

University of Gdańsk

Faculty of Chemistry

MSc Magdalena Anna Bojko

*Searching for peptides interacting with the PD-1
and PD-L1 immune checkpoint proteins for cancer
immunotherapies*

Doctoral Thesis

*Poszukiwanie peptydów oddziałujących z białkami immunologicznych
punktów kontrolnych PD-1 i PD-L1 wykorzystywanych w terapiach
nowotworowych*

Doctoral dissertation conducted at the Department of Biomedical
Chemistry

under the supervision of

prof. dr hab. Sylwia Rodziewicz-Motowidło

co-supervisor: dr Marta Spodzieja

Gdańsk 2023

*I would like to express my deepest gratitude to **prof. Sylwia Rodziewicz-Motowidło**, who generously provided knowledge, expertise, who guided and inspired me during the entire period of this doctoral dissertation.*

*This endeavour would not have been possible without **Ph.D. Marta Spodzieja** for her invaluable knowledge and patience, for late-night sessions, and moral support.*

*Special thanks to **prof. Peter Steinberger, Ph.D. Claire Battin, Ph.D. Adam Sieradzan, Ph.D. Paweł Niedziałkowski, Ph.D. Katarzyna Węgrzyn, MSc Mikołaj Kocikowski and MSc Małgorzata Kogut** for cooperation in carrying out my research for this doctoral dissertation.*

*I am also grateful to co-workers from **Department of Biomedical Chemistry** for the great atmosphere, exciting discussions and support.*

*I could not have undertaken this without **Marcin Witkowski** and my **Mom** their belief in me kept my spirits and motivation high during this process.*

This work was supported by the following sources:

- Polpharma Scientific Foundation (2020) project contractor - Grant from the Scientific Foundation of Polpharma - “Peptide immunomodulators as next generation inhibitors of the PD-1/PD-L1 checkpoints” (1/XVIII/19, 559-T070-0140-20)
Supervisor: prof. dr hab Sylwia Rodziewicz-Motowidło
- Research of Young Scientists: „Wykorzystanie białka PD-L1 jako biomarkera w diagnostyce chorób nowotworowych” (539 T070 B469 20), 2020-2021;
Supervisor: Magdalena Bojko
- Research of Young Scientists: „Poszukiwanie immunomodulatorów przeciwko tworzeniu się kompleksu białek kontrolnych PD-1/PD-L1” (538-8720-B251-18/19), 2019-2020;
Supervisor: Magdalena Bojko
- Research of Young Scientists: „Projektowanie i synteza fragmentów białka PD-L1 – poszukiwanie inhibitorów kompleksu białek PD-1/PD-L1” (538-8720-B726-17/18), 2018-2019;
Supervisor: Magdalena Bojko
- Research of Young Scientists: „Projektowanie i synteza peptydów hamujących formowanie się immuno-kompleksu białek PD-1/PD-L1” (538-8725-B360-16/17), 2017-2018;
Supervisor: Magdalena Bojko

Table of Contents

List of Abbreviations	7
Abstract.....	10
Streszczenie	13
I. Introduction.....	16
1. Cancer.....	16
1.1. Cancer treatment.....	16
1.1.1. Immunotherapy.....	18
2. Immune system.....	19
2.1. T lymphocytes and their receptors.....	20
2.2. Antigen presentation to T lymphocytes	21
2.3. Activation and inhibition of T lymphocyte.....	22
2.4. Immune checkpoint receptors and ligands.....	23
3. Immunoglobulin superfamily.....	25
3.1. Programmed cell death 1 - PD-1	26
3.1.1. Structure of the PD-1	26
3.1.2 Occurrence and function of PD-1	28
3.2. Programmed cell death 1 - ligand 1 (PD-L1) and 2 (PD-L2).....	30
3.2.1. Structure of the PD-L1	30
3.2.2. Structure of the PD-L2.....	32
3.2.3. Occurrence and function of PD-L1 and PD-L2.....	34
3.3. The crystal structures of the PD-1/PD-L1 and PD-1/PD-L2 complexes	35
3.3.1. The crystal structure of the PD-1/PD-L1 complex	35
3.3.2. The crystal structure of the PD-1/PD-L2 complex	37
4. The role of the tumour microenvironment in immuno-oncology.....	39
4.1. Therapy based on the immune checkpoint inhibition	40
4.2. The complexity in the PD-1/PD-L1 complex inhibition.....	41
5. Inhibitors of the PD-1/PD-L1 complex	42
5.1. Monoclonal antibodies targeting the PD-1/PD-L1 complex.....	42
5.1.1. Anti-PD-1 monoclonal antibodies	42
5.1.2. Anti-PD-L1 monoclonal antibodies	44
5.1.3. Results of the monoclonal antibodies therapy in the immune checkpoint inhibition	44
5.2. Peptides and peptidomimetics as inhibitors of the PD-1/PD-L1 complex formation...46	
5.2.1. Peptides and peptidomimetics inhibiting the PD-1/PD-L1 interactions	48
6. Selected techniques of the PD-1/PD-L1 potential inhibitors evaluation	54
6.1. SPR technique	54
6.2. Enzyme-linked immunosorbent assay - ELISA	57
6.3. Flow cytometry	58
II. Aim of the PhD thesis.....	61
III. Results.....	62
1. MM/GBSA analysis of PD-1/PD-L1 complex.....	62
2. Peptides targeting the PD-L1 protein	65
2.1. Designing and synthesis of peptides derived from the PD-1 protein.....	65
2.2. Study of binding of PD-1 based peptides to PD-L1 by the SPR technique	68

2.3. Stability of the designed peptides and their effects on the viability of chosen cell lines	73
2.4. Cell-Binding Assay and Competitive Inhibition	78
2.5. Cell-based PD-1/PD-L1 blocking bioassay	82
2.6. Conformational studies for peptide PD-1(122-138) ^{C123-S137C}	83
3. Peptides targeting the PD-1 protein	85
3.1. Design and synthesis of peptides derived from the PD-L1 protein	85
3.2. Study of binding of PD-L1 based peptides to PD-1 by the SPR and ELISA techniques	89
3.3. Stability of the designed peptides and their effects on the viability of chosen cell lines	98
3.4. Cell-Binding Assay and Competitive Inhibition	102
3.5. Stimulation assay	104
4. Analogues of PD-1(122-138)^{C123-S137C} targeting PD-L1 protein	110
4.1. Designing and synthesis of the analogues of PD-1(122-138) ^{C123-S137C} targeting the PD-L1 protein	110
4.2. Study of binding of PD-1(122-138) ^{C123-S137C} analogues to PD-L1 using the SPR technique	111
4.3. Stability of the designed analogues and their effects on the viability of chosen cell lines	112
4.4. Cell-Binding Assay and Competitive Inhibition	114
4.5. Stimulation assay	115
IV. Discussion	117
1. Analysis of the PD-1/PD-L1 interface	117
1.1. Analysis of the PD-1 interface	118
1.2. Analysis of the PD-L1 interface	120
2. The PD-1 and PD-L1 derived peptides	121
3. SPR analysis of the PD-1/PD-L1 complex – obstacles during analysis condition optimisation	123
3.1. Differences in binding of the PD-1 derived peptides to PD-L1 - analysis of the SPR data	124
3.2. Differences in binding of the PD-L1 derived peptides to PD-1 - analysis of SPR and ELISA data	125
4. Peptides evaluation in <i>in vitro</i> cellular assays	127
5. Conformation of peptide PD-1(122-138) ^{C123-S137C}	131
6. PD-1(122-138) ^{C123-S137C} peptide's loop modification and its influence on the interaction with PD-L1	132
7. Peptide PD-1(122-138) ^{C123-S137C} analogues evaluation in the <i>in vitro</i> cellular assays	134
V. Conclusions	136
VI. Materials and methods	137
1. Materials and general information	137
2. Peptides synthesis	138
3. Peptides cleavage	140
4. Formation of disulphide bridges	140
5. Peptide Purification	140
6. Peptides characterization	143
7. Testing of the peptides binding properties	148

7.1. The SPR Analysis on a CM5 sensor chips.....	148
7.2. The SPR Analysis on an SA sensor chips.....	148
7.3. Indirect ELISA	149
8. Peptides stability in RPMI 1640.....	150
9. Jurkat E6.1, CHO-K1, and BW5417 (TCS Ctrl) cell lines viability assay	150
10. Competitive assay at the cellular level	151
11. Testing of the peptides inhibition properties for the PD-1/PD-L1 complex formation	152
11.1. The PD-1/PD-L1 blocking bioassay – based on NFAT-RE induced luciferase.....	152
11.2. The PD-1/PD-L1 blocking bioassay – based on NF- κ B-RE induced eGFP	153

List of Abbreviations

Ab - antibody
Abu - 2-aminobutyric acid
ACN - acetonitrile
AKT - protein kinase B
ANOVA - analysis of variance
AP-1 - activator protein 1
APC - antigen presenting cell
APC - allophycocyanin
ATP - adenosine triphosphate
B cell - B lymphocyte
BATF - basic leucine zipper transcriptional factor ATF like
BMS - Bristol-Myers Squibb (name of the small molecules)
C1-set - constant-1 domain
C2-set - constant-2 domain
CD - cluster of differentiation
CD28 - cluster of differentiation 28
CD80 - cluster of differentiation 80
CD86 - cluster of differentiation 86
CDR - complementarity determining region
CHO - chinese hamster ovary
CTLA-4 - cytotoxic T lymphocyte antigen-4
DC - dendritic cell
DIC - N,N-diisopropylcarbodiimide
DIPEA - N,N-diisopropylethylamine
DLBCL - diffuse large B cell lymphoma
DMF - N,N-dimethylformamide
DSF - differential scanning fluorimetry
E. coli - *Escherichia coli*
EC₅₀ - half maximal effective concentration
ELISA - enzyme-linked immunosorbent assay
ESI-IT-TOF MS - electrospray ionization, ion trap, and time-of-flight mass spectrometry
FBS - fetal bovine serum
Fc - fragment crystallizable region
FCS - forward-scattered light
FDA - Food and Drug Administration
FOXP3 - forkhead box P3
FQY - fluorescence quantum yield
GAL-9 - galectin-9
GFP - green fluorescence protein

gMFI - geometric mean fluorescence intensity
HRP - horseradish peroxidase
HTRF - homogeneous time resolved fluorescence
HVEM - herpes virus entry mediator
I-O - immune-oncology
I-set - intermediate domain
ICI - immune checkpoint inhibitor
ICOS - inducible T cell co-stimulator
ICOS-L - inducible T cell co-stimulator-ligand
Ig-like - immunoglobulin-like
IgSF - immunoglobulin superfamily
irAE - immune related adverse events
ITIM - immunoreceptor tyrosine-based inhibitory motif
ITSM - immunoreceptor tyrosine-based switch motif
k_a - association rate constant
K_D - dissociation constant/equilibrium dissociation constant
k_d - dissociation rate constant
LIGHT, (TNFRSF14) - tumour necrosis factor ligand superfamily member 14
mAb - monoclonal antibody
mb CD3 - membrane-bound anti-human CD3 single-chain variable fragment
MHC - major histocompatibility complex
MM/GBSA - molecular mechanics generalized Born surface area
MM/PBSA - molecular mechanics Poisson–Boltzmann surface area
MREMD - multiplexed-replica exchange molecular dynamics
NF-κB - nuclear factor κB
NFAT - nuclear factor of activated T cells
NFAT-RE - NFAT response element
Nle - norleucine
NMR - nuclear magnetic resonance
NNKTL - nasal natural killer/T cell lymphoma
NSCLC - non-small cell lung cancer
Oxyma Pure - ethyle cyano(hydroxyamino)acetate
PBMC - peripheral blood mononuclear cells
PD-1 - programmed cell death 1
PD-L1 - programmed cell death 1 - ligand 1
PD-L2 - programmed cell death 1 - ligand 2
PDB - Protein Data Bank
Pdcd^{-/-} mice - PD-1-deficient mice
PE - R-Phycoerythrin
PI2K - the phosphoinositide 3-kinase
PK - pharmacokinetic
PPI - protein-protein interaction
RAS - rat sarcoma virus
RGMb - repulsive guidance molecule b

RP-HPLC - reversed phase-high performance liquid chromatography
RPMI 1640 - Roswell Park Memorial Institute 1640 medium
RU - resonance unit
SA - streptavidin sensor
scFv - single-chain variable fragment
SD - standard deviation
SHP-2 - Src homology region 2 domain-containing phosphatase
SP - signalling peptide
SPPS - solid-phase peptide synthesis
SPR - surface plasmon resonance
SSC - side-scattered light
T cell - T lymphocytes
TBTU - 2-(1H-benzotriazole-1-yl)-1, 1, 3, 3 -tetramethylammonium tetrafluoroborate
Tc - cytotoxic T cell
TCR - T cell receptor
TCS - T cell stimulator cells
TF - transcription factors
Th - helper T cell
TIM3 - mucin domain-containing protein 3
TIPS - triisopropylsilane
TM - transmembrane domain
TMB - tetramethylbenzidine
TNF - tumour necrosis factor
TNFR1 - tumour necrosis factor receptor 1
TNFRS - tumour necrosis factor receptor superfamily
TNFS - tumour necrosis factor superfamily
Treg - regulatory T cell
UNRES - UNited RESidue
V-set - variable domain
ZAP70 - zeta-chain-associated kinase 70

Abstract

Cancer is a group of diseases that humanity is facing since the beginning of its existence. The number of cancer cases grows each year and it is estimated that it may reach around 60 million new cases by 2050. This forces the governments and scientists to work on new anticancer therapies, prevention and treatment programs. Nowadays, there are many different approaches to treating cancer. Often, the therapy combines more than one type of treatment; however, the results are not always effective. In the last two decades, a lot of attention has been devoted to the immune-oncology, especially immune checkpoints inhibition. For their work on this subject, the two scientist, Thasuku Honjo and James P. Allison, received the 2018 Nobel Prize in Physiology and Medicine. Immune checkpoints are responsible for the modulation of immune response through the regulation of T lymphocytes activity. One of the best-known and most characterized inhibitory immune checkpoint is PD-1 with its ligand PD-L1. Blocking the binding between those molecule may have many potential clinical applications and their antagonists can be applied in cases of cancer and infectious diseases.

Currently, there are many approaches to blocking the formation of the proteins belonging to the immune checkpoints bringing patients new hope and opportunities for recovery. However, FDA-approved cancer therapies are mostly based on mAbs which have many side effects and are not always effective. Moreover, the cost of the annual therapy per patient consisting of a single agent blocking the PD-1/PD-L1 complex can reach more than USD 100,000. Combination therapy, using at least two mAbs, brings better effects; however, it is even more expensive and, therefore, less available to oncology patients. All this make it necessary to search for new, better and more affordable therapies that block the PD-1/PD-L1 axis, capable of restoring the function of the immune system. In my research, I focused on finding the peptide inhibitors of the PD-1/PD-L1 complex formation, able to restore functions of the immune system. To design the peptides, I used the crystal structure of the PD-1/PD-L1 complex and information obtained from the MM/GBSA analysis.

In the first stage of my research, I obtained thirteen linear and cyclic peptides with disulphide bridges, derived from the PD-1 structure. Using the SPR technique, I determined their affinity for PD-L1. The strongest binding was received for peptides

(10) and (7) but six other compounds interacted with the protein. All peptides that bound to PD-L1 were chosen for further evaluation. I examined their stability in RPMI 1640 medium with 10% FBS, used in cell culture, and their influence on the viability of three cell lines used in the further experiments. For most of the tested compounds, I observed a decrease in their concentration. However, I did not observe any additional signals in the chromatograms received from the HPLC analysis, which may indicate that they were not a subject of the degradation process, but could interact with the medium components. Subsequently, I examined the effect of peptides on cell viability. I performed this assay on three cell lines - CHO-K1, Jurkat E6.1 and TCS Ctrl (modified BW5417). The Jurkat E6.1 cells were negatively affected only by the highest tested concentration of some of the examined peptides (150 μ M). The CHO-K1 and TCS Ctrl were more sensitive to the compounds. The tested peptides showed a cytotoxic effect on these cell lines in a wider spectrum than in the case of Jurkat E6.1. I also examined the ability of the PD-1 derived peptides to compete with the PD-1 protein for binding to PD-L1 present on the cell surface and I determined whether they possess the ability to inhibit the formation of the PD-1/PD-L1 complex in a test by restoring NFAT mediated luciferase expression. The results of my research show that peptides (7) and (10) partially inhibit the formation of the protein-protein complex. Moreover, peptide (7) competes with PD-1 for binding to PD-L1.

The second approach to blocking the PD-1/PD-L1 complex consisted in designing peptides derived from PD-L1. I obtained seventeen linear and cyclic peptides with disulphide bridges. The PD-L1 derived peptides were tested in similar approaches to the PD-1 derived peptides. I examined their ability to compete with the PD-L1 protein for binding to PD-1 on the cell surface and their inhibitory properties against the PD-1/PD-L1 complex by measuring the expression of eGFP under the transcription factor NF- κ B. In the competitive assay, peptides (L1) and (L11) prevent PD-L1 from binding to PD-1 in a concentration-dependent manner; moreover, peptide (L11) from all the PD-L1 derived peptides stimulates the eGFP expression by inhibition of the PD-1/PD-L1 complex formation in a concentration-dependent manner. This peptide also exhibits one of the strongest affinity for the PD-1 protein.

Based on the data received for the PD-1 derived peptides, I chose peptide (10) as parent peptide to design its analogues. I designed six compounds but only four of them were subject to further analysis due to problems arising during the synthesis. To all peptide

(10) analogues, I introduced modifications in the loop to stabilize their structure and thus improve their affinity for PD-L1. The modifications have not increased the binding strength of the peptides to PD-L1 compared to peptide (10); however, they have influenced their stability and interaction with the components of the medium. These compounds also had a less negative effect on the cells used in the cell assays. In the cell functional assay, conducted to examine the competitive properties of peptide (10) analogues, it can be observed that changes introduced in the sequence of A3 lead to the displacement of PD-1 from the complex with PD-L1 in a dose-depending manner. In the stimulation assay based on a reporter gene expression system (NF- κ B::eGFP), peptide (10) and analogues A3, A4 and A5 restore the eGFP expression only at the highest concentration used.

The market of therapeutic peptides is growing annually and it is estimated to reach USD 50.60 Billion by 2026. The clinical trials focusing on the development of immunoncology therapies using peptides and peptidomimetics in their approach, are becoming increasingly common. The molecules obtained in this work, after further modifications of their structure, may also be used as therapeutics in immuno-oncology.

Streszczenie

Nowotwory to grupa chorób, z którymi ludzkość boryka się od początku istnienia. Liczba zachorowań na raka rośnie każdego roku i szacuje się, że do 2050 roku może osiągnąć około 60 milionów nowych przypadków. Zmusza to rządy państw i naukowców do pracy nad nowymi terapiami przeciwnowotworowymi oraz programami profilaktyki i leczenia. Obecnie istnieje wiele różnych podejść do leczenia raka. Często terapia przeciwnowotworowa łączy więcej niż jeden rodzaj leczenia, jednak jej efekty nie zawsze są zadowalające. W ostatnich dwóch dekadach wiele uwagi poświęcono immunoonkologii, a zwłaszcza hamowaniu punktów kontrolnych układu immunologicznego. Za prace nad tym zagadnieniem, w 2018 roku dwóch naukowców, Thasuku Honjo i James P. Allison, otrzymało Nagrodę Nobla w dziedzinie fizjologii i medycyny. Punkty kontrolne układu odpornościowego są odpowiedzialne za modulację odpowiedzi immunologicznej, poprzez regulację aktywności limfocytów T. Jednym z najlepiej poznanych i najlepiej scharakteryzowanych punktów kontrolnych hamujących odpowiedź układu odpornościowego jest białko PD-1, tworzące kompleks ze swoim ligandem, białkiem PD-L1. Zablokowanie wiązania się tych molekuł może mieć wiele potencjalnych zastosowań klinicznych, a związki hamujące tworzenie kompleksu PD-1/PD-L1 mogą znaleźć zastosowanie w leczeniu nowotworów i chorób zakaźnych.

Obecnie istnieje wiele podejść mających na celu blokowanie tworzenia kompleksów przez białka należące do punktów kontrolnych układu immunologicznego, co daje pacjentom nadzieje i nowe możliwości powrotu do zdrowia. Jednak zatwierdzone przez FDA terapie przeciwnowotworowe w większości oparte są na przeciwciałach monoklonalnych, które przyczyniają się do wystąpienia wielu skutków ubocznych i nie zawsze są skuteczne. Ponadto koszt rocznego leczenia jednego pacjenta złożony z jednego przeciwciała blokującego kompleks PD-1/PD-L1 może sięgać nawet ponad 100 000 USD. Terapia skojarzeniowa, przy użyciu co najmniej dwóch przeciwciał monoklonalnych, przynosząca lepsze efekty, jest jeszcze droższa a przez to mniej dostępna dla pacjentów onkologicznych. Wszystko to sprawia, że konieczne jest poszukiwanie nowych, lepszych i bardziej przystępnych cenowo terapii blokujących wiązanie się białka PD-1 z PD-L1. W swoich badaniach skupiłam się na poszukiwaniu

peptydowych inhibitorów tworzenia kompleksu PD-1/PD-L1, zdolnych do przywracania funkcji układu odpornościowego. Do zaprojektowania peptydów, wykorzystałam strukturę krystaliczną kompleksu PD-1/PD-L1 oraz informacje uzyskane z analizy MM/GBSA.

W pierwszym etapie moich badań otrzymałam trzynaście peptydów liniowych oraz cyklicznych z mostkami disulfidowymi, wywodzących się ze struktury białka PD-1. Wykorzystując technikę SPR określiłam ich powinowactwo do białka PD-L1. Wiązanie do białka zaobserwowałam dla peptydów **(10)** i **(7)**, ale sześć innych związków również oddziaływało z celem molekularnym. Wszystkie peptydy, które wiązały się do białka PD-L1 poddałam dalszej analizie. Zbadałam ich stabilność w pożywce RPMI 1640 (z 10% FBS), używanej w hodowli komórkowej oraz ich wpływ na żywotność trzech linii komórkowych, wykorzystywanych w dalszych doświadczeniach. Dla większości badanych związków, zaobserwowałam zmniejszenie się ich stężenia po dodaniu do pożywki oraz po 24 godzinach inkubacji. Nie zaobserwowałam jednak dodatkowych sygnałów na chromatogramach uzyskanych podczas analizy z wykorzystaniem HPLC, co może wskazywać, że nie były one przedmiotem degradacji, natomiast mogły oddziaływać ze składnikami pożywki. Następnie sprawdziłam wpływ peptydów na żywotność komórek. Test ten wykonałam dla trzech linii komórkowych - CHO-K1, Jurkat E6.1 i TCS Ctrl (zmodyfikowane BW5417). Na komórki Jurkat E6.1 negatywny wpływ miały jedynie najwyższe stężenia niektórych z peptydów (150 μ M). Linie CHO-K1 i TCS Ctrl okazały się bardziej wrażliwe na działanie związków. Badane peptydy wykazały efekt cytotoksyczny w szerszym spektrum niż w przypadku linii komórkowej Jurkat E6.1. Sprawdziłam również, czy otrzymane przez mnie związki konkurują z białkiem PD-1 o wiązanie się z PD-L1 obecnym na powierzchni komórek oraz określiłam czy posiadają zdolności do hamowania tworzenia kompleksu PD-1/PD-L1 w teście komórkowym polegającym na przywróceniu ekspresji lucyferazy poprzez aktywację czynnika transkrypcyjnego NFAT. Wyniki moich badań pokazują, że peptydy **(7)** i **(10)** w pewnym stopniu hamują tworzenie się kompleksu białko-białko. Ponadto peptyd **(7)** konkuruje z PD-1 o wiązanie się z PD-L1.

Drugie podejście do blokowania kompleksu PD-1/PD-L1 polegało na zaprojektowaniu peptydów, wywodzących się ze struktury białka PD-L1. Otrzymałam siedemnaście peptydów, które były liniowe lub posiadały mostek disulfidowy. Peptydy pochodzące z białka PD-L1 testowałam w podobny sposób jak peptydy pochodzące z białka PD-1.

Zbadałam ich zdolność do konkurowania z białkiem PD-L1 o wiązanie się z PD-1 znajdującym się na powierzchni komórki oraz ich właściwości hamujące względem kompleksu PD-1/PD-L1 poprzez pomiar ekspresji eGFP wyindukowanego za pośrednictwem czynnika transkrypcyjnego NF- κ B. W teście kompetycyjnym peptydy **(L1)** i **(L11)** zakłócają wiązanie się PD-L1 do PD-1 w sposób zależny od stężenia, ponadto **(L11)** jako jedyny stymulował ekspresję eGFP poprzez hamowanie tworzenia się kompleksu PD-1/PD-L1 w sposób zależny od stężenia. Peptyd **(L11)** jest również jednym ze związków najsilniej wiążących się do białka PD-L1.

Na podstawie wyników otrzymanych dla peptydów wywodzących się z białka PD-1, wybrałam peptyd **(10)** jako cząsteczkę wiodącą do zaprojektowania jego analogów. Zaprojektowałam sześć związków, jednak tylko cztery z nich zostały poddane dalszej analizie, ze względu na problemy powstałe podczas syntezy. Do wszystkich analogów peptydu **(10)** wprowadziłam zmiany w pętli, aby ustabilizować ich strukturę i przez to poprawić ich powinowactwo do PD-L1. Wprowadzone modyfikacje nie zwiększyły siły wiązania się z białkiem PD-L1, w porównaniu do peptydu **(10)**, jednak wpłynęły na ich stabilność i wiązanie się ze składnikami pożywki. Związki te miały również dużo mniej negatywny wpływ na komórki, wykorzystywane w testach. W funkcjonalnym teście komórkowym, przeprowadzonym w celu zbadania właściwości kompetycyjnych analogów peptydu **(10)**, zaobserwowałam, że zmiany wprowadzone w sekwencji **A3** prowadzą do wypierania białka PD-1 z kompleksu z PD-L1 w sposób zależny od dawki. W teście stymulacji opartym na systemie ekspresji genu reporterowego (NF- κ B::eGFP) analogi **A3**, **A4** i **A5** podobnie jak peptyd **(10)** przywracają ekspresję eGFP tylko w najwyższym zastosowanym stężeniu.

Rynek peptydów terapeutycznych rośnie z roku na rok i szacuje się, że do 2026 roku osiągnie wartość 50,60 mld USD. W badaniach klinicznych nad rozwojem terapii immunookologicznych coraz częściej można spotkać terapie wykorzystujące w swoim podejściu peptydy i peptydomimetyki. Otrzymane w tej pracy cząsteczki, po dalszych modyfikacjach struktury w celu zwiększenia ich aktywności również będą mogły znaleźć zastosowanie jako terapeutyki w immunoonkologii.

I. Introduction

1. Cancer

Cancer is not one disease. It is a group of diseases connected with uncontrolled growth of cells caused by multiple sequential mutations. Cancer cells no longer fulfil its biological purpose and do not behave as regular cells. They grow without a signal that tells them to grow and they ignore the signal which tells them to stop¹. There are three main carcinogens: physical (caused e.g. by ionizing or ultraviolet radiation), chemical (caused e.g. by pesticides or polycyclic aromatic hydrocarbons) and infection induced (caused e.g. by the *Helicobacter pylori* or human papillomavirus)¹. Together with the socioeconomic development, external environmental factors have gained greater influence on the number and rate of the genetic “mistakes”, which can lead to cancer development².

Cancer has been known to the mankind for ages. The first description of tumour in human tissues was found in an Egyptian papyrus dated 1500 B.C. Moreover, there is evidence that even dinosaurs living 250 to 65 million years ago suffered from cancer³. It is estimated that only in 2020 there were reported more than 19 million new cancer cases and almost 10 million deaths worldwide⁴. In comparison with year 2000, this number increased by 9 million new cases and 4 million deaths⁵. This escalation reflects growth and aging of the worldwide population. It is estimated that this number will triple by the year 2050, which put pressure on governments and scientists to work on new anticancer therapies, prevention and treatment programs⁶.

1.1. Cancer treatment

There are different approaches to treat cancer and they depend on the specific type of cancer. Moreover, new ways of treatment are constantly developed to find better therapy, which will prolong lives of patients, improve their quality, be more affordable and have less adverse effects. Cancer treatment is usually complex and combines a couple of therapies at once. The most common cancer treatment options are presented in Figure 1.



Figure 1. *The most common methods of cancer treatment⁷.*

Predominantly, cancer treatment can be divided into two approaches: “local” and systemic. The first one consists of surgery and radiation therapy and its goal is to remove cancer. It can be done during the surgery or by using high-energy waves or particles such as X and gamma rays, protons or electron beams. The second one includes treatments connected with delivering medicines to the patient and can be divided into chemotherapy, hormone, targeted therapy or immunotherapy. Chemotherapy is the most frequently used method of treating cancer and it applies chemotherapeutic agents focused on blocking the mechanism characteristic of cancer cell that leads to cell death. However, this approach affects also healthy cells. Hormone therapy is implemented when a cancer is fuelled by the hormones. It is commonly used in breast and prostate cancer. Hormone therapy leads to blocking the effects of hormones. Another method is targeting therapy, which focuses on specific abnormalities within cancer cells. For example, a molecular target located in the cancer cell. Moreover, there is also a treatment that consists of restoring or amplifying body’s natural immune system to attack cancer cells. This is called immunotherapy or immunoncology (I-O) and it is a relatively new anticancer treatment^{8,9}. Due to the fact that my doctoral thesis focuses on the topic of immunotherapy in cancer treatment and especially one of the approaches of restoring our own immune system’s mechanism against the cancer cells further in this work, I will present closer the subject of the I-O.

1.1.1. Immunotherapy

In last two decades cancer immunotherapy has gained an important role in cancer treatment. In contrary to other approaches I-O does not target tumour directly but stimulate host immune system to make a stand against the enemy which inhibits the immune response¹⁰. The beginning of this concept is dated on nineteenth century and was initiated by a German pathologist Rudolf Virchow, who studied cellular pathology, as a first recognized leukaemia and observed immune infiltration in human tumors^{11,12}. Since that date I-O has evolved, and basing on the mechanism of action, can be divided into active and passive immunotherapy, those approaches are presented in the Figure 2. In general, passive therapy adopt *ex vivo* activated or pre-treated cells taken from the host body or grown in the laboratory and administrate them to patient to restore deficient immune function⁷. This type of therapy produces immediately action. By contrast, the active approaches act *in vivo* by stimulating immune system against the cancer. The example of active immunotherapy can be immune checkpoints inhibition^{7,10}. This type of cancer treatment will be discussed more broadly in chapter 4.1. as it is connected with my doctoral research. For better understanding immunotherapy basing on immune checkpoint inhibition the immune system and mechanisms standing behind growing interest of it use in cancer treatment will be described.

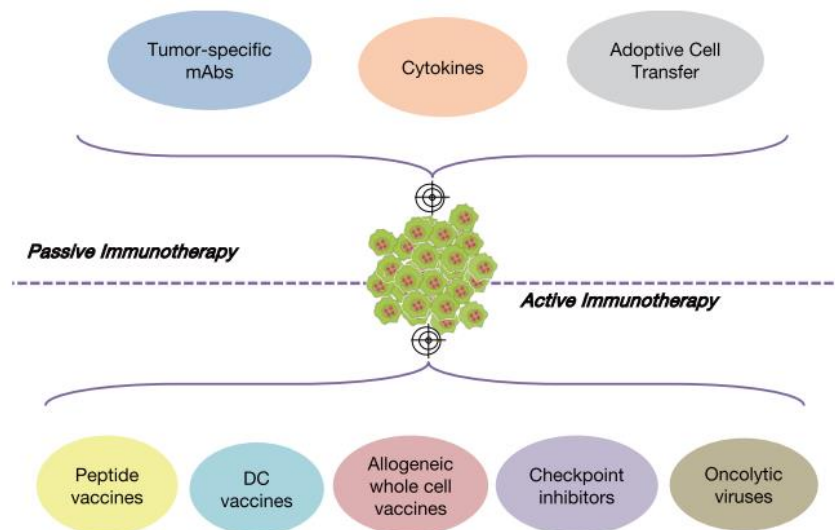


Figure 2. Approaches of I-O classified into passive and active immunotherapy⁷.
mAbs - monoclonal antibodies; DC - dendritic cells.

2. Immune system

Immune system is body's defence in the word full of microbes, viruses and parasites. It ensures homeostasis of human organism by identifying of threats from surrounding environment and from ours own defect cells¹. The main tools of immune system are immune cells having their origin in stem cells. They may be divided into granulocytes and lymphocytes (Figure 3). The first group of immune cells takes part in mechanism triggered by innate immune system. They provide first line of defence – immediate but not specific. In contradiction to granulocytes, lymphocytes are responsible for adaptive immune response which take longer time than innate one, however, is more precise. The main weapon of adaptive immune system are T lymphocytes (T cells) with T cell receptors (TCRs) and B lymphocytes (B cells) with their specialized antibodies^{1,13}. The innate and adaptive immune systems cooperate with each other. The first one gives time to the second one which defence mechanisms are more time-consuming.

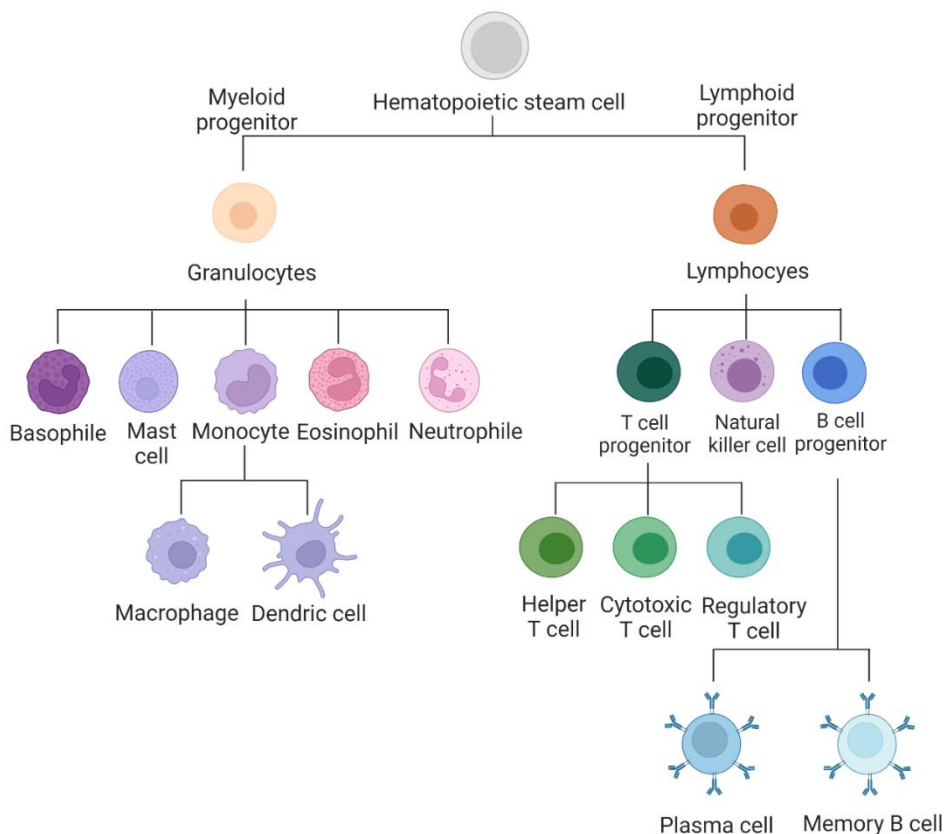


Figure 3. Cells of immune system¹⁴.

The B and T cells take part in the main types of immune response - humoral (antibody-mediated) and cellular (cell-mediated). It should be noted that above mentioned immune responses occur simultaneously only with slight predominantly of

one type of response. Antibody-mediated immunity depends on recognition of antigen by antibody (Ab) produced by B cells and will not be discussed further in this work. The second type of immune response relies on T lymphocytes, mainly on recognition of antigens by T cell receptors located on T lymphocytes^{1,13,15}.

2.1. T lymphocytes and their receptors

T cells are one of the most important cells in immune system. They develop from hematopoietic stem cells in the bone marrow but cease maturation events in thymus. The T cells can be divided into three main subtypes, namely, cytotoxic (Tc), helper (Th) and regulatory (Treg) cells. Each of those cells populations have varied functions and different molecular receptors presented on their surface in the form of cluster of differentiation (CD) molecules which support T cell activation. Moreover, they recognized antigens presented by strictly defined class of major histocompatibility complex (MHC) molecules. Characterization of T cells subpopulations is show in Table 1.

Table 1. Characterization of T cells subpopulations¹.

T LYMPHOCYTE			
Types of lymphocytes	Cytotoxic T cells	Helper T cells	Regulatory T cells (suppressor)
Abbreviation	Tc	Th	Treg
Function	Have ability to kill infected and body's own cells. Tc have to directly bind to infected cell.	Support humoral and cell-mediated immune response. They simplify activation, proliferation and differentiation of B and T cells.	Regulate/suppress function of Tc and Th. Prevent from long-term, superfluous agitation.
CD molecule supporting T cell activation	CD8	CD4	CD4, CD8, CD25, FOXP3*
Class of MHC molecule interacting with TCR and cluster of differentiation molecule	MHC I	MHC II	-

*FOXP3 - forkhead box P3.

On the surface of T cells are located earlier mentioned TCRs (around 5×10^4 per one T cell), which are surface proteins responsible for binding with antigen, exposed by antigen presenting cells (APCs)^{16,17}.

TCR is a transmembrane heterodimeric receptor with two polypeptide chains linked by disulphide bridge. TCR constituted of two constant domains ($C\alpha$ and $C\beta$) and two variable regions ($V\alpha$ and $V\beta$) (Figure 4). In both variable domains can be distinguish

three complementarity determining regions (CDRs) responsible for antigen binding. Moreover, on T cells surface can be find aforementioned CD proteins, which vary for different subpopulations of T cells. Both TCR polypeptide chains, α and β , create complex in cell membrane with CD3 molecule which mediate in transmission of the T cell activation signal. Additionally, TCR-CD3 complex interacts in the cell membrane with CD8 and CD4^{1,13,15,18}.

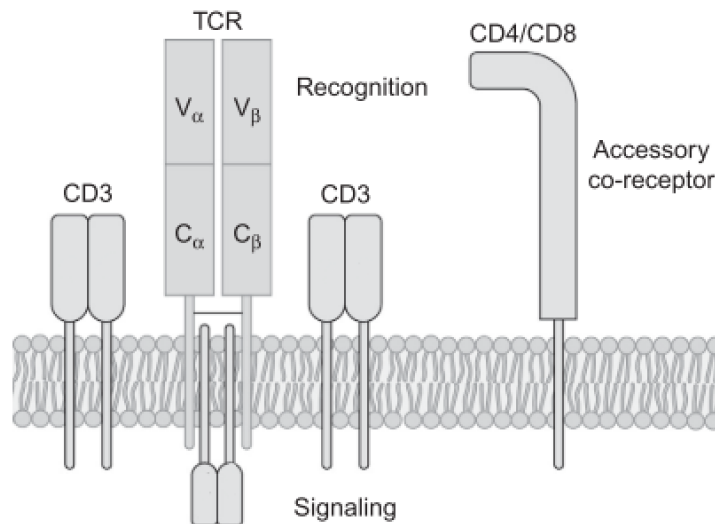


Figure 4. Types of receptors on T cell surface¹⁵.

2.2. Antigen presentation to T lymphocytes

Antigen is an agent capable to stimulate immune response. It can be distinguished two main types of antigens: foreign antigens (pathogens, toxins, pollens) and autoantigens (body's cells under pathological conditions). T cells recognize only antigens in form of short peptides presented by MHC molecules located on surface of APC. APCs are involved in innate and adaptive immune response. They process and present antigens for recognition by the appropriate TCR. APC are a heterogeneous group of cells which can be divided into professional APC, which include macrophages, dendritic cells, B cells, and nonprofessional APC which include vascular endothelial cells and thymic epithelial cells^{16,17}.

MHC molecules are glycoproteins which function is presenting antigens to TCRs. Antigens presented by MHC molecules are peptides arise through enzymatic digestion of the proteins having it origins in aforementioned foreign or autoantigens. MHC

molecules can be divided into two classes MHC class I and MHC class II. This classification is based on the protein processing pathway into peptides. MHC class I molecules bind and present endogenous-derived peptides, which are digested by proteolytic enzymes in cytoplasm and loaded to MHC I in endoplasmic reticulum. Those antigens originate from microorganism and parasites developing intracellularly and from cancer cells. MHC I peptides usually contain 8-10 amino acid residues¹⁹. Antigens presented by the MHC class I are recognized by CD8 T cells (Tc) specific for presented peptide. MHC class I molecules are found on the surface of almost all nucleated cells. On the contrary, MHC class II are surface molecules present on professional APC – macrophages, B cells and DC. This class of molecules present exogenous-derived peptides containing 13-17 amino acid residues¹⁹. In this type of antigen presentation whole viruses or bacteria are engulfed by endocytose and enclosed in an endosome where it is digested by proteolytic enzymes and loaded to MHC II. Antigens presented by the MHC class II are recognized by CD4 T cells (Th) specific for presented peptide^{1,15,19}.

2.3. Activation and inhibition of T lymphocyte

Control of immune system, its activation, occurs through at least two signals from connection of APCs with T cells. Primary signal is aroused by detection of peptides (antigens) presented by MHC molecules on APCs by T cell receptor on T cells. Moreover, to complete first signal CD8 or CD4 molecules present on Tc or Th have to bind to MHC I (activation of Tc, describe as lymphocytes CD8⁺) or MHC II (activation of Th, describe as lymphocytes CD4⁺) respectively (Figure 5, Signal I). However, it is only first step to activate immune system. The second one is controlled by co-stimulatory and co-inhibitory receptors also known as immune checkpoints. To induce second signal immune checkpoint receptor, one of the proteins belonging to cluster of differentiation 28 (CD28) family, located on T cell has to bind to its ligand, belonging to B7 proteins family, on APC (Figure 5, Signal II). Those two signals are necessary to stimulate or inhibit immune response. Absence of a second signal may lead to T cell anergy (inactivation). Those two signals are necessary for complied activation of T cells. Lymphocytes CD8⁺ secrete cytokines which cause death of target cell by apoptosis. On the contrary, T cells CD4⁺ secrete cytokines which lead to B cells and Tc proliferation^{1,15}. The response of immune system undergoes sustained balance

between positive and negative signals which activate or inhibit its response. Those mechanisms prevent us from autoimmune diseases, infections and development of damaged (mutated) cells. Therefore, immune system evolved mechanisms enable to recognition “self” from “non-self” by detecting proteins located on the cell surface which are tools used to maintain homeostasis^{1,15}.

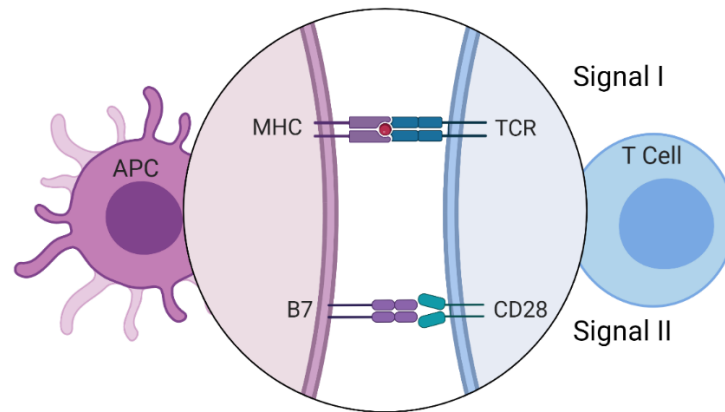


Figure 5. Model of two stage T cell activation²⁰.

2.4. Immune checkpoint receptors and ligands

Immune checkpoint proteins mentioned in the previous paragraph are crucial for full activation or inhibition of T cells. Those proteins can be divided into co-stimulatory and co-inhibitory receptors. Both types of the receptors have to bind to its ligand on APC to induce T cell activation signal which stimulates or inhibits immune response, respectively. The first group of receptors is responsible for co-activation of T cells against pathogens and body’s cells under pathological condition. To co-stimulatory receptor-ligand pairs following molecules can be included: CD28 receptor and its ligands cluster of differentiation 80 and 86 (CD80 and CD86), and inducible T cell co-stimulator (ICOS) and its ligand (ICOS-L). The second group of immune checkpoints constitute co-inhibitory molecules responsible for negative stimulation of T cells. Their main function is surveillance of immune system against autoaggression events. The best-known inhibitory immune checkpoints are cytotoxic T lymphocyte antigen – 4 (CTLA-4) interacting with CD80 or CD86, programmed cell death - 1 (PD-1) interacting with programmed cell death 1 – ligand 1 or ligand 2 (PD-L1 and PD-L2, respectively)²¹ and T cell immunoglobulin and mucin domain-containing protein 3

(TIM3) and its ligand galectin-9 (GAL-9)²². Exemplary co-stimulatory and co-inhibitory receptors, and their ligands are presented in the Figure 6.

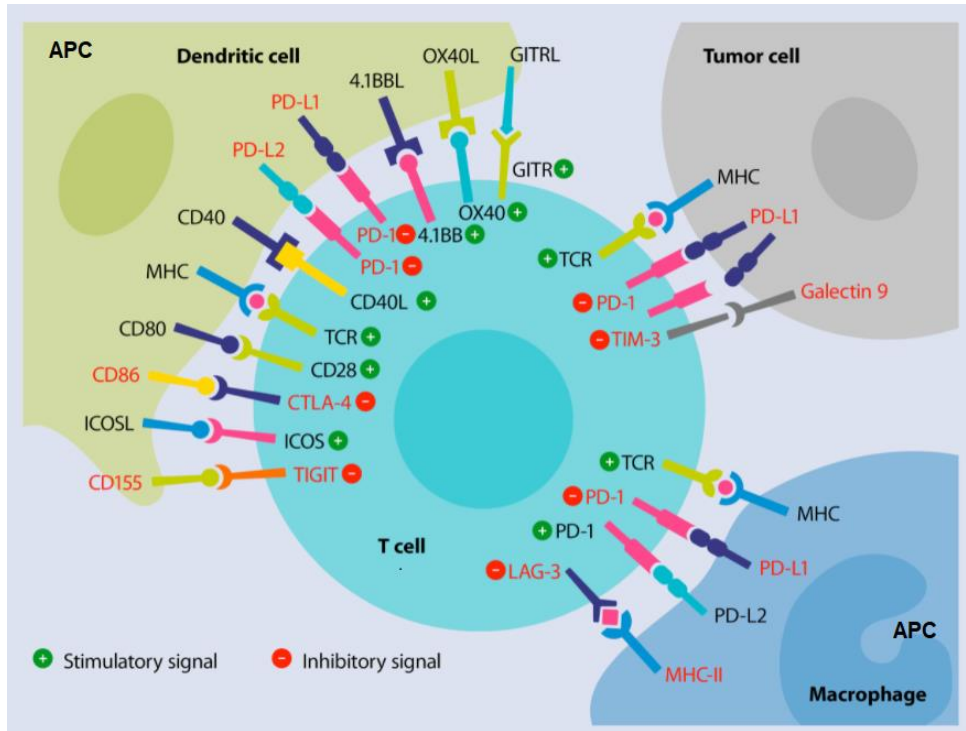


Figure 6. Examples of co-stimulatory and co-inhibitory pairs of molecules. Plus marks show co-stimulatory molecules, whereas minus marks show co-inhibitory molecules²³.

Immune checkpoints receptors and their ligands belong to two main protein superfamilies:

- Tumour necrosis factor receptor superfamily (TNFRS) and their ligands tumour necrosis factor superfamily (TNFS) – representatives of this protein receptor superfamily are tumour necrosis factor receptor 1 (TNFR1) and herpes virus entry mediator (HVEM) and their ligands tumour necrosis factor (TNF) and tumour necrosis factor ligand superfamily member 14 (TNFRSF14, LIGHT), respectively^{24,25};
- Immunoglobulin superfamily (IgSF) - representatives of this protein superfamily are receptors CD28, CTLA-4 and PD-1 and its ligands CD80, CD86 and PD-L1, PD-L2, respectively²⁶.

The IgSF protein superfamily and three of its representatives PD-1, PD-L1 and PD-L2 will be discussed and characterized in more details in the next chapter.

3. Immunoglobulin superfamily

Immunoglobulin superfamily is a widely diverse group of protein receptors and ligands with divergent functions and sequences, connected with similarities in the tertiary structure, namely by immunoglobulin-like (Ig-like) domain²⁷. In general, Ig homology units consist of two antiparallel β -sheets containing 70-100 amino acid residues grouped into 7-9 β strands stabilized by disulphide bridge. Each β -strand is formed by 5-10 amino acid residues^{28,29}. The Ig domains can be classified into four groups which are presented in the Figure 7:

- V-set – variable domain, it consists of 9 β strands;
- C1-set – constant-1 domain, it is standard IgC domain, it consists of 7 β strands;
- C2-set – constant-2 domain, it consists of 7 β strands (the same as C1-set) but it is sequentially similar to V- set;
- I-set – intermediate domain, IgI domain resembles the IgV with small differences exhibiting in shorter C' strand and lacking C'' strand.

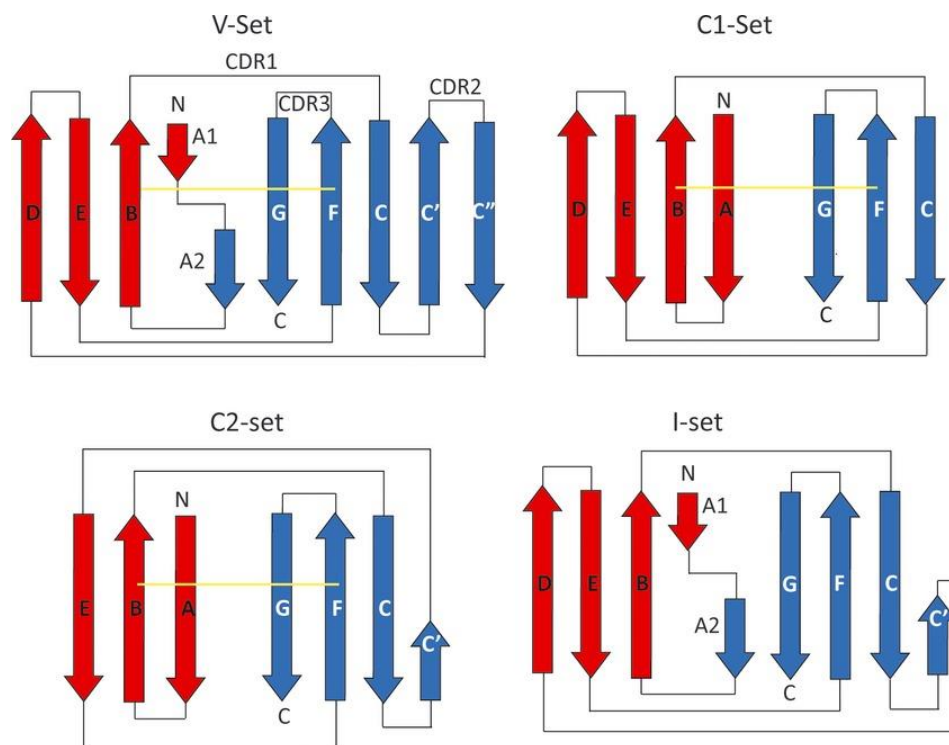


Figure 7. Topology of four main immunoglobulin domains³⁰.

3.1. Programmed cell death 1 - PD-1

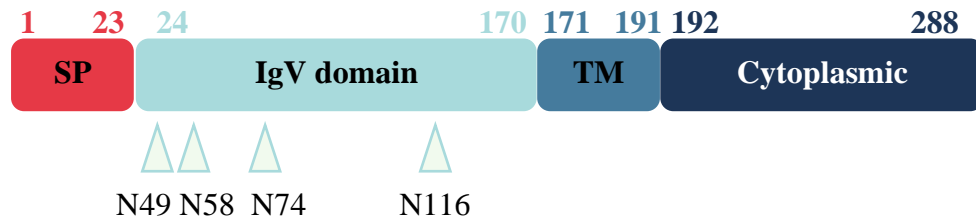
Programmed cell death 1 (PD-1, CD279) is a protein receptor which belongs to the immunoglobulin superfamily³¹ and takes part in negative regulation of immune response^{32,33}.

3.1.1. Structure of the PD-1

PD-1 is a protein containing 288 amino acids of molecular weight of 50-55 kDa³⁴⁻³⁶. It consists of a signalling peptide (length: 23 amino acids), an extracellular region in IgV topology (length: 147 amino acids), transmembrane helical region separating IgV domain from a cytoplasmic domain (length: 21 amino acids) and the cytoplasmic domain (length: 97 amino acids)^{34,37}. This is a typical structure for type I transmembrane glycoprotein (Figure 8A and 8B). IgV domain of PD-1 has four potential N-linked glycosylation sites in positions 49, 58, 74 and 116 (triangles in the Figure 8A)³⁸. The cytoplasmic domain has two tyrosine residues. The proximal one to a cell membrane constitutes an immunoreceptor tyrosine-based inhibitory motif (ITIM), whereas the distal tyrosine residue is a part of the immunoreceptor tyrosine-based switch motif (ITSM). Both of them are essential for the inhibitory function of PD-1^{39,40}.

The extracellular domain of PD-1 occurs as a monomer on the cell surface, in solution and in the crystallized form⁴¹. PD-1 structure is stabilized by only one intrachain disulphide bond (Figure 8B, red)^{32,42}. Contrary to the other members of CD28 family, such as CD28, CTLA-4, and ICOS, PD-1 cannot form a homodimer as it lacks cysteine residues proximal to the cell surface^{32,42,43}.

A



B

	10	20	30	40	50
MQIPQAPWPV	VWAVLQLGWR	PGWFLDSPDR	PWNPPTFSPA	LLVTEGDNA	
	60	70	80	90	100
TFTCSFSNTS	ESFVLNWYRM	SPSNQTDKLA	AFPEDRSQPG	QDCFRFVTQL	
	110	120	130	140	150
PNGRDFHMSV	VRARRNDSGT	YLCG AISLAP	KAQIKESLRA	ELRVTERRAE	
	160	170	180	190	200
VPTAHPSPSP	RPAGQFQTLV	VGVVGGLLGS	LVLLVWVLAV	ICSRAARGTI	
	210	220	230	240	250
GARRTGQPLK	EDPSAVPVFS	VDYGELDFQW	REKTPEPPVP	CVPEQTEYAT	
	260	270	280		
IVFPSGMGTS	SPARRGSADG	PRSAQPLRPE	DGHCSWPL		

Figure 8. A) Schematic diagram of PD-1 protein. SP - signalling peptide; TM - transmembrane domain; triangles - potential N-linked glycosylation sites. B) Amino acid residues sequence of PD-1. The disulphide bridge connecting cysteine residues is marked red.

PD-1 protein forms two β -sheet structures with antiparallel β strands. The extracellular domain between 24th and 170th amino acid residues bears resemblance to IgV topology and is arranged in two β sheets (G'GFCC' and AA'BED) stabilized by a disulphide bond between C54 and C123 (Figure 9). In addition, the strongly conserved four amino acid residues, R94, F95, D117 and G119, typical of many V-set sequences, can be found in the extracellular domain of PD-1^{34,42}.

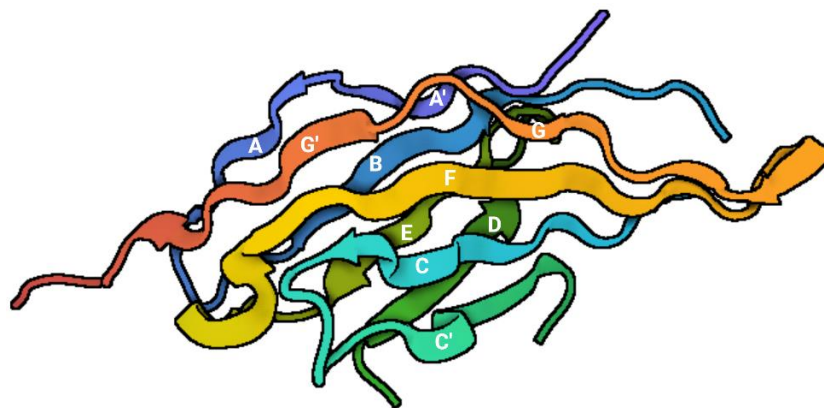


Figure 9. Structure of the extracellular domain of PD-1 protein (PDB ID: 3RRQ)⁴².

3.1.2 Occurrence and function of PD-1

PD-1 is expressed on activated T cells (CD4⁺ and CD8⁺) and in small amounts occurs on naïve T cells and B cells, dendritic cells, monocytes, and natural killer T cells^{34,39}. PD-1 occurs not only in transmembrane form but an extracellular soluble domain of this protein can be secreted into sera (sPD-1) by peripheral blood mononuclear cells (PBMC)⁴⁴.

ITSM and ITIM motifs of PD-1 undergoes phosphorylation upon stimulation by its ligand which enable binding of Src homology region 2 domain-containing phosphatase (SHP-2)⁴⁵ (Figure 10). SHP-1 is also recruited in PD-1 signalling pathway, however only in the absence of SHP-2⁴⁶. Moreover, not only the inhibitory signal is transferred through ITSM and ITIM but the ITSMs from two PD-1 may bind SHP-forming PD-1 homodimer⁴⁷. These phosphatases dephosphorylate critical proteins from stimulating signalling triggered by TCR/MHC and also CD28/CD80/86, among others they influence Zeta-chain-associated protein kinase 70 (ZAP70) and the phosphoinositide 3-kinase (PI3K) - protein kinase B (AKT) and rat sarcoma virus (RAS)⁴⁵. This leads to diminish of transcription factors (TFs), namely, activator protein 1 (AP-1), nuclear factor κ B (NF- κ B) and nuclear factor of activated T cells (NFAT), responsible for T cell activation, proliferation, cytokine production, and cytolytic function³⁶. Moreover, PD-1 may influence T cell function through increasing expression of basic leucine zipper transcriptional factor ATF like (BATF), which is connected with avoiding autoimmunity through T cell exhaustion⁴⁸.

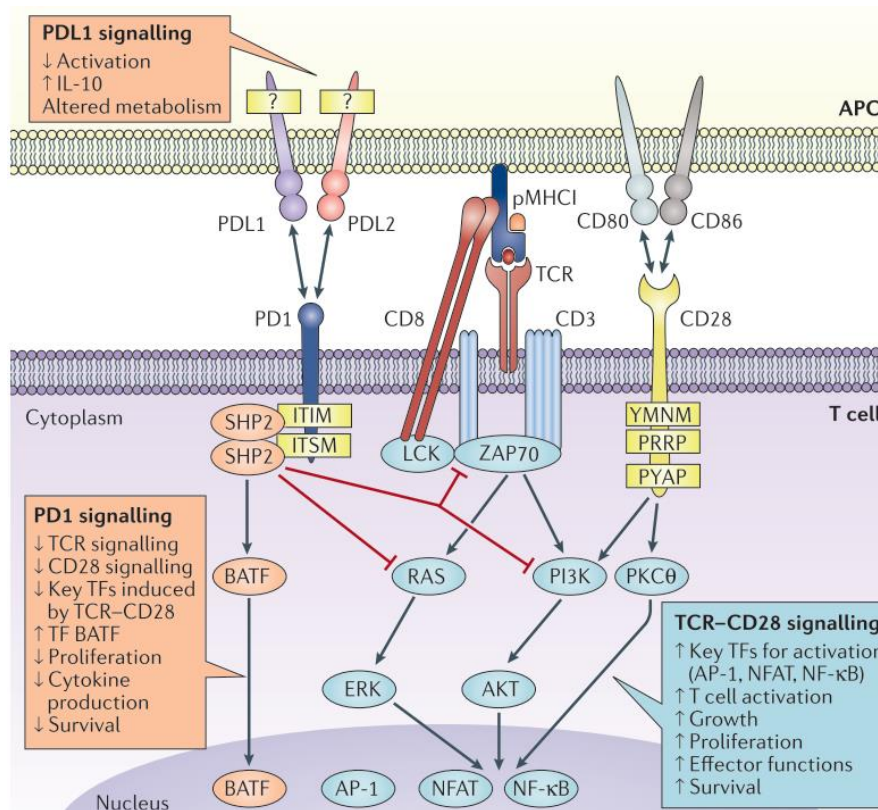


Figure 10. PD-1 signalling pathway⁴⁹.

The PD-1 protein participates in the establishment and sustain immunological self-tolerance. Generating of the PD-1-deficient mice (Pcd⁻¹ mice) led to unveiled the function of PD-1 protein which is regulation of adaptive immune response. Experiments on Pcd⁻¹ mice revealed correlation of the PD-1 deficiency with development of autoimmunity diseases such as systemic lupus erythematosus^{50,51}, dilated cardiomyopathy⁵², acute type I diabetes^{53,54}, multiple sclerosis⁵⁵ and allergy⁵⁶. Additionally, the extracellular region of sPD-1 secreted to sera can attenuates the PD-1 pathway and leads to progression of autoimmune disease. sPD-1 occurrence in synovial fluid of patients with rheumatoid arthritis worsens the disease⁵⁵. Targeting PD-1 protein can have many potential clinical applications (Figure 11). PD-1 antagonists can be applied in case of cancer and infectious diseases where activation of immune system is desired. On the other hand, the PD-1 pathway agonists can be useful agents in autoimmunity diseases, allergy and prevention of transplant rejection where the deactivation of immune system is seek aspect³⁶.

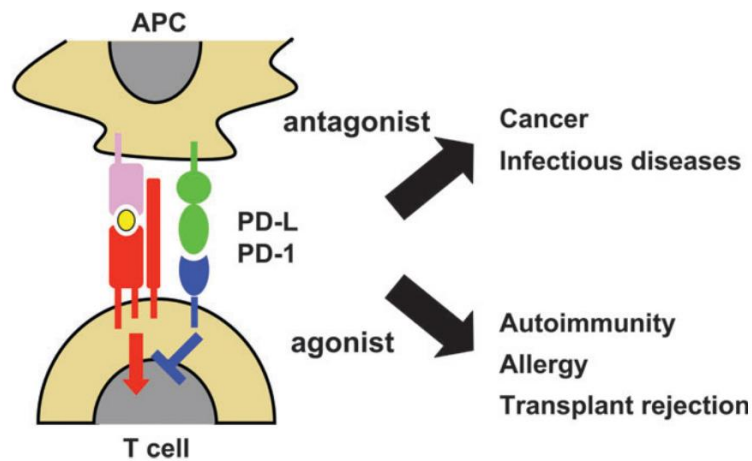


Figure 11. Potential application of PD-1 antagonists and agonists³⁶.

Moreover, the PD-1 molecule was found on cancer cells in cancer types such as non-small cell lung cancer (NSCLC), melanoma and different types of sarcomas⁵⁷⁻⁵⁹. Appearance of PD-1 protein on the tumour cells leads to complications during I-O therapies targeting PD-1 protein, like promoting hyperprogression of tumour growth⁵⁷. Presence of PD-1 on tumour cells may create a demand for changing approach in immune therapy blocking PD-1/PD-L1 complex consisting in targeting PD-1 protein. Shifting attention to therapy focusing only on targeting PD-L1 protein or routine determination of PD-1 protein on cancer cells before choosing way of action may lead to a better therapeutic effect.

3.2. Programmed cell death 1 - ligand 1 (PD-L1) and 2 (PD-L2)

PD-1 receptor has two known naturally occurring ligands: PD-L1 and PD-L2⁶⁰. Structure, expression and functions of both of them are presented in the following chapters.

3.2.1. Structure of the PD-L1

Programmed cell death 1 ligand 1 (CD274, B7-H1, PD-L1) is a type I transmembrane glycoprotein. PD-L1 protein consists of 290 amino acid residues of a molecular weight of 40 kDa. It is composed of a signalling peptide (length: 18 amino acids), extracellular domain (length: 220 amino acid residues) where antiparallel N-terminal IgV and C-terminal IgC2 - type domains typical for B7 family can be identified, transmembrane – helical domain (length: 21 amino acid residues) and cytoplasmic domain (length:

31 amino acid residues) (Figure 12A and 12B)^{36,43,61}. PD-L1 as its receptor forms a monomer on the cell surface, in solution, and in the crystallized form^{61,62}. Extracellular domain of PD-L1 has four potential N-linked glycosylation sites in positions 35, 192, 200 and 219 (triangles in the Figure 12A)^{61,63}.

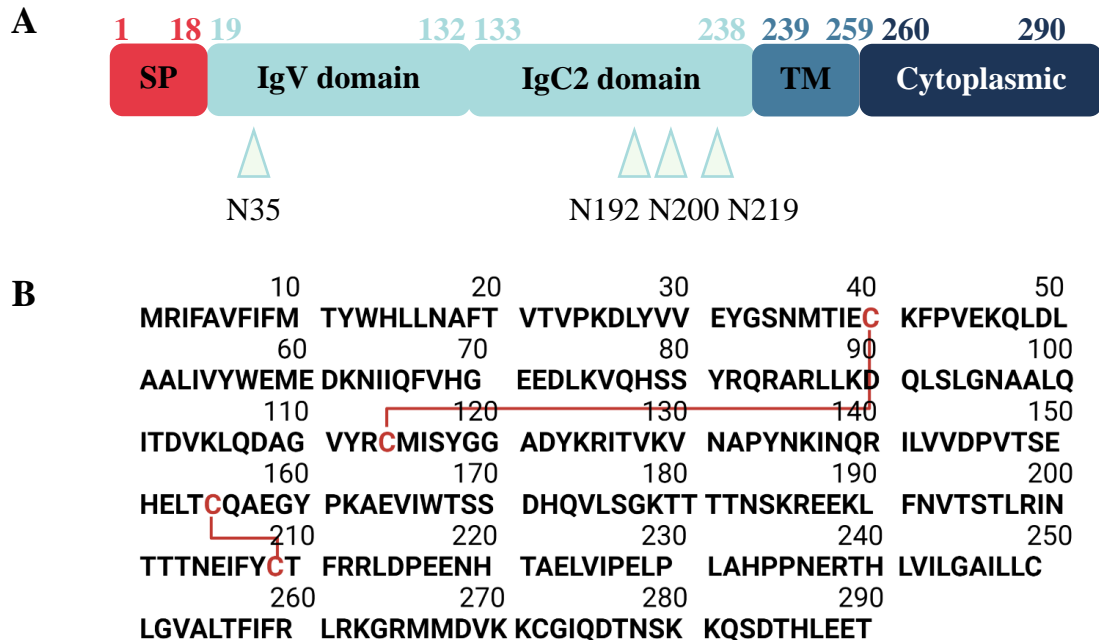


Figure 12. A) Schematic diagram of PD-L1 protein. SP -signalling peptide; TM - transmembrane domain; triangles - potential N-linked glycosylation sites. B) Amino acid residues sequence of PD-L1. The disulphide bridges connecting cysteine residues are marked red.

In PD-L1 β strands in IgV extracellular domain constitute two β sheets containing BED and AGFCC'C'' strands. Short 3_{10} helix domains connect the B-C, C''-D, D-E, E-F strands. The IgV domain covers positions 19-132 in the protein. IgC domain is proximal to the cell surface and consists of two β sheets ABED and CFG, typical for IgC2 domain. The IgC domain is in positions 133-238 (Figure 13). IgV and IgC2 domains in PD-L1 are stabilized by disulphide bonds between C40_L-C114_L, and C155_L-C209_L, respectively (Figure 12, red lines) (in this work, amino acid residues from PD-L1 will be marked with "L")^{61,63}.

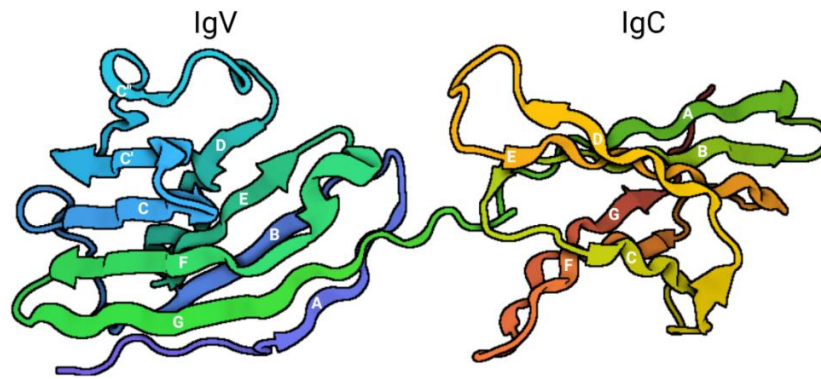


Figure 13. Structure of the extracellular domain of PD-L1 protein (PDB ID: 3BIS)⁶¹.

3.2.2. Structure of the PD-L2

Programmed cell death 1 ligand 2 (CD273, B7-DC, PD-L2) is a type I transmembrane glycoprotein³⁶ consisting of 273 amino acid residues of a molecular weight of 31 kDa. It contains a signalling peptide (length: 19 amino acids), extracellular domain (length: 201 amino acid residues) where N-terminal IgV and C-terminal IgC2 type domains can be identified, transmembrane – helical domain (length: 21 amino acid residues) and cytoplasmic domain (length: 32 amino acid residues) (Figure 14A and B). PD-L2 like PD-L1 forms a monomer on the cell surface. Extracellular domain of PD-L2 has five potential N-linked glycosylation sites in positions 37, 64, 157, 163 and 189 (triangles in the Figure 14A)^{32,36,64}.

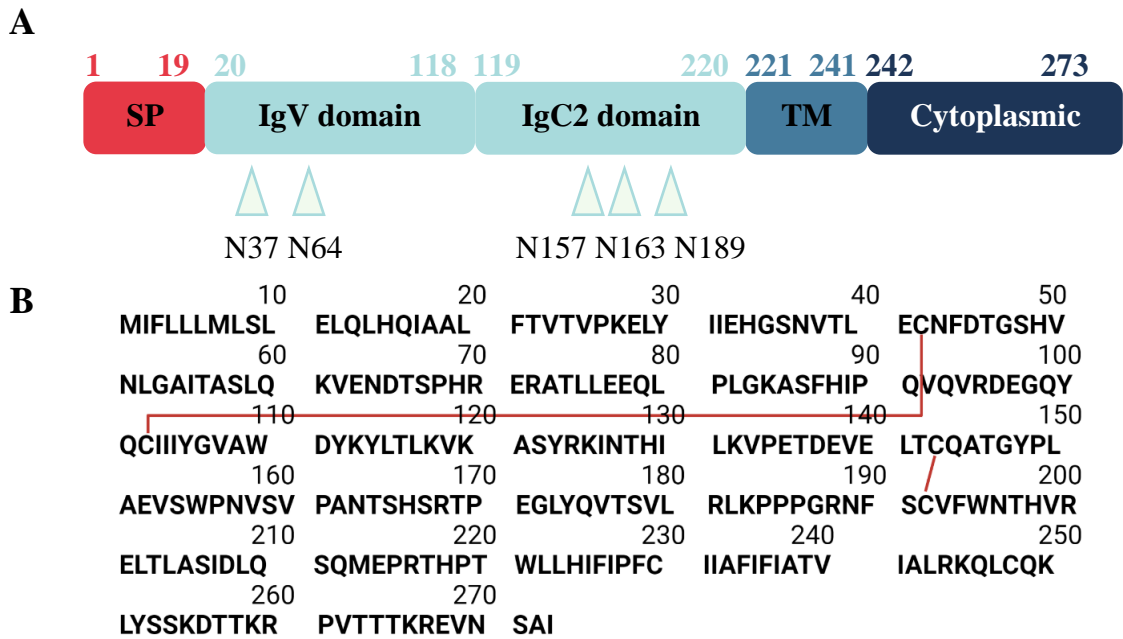


Figure 14. Schematic diagram of PD-L2 protein. SP - signalling peptide; TM - transmembrane domain; triangles - potential N-linked glycosylation sites. B) Amino acid residues sequence of PD-L2. The disulphide bridges connecting cysteine residues are marked red.

The β strands in IgV extracellular domain constitute two β -sheets containing ABED and A'GFCC' strands and it is in position 20-118 in protein. The IgV domain in PD-L2 protein lacks the C'' strand, which is typical for this group (Figure 15). The IgC2 domain is proximal to the cell surface and consists of two β sheets containing ABED and GFC strands, typical for C2 domain. The IgC2 domain is in positions 119-220. IgV and IgC2 domains in PD-L2 are stabilized by disulphide bonds between C42_{L2}-C102_{L2}, and C143_{L2}-C192_{L2}, respectively (in this work, amino acid residues from PD-L2 will be marked with "L2") (Figure 14B, red lines).

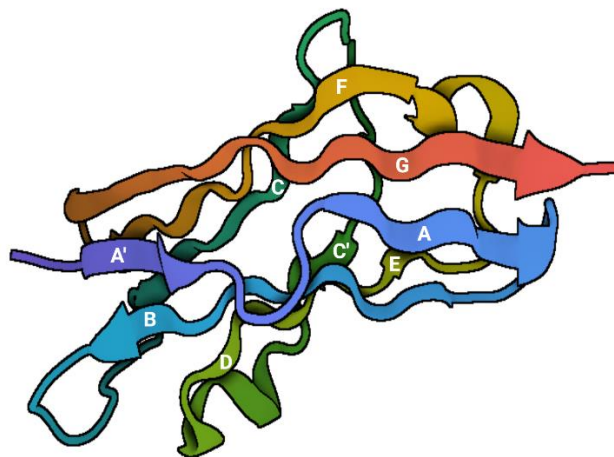


Figure 15. Structure of PD-L2 IgV domain (PDB ID: 6UMT)⁶¹.

3.2.3. Occurrence and function of PD-L1 and PD-L2

PD-L1 is expressed on professional and non-professional APC⁶⁵ and hematopoietic and nonhematopoietic cells⁶⁶. Moreover, PD-L1 protein can overexpressed in different tumour types presented in Figure 16. PD-L1 expression on cancer cells inhibits cytolytic activity of T cells CD8⁺⁶⁷.

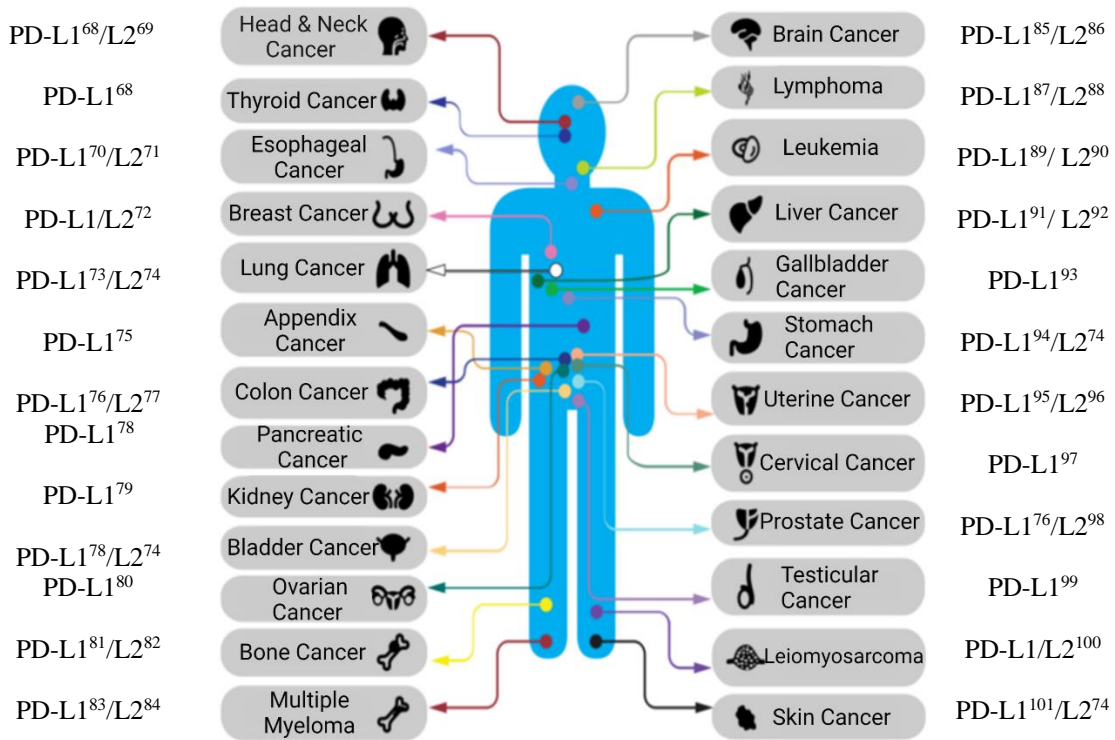


Figure 16. Schematic diagram of PD-L1 and PD-L2 expression on cancer cells.

PD-L1, analogous to PD-1, occur not only in transmembrane form but can be secreted to sera in a soluble form (sPD-L1). Monocytes, macrophages, and DC may secrete the sPD-L1 into sera^{102,103}. Furthermore, soluble form of PD-L1 protein may be detected in the sera of malignant melanoma¹⁰³, renal carcinoma, nasal natural killer/T cell lymphoma (NNKTL)^{104,105}, diffuse large B cell lymphoma (DLBCL)¹⁰⁶, myeloma¹⁰⁷, and hepatocellular carcinoma patients¹⁰⁸. High level of sPD-L1 impacts overall survival and, in some cases, is associated with increased mortality in cancer patients^{102,105,109}. It is reported that tumour-secreted sPD-L1 appearing in sera is a biologically active, receptor-binding domain which is capable to deliver immunosuppressive signals to T cells. Moreover, sPD-Ls can be found in placenta which led to theory that PD-1/sPD-Ls pathways are responsible for feto-maternal tolerance. This theory was confirmed on murine abortion model where murine were treated with anti-PD-L1 antibody (Ab)

which led to increase of the abortion rate from 18% to 86% in the case of anti-PD-L1 Ab supplementation¹¹⁰.

PD-L2 protein expressed in more narrow spectrum than PD-L1, is expressed on activated dendritic cells, macrophages and mast cells^{36,60,111}. Although the PD-L2 has different expression pattern compared to PD-L1, its role is inhibition of immune response through PD-1 pathway⁶⁷. However, it also influences immune response stimulation through binding with repulsive guidance molecule b (RGMB), which is a co-receptor for bone morphogenetic proteins^{112,113}. The PD-L2 protein can overexpressed in different tumours types presented in Figure 16. As in case of PD-L1, PD-L2 expression on cancer cells inhibits cytolytic activity of T cells CD8⁺⁶⁷.

PD-L2, like PD-1 and PD-L1, occur not only in transmembrane form but can be secreted to sera in a soluble form (sPD-L2). Activated leukocytes may secrete the sPD-L2 into sera. Furthermore, soluble form of PD-L2 protein may be detected in the sera of lymphoid malignancies¹¹⁴, epithelial ovarian cancer¹¹⁵ and urothelial bladder cancer¹¹⁶. Interestingly, in some tumours the level of sPD-L2 is reduced compared to healthy controls^{115,117,118}. Moreover, Takeuchi M. et al.¹¹⁹ reported that tumour-secreted sPD-L2 appeared in sera does not have its ability to bind to PD-1. As of now, the role and function of sPD-L2 remains unclear and requires further investigation. Changes in the level of sPD-L2 are observed not only in cancer patients but in diseases like systematic sclerosis, rheumatoid arthritis, systemic lupus erythematosus, viral haemorrhagic fever and COVID-19¹²⁰⁻¹²⁴.

3.3. The crystal structures of the PD-1/PD-L1 and PD-1/PD-L2 complexes

3.3.1. The crystal structure of the PD-1/PD-L1 complex

The first structure of the PD-1/PD-L1 complex based on crystals of the human proteins was obtained by Zak et al. in 2015 (Figure 17)⁶². The receptor and its ligand 1 form a complex in an 1:1 stoichiometry^{42,61,62}. The total surface area of the protein-protein complex interface covers 1.970 Å² and involves the front faces of the β sheets of the IgV domains from both proteins (GFCC' β sheets). Additionally, the rearrangements in

the CC' loop (M70-D77), in the form of a 90° twist, can be observed in the PD-1 protein extracted from the complex and is confirmed by molecular dynamic¹²⁵.

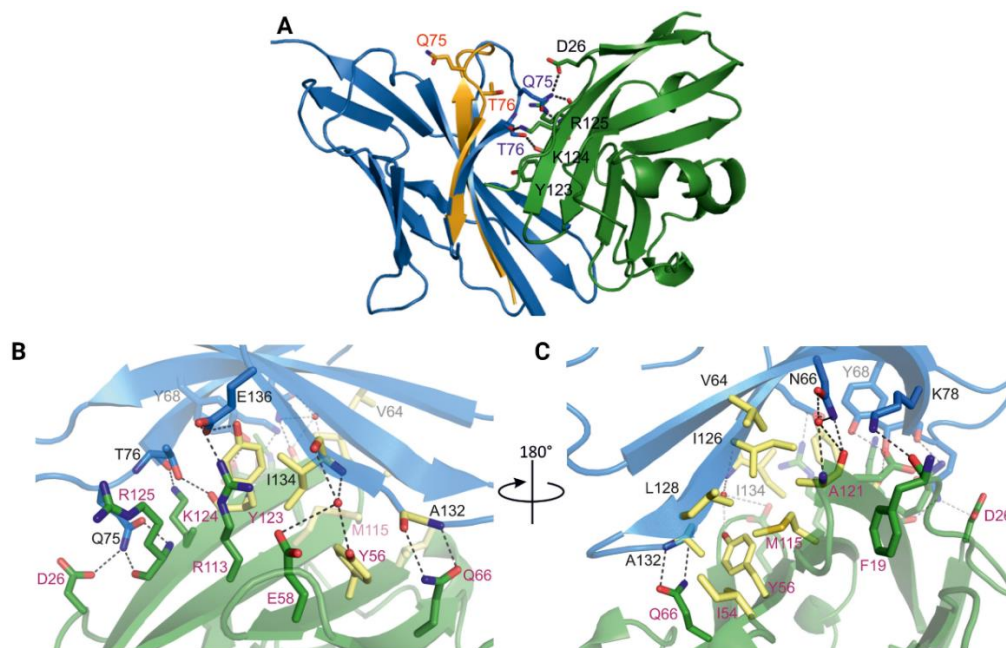


Figure 17. A) The PD-1/PD-L1 complex (PDB ID: 4ZQK) and zoom on the complex interface. B) Front-side of the interface. C) back-side of the interface. PD-1 is coloured blue; PD-L1 – green; the hydrophobic core of the interaction is coloured yellow; sticks - residues taking part in the complex formation; black dashed lines – hydrogen bonds⁶².

Both polar and nonpolar interactions participate in the complex formation. Hydrophobic residues from the PD-1 and PD-L1 β sheets form a core consisting of V64, I126, L128, A132, I134 and I54_L, Y56_L, M115_L, A121_L, Y123_L, respectively (Figure 17 amino acid residues coloured yellow). The hydrophobic core is surrounded by the hydrophilic residues. Moreover, the amino acid residues responsible for forming the receptor-ligand interface and types of interactions are presented in Table 2.

Three main hotspots can be defined in the protein-protein interaction (PPI) interface, two pockets and one groove, formed in the surface of the PD-L1 protein. I134 and I126 are PD-1 amino acids residues and they are accommodated by pockets formed in the structure of PD-L1. Side chains of PD-L1 amino acid residues composing the I134 pocket are as follow Y56_L, E58_L, R113_L, M115_L and Y123_L. The I126 pocket consists of M115_L, A121_L, Y123_L. The third structure is a shallow groove accommodating three PD-1 amino acids residues Y68, Q75 and T76 and is composed by PD-L1 residues: D122_L, Y123_L, K124_L, R125_L and D26_L. This structure is the donor and acceptor of a large number of hydrogen bonds; however, due to the depth of the well structure, it can generate complications for efficient designing of potential inhibitors⁶².

Table 2. Amino acid residues and types of interaction responsible for the PD-1/PD-L1 complex formation⁶².

PD-1	PD-L1	Type of bond/interaction	Groups taking part in interaction
I134	Y123 _L	Alkyl- π	side chains
Y68	Y123 _L	π - π	side chains
E136	R113 _L	salt bridge	side chains
N66	A121 _L	H bond	amid hydrogen from side chain with carbonyl oxygen from main chain
Y68	D122 _L	H bond	hydroxyl hydrogen from side chain with carboxyl oxygen from side chain
Q75	R125 _L	H bond	carbonyl oxygen from side chain with amid hydrogen from main chain
Q75	D26 _L	H bond	amid hydrogen from side chain with carboxyl oxygen from side chain
T76	Y123 _L	H bond	hydroxyl hydrogen from side chain with carbonyl oxygen from main chain
T76	K124 _L	H bond	carbonyl oxygen from main chain with amine hydrogen from side chine
K78	F19 _L	H bond	amine hydrogen from side chine with carbonyl oxygen from main chain
A132	Q66 _L	H bond	amide hydrogen from main chain with carbonyl oxygen from side chain
I134	Y56 _L	H bond/water mediated	amide hydrogen from main chain with hydroxyl hydrogen from side chain
I134	E58 _L	H bond/water mediated	carbonyl oxygen from main chain with carboxyl oxygen from side chain
E136	Y123 _L	H bond	carboxyl oxygen from side chain with hydroxyl hydrogen from side chain

3.3.2. The crystal structure of the PD-1/PD-L2 complex

Until 2019, crystal structure of the human PD-1/PD-L2 complex was not obtained¹²⁶. In recent years, Tang S. and Kim PS.¹²⁶ obtained an X-ray crystal structure of the human PD-1 triple-mutant N74G, T76P and A132V with the IgV domain of the PD-L2 protein. This complex was obtained at a 2.0 Å resolution. The receptor and its ligand 2 form a complex in an 1:1 stoichiometry (Figure 18).

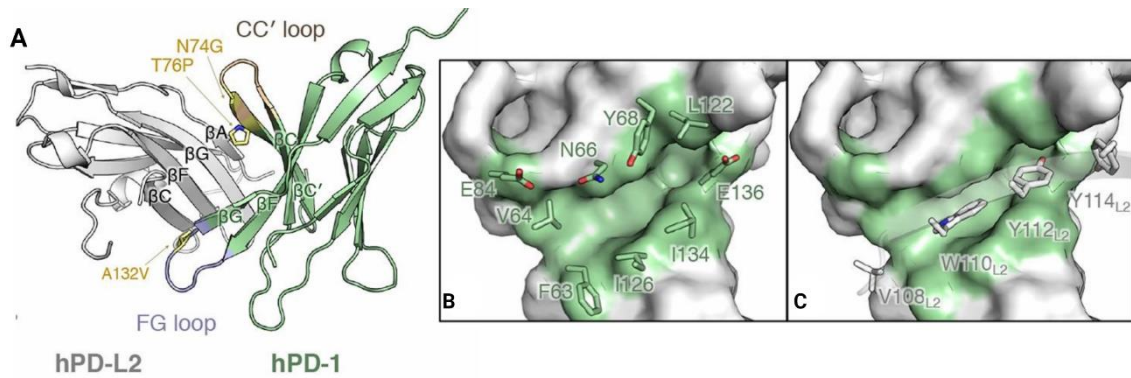


Figure 18. A) The complex of PD-1 triple mutant with its ligand PD-L2 (PDB ID:6UMT). B-C) The Zoom on the PD-1 structure taking part in the complex formation; B) with the PD-1 residues taking part in complex formation, C) with PD-L1 residues taking part in complex formation. PD-1 is coloured pale green, PD-L1 – gray, CC' loop – wheat, FG loop – light blue; Sticks – residues taking part in the complex formation.

The total surface area of the PD-1 mutant and the PD-L2 proteins complex interface covered 1.840 \AA^2 and involved the front faces of the β sheets of the IgV domains from both proteins (GFCC' β sheets). Interaction surface for both PD-1's ligands overlap and cover a similar interface¹²⁶. However, PD-L1 and PD-L2 IgV domains, interacting with its receptor, strongly differ from each other¹²⁷. PD-L2 interaction with PD-1 induces rearrangements in the CC' (M70-D77) and FG (S127-Q133) loops. Moreover, binding of PD-L2 to the PD-1 protein forces changes in C, F, G strands and C'D loop leading to the formation of a deep pocket in the PD-1 protein which accommodates two aromatic residues from the PD-L2 protein, namely, W110_{L2} and Y112_{L2}. The rearrangements cover F63, V64, N66 and Y68 from C strand, L122, G124 and I126 from F strand, I134 and E136 from G stand and E84 from C'D loop. This cavity also occurs in the PD-1 protein triggered by PD-L1 and accommodates only one side of the chain of aromatic Y123_L. The rearrangement induced by ligand 2 is more than twice bigger than the one forced by ligand 1 upon binding to its receptor, covering an area of 170 \AA^3 and 80 \AA^3 , respectively¹²⁶. Those differences in structural rearrangements in the PD-1 protein and the size of the binding pockets could be the reason for the diverse dissociation constant. The value of the dissociation constant (K_D) of the PD-1/PD-L1 complex differs depending on the analytical method and is estimated at 1.15-8.2 μM . Whereas, for PD-1/PD-L2, it is 2.6 μM (Table 3 in chapter 5.1.1.)^{42,128}.

4. The role of the tumour microenvironment in immuno-oncology

Cancer cells and the stroma supporting the cancer cells create a tumour (neoplasm)¹. The tumour is characterised by a unique microenvironment composed of proliferating tumour cells, tumour stroma cells, inflammatory cells, blood vessels and a variation of associated tissue cells necessary for the tumour growth and survival. The tumour environment is comprised of T and B lymphocytes, dendritic cells and occasional macrophages and natural killer cells. The scheme of the tumour microevent is presented in Figure 19¹²⁹. The specificity of the tumour microenvironment is characteristic for different types of cancer, which fully control its molecular and cellular surrounding focusing on evading the host's immune system. Tumour cells change their surface protein profile by expressing immune checkpoint ligands such as PD-L1, PD-L2, CD80 and CD86¹³⁰. Tumours through genetic instability, manifested by changing the surface protein and their mutation, may actively affect the antitumour immune response. Moreover, the patient's survival depends on the tumour's constitution^{1,129}.

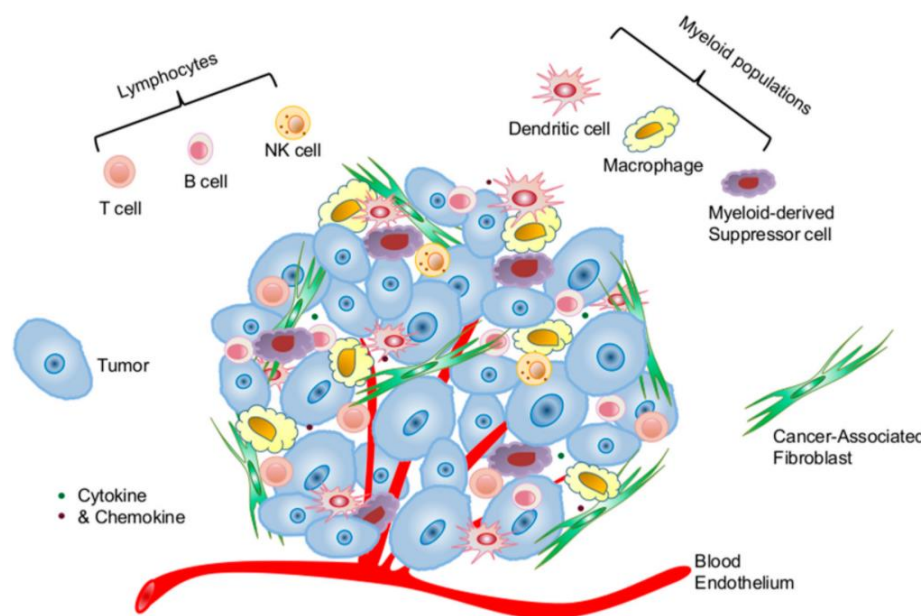


Figure 19. Scheme of tumour microenvironment¹³¹.

In search of a new cancer treatment, attention is drawn to the pairs of receptor-ligand belonging to inhibitory checkpoint proteins. As mentioned earlier, many ligands are expressed on cancer cells and are used as an escape mechanisms from immune surveillance. Blocking the interaction between receptors on T cells (CTLA-4, PD-1, TIM3) and their ligands (CD80/CD86, PD-L1/PD-L2 and GAL-9) on cancer cells

restores the function of the immune system by leading to the activation of T cell proliferation and cytokine production which are actively fighting the cancer cells¹³².

4.1. Therapy based on the immune checkpoint inhibition

Independent research conducted by Thasuku Honjo and James P. Allison during the 1990s focusing on the immune cell proteins led to the development of immunotherapies consisting of blocking immune checkpoint complexes. Moreover, those studies led to winning by them the 2018 Nobel Prize in Physiology and Medicine. Along with the developing knowledge regarding new checkpoint proteins, the number of monoclonal antibodies blocking those complexes has increased. Approval of ipilimumab, mAb anti-CTLA-4, in 2011 by Food and Drug Administration (FDA)¹³³ was a milestone in anticancer immunotherapy based on blocking the immune checkpoint proteins and introduced new criteria for the assessment of clinical responses against new immunotherapeutics¹³⁴. In the following years, mAb anti-CTLA-4 - ipilimumab¹³³, anti-PD-1 - nivolumab¹³⁵ and pembrolizumab¹³⁶, and anti-PD-L1 - atezolizumab¹³⁷ and durvalumab¹³⁸ gained approval from FDA. As already mentioned (in chapter 2.4.), PD-1 and CTLA-4 are receptors located on T cells, they interact with ligands, PD-L1, PD-L2 and CD80, 86 on the APC or cancer cells, respectively, leads to the deactivation of the T cell (Figure 20). Disruption of this axis diminishes the inhibitory signal and activates the T cell response manifesting through their proliferation and cytokine production³⁶.

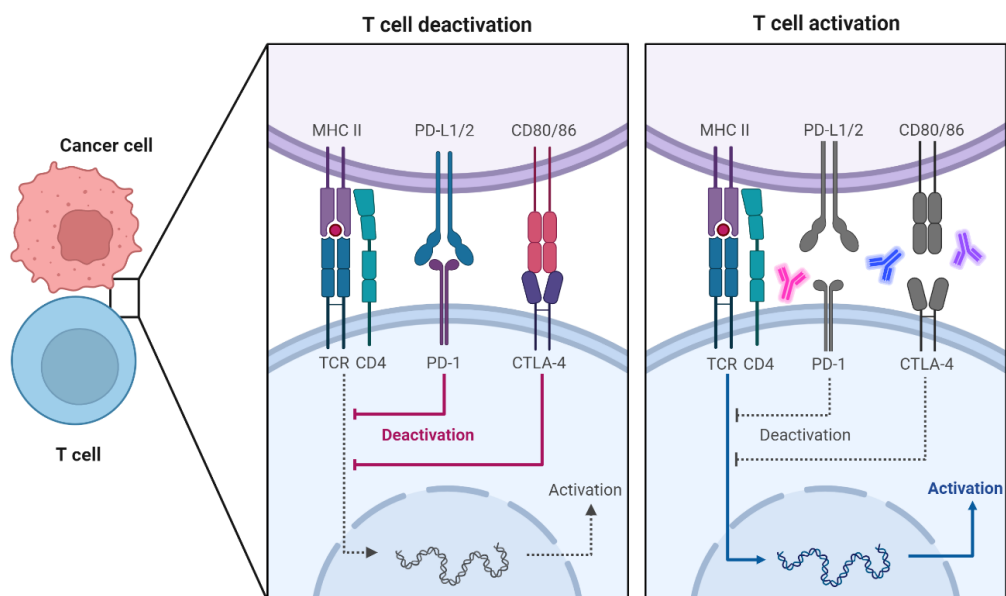


Figure 20. The scheme of activation and deactivation of T cells by the blocking of the immune checkpoint protein¹³⁹. Grey dotted line indicates that the signalling pathway is deactivated.

4.2. The complexity in the PD-1/PD-L1 complex inhibition

The main function of the PD-1/PD-L1 complex is the inhibition of T cell activation. However, the relation between those proteins is more complex (Figure 21). PD-1 may interact with PD-L1 in a *cis* and *trans* geometry, depending on the localisation of those two proteins¹⁴⁰. If they express on the surface of different cells (i.e. T cell and APC or cancer cells), they interact in a *trans* geometry (Figure 21A) and if they are localised on the same cell, they bind in *cis* (Figure 21B). In the second arrangement, if those proteins are localised on the APC or cancer cell, PD-L1 lose the ability to inhibit T cells, what is a positive aspect in cancer treatment. Although, when the anti-PD-1 treatment will be introduced, it may release *cis* bonded PD-L1 and enable the creation of *trans* PD-1/PD-L1 complex (Figure 21B)¹⁴⁰.

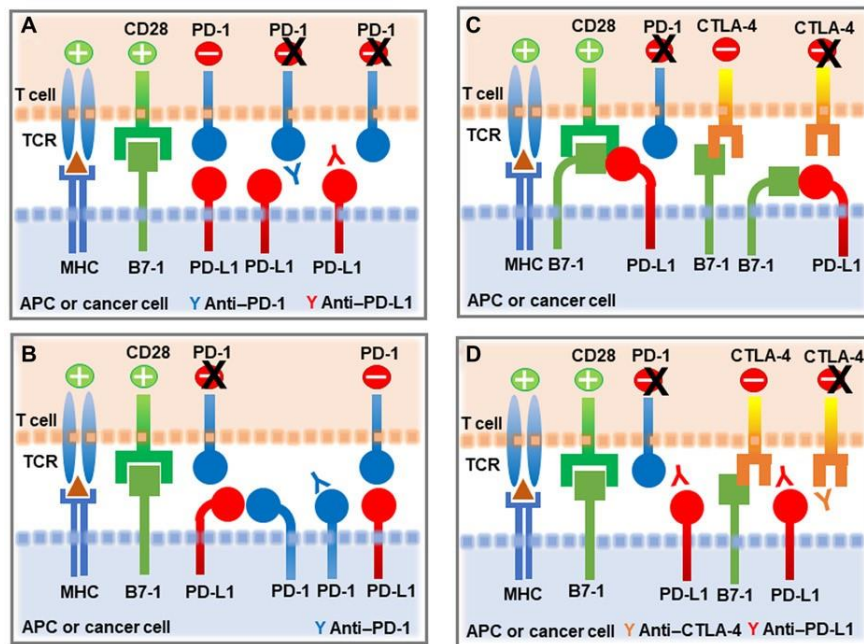


Figure 21. Scheme of PD-1 and PD-L1 interactions¹⁴¹.

Moreover, PD-L1 may interact with B7.1 (CD80) in a *cis* geometry¹⁴², what interrupts the PD-1/PD-L1 complex in *trans* - leading to a PD-1 mediated stimulation of T cells (Figure 21C)¹⁴³. To make the situation even more complex, B7.1 interacts with CD28 (what stimulates T cells) and CTLA-4 (what inhibits T cell stimulation). PD-L1/B7.1 interaction does not disrupt the CD28/B7.1 complex but influences B7.1 binding to CTLA-4¹⁴⁴. When we introduce an anti-PD-L1 therapy, not only the PD-1/PD-L1 complex can be disrupted but also PD-L1/B7.1 what leads to the disengagement of B7.1 which can bind CTLA-4 and activate the inhibitory pathway signalling (Figure 21D)¹⁴⁴.

In such a complicated arrangements, introducing the immune checkpoint anticancer therapy has to be truly planned and combining therapies of a few blocking agents may bring benefits to cancer patients.

5. Inhibitors of the PD-1/PD-L1 complex

In 2011, the first agent blocking immune checkpoint proteins complex was approved by FDA to treat metastatic melanoma¹³³. Since then many research groups and pharmaceutical companies have focused on finding immunomodulators of the immune checkpoint complexes. Extensive attention was placed on the PD-1 protein and its ligands, mostly PD-L1. Apart from the aforementioned (in chapter 4.1.) monoclonal antibodies approved by FDA, there are many ongoing studies focusing on finding new monoclonal antibodies and small molecules targeting the PD-1/PD-L1 axis. Many of those compounds are at the starting phase of the research but many of them have already reached clinical trials. Only last year there were more than two thousand ongoing clinical trials with single-agent or combinatory approaches consisting in inhibiting the PD-1/PD-L1 complex^{145,146}.

5.1. Monoclonal antibodies targeting the PD-1/PD-L1 complex

In the last decade, several studies regarding monoclonal antibodies anti-PD-1 or anti-PD-L1 were published. Each year their number and the amount of information regarding their affinity, effectiveness and side effect increase. Each year new structures of monoclonal antibodies with the PD-1 or PD-L1 protein complexes are published.

5.1.1. Anti-PD-1 monoclonal antibodies

In recent years, FDA approved four mAb anti-PD-1 – pembrolizumab, nivolumab, cemiplimab and tislelizumab for treatment of several types of cancer. The structure of the complex of PD-1 with pembrolizumab, nivolumab and tislelizumab has already been disclosed while information regarding the structure of PD-1/cemiplimab is still missing¹⁴⁷⁻¹⁵⁰. Four X-ray structures of PD-1/pembrolizumab were reported (Table 3). Those structures provide vital information on the interface of the PD-1/mAb complexes. Pembrolizumab is one of the first mAb approved by FDA, its binding site involves PD-1 amino acids residues taking part in the PD-L1 recognition. The

PD-1/pembrolizumab interaction covers 26 of PD-1's amino acids and may be divided into two sites. Residues from flexible C'D loop create site I of the interaction and amino acids from C, C' and F strands create site II. The complex involves hydrophobic interactions, direct and water mediated H-bonds and two salt bridges. Only site II covers the surface involved in the PD-L1 recognition and site I is mostly responsible for affinity of PD-1 to antibody¹⁴⁷⁻¹⁵⁰. Interaction surface between nivolumab and PD-1 has also been determined using X-ray crystallography. Two crystallographic structures of the PD-1/nivolumab complex were obtained (Table 3). The PD-1 interaction surface with nivolumab is smaller than the one with pembrolizumab and involves N-terminal loop of PD-1, which is located outside the IgV domain and is not involved in the PD-L1 binding^{38,151}. Despite diverse epitopes, nivolumab and pembrolizumab manifest similar inhibition mechanism involving flexible loops of PD-1, outside the binding site of PD-L1, covering only a minor part of the PD-1/PD-L1 interaction surface. Those antibodies induce structural rearrangements in N-terminal, BC, C'D and FG loops of PD-1, stabilizing the PD-1/mAb complexes.

Table 3. The affinity between PD-1 with its natural ligands and their antibodies approved by FDA as a therapeutic agent.

	Complex	PDB ID	Affinity (K _D)	Year of approval by FDA
	PD-1/PD-L1	4ZQK ⁶²	1.15-8.2 μM ^{42,128}	-
	PD-1/PD-L2	-	2.06 μM ^{32,42}	-
	PD-1 ^{N74G,T76P,A132V} /PD-L2	6UMT ¹²⁶	2.6 nM ¹²⁶	-
Anti-PD-1 mAb	PD-1/nivolumab	5GGR/ 5GGQ ¹⁵¹ 5WT9 ³⁸	1.45 nM ³⁸	2014
	PD-1/pembrolizumab	5JXE ¹⁴⁷ 5GGS ¹⁴⁸ 5B8C ¹⁴⁹ 5DK3 ¹⁵⁰	27 pM ¹⁴⁷	2014
	PD-1/tislelizumab	7BXA ¹⁵² 7CGW ¹⁵³	114 pM ¹⁵³	2021
	PD-1/cemiplimab ¹⁵⁴	ND	ND	2018
Anti-PD-L1 mAb	PD-L1/atezolizumab	5X8L ¹⁴⁸	400 pM ¹⁵⁵	2016
	PD-L1/avelumab	5GRJ ¹⁵⁶	42 pM ¹⁵⁶	2017
	PD-L1/durvalumab	5X8M ¹⁴⁸ 5XJ4 ^{38,157}	667 pM ¹⁵⁷	2017

The crystallographic structures of the complex of PD-1 with tislelizumab was published recently by Lee et al.¹⁵² and Hong et al.¹⁵³. The obtained structures show that epitope recognised by this mAb is similar to the binding site of PD-L1 and covers the front β-sheet of PD-1. On the contrary to the interaction surface of pembrolizumab and

nivolumab with PD-1, tislelizumab does not involve the flexible loops while binding to PD-1. Additionally, it does not lead to structural changes of the target molecule. The affinity between PD-1/nivolumab, pembrolizumab and tislelizumab is three to five orders of magnitude bigger than in the case of the PD-1/PD-L1 complex and it is 1.45 nM, 0.027 nM and 0.114 nM, respectively, while the value of dissociation constant of PD-1/PD-L1 is about 1.15-8.2 μM ^{38,42,147,153}.

5.1.2. Anti-PD-L1 monoclonal antibodies

Recently, three mAb anti-PD-L1, atezolizumab, avelumab and durvalumab, were approved by FDA and yielded promising results in clinical trials. The crystal structure of all the PD-L1/mAb complexes was solved and deposited in the PDB database (Table 3). The structural studies revealed the PD-L1 interface for the mentioned antibodies. The binding site of atezolizumab covers BC, CC', C'C'' and FG loops of PD-L1. The region binding durvalumab focuses on N-terminal of PD-L1 and CC' loop, additionally, this loop is the binding site for avelumab. Although these mAbs interact with PD-L1 through partially different binding sites, they all create interactions with five amino acid residues from the front β sheet of PD-L1, namely Y56_L, E58_L, R113_L, M115_L and Y123_L which are crucial for creating the complex with PD-1^{148,151,156,157}. As in the case of anti-PD-1 antibodies, the binding affinity of the PD-1/PD-L1 complex is weaker than the binding affinity of PD-L1/mAb and is reported to be 400, 42 and 667 pM, respectively, for atezolizumab, avelumab and durvalumab and the buried surface area of complexes with PD-L1 is 2106, 1865, 1624 \AA^2 ^{156,157}.

5.1.3. Results of the monoclonal antibodies therapy in the immune checkpoint inhibition

Immune checkpoint inhibitors (ICIs) such as mAbs showed promising results in a growing spectrum of cancer types including NSCLC and melanoma, where only monotherapy brings encouraging effects with an objective response rate of 40-50% and 50%-60% for combinatory therapy including at least two immunotherapeutics (anti-CTLA-4 and anti-PD-1)^{158,159}. Moreover, the median progression-free survival for patients with untreated melanoma in nivolumab and ipilimumab treatment was 14 months¹⁶⁰. Thanks to the positive effects in clinical trials and the expanding number

of FDA approved monoclonal antibodies, they are taking an increasingly significant place among cancer drugs. The predictions for the I-O market size is estimated at USD 35 billion by 2023 whereof the cost of annually therapy per patient consisting of a single agent (monoclonal antibody) blocking the PD-1/PD-L1 complex can reach more than USD 100,000 and the cost of combination therapies bringing better effects is even less available for a wider circle of cancer patients^{161,162}. Not only the cost of monoclonal antibodies is a disadvantage of this kind of immunotherapy. During treatments with mAb, there were observed immune related adverse events (irAEs) and even cases of death were reported¹⁶³. The combination therapies more often led to high-grade irAEs. Specifically, the combination of nivolumab with ipilimumab led to high-grade irAEs in 59% of patients with advanced melanoma, while nivolumab and ipilimumab monotherapy caused irAEs in 23% and 28% of patients, respectively¹⁶⁴. The most frequently side effects occurring during immunotherapy consisting of immune checkpoint inhibition can include headache, pneumonitis, diarrhoea, fatigue, rashes and itchiness, kidney infections, problems with some hormone levels, decreased appetite, fever and chills^{163,165}. The most common irAEs are presented in Figure 22. It is worth mentioning that the latest research shows that the anti-PD-1 treatment can lead to the onset of type I diabetes¹⁶⁶. This information provides a basis for the assumption that anti-PD-1 therapy can unfortunately lead to the onset of other autoimmune diseases connected with the PD-1/PD-L1 regulation functions.

It is worth mentioning that anti-PD-1 mAbs inhibit interaction between PD-1 and its both ligands PD-L1 and PD-L2, while FDA approved anti-PD-L1 antibodies are inhibitors targeting only the PD-1/PD-L1 complex not interfering in the PD-1/PD-L2 axis. Anticancer therapies with selective agents targeting only the PD-1/PD-L1 complex can prevent additional irAEs associated with blocking of the PD-1/PD-L2 complex^{112,167}.

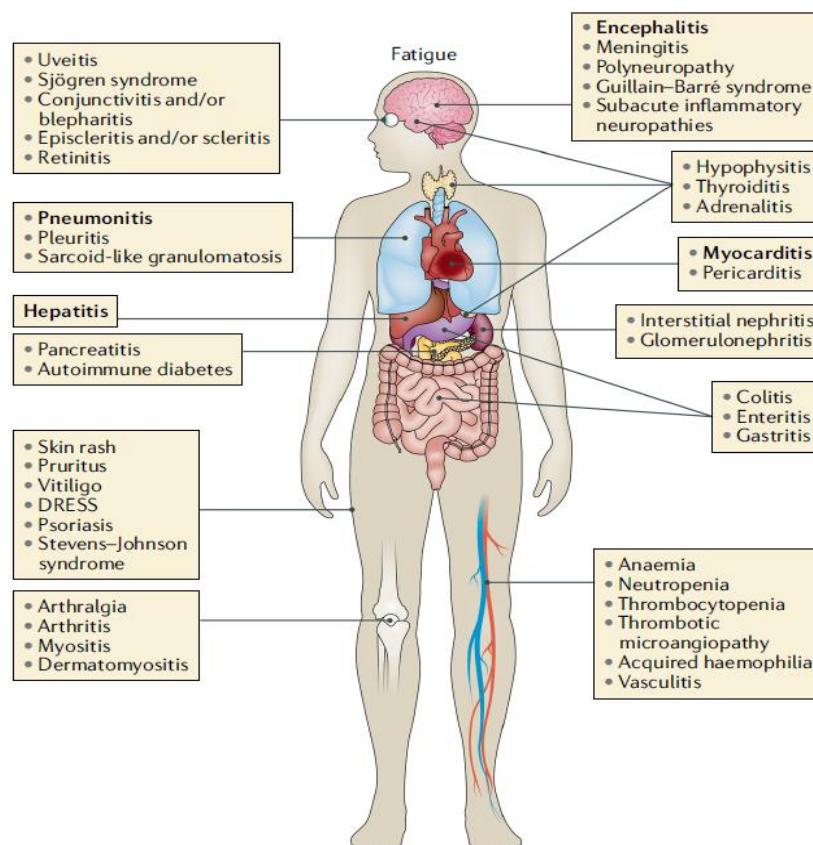


Figure 22. The most common irAEs caused by ICI therapy¹⁶⁸.

5.2. Peptides and peptidomimetics as inhibitors of the PD-1/PD-L1 complex formation

The usage of therapeutic peptides which are gaining a greater value on the drug market each year could be an alternative for the monoclonal antibodies. It is estimated that peptide therapeutics market is going to reach USD 50.60 Billion by 2026 ¹⁶⁹. Peptides as therapeutics have many advantages including high selectivity for the target molecule, good biocompatibility with human organism and through their smaller size, they demonstrate a better tumour penetration in comparison to monoclonal antibodies. Peptides exhibit low accumulation in tissues, their metabolic pathways are well known and their degradation products are only amino acids. However, peptides are characterised by poor metabolic stability, bioavailability and sometimes poor solubility which may reduce their therapeutic potential. Peptides are often the starting point for designing peptidomimetics, which show greater stability against proteolytic enzymes, better affinity and selectivity for the target molecule. Peptidomimetics contain structural and biological features of peptides and are characterised by easy modularity increasing

their structural diversity and flexibility leading to better adaptability to the molecule surface and recognition of binding pockets in the target proteins. Moreover, another advantage of peptides and peptidomimetics is the developed, standardised, optimised and relatively easy to modify synthesis protocol with lower costs of production compared to monoclonal antibodies^{170–173}. The aforementioned compounds, compared with antibodies, are more rapidly removed from plasma and consequently exhibit a shorter pharmacokinetic (PK) profile. Comparison of the PK profile of antibodies and small molecules is presented in Figure 23.

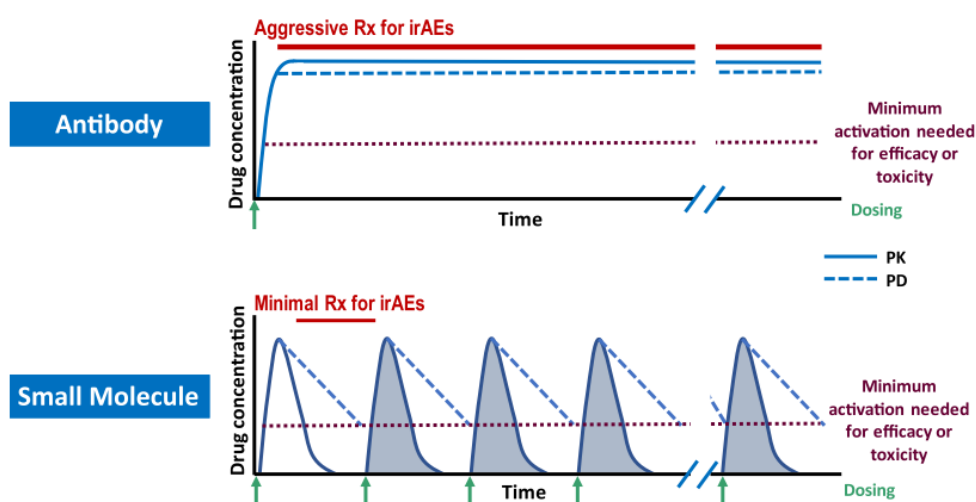


Figure 23. Comparison of the PK profile of antibodies and small molecules. PD – pharmacodynamic; Rx - prescription^{174,175}.

The half-life of antibodies is estimated at 15-20 days, whereas peptides are degraded within several hours. As a result, the administration timelines differ between those two classes of compounds what offer flexibility in dosing (Figure 23, green arrows). Small molecules require more frequent administration to achieve the minimum concentration required for efficacy than antibodies, therefore, they only periodically achieve the concentration in which the non-specific activation of the immune system can occur leading to irAEs, while the concentration of antibodies is high and constant, during their whole lifetime, causing unwanted side effects mentioned earlier (chapter 5.1.3).¹⁷⁴. Regardless of the chosen therapeutic, whether it is therapy based on monoclonal antibodies or peptides to decrease irAEs and other side effects, there is need to find proper biomarkers which indicate the selection of a proper therapy depending on the tumour microenvironment¹⁷⁶.

5.2.1. Peptides and peptidomimetics inhibiting the PD-1/PD-L1 interactions

In response to the growing knowledge regarding the PD-1/PD-L1 complex interface and the interaction mechanism between proteins and mAb anti-PD-1 and anti-PD-L1, the number of alternative inhibitors to mAb has increased. In last years, linear¹⁷⁷, branched¹⁷⁸ and macrocyclic peptides¹⁷⁹, peptidomimetics¹⁸⁰, D-peptides¹⁸¹ and small molecules¹⁸² were designed and tested. Many approaches were used to design the peptides e.g. rational designing based on hot-spots and the structure of the PD-1/PD-L1 complex¹⁸³, phage display¹⁸¹ and computational methods¹²⁸. Chosen published and patented peptides are presented in Tables 4 and 5, and described here and in the discussion.

In 2014 the Laboratoires Pierre Fabre and Aurigene have announced a collaboration on developing compound AUNP-12 as a PD-1/PD-L1 complex inhibitor in immunoncology¹⁷⁸. AUNP-12 was previously patented in 2011 as one of immunosuppression modulating compounds and compounds from the BC loop of human PD-1 (Table 4, no. 1)^{179,184}. AUNP-12 is a branched peptide consisting of three fragments of the PD-1 protein: part I - amino acid residues S57NTSGSF63 from BC loop, connected via lysine residues with part II - amino acid residues F95RVTQL100 from D strand and part III - amino acid residues A129PKAQIKE136 from FG loop. This 29-mer peptide reduced the tumour growth in the model of mouse melanoma by 44%. Additionally, it inhibited the cell growth in breast, kidney and metastatic lung cancers without significant toxicity at the same time at any of the tested doses^{178,185}. AUNP-12 is one of the most active PD-1/PD-L1 complex inhibitor patented by Aurigene exhibiting a half maximal effective concentration (EC₅₀) value of 0.41 nM and 0.72 nM in rat PBMC proliferation assay on cells lines expressing human PD-L1 and PD-L2, respectively^{178,185}. However, despite of the potency of AUNP-12, the latest research conducted by Musielak et al. determined, based on the outcome of the nuclear magnetic resonance (NMR) binding assay, homogeneous time resolved fluorescence (HTRF) assay and PD-1/PD-L1 inhibition bioassay, that this peptide does not bind to PD-L1 nor to PD-1 and does not interfere in the complex between them¹⁸⁶. This subject requires further investigation to define the mode of action and the binding target of this molecule.

In 2015 Chang et al.¹⁸¹ designed a series of linear peptides consisting of D-amino acids using a mirror-image phage display method (Table 4, no. 8-13). D-amino acids increased the stability of peptides in comparison to peptides consisting of L-amino acids. In surface plasmon resonance (SPR) experiment, PPA-1 (Table 4, no. 8) peptide exhibited the strongest affinity to PD-L1 from the whole series of D-peptides, reaching K_D value of 0.51 μ M. Additionally, in tests with tumour-bearing mice models, PPA-1 peptide inhibits CT26 tumour cells growth¹⁸¹.

Throughout the years, many linear peptides were designed, worth noting are the rationally designed peptides being fragments of the PD-1 or PD-L1 protein. Peptide PL120_L-131_L was designed based on the PD-L1 protein and consists of the amino acid residues from G120 to N131 (Table 5, no. 18). It interacts with the PD-1 binding groove mimicking its natural ligand. In the tests, this 12-mer linear peptide reversed the apoptotic signal in murine primary lymphocytes and Jurkat cells induced by sPD-L1¹⁷⁷. In the same tests, the inhibition properties of peptide PD64-78 for blocking the PD-1/PD-L1 complex were investigated (Table 5, no. 19)¹⁷⁷. Peptide PD64-78 is a fragment of the PD-1 protein, containing amino acid residues from M64 to K78. In comparison to peptide PL120_L-131_L (fragment of PD-L1), peptide PD64-78 did not inhibit the PD-1/PD-L1 interaction in the PD-1/PD-L1 blockade bioassay¹⁷⁷. However, hexapeptide – P1, reported by Wang et al.¹⁸⁷ consisting of amino acids from the PD-1 protein sequence, from S73 to K78 (Table 4, no. 2) increased drug-induced apoptosis in PD-L1 expressing pancreatic cancer cells¹⁸⁷. Almost all reported linear peptides have a lower affinity to their targets than PD-L1 to its receptor (Table 4 and 5); however, a biological effect caused by those peptides has been observed. Peptide TPP-1 (Table 4, no. 14), targeting PD-L1, has the highest reported affinity among the linear peptides, inhibitors of the PD-1/PD-L1 complex, with K_D value of 95 nM. This molecule can reactivate T cells by blocking the PD-1/PD-L1 complex leading to a decrease of tumour growth in mice model by 56% compared with control¹⁸⁸.

Table 4. The peptides and peptidomimetics described in the literature potentially interacting with the PD-L1 protein. D-amino acids are marked with a lowercase letter. NB - no binding; ND - no data; JD - no name given by the authors.

No.	Peptide name	Amino acid sequence	Affinity (K _D) [μM]	Method of peptide designing	The year of publication
1	AUNP-12 ^{184,189,190} (compound 8)	SNTSESF-NH ₂ SNTSESFKFRVTQLAPKAQI KE-NH ₂	-	Rational design basing on PD-1 protein amino acid sequence	2014
2	P1 ¹⁸⁷ PD-1(73-78)	SNQTDK	-	Rational design basing on PD-1 protein amino acid sequence	2012
3	P2 ¹⁸⁷ - control	ADTKRI	-	Rational design basing on PD-1 protein amino acid sequence	2012
4	L8 ¹⁹¹	SLPSTTTMRLTS	-	ND	2014
5	JD ¹⁹²	ANGSRLV	-	ND	2014
6	S10 ¹⁹³	WSHGGHQHFIRE	-	ND	2014
7	p101 ¹⁹⁴⁻¹⁹⁶	FFIVIRDRVFRGS _{cc}	-	ND	2014
8	PPA-1 ¹⁸¹	nkskptdrqyhf	0.51	Phage display/mirror	2015
9	PPA-2 ¹⁸¹	khahhthnlrlp	1.13	-image phage display	
10	PPA-3 ¹⁸¹	aakmgdhlhggq	NB		
11	PPA-4 ¹⁸¹	mnrerypkpyy	22		
12	PPA-5 ¹⁸¹	tlyqrpstnler	NB		
13	PPA-1 - scramble ¹⁸¹	rhtndysqfyfk	NB		
14	TPP-1 ¹⁸⁸	SGQYASYHCWCWRDPGRS GGSK	0.095	Random bacterial surface display method	2018
15	IMB-P6-10 ¹⁹⁷	LTCSLAPNIISAL	-	In silico proteolysis of hPRDX5/rational design	2019
16	IO103 ¹⁹⁸ PD-L1(9-27)	FMTYWHLNNAFTVTVPKDL		Rational design basing on PD-L1 protein amino acid sequence	2019
17	IO101 ¹⁹⁸ PD-L1(15-23)	LLNNAFTVTV		Rational design basing on PD-L1 protein amino acid sequence	2019
18	PD-L1Pep-1 ¹⁹⁹	CLQKTPKQC	0.373	Phage display	2020
19	PD-L1Pep-2 ¹⁹⁹	CVRARTR	0.281	Phage display	2020
20	HS1 ¹⁸³ PD-1(121-137)	YCGAISLAPKAQIKES	-	Rational design basing on PD-1 protein amino acid sequence	2021
21	HS2 ¹⁸³	CGAISLAPKAQIKES	-	Rational design basing on PD-1 protein amino acid sequence	2021
22	HS3 ¹⁸³	CGAISLAPKLQIKES	-	Rational design basing on PD-1 protein amino acid sequence	2021
23	HS4 ¹⁸³	GAISLAPKLQINE	-	Rational design basing on PD-1 protein amino acid sequence	2021
24	HS5 ¹⁸³	GAISLAPKLQINe	-	Rational design basing on PD-1 protein amino acid sequence	2021
25	HS6 ¹⁸³	H ₂ N-GAISLAPKLQINEG-CO (C,N-terminal lactam peptide)	-	Rational design basing on PD-1 protein amino acid sequence	2021
26	HS7 ¹⁸³	GAISLAPKLQIND	-	Rational design basing on PD-1 protein amino acid sequence	2021
27	OPBP-1 ²⁰⁰	GQSEHHMRVYSF	0.667	Liquide-phase phage display	2021

Table 5. The peptides and peptidomimetics described in the literature potentially interacting with the PD-1 protein. D-amino acids are marked with a lowercase letter. NB – no binding; ND - no data; JD - no name given by the authors.

No.	Peptide name	Amino acid sequence	Affinity (K _D) [μM]	Method of peptide designing	The year of publication
1	Ar5Y_1 ¹²⁸	FNWDYSWKSERLKEAYD L	3.39	Computational methods	2016
2	Ar5Y_2 ¹²⁸	FNWDYSLEELREKAKYK	3.14		
3	Ar5Y_3 ¹²⁸	TEKDYRHGNIRMKLAYDL	3.13		
4	Ar5Y_4 ¹²⁸	GNWDYNSQRAQLYNQ	1.38		
5	Ar5Y_4 W3A ¹²⁸	GNADYNSQRAQLYNQ	8.08		
6	Ar5Y_4 D4A ¹²⁸	GNWAYNSQRAQLYNQ	18.94		
7	Ar5Y_4 Y5A ¹²⁸	GNWDANSQRAQLYNQ	20.15		
8	Ar5Y_4 R9A ¹²⁸	GNWDYNSQAAQLYNQ	21.20		
9	Ar5Y_4 Y13A ¹²⁸	GNWDYNSQRAQLANQ	10.23		
10	Ar3_ref ¹²⁸	ADYK	370.4		
11	Ar3_1 ¹²⁸	WDYD	22.3		
12	Ar4_1 ¹²⁸	GIDYEERWK	28.28		
13	Ar4_2 ¹²⁸	LDYDGRLSQ	83.90		
14	Ar5M_1 ¹²⁸	LDYGDKREGQMAE	21.60		
15	Ar5M_2 ¹²⁸	LDYVNRKMYQ	3.32		
16	PDLong1 (PD-L1 9-28) ²⁰¹	FMTYWHELLNAFTVTVPKD L	-	Rational design basing on PD-L1 protein amino acid sequence	2016
17	PDLong2 (PD-L1 242-264) ²⁰¹	VILGAILLCLGVALTFIFRL RKG	-		
18	PL120 _L -131 _L ¹⁷⁷	GADYKRITVKVN	ND	Rational design basing on PD-L1 protein amino acid sequence	2018
19	PD64-78 ¹⁷⁷	VLNWYRMSPSNQTDK	ND	Rational design basing on PD-1 protein amino acid sequence	
20	WANG-003 ²⁰²	KRWWR	3.3	Computational methods	2019
21	WANG-004 ²⁰²	FRWWR	1.6		
22	WANG-005 ²⁰²	RRWQWR	5.1		
23	WANG-006 ²⁰²	YVAM	NB		
24	WANG-007 ²⁰²	YVAE	NB		
25	YT-16 PDL1(112-127) C114-C125 ²⁰³	YRCMISYGGADYKCIT (C- C)	0.0178	Rational design basing on PD-L1 protein amino acid sequence/ Computational methods	2019
26	PDL1(112-127) C114-C125; Y118- P ²⁰³	YRCMISPGGADYKCIT	-		
27	PDL1(112-127) C114-C125; D122- E ²⁰³	YRCMISYGGAEYKCIT	-		
28	PDL1(112-127) C114-C125; Y118-P, D122-E ²⁰³	YRCMISPGGAEYKCIT	-		
29	PDL1(112-127) C114-C125; S117- T ²⁰³	YRCMITYGGGDYKCIT	-		
30	PDL1(112-127) C114-C125; S117-T;	YRCMITPGGGDYKCIT	-		

	Y118-P ²⁰³				
31	PDL1(112-127) C114- C125;S117T;D122- E ²⁰³	YRCMITYGGGEYKCIT	-		
32	PDL1(112-127) C114-C125; S117-T; Y118-P; D122-E ²⁰³	YRCMITPGGGEYKCIT			
33	DS-I ²⁰⁴ 54-68	IVYWEMEDKNIIQFV	-	Rational design basing on PD-L1 protein amino acid sequence/ Computational methods	2019
34	DS-II ²⁰⁴ 110-132	GVYRCMISYGGADYKRIT VKVNA	109		
35	DS-II [C111-C127] ²⁰⁴ 110-132	GCYRCMISYGGADYKRIC VKVNA	28		
36	ΔDS-II [C111-C127] ²⁰⁴ 111-127	CYRCMISYGGADYKRIC	17.5		
37	ΔDS-II [C110-C128] ²⁰⁴ 110-128	CVYRCMISYGGADYKRIT C	11.6		
38	CLP001 ²⁰⁵	HYPFRPHANQAS	0.534	Phage display	2019
39	CLP002 ²⁰⁵	WHRSYYTWNLNT	0.366		
40	CLP003 ²⁰⁵	WHFSYNWRWLPP	0.117		
41	CLP004 ²⁰⁵	DYHDPSLPTLRK	0.544		
42	P1.1 ²⁰⁶ PD-L1(113-126)	RCMICYGGADYKRI	3.66	Rational design basing on PD-L1 protein amino acid sequence	2020
43	P1.2 ²⁰⁶	RCMISYpGADYKRI	83.05		
44	P1.3 ²⁰⁶	RTMIWYpGAWYKRI	1.80		
45	P1.4 ²⁰⁶	RTCITYpGADYCRI	474		
46	P2.1 ²⁰⁶	RTMIWYpPAWYKRI	29.20		
47	P2.2 ²⁰⁶	RTMIWYAAAWYKRI	55.20		
48	P2.3 ²⁰⁶	RTMIWYGpAWYKRI	129.00		
49	Q1 PD-L1(110-129)	GVYRCMISYGGADYKRIT VKV	-	Rational design basing on PD-L1 protein amino acid sequence/ Computational methods	2020
50	Pep1 ²⁰⁷	LETWFGKEILVKT	140.0		
51	Pep2 ²⁰⁷	VFELRHSKRKDSRTVY	127.0		
52	Pep3 ²⁰⁷	TSEVDNGVGKPKQKHS	81.1		
53	Pep4 ²⁰⁷	TFKVEDRYGQQQILD	22.7		
54	Pep6 ²⁰⁷	KSKAVNRVSQSEM	66.4		
55	Pep9 ²⁰⁷	LEYWSSGSTMVYGL	36.4		
56	Pep10 ²⁰⁷	LERHDFGDGRARYEE	39.0		
57	Pep14 ²⁰⁷	QYRCNGTSSKGSQAIIITL RV	10.9		
58	PD-i1 ²⁰⁸	[TnTDYnPtLI]	-	computation methods	2020
59	PD-i2 ²⁰⁸	[vpTSYSpDDv]	-		
60	PD-i3 ²⁰⁸	[TMYLerRYpD]	102		
61	PD-i4 ²⁰⁸	[LddRYpnLPM]	-		
62	PD-i5 ²⁰⁸	[DDqSWNiPfs]	-		
63	PD-i6 ²⁰⁸	[WwVpEakD]	30		
64	PD-i7 ²⁰⁸	[NsDYTyPF]	-		
65	IMB-P6-10 ¹⁹⁷	LTCSLAPNIISAL	-	hPRDX5-based peptide	2020
66	WQ-20 ²⁰⁹	-	305	Phage display	2020
67	QP-20 ²⁰⁹	-	10.7		
68	HD-20 ²⁰⁹	-	3.41		
69	SQ-20 ²⁰⁹	-	5.16		

70	C8 ²¹⁰	[CKWYRPSEC]	0.64	Phage display	2020
71	nABP284 ²¹¹	SRLKEIANSPTQFWRMVA RNTLGNGAKQSLNIEHAR L	11.8	Phage display/ computation methods	2021
72	nABPD1 ²¹¹	SHHHRLSRLKEIANSPTQF WRMVARNTLGNGAKQSL NIEHARL	0.0119		
73	JD1 ²¹²	RRWWRR	4.01	Peptide library	2021
74	JD2 ²¹²	RRQFW	4.38		

Molecules which can be potent agents blocking the PD-1/PD-L1 pathway may be also cyclic and macrocyclic peptidomimetics. Examples of these compounds are presented in the patents released by two companies Aurigene¹⁷⁹ and Bistol-Myers Squibb²¹³. Two macrocycles from the BMS patent, BMS-57 and BMS-71, were thoroughly tested by Magiera-Mularz et al.¹⁸⁰. They confirmed that those peptides interact with PD-L1 performing differential scanning fluorimetry (DSF), NMR-titration, and that they efficiently inhibit the interaction between PD-1 and PD-L1 by restoring the activity of NFAT response element (NFAT-RE) signalling in the PD-1/PD-L1 inhibition bioassay showing EC₅₀ at the level of 293 nM and 566 nM for BMS-57 and BMS-71, respectively. Moreover, the X-ray structures of both peptidomimetics with PD-L1 (BMS-57 PDB ID: 5O4Y, BMS-71 PDB ID: 5O45) were solved and interfaces of their interactions were described in details. The PD-L1 binding site interacting with peptides BMS-57 and BMS-71 partially overlaps the hotspots of PD-1. The analysis of the interface shows the importance of hydrophobic interactions in potential inhibitors designing¹⁸⁰. The aforementioned peptides were investigate further by Miao et al.²¹⁴, who designed and tested cycled-analogues, with peptide JMPDP-027 as a most potent of them. It shows dose-dependent restoring activity of T cells in the PD-1/PD-L1 inhibition bioassay showing EC₅₀ at the level of 5.9 nM²¹⁴.

Different approaches of blocking the PD-1/PD-L1 interaction can be found in the widely discussed reviews. Large fraction of the potential PD-1/PD-L1 inhibitors is composed from small-molecules²¹⁵⁻²²²; however, they will not be discussed in this dissertation as my work focused on the peptides.

6. Selected techniques of the PD-1/PD-L1 potential inhibitors evaluation

In the last decade, the development of the PD-1/PD-L1 complex inhibitors flourished and the knowledge regarding biological functions of PD-1 and PD-L1 expands each year^{215–222}. From the compound to a drug, there is a long way to “walk”. At the beginning of this journey, it is important to choose a proper way to screen potential inhibitors. The workflow of protein-protein interaction inhibitor development differs depending on the chosen approach and it is a cycle starting from drug designing, going through synthesis, binding to the target and biological effect evaluation and coming back to drug structure improving evaluation. A simplified diagram of PPI potential inhibitor development is presented in Figure 24^{223,224}. In the next chapter, I bring closer the selected methods used during my research.

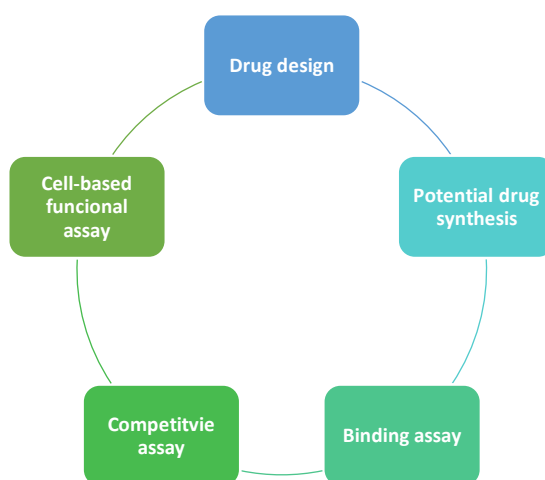


Figure 24. Simplified scheme of the early phase of drug development.

6.1. SPR technique

The SPR is an optical technique that allows for label-free, real time analysis and characterisation of the biomolecular interactions. In the SPR technique, the polarised light hits the electrically conducting surface (gold) at the biosensor between the buffers. This event generates plasmons, which lead to the reduction of intensity of the reflected light and is called a resonance angle (θ). The resonance angle is proportional to the mass of analyte bound to the biosensor (Figure 25) and is expressed in resonance units (RU) describing the final concentration of the bound ligand²²⁵. In general, when the injected

analyte binds to the ligand immobilized on the sensor surface, the change in the resonance angle occurs and is registered by the detector.

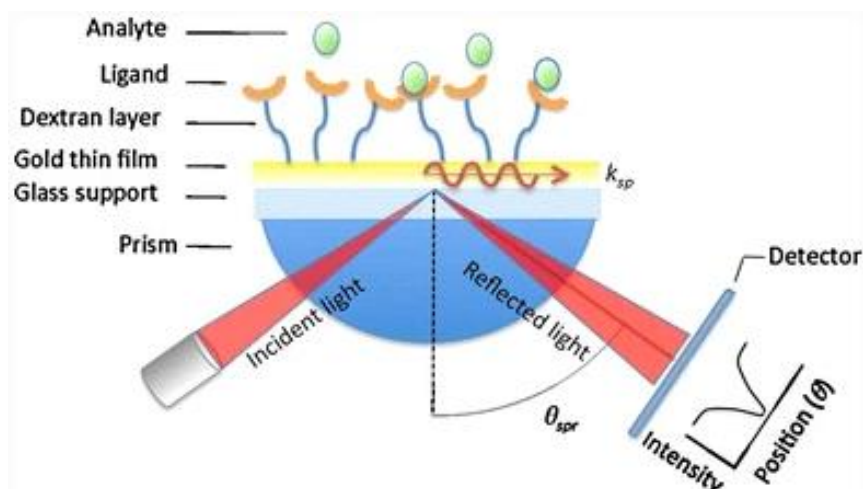


Figure 25. Detection basis in the SPR technique²²⁶.

In the SPR analysis, sensor chips consisting of a gold layer covering the glass surface are usually used (Figure 26 A). Moreover, the gold surface is covered by a monolayer of covalently bonded alkanethiol molecules forming the surface matrix for further modifications. Depending on the properties and the nature of the tested molecule immobilized on the sensor surface, it may be attached by three main approaches:

- Covalent – sensors with carboxyl or carboxymethyl groups (Sensor Chips CM3, CM5, CM6) (Figure 26C);
- High affinity – pre-coated with molecules exhibiting a high affinity for the tagged ligands or antibodies e.g. biotin → streptavidin sensors (SA) (Figure 26B), poly His tag → nickel coated sensors (NTA) or fragment crystallizable region (Fc region) of IgG Ab → Protein a sensor (Protein A);
- Hydrophobic adsorption - pre-coated with a hydrophobic surface – attachment of liposomes and lipid bilayers (HPA, L1)²²⁷.

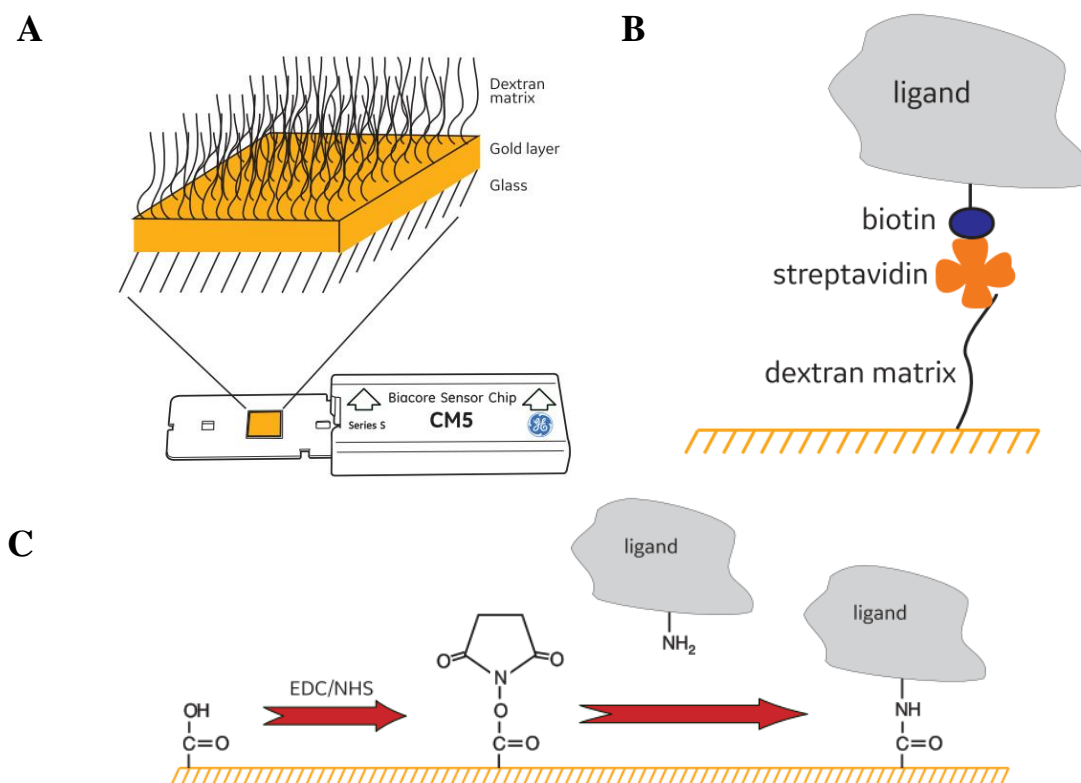


Figure 26. A) Scheme of the sensor chip surface on the CM- type. B) Configuration of molecules binding to the SA sensor chip. C) Chemistry of amine coupling of ligand to the CM-type sensor chip²²⁷.

In my doctoral research, I used CM5 and SA sensor chips presented in Figures 26B and C to evaluate binding properties of the designed peptides to the target molecule.

The data obtained during the SPR analysis are presented in the form of sensorgrams (Figure 27). The SPR technique can be used to obtain the data regarding the binding kinetics (rates of association and dissociation constants, k_a and k_d , respectively) and dissociation constant (K_D) of two species of molecules. Moreover, it can be utilised to estimate the concentration of the examined molecule and the amount of the active molecules in the sample.

K_D is ratio of the dissociation rate constant and the association rate constant (k_d/k_a), between a ligand and receptor. The k_a defines how quickly the molecule binds to the target and the k_d defines how quickly the molecule dissociates from the target. The k_a rate is concentration dependent (unit $M^{-1}s^{-1}$); however, the k_d is concentration independent (s^{-1}). The affinity and K_D are related. The high affinity is characterised by the low value of K_D - quick recognition of the target by the molecule (high k_a) and high stability of the complex between the molecule and the target (low k_d). The affinity is

defined as “attractiveness” of two molecules to each other manifested by the creation of non-covalent interactions. The bigger affinity is the quicker and longer interaction²²⁸.

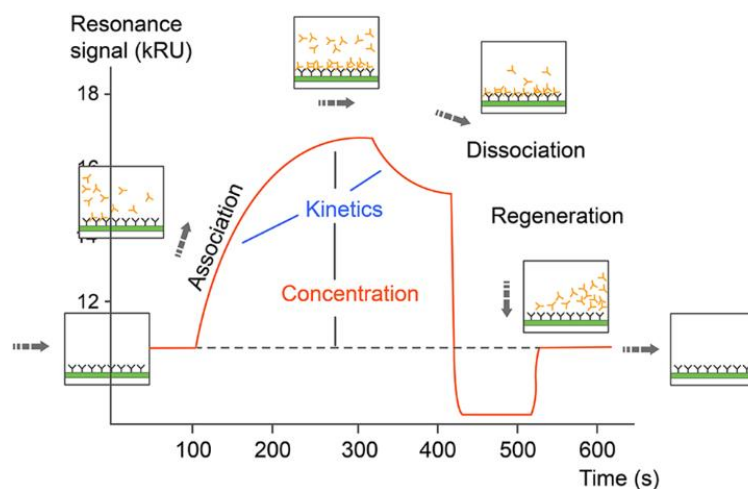


Figure 27. Scheme of the SPR sensorgrams data²²⁹.

6.2. Enzyme-linked immunosorbent assay - ELISA

ELISA is an immunological technique used for the detection and quantitative analysis of antigens, antibodies and proteins²³⁰. Initially, the ELISA was used in life sciences and the analysis of toxins contained in food, however, due to its numerous advantages, it quickly became the basic test in drug development, clinical and diagnostic laboratories^{230,231}.

ELISA may be distinguished into four main varieties: direct, indirect, sandwich and competitive ELISA (Figure 28). The test is frequently performed on 96- or 384-well polystyrene or polypropylene plates. The choice of the plate depends on the requirements of the tested molecules. The plates surface may be modified by the nickel ions Ni^{2+} or streptavidin which selectively binds His-tag and biotin, respectively. In direct ELISA, plates are primary coated with molecules which bind to the plate. After each step of the assay, unbound particles are washed away with wash buffer. Free, unbound sites of the plate are blocked with blocking agents to prevent non-selective binding of proteins to the plate in subsequent steps of the assay. This step is not required in the case of selectively binding molecules. Bovine albumin, skim milk, fish gelatine as well as commercially available buffers are used as blocking buffers. In the next step, the enzyme labelled antibody which detects the molecule bound to the plate is added. After incubation, unbound conjugates are washed off and a chromogenic substrate

recognising the enzyme on the antibody is added to the system and catalyse the coloured enzyme-substrate reaction which is measured by the use of spectrophotometer^{231,232}. In my doctoral research, I performed indirect ELISA which differs from the direct one only by one step - the detected protein is not conjugated with the enzyme and the enzyme labelled antibody has to be added to the plate in an additional step. Apart from the direct and indirect ELISA, we may distinguish sandwich ELISA which contains one more step compared with the indirect one. In sandwich ELISA, the plate is coated with a specific antibody, subsequently the sample is added which in the next step is detected by capture antibody. In the last step, the captured antibody is recognised by the enzyme labelled antibody which reacts with the chromogenic substrate. In competitive ELISA, two ligands – labelled and without a label, compete for binding with the target molecule bound to the plate^{231,232}.

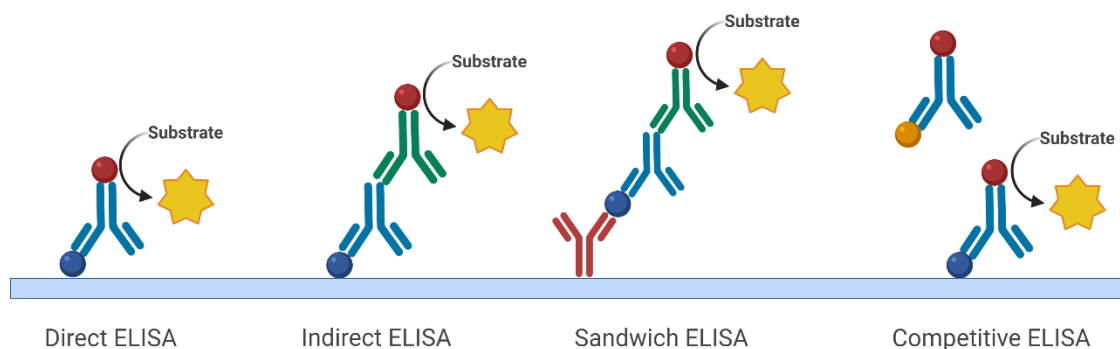


Figure 28. Scheme of the four different ELISA approaches.

Enzymes most commonly used in ELISA are:

- horseradish peroxidase (HRP) - changes to a blue colour in the presence of tetramethylbenzidine (TMB) as a substrate;
- glucose oxidase - changes to a brown colour in the presence of 5-aminosalicylic acid as a substrate;
- alkaline phosphatase - changes to a yellow colour in the presence of p-nitrophenol phosphate^{231,232}.

6.3. Flow cytometry

Flow cytometry is a technique that enables a multi-parametric analysis of a single cell or particles in fluids. It involves the fluorescence conjugated Abs (R-Phycoerythrin - PE, Allophycocyanin - APC), fluorescent dyes (e.g., propidium

iodide), or expression of fluorescence proteins (e.g. green fluorescence protein, GFP). This technique enables immunophenotyping involving one fluorochrome or multi-colour panels for a complex analysis of several parameters. Flow cytometry analyses cell after cell as they flow through the single or multiple lasers (Figure 29A). The measurements are determined by light beam scattering, which is measured in two directions (Figure 29B). One is measured along the path of the laser and is described by forward-scattered light (FCS) which indicates size or area of the cell. The visible light scattering at 90° direction is described by the side-scattered light (SSC) which is mostly reflected and refracted light which enable identification of granularity. Light scattering is fluorescence independent. Corelation of SSC and FCS allows in some degree for cell differentiation from the heterogeneous population (Figure 29C)^{233,234}.

Basic components used in flow cytometry are fluorescent molecules which have defined excitation and emission spectrums. These molecules are excited by the use of laser and then emitted light goes through the optical filters which direct it to the appropriate detector, depending on the wavelength. More developed equipment has multiple laser systems. At the end in the electronic system, the detected light beam is transformed to a voltage pulse. Each signal coming from one cell is transformed and visualised into one- and two-dimensional plots^{233,234}.

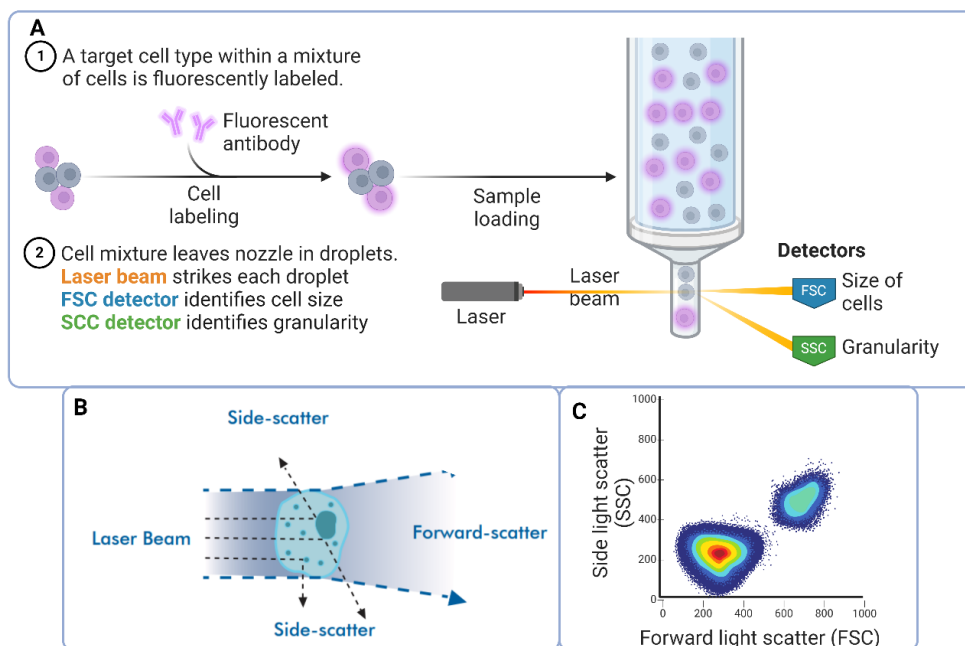


Figure 29. A) Scheme of flow cytometry. B) FSC and SSC light measuring directions. C) Two parameters histogram – dot plot enabling separation of different cell populations by the SSC and FSC²³⁵.

Flow cytometry has many application in different fields. In immunology, it is often used for immunophenotyping, measuring antigen specific responses, proliferation, apoptosis and intracellular cytokine analysis. In molecular biology, it may be applied for analysis of cell cycle or signal transduction. Moreover, it may be used in cancer biology, disease monitoring and diagnostic^{233,234}. In my research, I adapted the flow cytometry to evaluate the potential of the designed peptides for competing for binding to the target molecule with a native partner. Moreover, I used this technique to assess the ability of the designed peptides to inhibit the PD-1/PD-L1 complex formation in the functional cellular assay based on the PD-1 expressing NF- κ B::eGFP reporter cell line. Both experiments will be discussed more widely in the chapter focusing on the results.

II. Aim of the PhD thesis

Immune checkpoints are responsible for the modulation of the immune response by the regulation of the T lymphocyte activity. One of the best known and most characterized inhibitory immune checkpoint is PD-1 with its ligand PD-L1. Targeting the PD-1/PD-L1 axis can have many potential clinical applications. PD-1 and PD-L1 antagonists can be applied in the cases of cancer and infectious diseases. Nowadays, in the clinical practice, there are many approaches to blocking the proteins complex formation bringing patients new hopes and possibilities. FDA approved a series of cancer therapies focusing on immune checkpoints, mostly based on mAbs. Unfortunately, mAbs have many side effects and are not always effective. Moreover, the cost of an annual therapy per patient consisting of a single agent blocking the PD-1/PD-L1 complex can exceed USD 100,000. The cost of combination therapies is even less available for a wider range of cancer patients. Therefore, it is important to work on a more affordable drug therapy blocking the PD-1/PD-L1 axis. **The main aim of my research is to find the peptide inhibitors of PD-1/PD-L1 complex formation, able to restore functions of the immune system.** In my research, I focused on designing, synthesizing, and investigating the interaction of two peptide groups of inhibitors with the cellular target of which is the PD-1 or PD-L1 protein.

III. Results

To fulfil the aim of my research, I decided to apply the molecular mechanics generalized Born surface area (MM/GBSA) analysis calculated for the PD-1/PD-L1 complex. This analysis allows me to broaden the knowledge regarding the protein complex and to better understand the interactions between the PD-1 and PD-L1 proteins. In the next step, basing on the crystal structure of the PD-1/PD-L1 complex and results from MM/GBSA, I designed peptides targeting PD-L1 and PD-1. Next, I synthesised and purified the designed peptides. I studied their interaction with a target molecule using the SPR technique or ELISA, which enabled me to select the leading peptides for further research. For the chosen peptides, I run cell-based competition assays to select peptides competing with the ligand for binding with the target. Moreover, I performed an inhibitory bioassay to check if they block the PD1/PD-L1 complex formation. Before *in vitro* studies, I checked peptides stability in the medium used in the cell assays and investigated the cell lines viability in experimental conditions.

1. MM/GBSA analysis of PD-1/PD-L1 complex

The first step of my research was increasing the knowledge regarding the interaction between PD-1 and PD-L1. For this purpose, MM/GBSA calculations for the PD-1/PD-L1 complex (PDB ID: 4ZQK) were performed. MM/GBSA is a widely used method for binding free energy prediction in molecular studies and for *in silico* characterisation of receptor/ligand interactions²³⁶. All the all-atom molecular dynamics (MD) simulations of the proteins complex were performed by MSc Małgorzata Kogut from the Department of Theoretical Chemistry (Faculty of Chemistry, University of Gdańsk). My contribution to this part of the research was the final interpretation of the received data.

At the beginning, the per-residue energy decomposition was designated to study the total contribution of each amino acid residue of PD-1 and PD-L1 proteins in the formation of the complex (Figure 30). Furthermore, the pairwise per-residue energy decomposition and the fraction of contacts between PD-1 and PD-L1 were analysed (Table 6). The per-residue energy decomposition calculates the input of the energy of

a single residue by summing its interactions over all residues in the system (complex). While the pairwise per-residue describes the input of specific residue pairs in the system²³⁷.

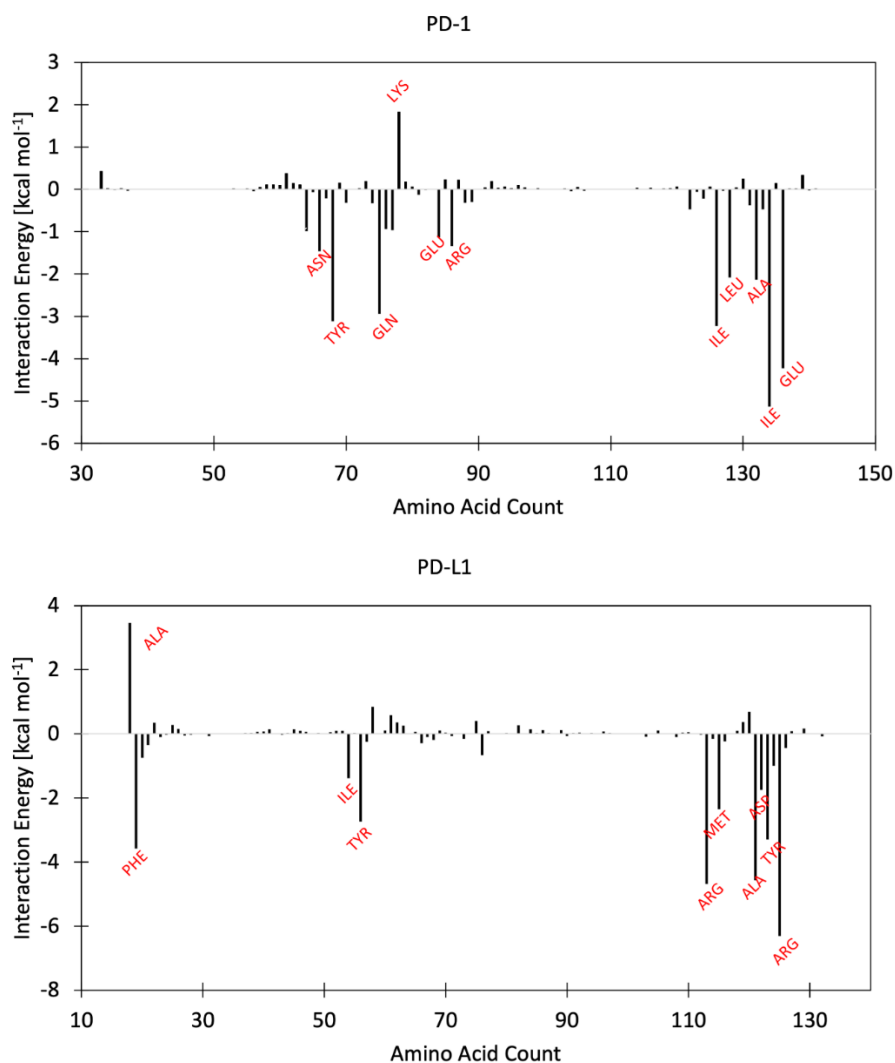


Figure 30. The per-residue energy decomposition analysis calculated for the PD-1 (top) and PD-L1 (bottom) amino acid residues. The cut down for “strong” interaction energy - the ΔG value - has to be at least -1 kcal/mol or lower²³⁸.

The per-residue energy decomposition calculation has enabled the recognition of three fragments of PD-L1 and two fragments of PD-1 robustly involved in the complex formation. For PD-1, the important fragments are as follow: N66-R86 and I126-E136, and for PD-L1: A18_L-F19_L, I54_L-Y56_L and R113_L-R125_L.

Table 6. The pairwise per-residue energy decomposition between PD-1 and PD-L1 calculated using the MM-GBSA analysis method. The cut down for “strong” interaction energy - the ΔG value - has to be at least -3 kcal/mol or lower²³⁸.

Interaction energy [kcal/mol]	PD-1		PD-L1	
	Residue name	Residue number	Residue name	Residue number
-11.303	GLU	136	ARG	113
-9.797	GLU	84	ALA	18
-7.319	GLU	136	ARG	125
-6.381	ASP	77	LYS	124
-5.768	GLN	75	ARG	125
-5.572	LYS	78	PHE	19
-5.245	LYS	78	ASP	122
-5.200	TYR	68	ASP	122
-3.996	LYS	78	ALA	121
-3.904	ARG	86	ALA	18
-3.642	GLU	136	TYR	123
-3.090	GLN	75	ASP	26
-2.652	THR	76	LYS	124
-2.609	ASN	74	ARG	125
-2.600	ILE	134	TYR	123
-2.396	THR	76	ARG	125
-2.185	ALA	132	TYR	56
-2.107	TYR	68	TYR	123
-2.057	ASP	85	ALA	18
-1.954	ALA	132	GLN	66
-1.864	ASN	66	ASP	122
-1.860	ASN	66	ALA	121
-1.844	ILE	134	ARG	113

The architecture of the complex interface with the essential amino acid residues obtained from the MM/GBSA calculations is presented in Figure 31. The essential amino acids residues (red, purple, blue, and black areas) are located close to each other, forming a complex interface including R113_L, A18_L, R125_L, K124_L, F19_L, D122_L from PD-L1 and E136, E84, D77 and Q75 from the PD-1 protein. Comparison of these analyses allowed me to identify the crucial amino acid residues for the PD-1/PD-L1 complex formation, which are marked in bold in Table 7.

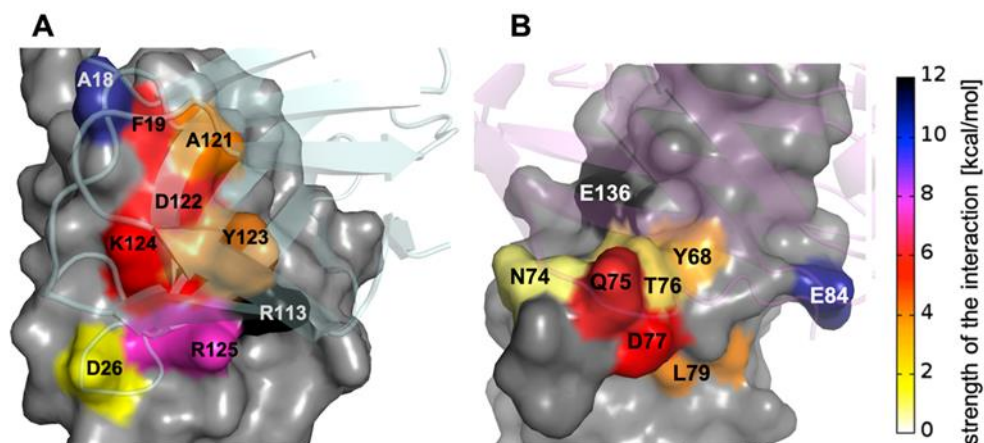


Figure 31. Visualization of the input of the most important amino acid residues from PD-L1 and PD-1 in the complex formation obtained from the pairwise per-residue energy decomposition method. In A), the grey surface area represents the structure of PD-L1 and the semi-transparent cartoon represents the PD-1 structure. In B), the grey surface area represents structure of PD-1 and the semi-transparent cartoon represents the PD-L1 structure. The amino acid residues with the biggest energy input for the complex formation are coloured black, with the lowest energy input coloured yellow, according to the energy scale on the right side of the figure²³⁸.

Table 7. Crucial amino acid residues received from the MM/GBSA energy decomposition analysis. The one with the strongest input in the complex formation in both decomposition methods are marked in bold. The cut down for “strong” interaction energy for per-residue calculation was set on -1 kcal/mol or lower and -3 kcal/mol for pairwise per-residue²³⁸.

	PD-L1 crucial amino acid residues for the PD-L1/PD-1 complex formation	PD-1 crucial amino acid residues for the PD-L1/PD-1 complex formation
Per-residue	F19_L , Y56 _L , R113_L , M115 _L , A121 _L , Y123_L , R125_L	N66, Y68 , Q75 , I126, L128, A132, I134, E136
Pairwise per-residue	A18 _L , F19_L , D26 _L , R113_L , A121 _L , D122 _L , Y123_L , K124 _L , R125_L	Y68 , Q75 , D77, K78, E84, R86, E136

2. Peptides targeting the PD-L1 protein

2.1. Designing and synthesis of peptides derived from the PD-1 protein

Basing on the MM/GBSA calculations and crystal structure of the PD-1/PD-L1 complex, I designed peptides derived from the PD-1 protein structure, potentially targeting PD-L1 and inhibiting the receptor/ligand interactions. As previously discussed, the PD-1 extracellular domain occurs in a β -sandwich form consisting of two β -sheets. The front one is composed of G'GFCC' strands and the back β -sheet includes AA'BED strands (Figure 32). The amino acid residues from the front part of the

receptor with the ones from the FG and CC' loops are responsible for the interactions with the PD-L1 protein.

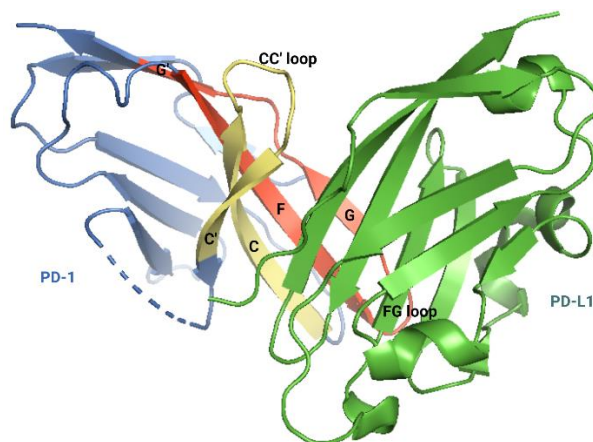


Figure 32. The structure of PD-1/PD-L1 complex (PDB ID: 4ZQK). The fragments of PD-1 protein which were used to construct two groups of peptides are marked: yellow - peptides from Group I and red – peptides from Group II. PD-1 is coloured blue, PD-L1 – green.

Taking this into consideration, I designed two groups of peptides (Table 8). Peptides from **1** to **4** (Group I) were constructed based on the fragments of CC' strands (Table 8) and the peptides from **5** to **13** (Group II) were assembled with amino acids residues from FGG' strands and FG loop (Table 8). Moreover, to enhance the affinity of the designed peptides to the target, I decided to introduce the intramolecular disulphide bonds into the eight peptides. Therefore, I exchanged selected amino acids, located opposite each other in the 3D structure of the PD-1 protein, for the cysteine residues. The introduction of such a modification should enable the β -hairpin formation as a short linear peptide probably will not adopt the β -hairpin conformation which in protein is stabilized by many interactions like hydrogen bonds or Van der Waals interactions. As it was reported elsewhere, the β -hairpin structure might be essential for the interaction with β -sheet-rich proteins such as PD-L1^{206,239,204}.

During the designing of peptides, not only the crystal structure of the PD-1/PD-L1 complex was considered but also MM/GBSA calculations performed in this work. That is why peptides PD-1(68-78) (**1**) and PD-1(62-80) (**2**) contain Y68, Q75, and T76 residues, crucial for the complex formation. Moreover, the sequence of (**1**) peptide includes D77 and peptide (**2**) N66, D77, and L79 ones. Group I was additionally expanded by the two peptides with an intramolecular disulphide bond, specifically PD-1(62-80)^(W67C-L79C) (**3**) and PD-1(62-80)^(R69C-D77C) (**4**). Group II can be divided into two parts. First part contains long peptides being disulphide bonded variations of the

linear peptide PD-1(119-142) (**5**) and containing I126, L128, A132, I134, and E136 – all essential amino acids residues for the complex formation from this part of the protein. This group includes PD-1(119-142)^(T120C-E141C) (**6**), PD-1(119-142)^(C123-S137C) (**7**), and PD-1(119-142)^(A125C-K135C) (**8**). The second part of Group II contains shorter analogues - peptides from (**9**) to (**12**) (Table 8). This group of peptides was designed as their longer analogues were poorly (**7**) and not soluble (**8**) in aqueous solutions. The analogue of peptide (**6**) was not designed as this peptide has the cysteine residues creating a disulphide bond placed in the penultimate position in the sequence and shortening of the sequence was not possible. In the end, I decided to design the short peptide PD-1(132-136) (**13**) containing three amino acids important for the complex formation.

Table 8. The amino acid sequences and position in the protein of the designed peptides²³⁸.

No		Peptide	Amino acid sequence
1.	Group I	PD-1(68-78)	Ac-YRNleSPSNQTDK-NH ₂
2.		PD-1(62-80)	Ac-SFVLNWyRNleSPSNQTDKLA-NH ₂
3.		PD-1(62-80) ^{W67C-L79C}	Ac-SFVLNcyRNleSPSNQTDKCA-NH ₂
4.		PD-1(62-80) ^{R69C-D77C}	Ac-SFVLNwYcNleSPSNQTCKLA-NH ₂
5.	Group II	PD-1(119-142)	Ac-GTYLAbuGAISLAPKAQIKESLRAEL-NH ₂
6.		PD-1(119-142) ^{T120C-E141C}	Ac-GCYLAbuGAISLAPKAQIKESLRACL-NH ₂
7.		PD-1(119-142) ^{C123-S137C}	Ac-GTYLCGAISLAPKAQIKECLRAEL-NH ₂
8.		PD-1(119-142) ^{A125C-K135C}	Ac-GTYLAbuGCISLAPKAQICESLRAEL-NH ₂
9.		PD-1(122-138)	Ac-LAbuGAISLAPKAQIKESLN-NH ₂
10.		PD-1(122-138) ^{C123-S137C}	Ac-LCGAISLAPKAQIKECL-NH ₂
11.		PD-1(122-138) ^{A125C-K135C}	Ac-LAbuGCISLAPKAQICESL-NH ₂
12.		PD-1(124-136) ^{A125C-K135C}	Ac-GCISLAPKAQICE-NH ₂
13.		PD-1(132-136)	Ac-AQIKE-NH ₂

Peptides were synthesized and purified. The peptide syntheses were carried out according to the solid-phase peptide synthesis (SPPS) technique using the Fmoc/tBu chemistry. The peptides were synthesised using an automatic microwave peptide synthesizer. The N-terminal amino group was acetylated and the C-terminal of peptides had the amide group. Those changes were introduced to mimic the native protein's charge state and enhance their stability for the enzymatic degradation. The obtained compounds were purified using the reversed phase - high-performance liquid chromatography (RP-HPLC) technique and the peptides molecular mass was confirmed

by electrospray ionization, ion trap, and time-of-flight mass spectrometry (LC ESI-IT-TOF MS) coupled with liquid chromatography. Peptides with intermolecular disulphide bonds have been subjected to an oxidation process. To prevent methionine oxidation, the methionine residues in position 69 were exchanged by its isosteres norleucine (Nle). The cysteine residues like methionine are susceptible to rapid oxidation; to prevent this, the cysteines in position 123 was substituted by 2-aminobutyric acid (Abu). It allows me to prevent problems related to dimerization by oxidation of the sulfhydryl groups of cysteines. The purification of long peptides with disulphide bridges, namely peptides (6)-(8), were hindered due to their poor solubility. The purification process ended with a low efficiency, which led to a few rounds of the peptides synthesis.

2.2. Study of binding of PD-1 based peptides to PD-L1 by the SPR technique

In the next step, I decided to test the affinity of the peptides to the PD-L1 protein using the SPR technique. Thanks to these measurements, it was possible to calculate the strength of the protein/peptide binding determined by the equilibrium dissociation constant (K_D). These measurements were performed in a close cooperation with Ph.D. Katarzyna Węgrzyn from the Intercollegiate Faculty of Biotechnology UG&MUG.

In the beginning, I decided to start the SPR measurements by obtaining the kinetic constant parameters for the interaction of the receptor with its natural ligand. For this purpose, the human glycosylated PD-L1 (expression system - HEK 293) was covalently immobilized on the surface of the CM5 sensor chip. Immobilized PD-L1 was titrated with human glycosylated PD-1-Fc protein (expression system - CHO) at a concentration range from 31 nM to 4 μ M (Figure 33A). In the applied experimental condition, the K_D for the interaction of PD-1 with PD-L1 was 1.56 μ M.

Binding of PD-1 protein to PD-L1

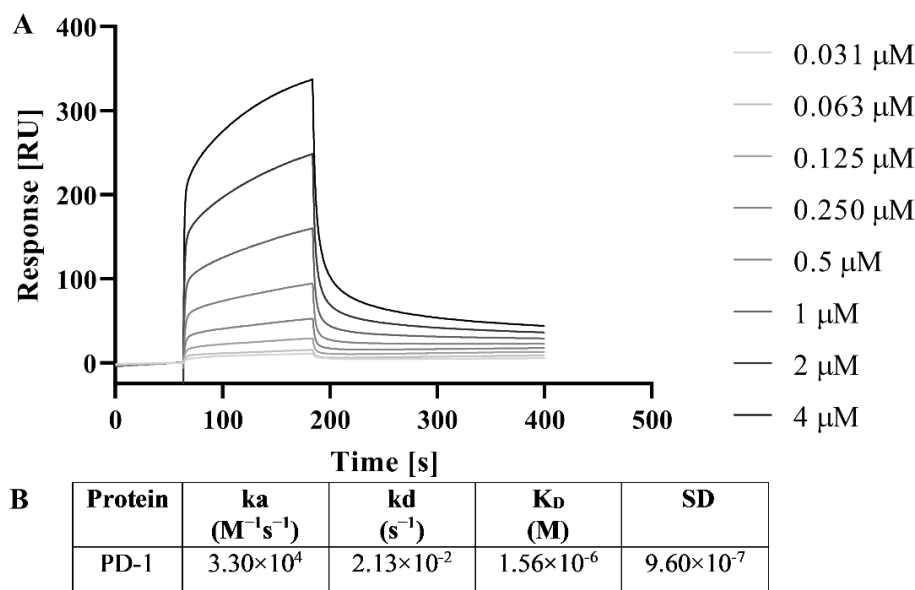


Figure 33. SPR profile of PD-L1 treated with different concentrations of PD-1. A) Sensorgrams showing the relation between the detected signal of different PD-1 concentrations binding to PD-L1 in time. B) The binding kinetics parameters from the SPR analysis were calculated with the Biacore T200 Evaluation Software²³⁸.

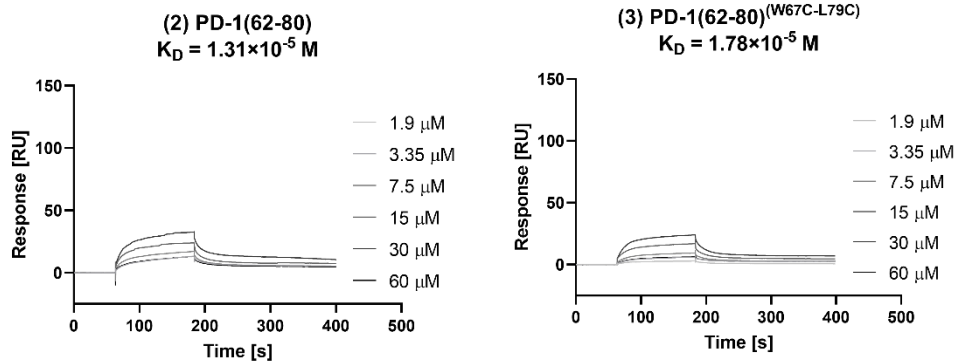
In the next step, the PD-1 derived peptides were subjected to a binding analysis using the SPR technique in the aforementioned conditions. The obtained results are shown in Figure 34 (peptides interacting with PD-L1) and 35 (peptides that show no interaction with PD-L1). The binding kinetics parameters have been collected in Table 9.

The differences in the strength of the interaction can be observed among the two groups of peptides. The peptides from Group I are characterized by a lower affinity to PD-L1 than the PD-1 or they are not interacting with the target protein at all. The shortest linear peptide from this group, peptide (1), shows no interaction with the PD-L1 protein. In contrary to peptide (1), its longer analogue, peptide (2), binds to PD-L1 with K_D 13.1 μM . However, the interaction is more than 8-times weaker than the one for PD-1. This group of peptides consists of two compounds with disulphide bonds. The strength of the interaction of peptide (3) is not substantially different from the one for peptide (2) (17.8 μM). Moreover, peptide (4), like peptide (1), shows no interaction with the protein (Figures 34 and 35).

Among Group II, eight from the nine peptides were analysed. Compound (8) was excluded as a result of poor solubility in standard buffers used in this technique and was rejected from further examination. Moreover, for linear peptide (9), and for peptides

(11) and (12), with disulphide bonds, the dissociation constant was not determined due to a weak binding or the lack of it (Figure 35). For peptide (5), the K_D was calculated; however, the affinity for PD-L1 was weaker than for the PD-1/PD-L1 complex, the obtained value was 57.8 μM . From the Group II, four peptides could be distinguished as they bound to ligand-1 with the same order of magnitude as its natural receptor. The highest affinity was determined for peptide (10), the obtained K_D for the PD-L1/peptide (10) complex was 1.52 μM (Figure 34). Its k_d was one of the two lowest obtained and it was $1.8 \times 10^{-3} \text{ s}^{-1}$, it was lower than k_d for PD-1. Peptides (7) and (6) exhibit a slightly weaker binding than peptide (10), and their K_D was 4.66 μM and 5.36 μM , respectively. Peptide (13) was the smallest molecule from among the tested peptides, it consisted of only five amino acid residues. As the resonance angle is proportional to the mass of analyte bound to the biosensor in this case, the signal reached only 13 RU (Figure 34), however, the K_D of its interaction with the ligand was 7.30 μM .

Group I



Group II

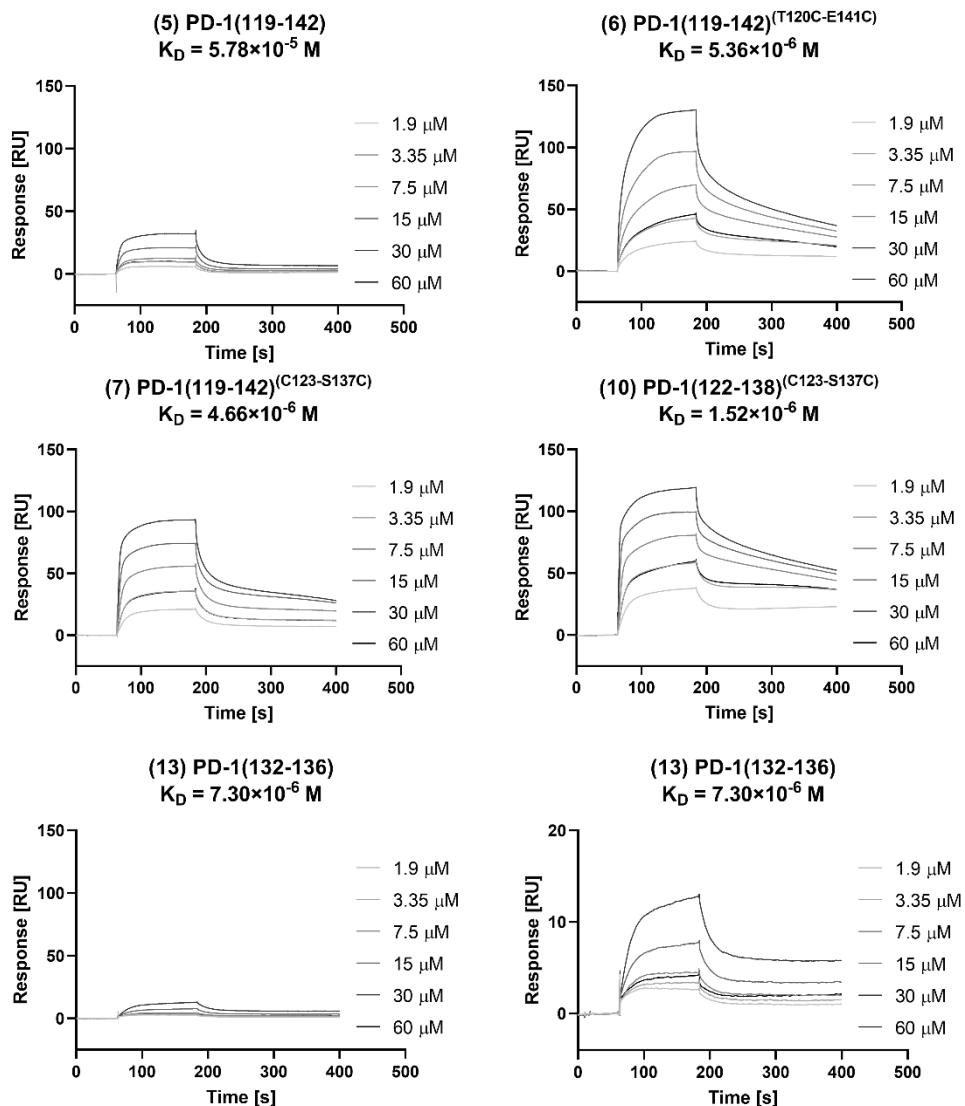


Figure 34. Sensorgrams of the PD-1 derived peptides interacting with PD-L1 analysed by the SPR technique. For peptide (13), binding to PD-L1 is shown in two different scales²³⁸.

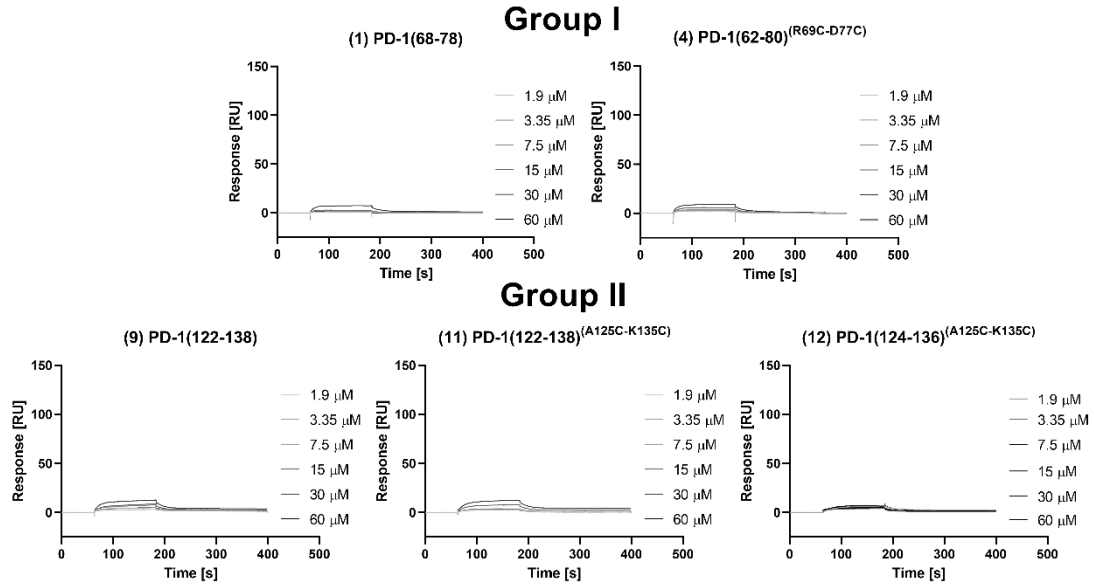


Figure 35. Sensorgrams of the noninteracting PD-1 derived peptides with PD-L1 analysed by the SPR technique²³⁸.

Table 9. Association and dissociation rates and dissociation constants calculated for the PD-1 derivate peptides binding to PD-L1 from the SPR data. The results were calculated using the Biacore T200 Evaluation Software from at least three independent titration analyses. The applied binding model 1:1. ND - not determined (no binding detected or binding too weak to establish reliable constants); SD – standard deviation²³⁸.

	No	Peptides	k_a ($M^{-1}s^{-1}$)	k_d (s^{-1})	K_D (M)	SD
Group I	1.	PD-1(68-78)	ND	ND	ND	ND
	2.	PD-1(62-80)	2.18×10^2	1.76×10^{-3}	1.31×10^{-5}	1.27×10^{-5}
	3.	PD-1(62-80) ^{W67C-L79C}	4.94×10^2	9.19×10^{-3}	1.78×10^{-5}	1.36×10^{-5}
	4.	PD-1(62-80) ^{R69C-D77C}	ND	ND	ND	ND
Group II	5.	PD-1(119-142)	1.45×10^2	4.27×10^{-3}	5.78×10^{-5}	4.11×10^{-5}
	6.	PD-1(119-142) ^{T120C-E141C}	9.97×10^2	3.17×10^{-3}	5.36×10^{-6}	4.02×10^{-6}
	7.	PD-1(119-142) ^{C123-S137C}	6.76×10^2	2.86×10^{-3}	4.66×10^{-6}	1.97×10^{-6}
	8.	PD-1(119-142) ^{A125C-K135C}	Not soluble in solution using in SPR measurements			
	9.	PD-1(122-138)	ND	ND	ND	ND
	10.	PD-1(122-138) ^{C123-S137C}	1.21×10^3	1.80×10^{-3}	1.52×10^{-6}	8.76×10^{-7}
	11.	PD-1(122-138) ^{A125C-K135C}	ND	ND	ND	ND
	12.	PD-1(124-136) ^{A125C-K135C}	ND	ND	ND	ND
13.	PD-1(132-136)	2.23×10^2	1.25×10^{-3}	7.30×10^{-6}	5.47×10^{-6}	

2.3. Stability of the designed peptides and their effects on the viability of chosen cell lines

The next step in my research was an evaluation of the selected peptides regarding their stability in the growth medium used for the cell lines culture and influence on the viability of cell lines used in the planned *in vitro* assays. For further evaluation, I chose only peptides interacting with the PD-L1 protein, namely peptides (2) and (3) from Group I and (5), (6), (7), (10), and (13) from Group II. The peptide selections was based on the data obtained from the SPR measurements. The first action was to check the stability of the selected peptides in Roswell Park Memorial Institute (RPMI) 1640 medium with 10% heat-inactivated fetal bovine serum (FBS) used in the cell-based tests. The composition of the RPMI 1640 medium was especially balanced for the growth of human T and B lymphocytes. It is distinguished from other mediums by high concentrations of vitamins and glutathione reducing agent²⁴⁰. The peptides were incubated for 24 hours in the RPMI 1640 medium. The checkpoints were set at time 0 and after 24 hours to correspond to the time points chosen in the viability cell assay. As a control, I used peptides dissolved in water in time 0 h. All samples were analysed using the RP-HPLC method and the percentage of stability was established by comparing the peak area of control in time 0 h with the peak area for collected samples incubated in RPMI 1640. The obtained results are presented in Figure 36.

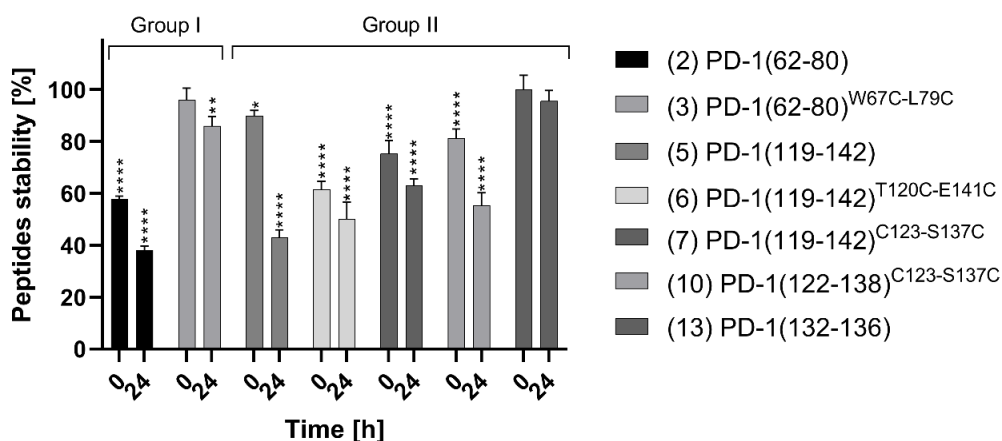


Figure 36. Peptides stability in the RPMI 1640 medium at times 0 and 24 h. The percentage of stability was established by comparing the peak area of control in time 0 h with the peak area for the collected samples. Results were obtained through the RP-HPLC analysis method. Results are shown for three experiments performed independently. Data are depicted as mean with SD (Mean +/- SD). Statistical analysis was performed using one-way analysis of variance (ANOVA) followed by the Dunnet's post-hoc test. ****: $p < 0.0001$, ***: $p < 0.001$, **: $p < 0.01$, *: $p < 0.05$ ²³⁸.

The best stability in RPMI 1640 with 10% FBS was achieved by two peptides, namely peptides **(3)** and **(13)**. A decrease of the peptide **(13)** content in the sample in time 0 h has not been observed and for peptide **(3)**, it was only a 4% decrease comparing to the control. After 24 hours, there was only a slight drop observed resulting in the received stability at the level of 96% for peptide **(13)** and 86% for peptide **(3)**. On the contrary, two linear peptides, **(2)** and **(5)**, show the biggest decrease of stability. For peptide **(2)** from Group I, it was a 42% and 62% decrease of content in time 0 and 24 hours of incubation, respectively. Where for peptide **(5)**, there was only a 10% decrease in time 0 h but after 24 hours of incubation further decrease of about 47% was observed. Three peptides, **(6)**, **(7)**, and **(10)**, from Group II with disulphide bonds show a moderate decrease in concentration in comparison to control. For time 0 h, the decrease was observed in the range of 19-38% and after 24 hours of incubation, it was 37-50%. It should be noticed that peptides might undergo many biological and chemical processes in a solution. For the tested peptides, I have not observed any additional signals in the HPLC chromatograms, what can indicate that they were not an object of the degradation process caused by the medium components (Figure 37). However, a reduction of the signal was observed. It can be caused by the interaction of the peptides or their degradation products with the serum albumin proteins during sample preparation which includes precipitation of medium components by ethanol and spinning. The process of non-specific binding of peptides with albumins was observed previously and may occur due to hydrophobic interactions with albumins²⁴¹⁻²⁴³.

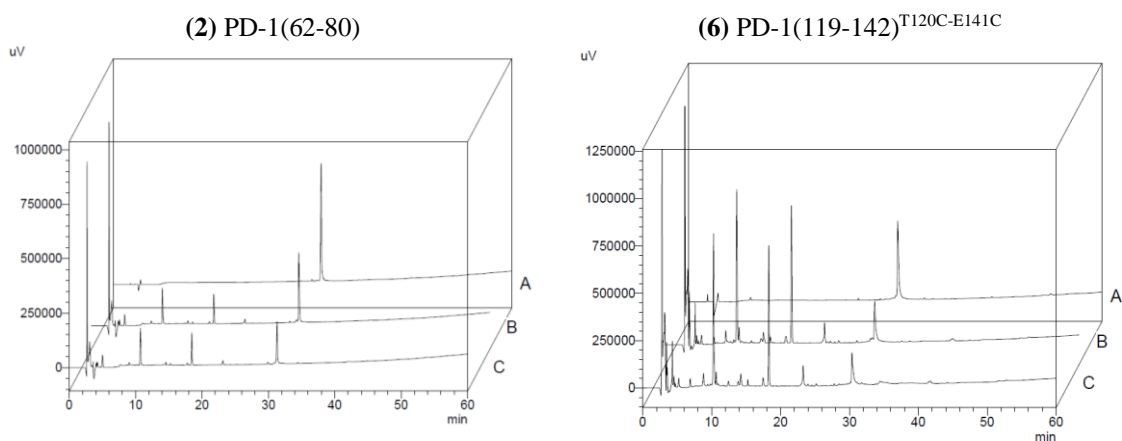


Figure 37. Chromatograms registered for peptides **(2)** and **(6)**. A) peptide in water $t=0$ h, B) peptide in medium $t=0$, C) peptide in medium $t=24$ h²³⁸.

Subsequently, I checked CHO-K1, Jurkat E6.1, and BW5417 (T cell stimulator, TCS Ctrl) cell lines viability after 24 hours of incubation with the selected peptides from

Groups I and II. The CHO-K1 is a hamster ovary cell line and Jurkat E6.1 is a human T lymphoblast cell line from a patient with acute T cell leukaemia. Both these cell lines were used in the inhibition bioassay. BW5147 is a T lymphoblast cell line from mice with lymphoma. This cell line was used in the competition assay. Cells were seeded on the 96-well plate and incubated with the peptides for 24 h. To estimate the number of viable cells, I used the CellTiter-Glo® luminescence-based assay, consisting of quantitative determination of adenosine triphosphate (ATP), which is related to the metabolically active cells and proportional to the living cells²⁴⁴. The mechanism of the assay is based on luciferase-luciferin reaction in which ATP and molecular oxygen are substrates. The reaction is catalysed by luciferase and is run in the presence of the aforementioned ATP, O₂, and additionally with the presence of Mg²⁺ (from the growth medium). The reaction leads to the emission of energy with the maximum intensity at 560 nm (yellow-green colour) (Figure 38)^{245,246}.

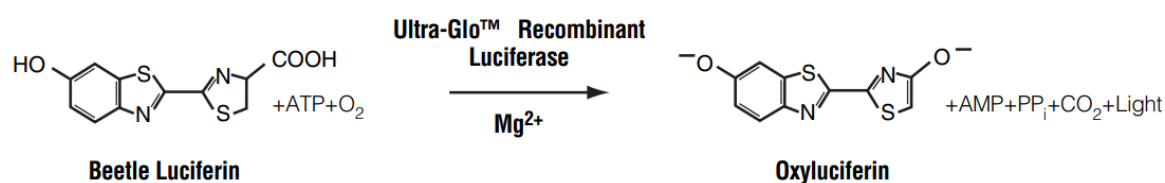


Figure 38. Luciferin-luciferase reaction²⁴⁵.

Each cell line was treated with six different peptide concentrations 150, 50, 16.7, 5.6, 1.9, and 0.62 μM. The peptides were not tested in higher concentrations as they precipitate in the cell culture medium during preparation of the stock solutions required for the tests. The concentrations were prepared by the serial dilution method. The results were compared to the non-treated cells and normalised.

Peptides from Group I, peptides (2) and (3), almost in all concentrations did not have a negative effect on the CHO-K1 cell line viability after 24 hours of incubation (Figure 39). Only peptide (2) led to a 20% decrease in cell viability at the highest concentration. Three peptides from Group II, peptides (5), (7), and (13), at the 150 μM concentration, strongly influenced the CHO K-1 cell viability leading to the decrease of viable cells to 47%, 76%, and 33% (Figure 39) compared with control, respectively. Peptides (6) and (10) showed a strong cytotoxic effect at this concentration. Additionally, peptides (5), (6), (7), and (10) at the second highest concentration (50 μM) led to a slight drop in the

number of viable cells in comparison to the control. Lower concentrations of the tested peptides, below 16.7 μM , do not show a negative effect on the CHO K-1 cell's viability.

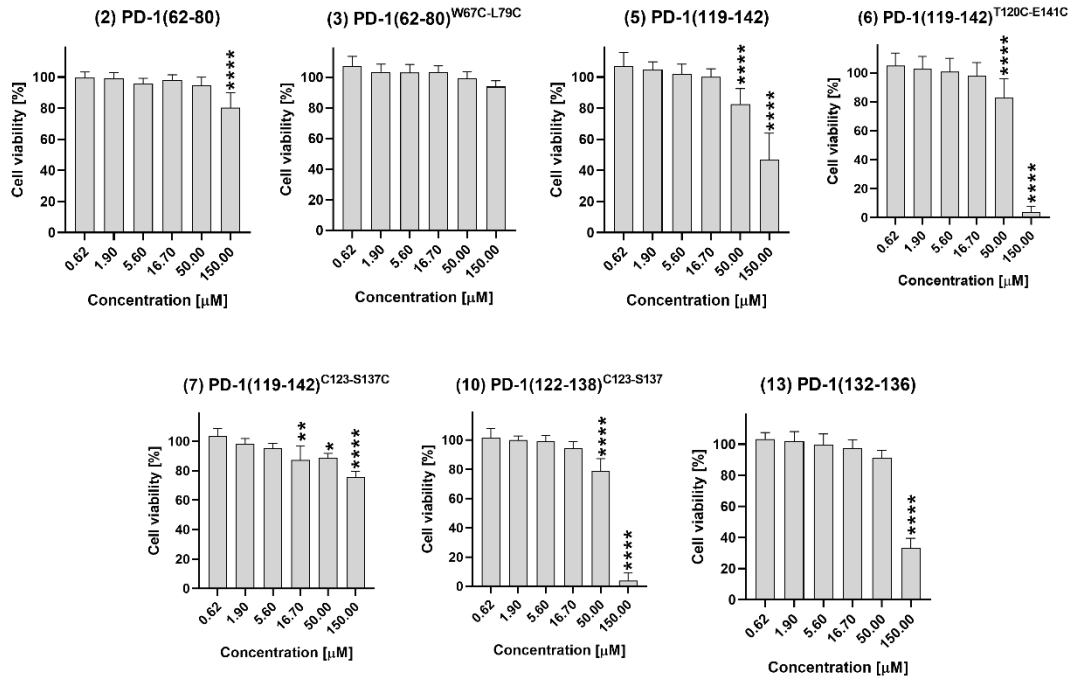


Figure 39. Cell viability assay used to define the influence of the PD-1 derived peptides on the CHO-K1 cell line after incubation for 24 hours. Results are shown for three experiments performed independently in triplicate. Data are depicted as mean with SD (Mean \pm SD). Statistical analysis was performed using one-way ANOVA followed by the Dunnet's post-hoc test. ****: $p < 0.0001$, ***: $p < 0.001$, **: $p < 0.01$, *: $p < 0.05$ ²³⁸.

The peptides from both groups had less influence on the viability of the Jurkat E6.1 cells than in the case of the CHO K-1 cells (Figure 40). In the experiment conditions, I observed only a slight drop of the cells viability in the case of peptides (2), (5), (7), and (10) and only for the concentration of 150 μM . The number of viable cells decreased by 17%, 27%, 25%, and 20% respectively. For lower concentrations, below 150 μM , the changes were not significant.

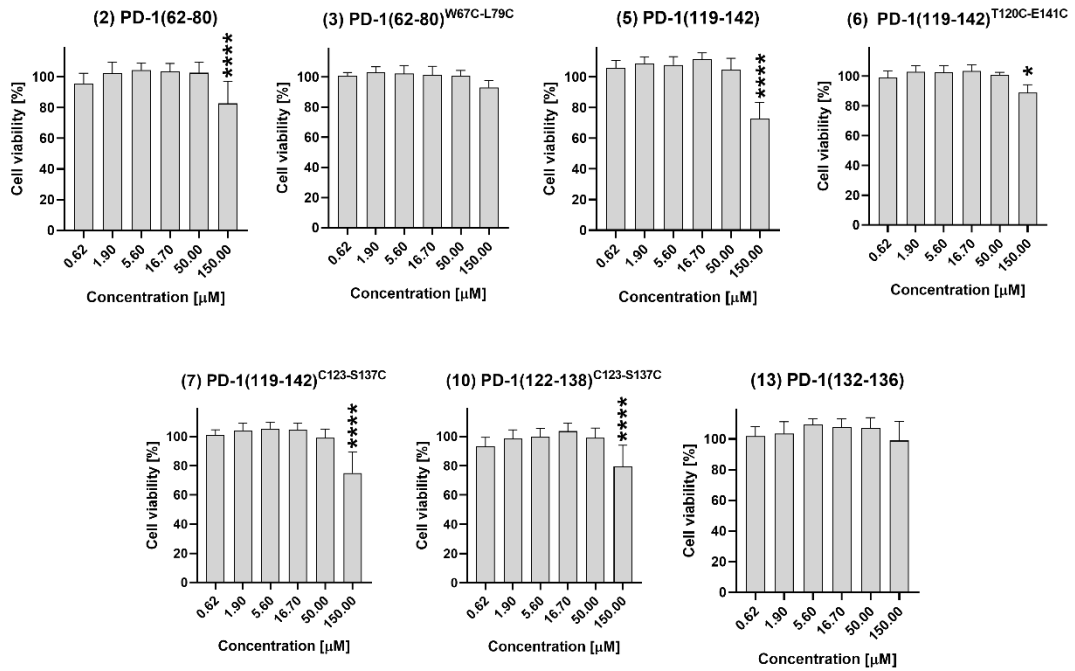


Figure 40. Cell viability assay used to define the influence of the PD-1 derived peptides on the Jurkat E6.1 cell line after incubation for 24 hours. Results are shown for three experiments performed independently in triplicate. Data are depicted as mean with SD (Mean +/- SD). Statistical analysis was performed using one-way ANOVA followed by the Dunnet's post-hoc test. ****: $p < 0.0001$, ***: $p < 0.001$, **: $p < 0.01$, *: $p < 0.05$ ²³⁸.

In the case of the TCS Ctrl cells, the tested peptides indicated a more intense effect on their viability than for the CHO K-1 and Jurkat E6.1 cells. The highest concentration had a strong negative effect on cell viability in all the tested peptides (Figure 41). It led to a decrease in the number of living cells below 20% for peptide (5) and (7) in comparison with the control. The concentration of 50 μM demonstrated the cytotoxic effect in the case of peptides (7) and (13), leading to a reduction of the living cell population to 37% and 48%, respectively. The remaining peptides at this and lower concentrations had a moderate impact on cell viability and the number of living cells in the tested condition fluctuated between 70% and 90%. Peptide, (10) at concentrations from 1.9 to 50 μM demonstrated a slight proliferating effect on the TCS Ctrl cells leading to an increase of viable cells up to 105-108% compared to the control.

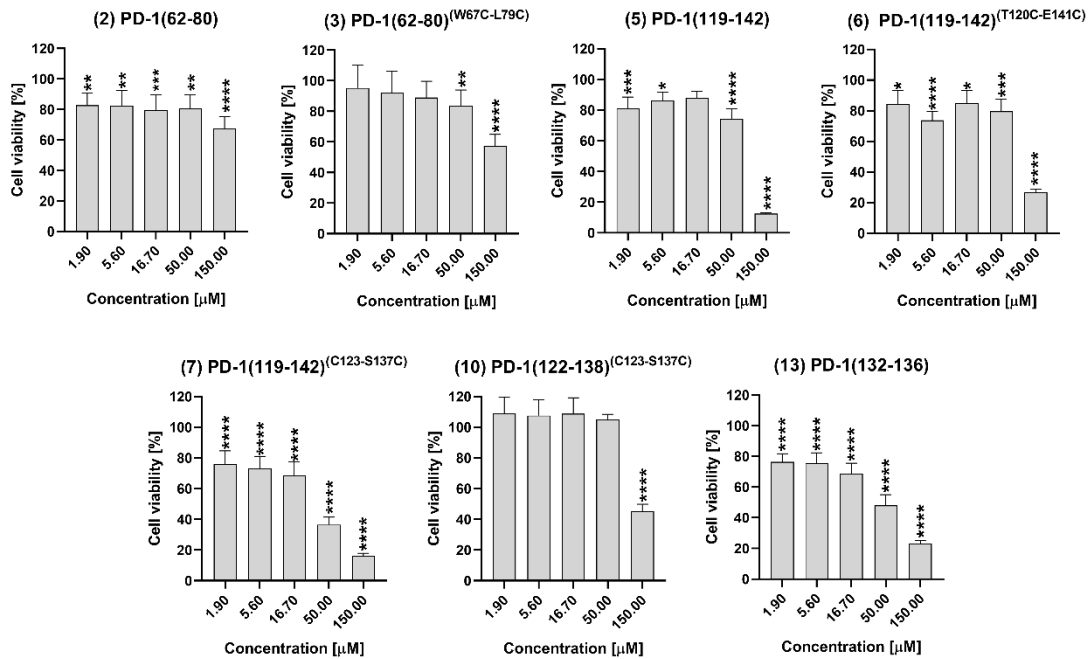


Figure 41. Cell viability assay used to define the influence of the PD-1 derived peptides on the TCS Ctrl cell line after incubation for 24 hours. Results are shown for three experiments performed independently in triplicate. Data are depicted as mean with SD (Mean +/- SD). Statistical analysis was performed using one-way ANOVA followed by the Dunnet's post-hoc test. ****: $p < 0.0001$, ***: $p < 0.001$, **: $p < 0.01$, *: $p < 0.05$.

2.4. Cell-Binding Assay and Competitive Inhibition

In the next step of my research, I performed a competitive bioassay for selected peptides (2), (3), (5), (6), (7), (10), and (13). These studies have been performed at the prof. Peter Steinberger laboratory from the Division of Immune Receptors and T cell Activation at the Medical University of Vienna under the supervision of Ph.D. Claire Battin. The assay was performed to examine the capacity of the peptides to displace the human glycosylated PD-1-Fc from the complex with PD-L1 located on the BW5417 cell line with the stable expression of PD-L1 (TCS PD-L1). In the assay, as a control, I used TCS without the expression of PD-L1 (TSC Ctrl). The idea of a competitive assay is to measure the binding of labelled ligand to a target in the presence of the second unlabelled-ligand. In experiment, the “target” was a PD-L1 protein, indirect labelled ligand was PD-1, and unlabelled ligands were peptides. The PD-1-Fc protein was detected by the anti-IgG Ab conjugated with a fluorescent label. In short, when peptide binds to the PD-L1 protein located on the TCS cell stronger than PD-1-Fc, we receive a lower signal from anti-IgG antibody with fluorochrome. If the peptide binds to the

PD-L1 with a lower affinity than PD-1, the more of the PD-1 molecules will bind to PD-L1 and we receive a stronger signal (Figure 42A).

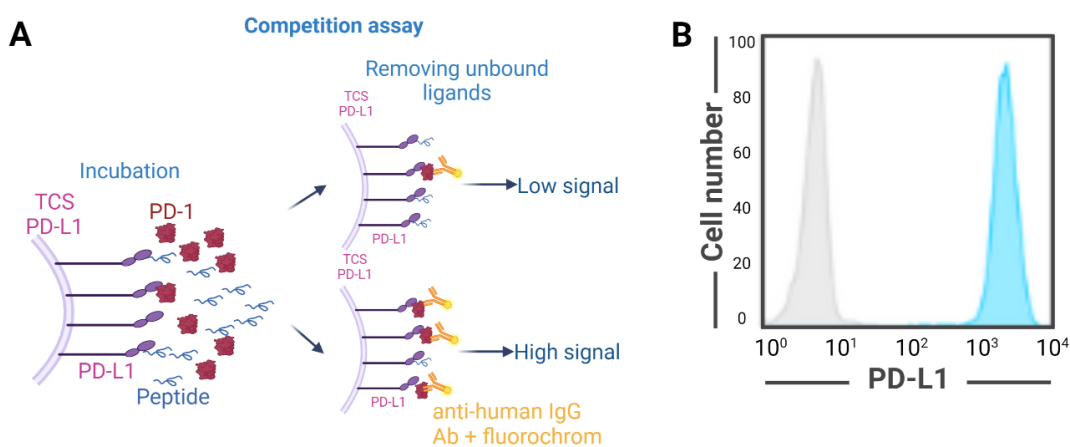


Figure 42. A) Schematic representation of the competition experiment. B) Flow cytometry analysis of TCS Ctrl and TCS PD-L1 confirming the presence or absence of PD-L1. Light grey histogram: staining of the control cells. Blue histogram: staining of the PD-L1 cells.

I confirmed the expression of PD-L1 on the TCS PD-L1 surface (Figure 42B, blue histogram) and the absence of PD-L1 on TCS Ctrl (Figure 42B, light grey histogram) by the flow cytometry technique. Before performing the competition assay, I optimised the condition of the test by investigating two different anti-human IgG Ab - PE-labelled donkey anti-human IgG antibody and APC-labelled mouse anti-human IgG antibody. These Abs recognize the Fc region of the PD-1 chimera protein used in this experiment. Differences between the PE- and APC-label are presented in Table 10. PE and APC are fluorescent proteins that after excitation emit light from the yellow-orange (574 nm) and red spectrum range (660 nm), respectively. The PE is more “bright” than APC. This difference is partially related to its higher extinction coefficient and quantum yield. It is also related with more energy requirements by the PE for excitation. Moreover, both proteins are conjugated with different anti-human IgG antibodies characterized by the different affinity to the target. Taking into consideration the aforementioned differences between those antibodies, I decided to examine which one will be more optimal for my planned experiment.

Table 10. Spectral properties of PE and APC.

Name	Short name	Excitation wavelength [nm]	Emission wavelength [nm]	Extinction coefficient [cm ⁻¹ M ⁻¹]	FQY ²
R-Phycoerythrin	PE	566	574	1,960,000	0.84
Allophycocyanin	APC	651	660	700,00	0.68

²FQY – fluorescence quantum yield in an aqueous buffer (pH 7.2)

Moreover, I tested four different concentrations (from 0.4 $\mu\text{g/ml}$ to 1 $\mu\text{g/ml}$) of the human PD-1 protein (Figure 43A and B) to choose the concentration of protein which can be detected by labelled anti-human IgG Ab and can saturate PD-L1 on the cell surface. This test was performed using the flow cytometry method. The obtained results show that the PE-labelled antibody yields a stronger response than the APC-labelled antibody what was expected and was more preferable for the test outcome as the difference between the control and the sample of interest was bigger. Additionally, the titration experiment performed for the PD-1 protein shows that the strongest signal was received for 1 $\mu\text{g/ml}$ of the tested protein. To confirm that this concentration of PD-1 is the most optimal for the experiment, I decided to examine two higher concentrations of the protein, namely 6.25 $\mu\text{g/ml}$ and 2.5 $\mu\text{g/ml}$ detected by PE-labelled Ab (Figure 43C).

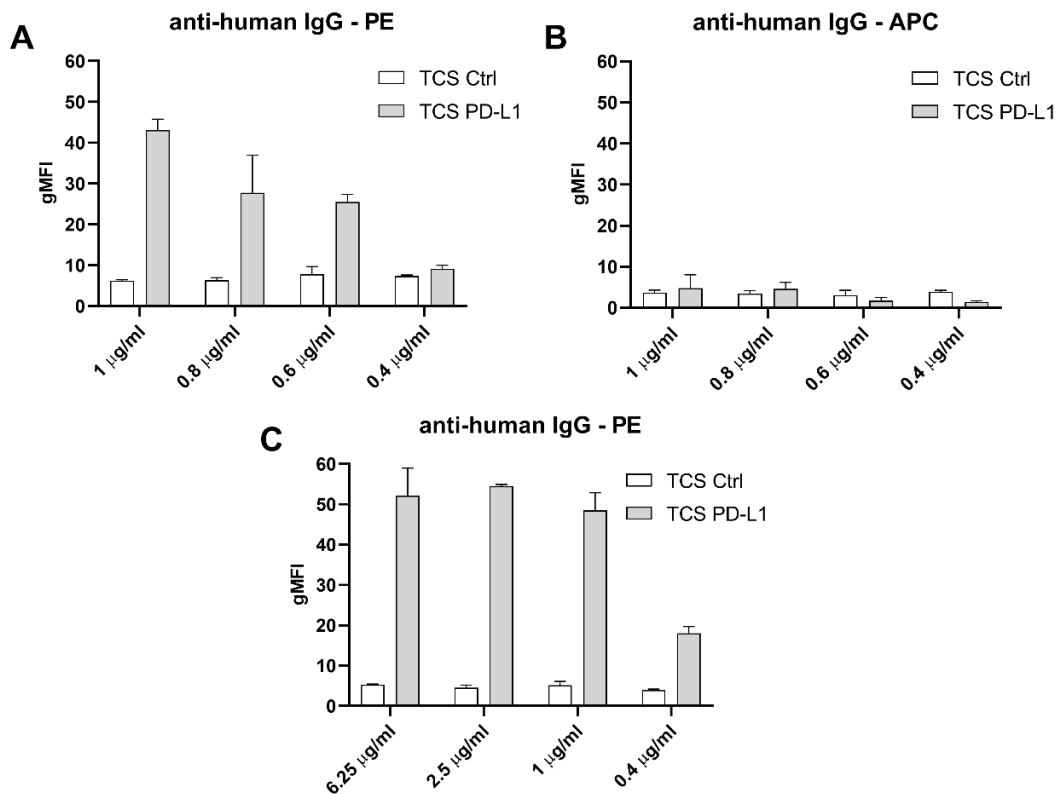


Figure 43. Optimization of the competition test condition. A, B) Comparison of two different anti-human IgG antibodies PE- and APC-labelled detecting human PD-1-Fc protein at four concentrations. C) Comparison of different PD-1 concentrations detected by the anti-human IgG PE Ab.

The obtained results show that the use of a higher concentration of the PD-1 protein than 1 $\mu\text{g/ml}$ is not required as this concentration saturates all available PD-L1 molecules on the cell surface. Taking together the obtained results, the binding of human PD-1-Fc

to the PD-L1 on the cell surface was detected with a PE-labelled donkey anti-human IgG antibody, and in the assay, I used the PD-1 protein at the concentration of 1 $\mu\text{g/ml}$.

In the final test, the target cells (TCS PD-L1) were incubated in test tubes with peptides at three different concentrations from 50 μM to 5.5 μM . The 150 μM concentration was excluded from further research due to the cytotoxic effect of the tested peptides on TCS Ctrl. As a competitor, PD-1-Fc was used. After incubation, anti-human IgG PE Ab was added to detect PD-1 bound to PD-L1. As control, TCS PD-L1 cells were incubated with the PD-1 protein (without peptides). Additionally, atezolizumab, mAb anti-PD-L1, which inhibits the PD-1/PD-L1 complex formation was used as a positive control (Figure 44).

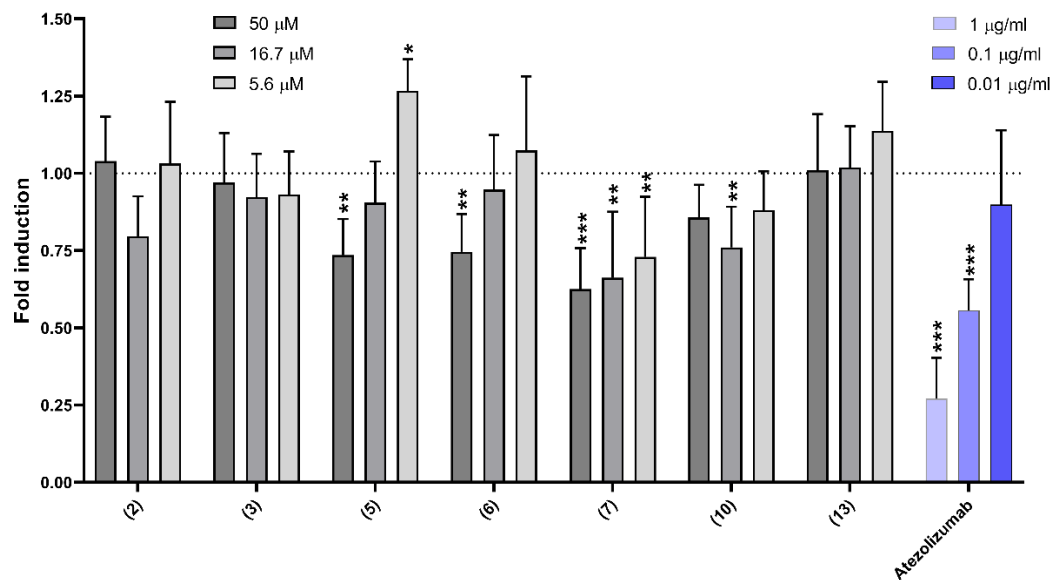


Figure 44. Competitive inhibition of peptides against the PD-1/PD-L1 complex formation. TCS PD-L1 was incubated with the indicated peptides used at final concentrations ranging from 50 μM to 5.6 μM . The bar diagram shows the fold induction of geometric mean fluorescence intensity (gMFI) for at least three experiments performed independently in triplicate. Data were normalised to the gMFI received for TCS PD-L1 treated by PD-1. Data are depicted as mean with SD (Mean \pm SD). Statistical analysis was performed using one-way ANOVA followed by the Dunnet's post-hoc test. ****: $p < 0.0001$, ***: $p < 0.001$, **: $p < 0.01$, *: $p < 0.05$.

The best inhibitory properties were received for peptide (7) for which the dose-dependent inhibition effect was observed and for highest concentration the complex inhibition was calculated on 37.5%. Peptides (5) and (6) significantly blocked the binding of PD-1 to PD-L1 at a concentration of 50 μM in 26.4% and 25.4%, respectively; additionally, they had a dose-dependent effect. Additionally, (10) blocked the binding of PD-1 to PD-L1, however, not in the concentration-dependent manner and

showed a significant inhibition only at the concentration of 16.7 μM . No blocking effect was seen for peptides (2), (3), and (13).

2.5. Cell-based PD-1/PD-L1 blocking bioassay

Subsequently, I evaluated the inhibition properties of the designed peptides for blocking the PD-1/PD-L1 axis in an *in vitro* bioluminescent reporter cell-based assay including two genetically engineered cell lines. Effector Jurkat E6.1 cell line stably expressed PD-1 and firefly luciferase reporter gene under NFAT response element (NFAT-RE) and the PD-L1 APC/CHO-K1 cell line was constructed on the CHO-K1 cell line and expressed PD-L1. When PD-1 binds to the PD-L1, the TCR signalling and luminescence mediated by NFAT-RE is suppressed, the “glowing” (luminescence) is reduced (Figure 45, left side). When the PD-1/PD-L1 axis is disrupted by the inhibitors, it activates TCR and NFAT-RE mediated firefly luminescence, and the “glowing” is restored (Figure 45, right side).

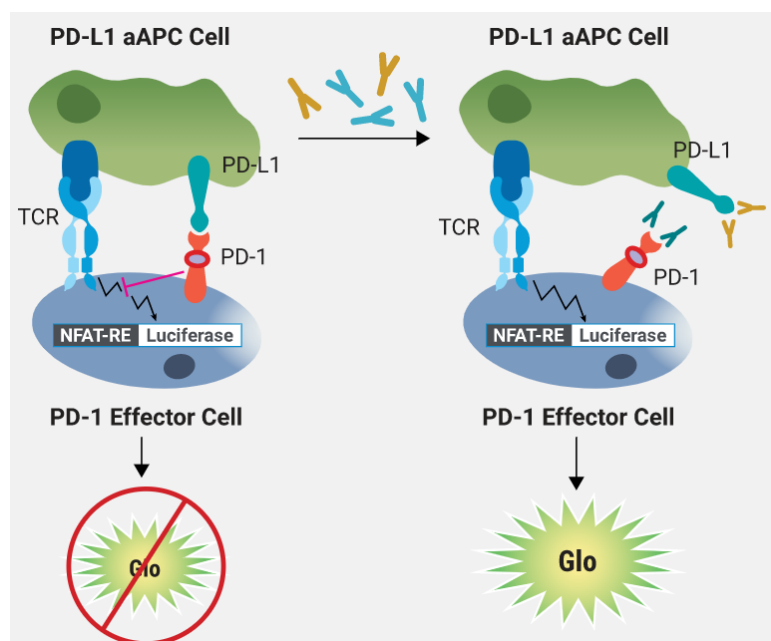


Figure 45. Scheme of PD-1/PD-L1 blocking bioluminescence assay²⁴⁷.

I performed the assay for the chosen peptides, selected on the basis of the SPR analysis from Groups I and II and tested them at five concentrations prepared using the serial dilution method from 50 μM to 0.62 μM . As a positive control, I used an anti-PD-1 antibody (Figure 46). As a untreated control, PD-1 effectors cells were co-cultured with the PD-L1 APC cells without the presence of an inhibitor.

The most active peptides from the inhibition bioassays were shown to be peptide (7) and (10). These compounds inhibit the PD-1/PD-L1 complex in a dose-dependent manner. It should be noted that they have similar amino acid sequences and differ only in length. Moreover, they have disulfide bonds in the same position. Additionally, linear peptide (5) shows concentration-dependent inhibitory properties at the concentration range from 16.7 μM to 0.62 μM but not 50 μM . For peptide (3), the inhibitory effect was seen for all tested concentrations, however, the effect was not correlated with the concentration. No inhibition was seen for peptides (2), (6), and (13) (Figure 46).

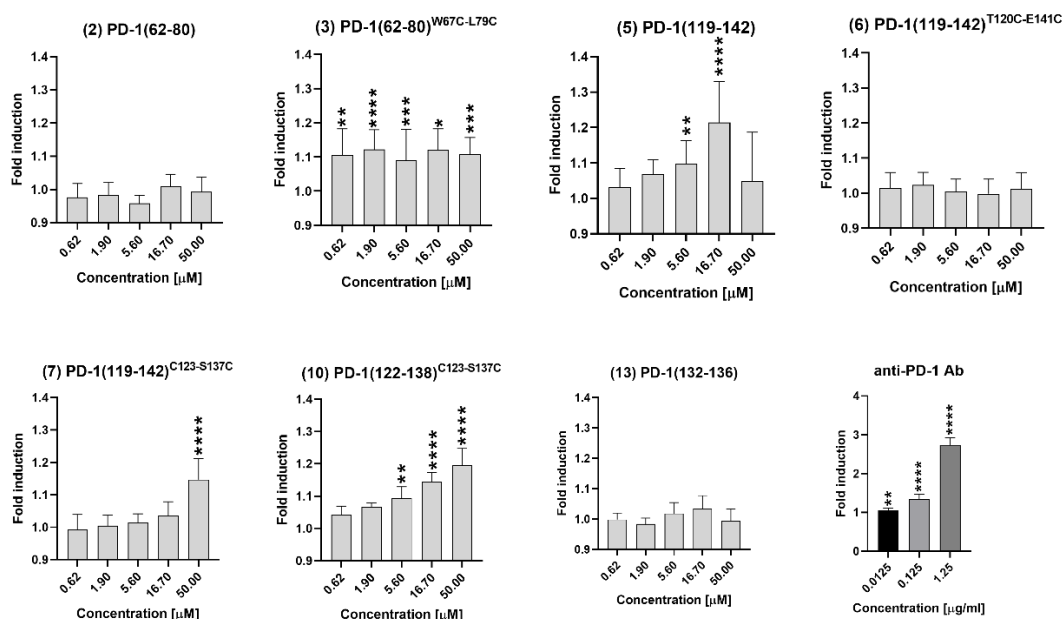


Figure 46. The inhibition of the PD-1/PD-L1 complex by the PD-1 derived peptides in a bioluminescent reporter cell-based assay. The activity of tested peptides is presented as a fold induction calculated by dividing the relative luminescence units (RLU) received for cells treated by the peptides by the RLU for the untreated control (RLU peptide/RLU control). Results are shown for three experiments performed independently in triplicate. Data are depicted as mean with SD (Mean \pm SD). Statistical analysis was performed using one-way ANOVA followed by the Dunnett's post-hoc test. ****: $p < 0.0001$, ***: $p < 0.001$, **: $p < 0.01$, *: $p < 0.05$ ²³⁸.

2.6. Conformational studies for peptide PD-1(122-138)^{C123-S137C}

In the next step, peptide (10) was chosen for a more detailed conformational analysis because of the best affinity to PD-L1. Regardless, it did not compete with the PD-1 protein in a concentration-dependent manner in the competition assay; however, it restores the NFAT-RE mediated luminescence in the PD-1/PD-L1 cell-based inhibition bioassay. Moreover, it is better soluble in aqueous solutions than its longer analogue

peptide (7), which yields better results in the competitive inhibition test, but not in the cell-based PD-1/PD-L1 blocking bioassay. Inhibitory properties and good solubility observed for peptide (10) provide the basics for further modifications and designing analogue peptides having a better blocking capacity. To collect more data regarding the structure of peptide (10) and its binding interface with PD-L1, conformational studies were performed. The NMR studies and 3D structure determination of peptide (10) were conducted by Ph.D. Emilia Sikorska. The docking of the obtained structure of peptide (10) to the PD-L1 protein, applying UNited RESidue (UNRES) force field and next multiplexed-replica exchange molecular dynamics (MREMD) were performed by Ph.D. Adam Sieradzan. Both of them are from the Faculty of Chemistry of Gdańsk University. I analysed the obtained structural results in correlation with biological data.

In this work, only selected data from the NMR results, molecular dynamics, and MREMD are presented, a broader analysis is available in the publication of Bojko et al.²³⁸. NMR analysis of peptide (10) was based on a data set achieved from the 2D total correlation spectroscopy (TOCSY) and 2D nuclear Overhauser enhancement spectroscopy (NOESY) measurements. NMR analysis confirmed the *trans* geometry in the peptide bonds and that sulfhydryl groups from cysteines are oxidated. 300 different structures of peptide (10) were received and were clustered in 10 conformational families. Two from ten families encompassed 72% peptide conformations which form a β -hairpin like structure stabilized by intermolecular hydrogen bonds and disulfide bridge (Figure 47). Those two structures were used for further docking studies.

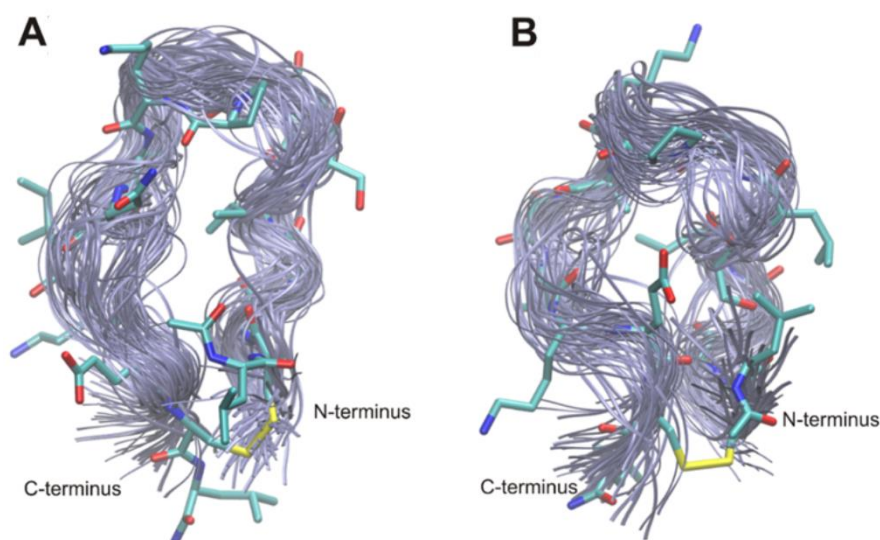


Figure 47. Superimposed conformations of dominant clusters of peptide (10). A) Family 1 consolidating 79 structures. B) Family 2 consolidating 65 structures²³⁸.

The four 3D structures of peptides were docked to PD-L1 applying UNRES force field and MREMD for better recognition of the PD-L1/peptide interface (Figure 48). Three structures of peptide (10) were used, namely the structure trimmed from the PD-1/PD-L1 crystal complex with cysteine residues in the appropriate position in the sequence and two selected clusters from the NMR data. For the method validation purpose, peptide (4) cut out from the crystal structure of the PD-1/PD-L1 complex served as a negative control (no binding with PD-L1 in the SPR analyses performed in this work). The analysis indicates that both conformation families obtained from NMR bind with PD-L1 in the same region as PD-1.

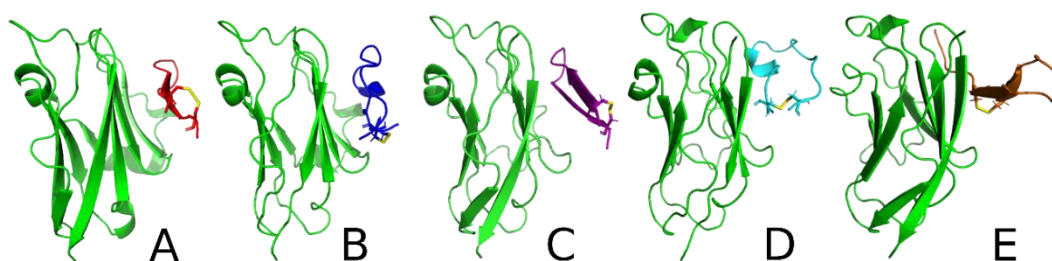


Figure 48. Four PD-L1/peptide (10) conformations structures. Origin of the peptide (10) structure: A) peptide structures were trimmed from the PD-1 protein, B) fragment of the PD-1 crystal structure with the peptide (10) sequence, C) and D) NMR family 1 and 2 restraints on peptide (10), respectively, E) fragment of the PD-1 crystal structure with the peptide (4) sequence. Points B-E presents the cluster with the lowest Root-mean-square deviation (RMSD) from the MREMD simulation²³⁸. PD-L1 is coloured green.

3. Peptides targeting the PD-1 protein

3.1. Design and synthesis of peptides derived from the PD-L1 protein

The approach of designing the PD-1 targeting peptides corresponds to the concept I have presented for the peptides targeting PD-L1. The amino acid sequences of peptides presented in this paragraph were derived from the PD-L1 protein and were designed based on the crystal structure of the PD-1/PD-L1 complex and the MM/GBSA calculations. As previously discussed, the PD-L1 extracellular IgV domain occurs in a β -sandwich motif consisting of two β -sheets. The front β -sheet is composed of AGFCC'C'' strands and the back one includes BED strands. The amino acid residues from the front part are responsible for stabilizing the interaction with the PD-1 (Figure 49). Taking this into consideration, I designed three groups of peptides - Group

I_L, II_L, and III_L (Table 11). Moreover, to enhance the affinity of the designed peptides to the flat PD-1 interface, I decided to introduce the intramolecular disulphide bonds into the seven peptides by exchanging selected amino acids, located opposite each other in the 3D structure of the PD-L1 protein, with the cysteine residues. The introduction of such a modification should allow the β -hairpin structure formation mimicking the structure of the PD-L1 protein and thus enhance the binding to the flat PD-1 interface^{206,239,204}.

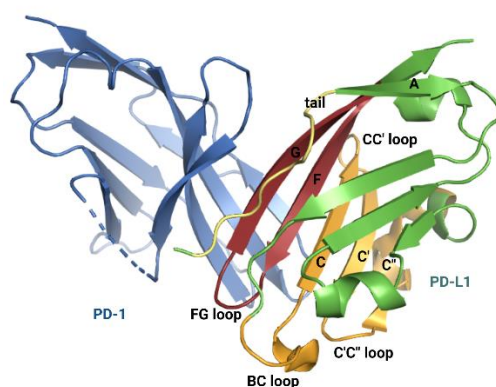


Figure 49. The structure of PD-1/PD-L1 complex (PDB ID: 4ZQK). The fragments of PD-L1 which were used to construct three groups of peptides are marked: yellow - peptides from Group I_L, orange - peptides from Group II_L, red - peptides from Group III_L. PD-1 is coloured blue, PD-L1 - green.

Group I_L consists of only one peptide, (**L1**), and constitutes the amino acid residues from the fragments of A strand's tail. Peptides from (**L2**) to (**L6**), belonging to Group II_L, are assembled with amino acids from CC'C'' strands, BC, CC' and C'C'' loops. Peptides from Group III_L are assembled from amino acid residues from FG strands and FG loop (Table 11). III_L Group is the most widely developed and consists of peptides from (**L7**) to (**L17**).

Peptide PD-L1(19-26) (**L1**) contains F19_L and D26_L important for the protein complex formation. In this part of the protein, A18_L is also important for the interaction; however, it adds a negative contribution to the potential energy of the interaction that destabilizes the protein complex, which is why it was not included in the (**L1**) peptide sequence. For this group, I have not designed any analogues due to the fact that this fragment in protein possesses a disordered structure. Its amino acid sequence is taken from flexible a strand tail, and the structure organization may lead to the loss of affinity to PD-1.

Group II_L consists of peptides from the middle part of the PD-L1 IgV domain. Firstly, I designed peptide PD-L1(52-68) (**L2**) containing – I54_L, Y56_L, E58_L, and Q66_L. The interactions of these residues with the PD-1 protein were observed in the crystal structure of the proteins (Table 2) and determined by the MM/GBSA analysis (Table 7). After the chemical synthesis of peptide (**L2**), I found that its solubility is very low. To enhance it, I prolonged the amino acid sequence in N- and C-terminal by adding hydrophilic amino acids from the protein sequence. I designed the following peptides: PD-L1(52-73) (**L3**), PD-L1(52-79) (**L4**), and PD-L1(45-68) (**L5**). At the end, I decided to examine the shortest peptide PD-L1(56-66) (**L6**), focusing only three amino acids important for stabilizing a complex and lacking hydrophobic residues of leucine (L53_L), isoleucine (I54_L), valines (V55_L, V68_L), and phenylalanine (F67_L) (Table 11).

During designing of the peptides from Group III_L, I focused on the C-terminus of PD-L1 containing FG strands and FG loop which are crucial for the PD-1/PD-L1 complex formation. Group III_L consists of long linear peptides PD-L1(111-127)^{M115Nle} (**L7**) and its shorter version PD-L1(113-126)^{M115Nle} (**L8**) containing - R113_L, A121_L, D122_L, Y123_L, K124_L, R125_L - all essential amino acids residues for the complex formation from the C-terminal part of the protein (Table 2 and Table 7). M115_L in these peptides was substituted by Nle due to the same reason as discussed previously. Despite the fact that according to the per-residue energy decomposition, it possesses negative energy and is valuable for proteins interaction. Group III_L was additionally, expanded by three peptides with intramolecular disulphide bonds PD-L1(113-126)^{(C114-K124C) M115Nle} (**L9**), PD-L1(110-128)^{(V111C-T127C) M115Nle} (**L10**), and PD-L1(111-127)^{(Y112C-I126C) M115Nle} (**L11**). In Group III_L, the analogues of linear peptide PD-L1(113-126) create a whole family, consisting of the aforementioned peptides (**L8**) and (**L9**) but also analogues of peptide (**L9**) where glycine 120 was exchanged with serine (**L12**), phenylalanine (**L13**), and glutamic acid (**L14**) (Table 11). The replacement of the G120_L residue in peptide (**L9**) with the mentioned amino acid residues was dictated by the fact that in the MM/GBSA calculations (per-residue energy decomposition), the G120_L residue slightly destabilizes the PD-1/PD-L1 complex and its substitution could improve the interaction of peptides with PD-1. Therefore, G120_L was replaced by the amino acid residues which can be donors and acceptors of additional hydrogen bonds and van der Waals interactions. I decided also to test the short peptide PD-L1(121-125) (**L15**) containing three amino acids important for the protein complex formation. As

aforementioned, M115_L is also important for the stability of the PD-1/PD-L1 complex, according to the MM/GBBSA analysis (Figure 30). Taking that into consideration, I decided to test peptide PD-L1(111-127) (**L16**) containing the methionine residue in position 115. Both peptides, (**L7**) and (**L16**), were tested to evaluate if these residues may influence the affinity. Moreover, I decided to synthesise peptide (**L17**) the analogue of peptide (**L13**) containing the Met in position 115, not Nle.

Table 11. The amino acid sequences and position in the protein of the designed peptides.

No.		Peptide	Amino acid sequence
L1	Group I _L	PD-L1(19-26)	Ac-FTVTVPKD-NH ₂
L2	Group II _L	PD-L1(52-68)	Ac-ALIVYWENleEDKNIIQFV-NH ₂
L3		PD-L1(52-73)	Ac-ALIVYWENleEDKNIIQFVHGEEED-NH ₂
L4		PD-L1(52-79)	Ac-ALIVYWENleEDKNIIQFVHGEEEDLKVQHS-NH ₂
L5		PD-L1(45-68)	Ac-EKQLDLAALIVYWENleEDKNIIQFV-NH ₂
L6		PD-L1(56-66)	Ac-YWENleEDKNIIQ-NH ₂
L7			PD-L1(111-127) ^{M115Nle}
L8		PD-L1(113-126) ^{M115Nle}	Ac-RAbuNleISYGGADYKRI-NH ₂
L9	Group III _L	PD-L1(113-126) ^(C114-K124C) M115Nle	Ac-RCNleISYGGADYCRIN-H ₂
L10		PD-L1(110-128) ^(V111C-T127C) M115Nle	Ac-GCYRAbuNleISYGGADYKRICV-NH ₂
L11		PD-L1(111-127) ^(Y112C-I126C) M115Nle	Ac-VCRAbuNleISYGGADYKRCT-NH ₂
L12		PD-L1(113-126) ^(C114-K124C) G120S; M115Nle	Ac-RCNleISYGSADYCRIN-H ₂
L13		PD-L1(113-126) ^(C114-K124C) G120F; M115Nle	Ac-RCNleISYGFADYCRIN-H ₂
L14		PD-L1(113-126) ^(C114-K124C) G120E; M115Nle	Ac-RCNleISYGEADYCRIN-H ₂
L15		PD-L1(121-125)	Ac-ADYKR-NH ₂
L16		PD-L1(111-127)	Ac-VYRAbuMISYGGADYKRIT-NH ₂
L17		PD-L1(113-126) ^(C114-K124C) G120F	Ac-RCMISYGFADYCRIN-H ₂

The peptides were synthesized and purified according to the same procedures as the PD-1 derived peptides. The obtained peptides were acetylated at the N-terminal amino group; and the C-terminal of peptides had the amide group. Peptides with intramolecular disulphide bonds were subjected to an oxidation process. If not pointed differently, the cysteine residue in position 114 was replaced by Abu, to prevent dimerization during the oxidation reaction. Additionally, all peptides from Group I_L and III_L were synthesized with a linker on the N-terminal consisting of five glycine residues

and biotin. A linker with biotin was added to the peptides for the evaluation process in the SPR measurements and ELISA.

The peptides from Group II_L were poorly soluble. Despite the use of water, different buffers, and organic solvents, they were not soluble in solutions acceptable in SPR and cellular assays. Difficulties with the solubility of peptides from Group II_L contributed to their exclusion from further analysis. The purification of peptides with disulfide bridges, namely peptides (L12), (L13), and (L17), was hindered due to their poor solubility. Moreover, after introducing a linker, consisting of five glycine residues and biotin, their further enhanced the problem with solubility. The efficiency of the purification process ended up being low, what led to a few rounds of the peptide synthesis.

3.2. Study of binding of PD-L1 based peptides to PD-1 by the SPR and ELISA techniques

The first attempt of obtaining the kinetic parameters of the PD-L1 derived peptides with PD-1 was performed in the conditions of analysis similar to the one mentioned in chapter 2.2. Human glycosylated PD-1 (express system – HEK 293) was immobilized on a CM5 sensor chip and its interaction with human glycosylated PD-L1-Fc (expression system - CHO) was measured. The obtained K_D was 1.04 μ M (Figure 50). In the case of the PD-L1 derived peptides, only for peptide (L1) the binding to PD-1 was detected and the K_D value was calculated ($K_D = 25.7 \mu$ M). Peptide (L16), at higher concentrations, precipitated and bound to the reference flow cell (Figure 50). For peptides (L7), (L9), (L10), (L11), and (L15), these problems were detected even at lower concentrations, which hindered the binding analysis. The examples of obtained sensorgrams are shown in Figure 51.

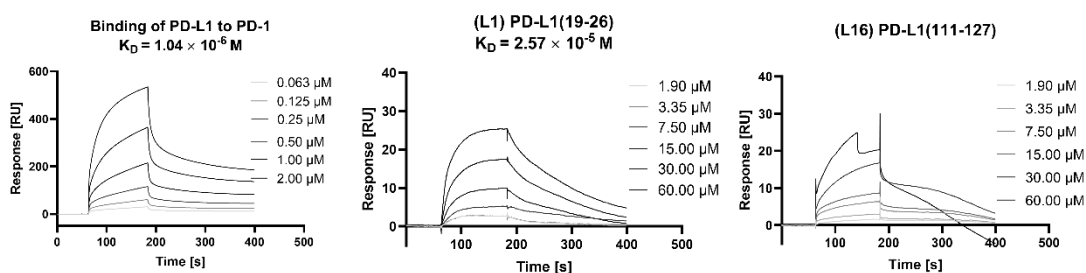


Figure 50. Binding of the PD-L1 protein and the PD-L1 derived peptides to PD-1 immobilized on a CM5 sensor chip surface.

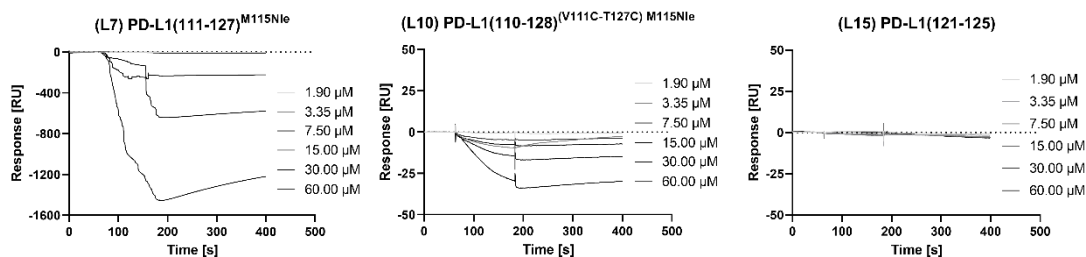


Figure 51. Binding of the PD-L1 derived peptides to the PD-1 protein immobilized on a CM5 sensor chip surface.

After encountering complications during the interaction analysis of the PD-L1 derived peptides with human glycosylated PD-1 immobilized on a sensor chip, I decided to examine an alternative configuration of the system. I immobilized the peptides by the biotin to the streptavidin sensor (SA) chips and titrated the peptides with human glycosylated PD-1. In order to perform this test, I synthesized peptides prolonged on the N-terminal by the five glycine linker and biotin.

Subsequently, I immobilized biotinylated (**L13**) peptide on the SA chip and measured the interaction with the PD-1 protein. Although some increase in response was detected when increasing the concentration of human glycosylated PD-1 was injected, the quality of the obtained results was insufficient for a reliable kinetic analysis. The response was only registered for the two highest tested concentrations. After obtaining the result, I took into consideration the molecular mass of the tested molecules. Molecular mass of the synthesized biotinylated peptides ranges between around 1100-2600 Da and the molecular mass of human glycosylated PD-1 is 30-40 kDa. The difference in the size of the tested molecules and the immobilization of the smaller molecule on the sensor may lead to the unavailability of the PD-1 binding pockets. To reduce the difference in the size of the tested molecules, I decided to examine the binding of the PD-L1 derived peptides (immobilized on a sensor chip) with the human PD-1 produced in the *Escherichia coli* (*E. coli*) system. This protein is characterized by the lack of post-translational glycosylation. The molecular mass of human PD-1 produced in the *E. coli* expression system is 13.5 kDa.

At the beginning, I measured the interaction between two proteins. To obtain the kinetic parameters of the interaction the human glycolyzed PD-L1 (with biotin) was immobilized on an SA sensor chip and titrated by PD-1 expressed in *E. coli*. at the concentration range from 310 nM to 10 μM (Figure 52A). For the highest

concentrations, the precipitation of PD-1 and its binding to the reference flow cell was observed. In the applied experimental condition, the K_D for the interaction of PD-1 with PD-L1 is 22.6 nM (Figure 52B).

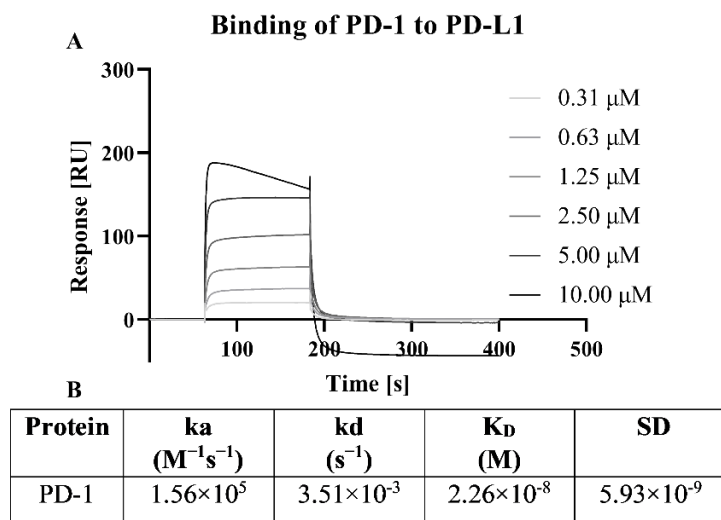


Figure 52. The SPR profile of PD-L1 treated by different concentrations of PD-1. A) Sensorgrams showing the relation between the detected signal of PD-1 binding to PD-L1 in time. B) The binding kinetics parameters from the SPR analysis calculated with the Biacore T200 Evaluation Software.

In the next step, the PD-L1 derived peptides were subjected to the binding analysis by the SPR technique. The biotinylated peptides were immobilized on the surface of the SA sensor chips and titrated with PD-1 (expressed in *E. coli*). The obtained results are shown in Figures 53 (peptides interacting with PD-1) and 54 (peptides that show no interaction with PD-1), and the binding kinetics parameters are collected in Table 12.

The peptide (**L1**) from Group I_L, in the applied conditions, shows no interaction with PD-1 (Figure 54) or the interaction is too weak to establish reliable K_D .

In the Group III_L, PD-1 bound to ten of the eleven peptides. PD-1 showed no interaction with the shortest linear peptide, (**L15**) (Figure 54). The weakest affinity was determined for linear peptide (**L7**), the obtained K_D for peptide (**L7**)/PD-1 complex was 198 μM (Figure 53). Peptide (**L16**) – the analogue of (**L7**) with methionine residue in position 115 instead of Nle, bound to PD-1 with K_D 3.20 μM , which is two orders of magnitude stronger than (**L7**). Another linear peptide which was tested, (**L8**), showed a stronger affinity to PD-1 than (**L7**); however, the difference is only about one order of magnitude and the obtained K_D was 14.9 μM . The analogues of peptide (**L8**) with a disulphide

bond, namely peptides (**L9**) and from (**L12**) to (**L14**), showed a comparable dissociation constants ranging between 52.4 - 33.5 μM . Peptide (**L17**), the analogue of (**L13**) with native M115_L instead of Nle, showed a stronger interaction with PD-1 than its precursor, reaching K_D of 1.99 μM , while for (**L13**) the K_D was calculated at 42.2 μM . Peptide (**L8**) and its analogues, (**L9**), (**L12**), (**13**) and (**L14**), displayed similar kinetic profiles with a slow dissociation rate between 6.97 - $1.94 \times 10^{-4} \text{ s}^{-1}$ (Table 12). Among the peptides with disulphide bonds, the highest affinity was obtained for PD-1 binding to peptide (**L11**). (**L11**)/PD-1 had a different kinetic profile than the other tested peptides from this group and it was similar to the kinetic profile of PD-1 binding to PD-L1 (Figure 52). The binding was characterized by fast association $k_a = 3.58 \times 10^3 \text{ M}^{-1}\text{s}^{-1}$ (Table 12). The longest peptide from this group, (**L10**), was characterized by the K_D of 22 μM , which was lower by one order of magnitude than for peptide (**L11**) which is shorter by only two amino acids and binds PD-1 almost eleven times stronger.

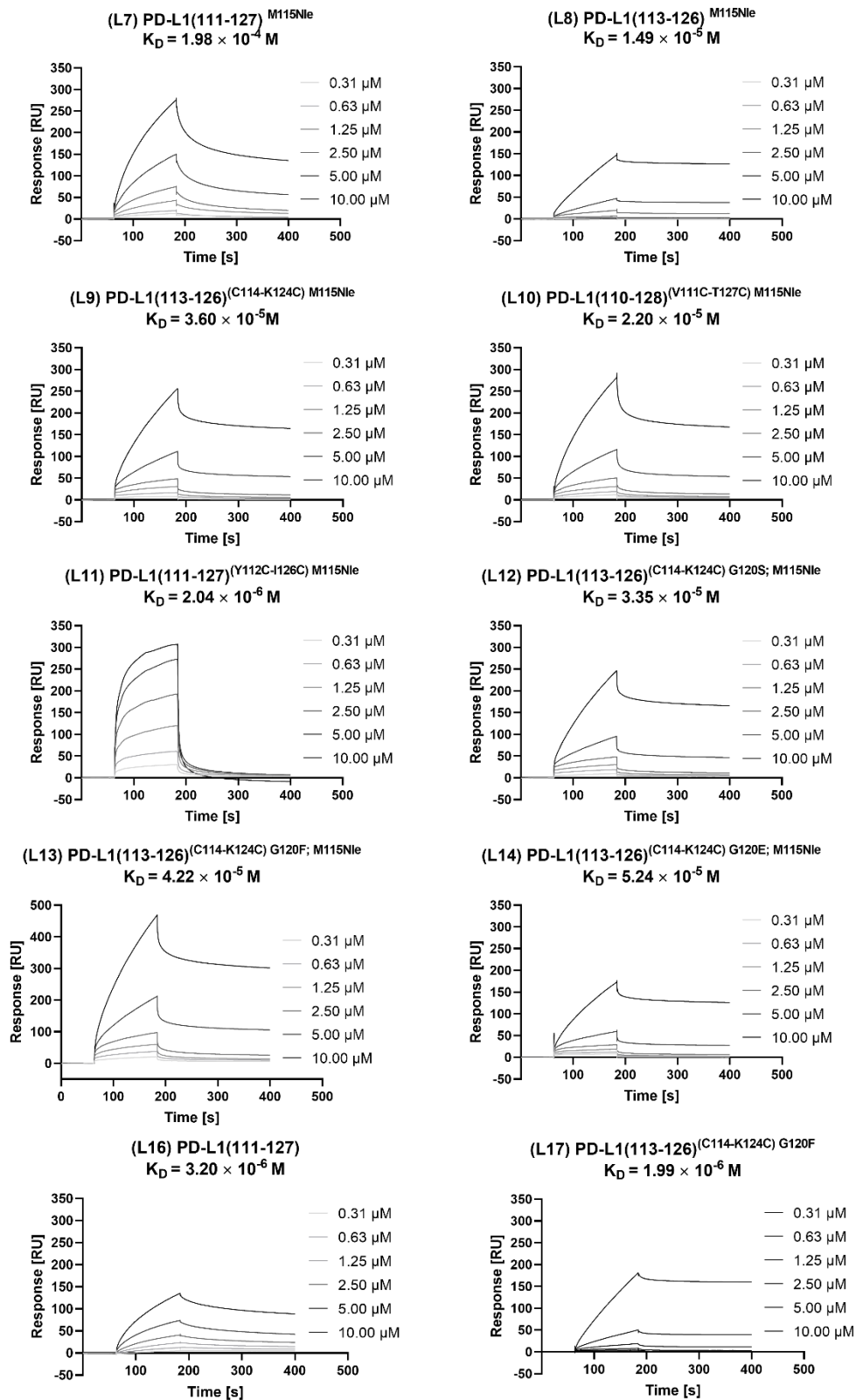


Figure 53. Sensorgrams of PD-1 interacting with the PD-L1 derived peptides analysed using the SPR technique.

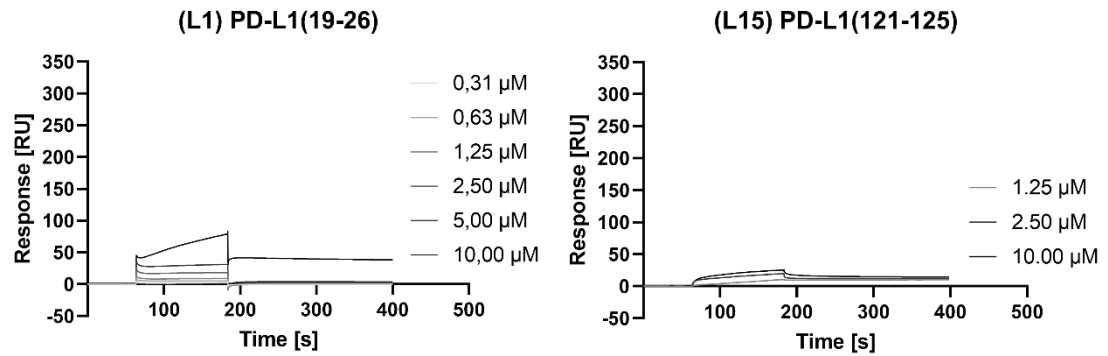


Figure 54. Sensorgrams of the noninteracting PD-L1 derived peptides with PD-1 analysed using the SPR technique.

Table 12. Association and dissociation rates and dissociation constants calculated for PD-1 binding to the PD-L1 derived peptides from the SPR data. Results were calculated using the Biacore T200 Evaluation Software from at least three independent titration analyses. The applied binding model 1:1. ND - not determined (no binding detected or binding too weak to establish reliable constants), SD – standard deviation

	No	Peptides	k_a ($M^{-1}s^{-1}$)	k_d (s^{-1})	K_D (M)	SD
Group I _L	L1	PD-L1(19-26)	ND	ND	ND	ND
Group III _L	L7	PD-L1(111-127) ^{M115Nle}	1.09×10^1	1.79×10^{-3}	1.98×10^{-4}	1.04×10^{-4}
	L8	PD-L1(113-126) ^{M115Nle}	2.47×10^1	1.94×10^{-4}	1.49×10^{-5}	9.92×10^{-6}
	L9	PD-L1(113-126) ^{(C114-K124C) M115Nle}	1.06×10^1	3.99×10^{-4}	3.60×10^{-5}	3.18×10^{-6}
	L10	PD-L1(110-128) ^{(V111C-T127C) M115Nle}	3.31×10^1	7.10×10^{-4}	2.20×10^{-5}	9.14×10^{-6}
	L11	PD-L1(111-127) ^{(Y112C-I126C) M115Nle}	3.58×10^3	6.70×10^{-3}	2.04×10^{-6}	5.17×10^{-7}
	L12	PD-L1(113-126) ^{(C114-K124C) G120S; M115Nle}	1.37×10^1	4.49×10^{-4}	3.35×10^{-5}	7.74×10^{-6}
	L13	PD-L1(113-126) ^{(C114-K124C) G120F; M115Nle}	1.94×10^1	6.97×10^{-4}	4.22×10^{-5}	2.88×10^{-5}
	L14	PD-L1(113-126) ^{(C114-K124C) G120E; M115Nle}	1.05×10^1	4.89×10^{-4}	5.24×10^{-5}	2.55×10^{-5}
	L15	PD-L1(121-125)	ND	ND	ND	ND
	L16	PD-L1(111-127)	5.31×10^2	1.67×10^{-3}	3.20×10^{-6}	6.89×10^{-7}
L17	PD-L1(113-126) ^{(C114-K124C) G120F}	1.39×10^2	2.91×10^{-4}	1.99×10^{-6}	2.09×10^{-7}	

During the SPR analyses, I used PD-1 produced in the *E. coli* system which is characterized by the lack of glycosylation. However, this system is not a native state in a human organism, where PD-1 undergoes post-translational N-glycosylation. Therefore, I decided to perform an indirect ELISA to confirm if the PD-L1 derived peptides interact with human glycosylated PD-1.

In my research, I performed indirect ELISA on streptavidin coated 96-well plates. The schematic procedure of the assay is presented in Figure 55. The biotinylated peptides were pre-coated on the plate (1). In the next step, the glycosylated PD-1-Fc was added (2). The Fc region in PD-1 is necessary for the detection of protein by the secondary antibody anti-human IgG Ab-conjugated with HRP (3). In the last step, I added TMB substrate to catalyse the enzymatic colour reaction (4). As more PD-1-Fc protein bind to the peptide immobilized on the plate, the absorbance will be more intense.

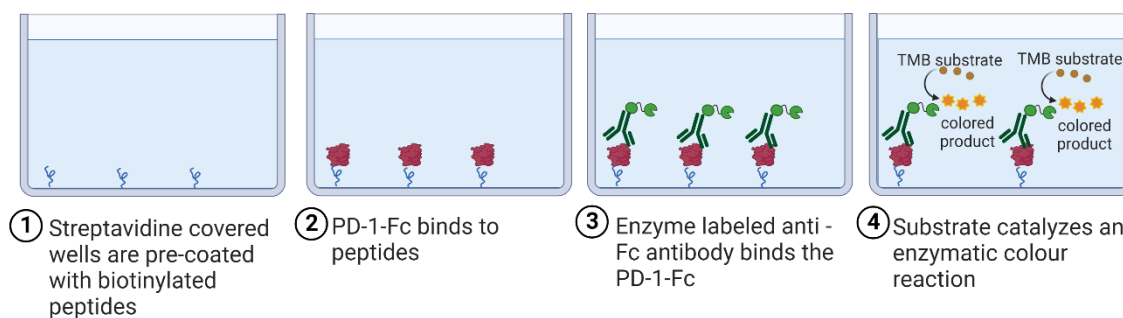


Figure 55. Scheme of indirect ELISA.

Before performing ELISA, I optimised the condition of the test by investigating the different concentrations of biotinylated peptides used to pre-coat the wells and different concentrations of human PD-1. Finally, I immobilized, on the streptavidin plate, four different concentrations of biotinylated (**L16**) peptide. (**L16**) is characterized by the one of the lowest K_D (strong binding) in the complex with PD-1 obtained in SPR and it served as a reference peptide. I started from 20 $\mu\text{g/ml}$ of peptide and made 10-fold dilutions. I prepared the PD-1 protein in 2-fold dilutions starting from 4 $\mu\text{g/ml}$. For the highest tested peptide concentration, I observed the smoothest concentration-dependent response for PD-1 (Figure 56). For lower peptide concentrations, the concentration-dependent response for PD-1 was not as clearly defined. I also tested a higher peptide concentration to pre-coat the plate, however, no significant changes in the absorbance signal were observed. That can indicate that 20 $\mu\text{g/ml}$ of peptide is sufficient to saturate the well surface. Though, to test the peptides binding to PD-1, I pre-coated wells using 20 $\mu\text{g/ml}$ of peptides and a wider spectrum of PD-1 concentration than in the optimization step; as a positive control, I pre-coated the plate with biotinylated PD-L1 (Figure 57).

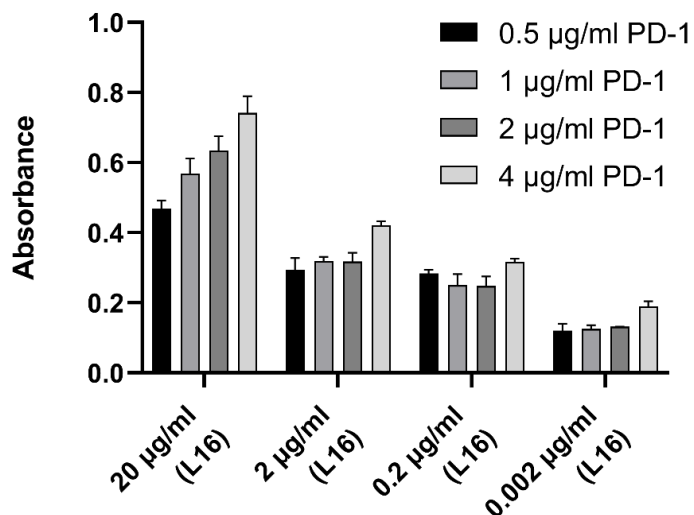


Figure 56. *Optimization of the ELISA condition.*

The titration assay showed that PD-1 binds to all tested PD-L1-derived peptides in a concentration-dependent manner (Figure 57). The strong binding of PD-1 was observed to peptide (L7) with a statistical significance for all examined concentrations. Slightly weaker interaction with PD-1 was observed for peptide (L9). This peptide significantly binds the PD-1 at a concentration above 1 µg/ml. PD-1 from concentration of 1 µg/ml and higher binds to peptides (L11), (L12), (L13), (L14), and (L16) with a statistical significance.

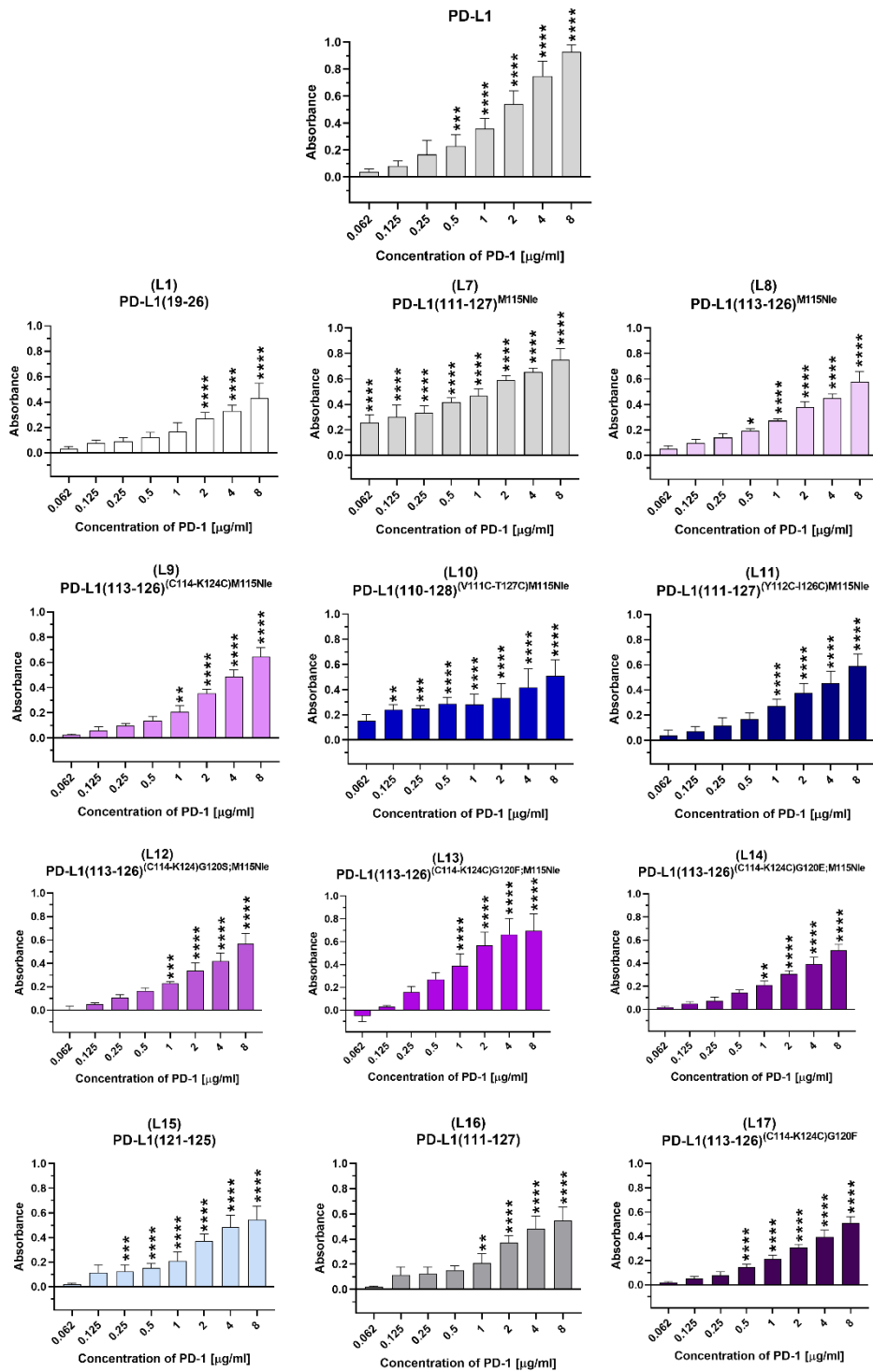


Figure 57. Binding of PD-1 to the PD-L1 and the PD-L1 derived peptides analysed using indirect ELISA. Results are shown for three experiments performed independently in triplicate. Data are depicted as mean with SD (Mean \pm SD). Statistical analysis was performed using one-way ANOVA followed by the Dunnet's post-hoc test. ****: $p < 0.0001$, ***: $p < 0.001$, **: $p < 0.01$, *: $p < 0.05$.

3.3. Stability of the designed peptides and their effects on the viability of chosen cell lines

The next step of my research was the evaluation of the selected peptides regarding their influence on the viability of cell lines used in the planned *in vitro* assays and the stability in the medium used in cell cultivation. The first action, as in the case of the PD-1 derived peptides, was the assessment of their stability in the RPMI 1640 medium with 10% of heat-inactivated FBS. As a control, I used peptides dissolved in water in time 0 h. The procedure for the stability experiment and cell viability assay was described previously in chapter 2.3. The obtained results are presented in Figure 58.

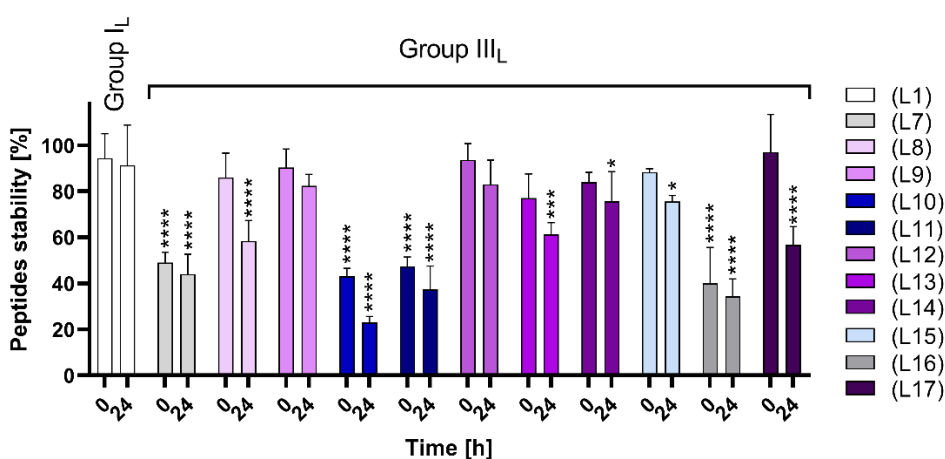


Figure 58. Peptides stability in the RPMI 1640 medium at time 0 and 24 h. The percentage of stability was established by comparing the peak area of control in time 0 h with the peak area for the collected samples. Results were obtained through the RP-HPLC analysis method. Results are shown for three experiments performed independently. Data are depicted as mean with SD (Mean \pm SD). Statistical analysis was performed using one-way ANOVA followed by the Dunnet's post-hoc test. ****: $p < 0.0001$, ***: $p < 0.001$, **: $p < 0.01$, *: $p < 0.05$.

The best stability in RPMI 1640 with 10% FBS was received for peptide (L1) from Group I_L. For this peptide, a 6% decrease in the peptide content in time 0 h was observed compared to the control. Between time 0 and 24 h additional, but only slight, drop of the peptide content was noticed (about 3%).

For all peptides from Group III_L the decrease of the peptide amount compared with the control was detected. For the shortest linear peptide (L15) (Figure 59), a moderate decrease in concentration was observed and its content level compared to the control was 88% and 76% for time 0 and 24 h, respectively. Two linear peptides (L7) and (L16), differing by about one amino acid residue, Nle or Met in position 115, were characterized by a significant drop of concentration in time 0 h to the level of 49% and

40%, respectively. After 24 h of incubation, a further decrease of the peptides content was registered and it reached 44% and 34% of the control. For the last linear peptide from this group, **(L8)**, a minor drop of the concentration lower than for its longer analogue, **(L7)**, was observed. In time 0 h, its content was set at the 86% and after 24 h at 58%. Five peptides, **(L9)**, **(L12)**, **(L13)**, **(L14)**, and **(L17)**, disulfide bonded analogues of **(L8)**, showed a moderate decrease of concentration in time 0 h and further decrease after 24 h compared to the control. For time 0 h, the decrease in the range of 3-16% was detected and after 24 hours of incubation, it was 17-43%. The two longest disulphide bonded peptides from this group, peptide **(L10)** and **(L11)**, exhibited the strongest drop of the content for about 57% and 53% in time 0 h and a further decrease for 20% and 14% after 24 h of incubation (Figure 59).

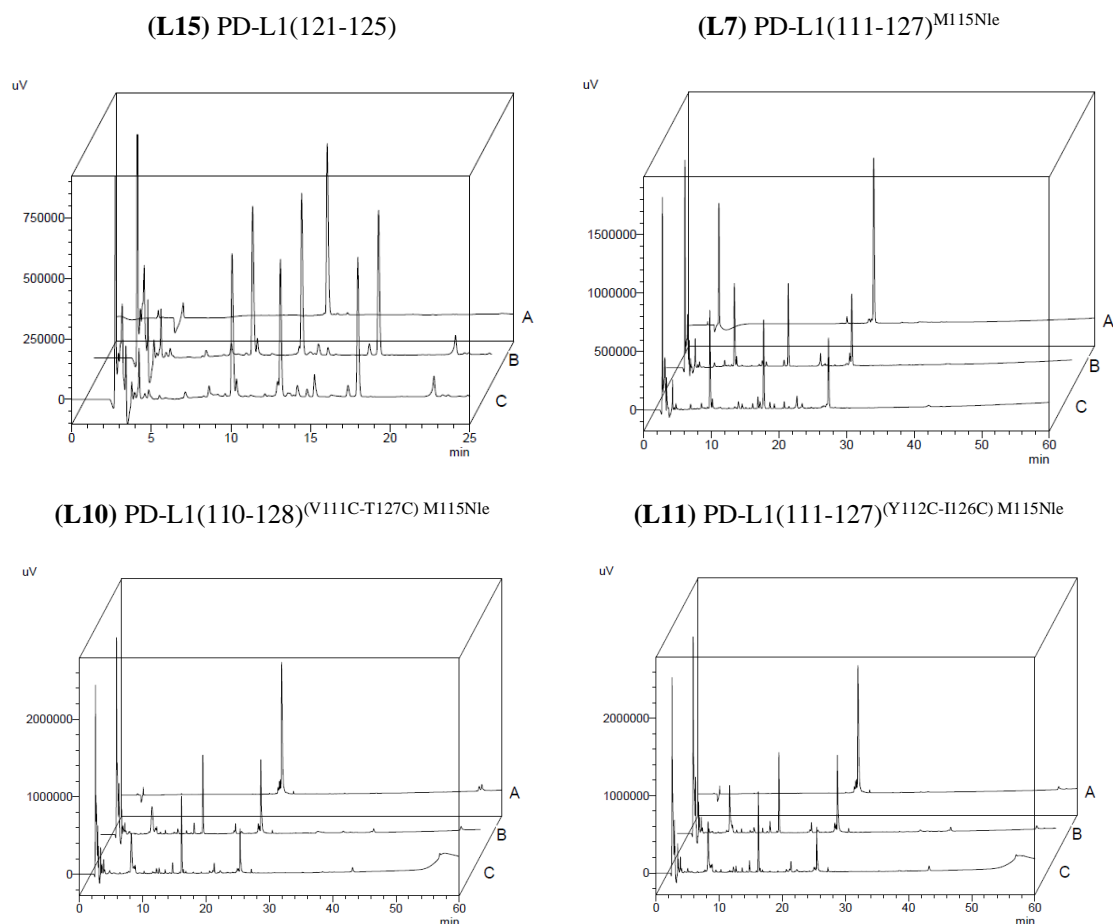


Figure 59. Chromatograms registered for peptides **(L15)**, **(L7)**, **(L10)**, and **(L11)**. A) peptide in water $t=0$ h, B) peptide in medium $t=0$ h, C) peptide in medium $t=24$ h.

Subsequently, I evaluated the viability of the Jurkat E6.1 cell line and TCS Ctrl after the treatment with the PD-L1-derived peptides for 24 h. The test was performed in the same conditions as in the case of peptides derived from the PD-1 protein and which was

described in chapter 2.3. In this part of my research, the influence of peptides on the CHO-K1 cell line was not evaluated. CHO-K1 cell line was not used in further research due to the change of the functional cell assay. The results were compared to the non-treated cells and normalised (Figure 60). Five examined peptides, (L7), (L11), (L12), (L13), and (L17) had a significant negative effect on the viability of the Jurkat E6.1 cell line at the highest tested concentration leading to the decrease of the number of living cells to 68%, 82%, 38%, 3%, and 9%, respectively. For the lower concentrations, the changes were not significant.

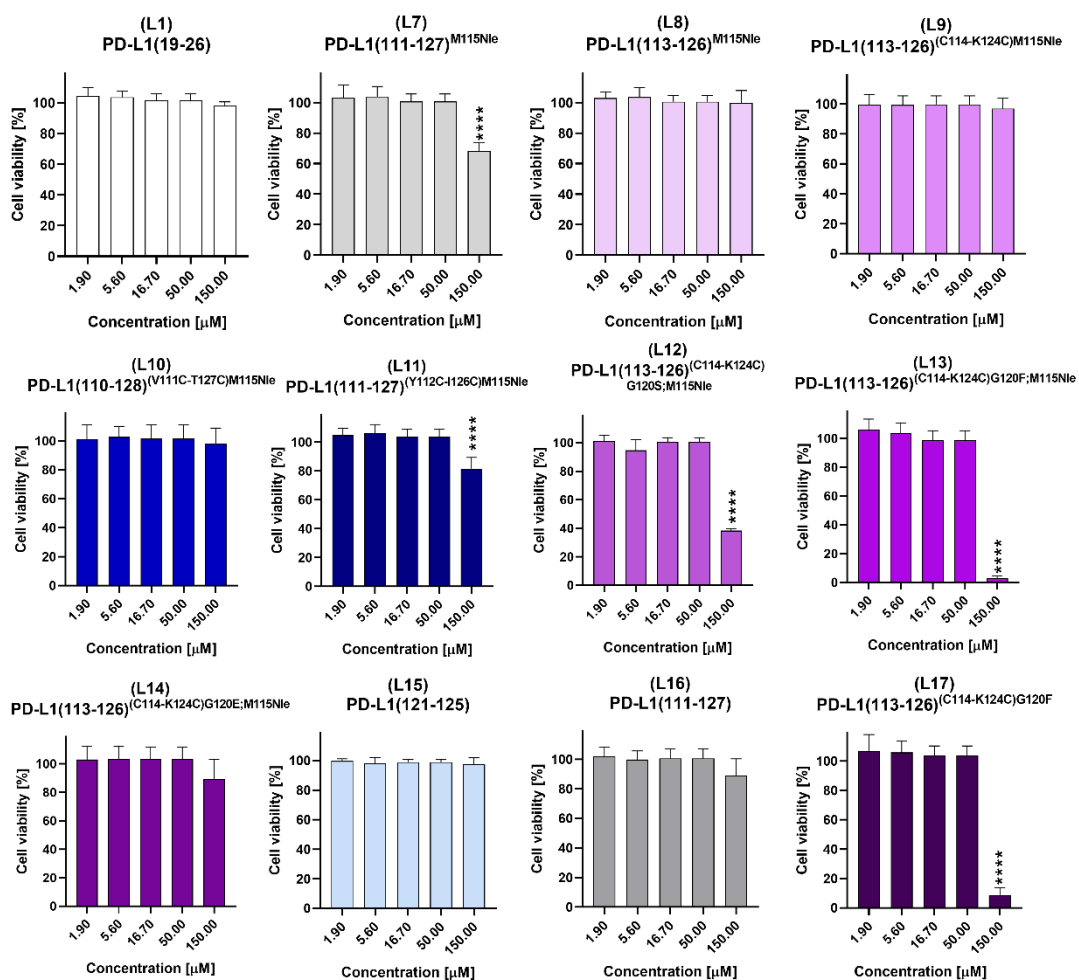


Figure 60. Cell viability assay used to define the influence of the PD-L1 derived peptides on the Jurkat E6.1 cell line after incubation for 24 hours. Results are shown for three experiments performed independently in triplicate. Data are depicted as mean with SD (Mean +/- SD). Statistical analysis was performed using one-way ANOVA followed by the Dunnet's post-hoc test. ***: $p < 0.0001$, **: $p < 0.001$, *: $p < 0.01$, *: $p < 0.05$.

In the case of the TCS Ctrl cells, the tested peptides affected them more intense than the Jurkat E6.1 cells. Only the highest concentration of peptide (L12) had a negative effect

on cell viability (Figure 61). Similar to the peptide (**10**) analogues, the rest of the PD-L1 derived peptides led to the TCS Ctrl cells proliferation. This effect was the most strongly observed for peptide (**L7**) which led to a statistically significant proliferation at all tested concentrations. For this peptide, an increase of living cells was between 23-27% compared to the control. Moreover, for eight peptides, the increase of living cells above 20% was noticed, namely for peptides (**L1**), (**L8**), (**L11**), (**L12**), (**L14**), (**L15**), and (**L17**).

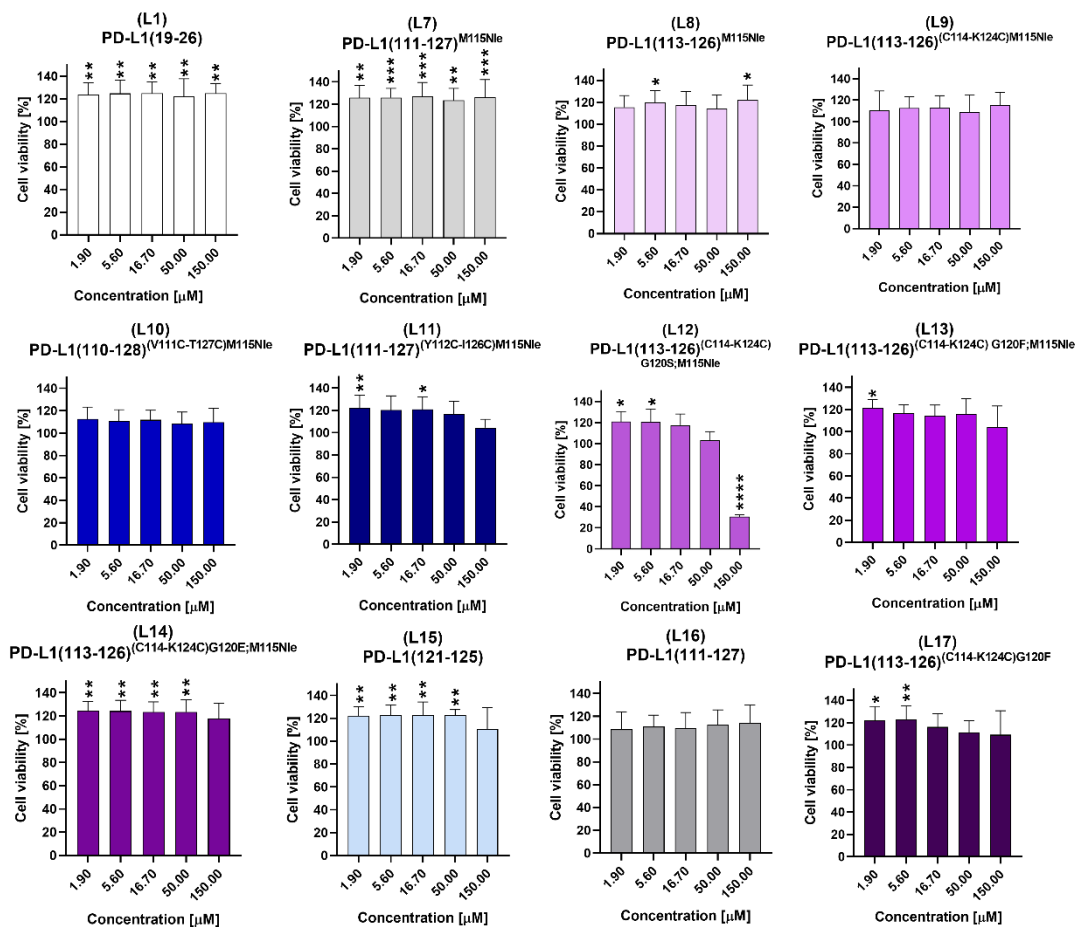


Figure 61. Cell viability assay used to define the influence of the PD-L1 derived peptides on the TCS Ctrl cell line after incubation for 24 hours. Results are shown for three experiments performed independently in triplicate. Data are depicted as mean with SD (Mean +/- SD). Statistical analysis was performed using one-way ANOVA followed by the Dunnet's post-hoc test. ****: $p < 0.0001$, ***: $p < 0.001$, **: $p < 0.01$, *: $p < 0.05$.

3.4. Cell-Binding Assay and Competitive Inhibition

The binding and competitive properties of the PD-L1 derived peptides against PD-L1 were studied using the PD-1 expressing Jurkat E6.1 cell line (J-NF- κ B::eGFP PD-1, J-PD-1). I performed these studies in prof. Peter Steinberger laboratory from the Division of Immune Receptors and T cell Activation at the Medical University of Vienna under the supervision of Ph.D. Claire Battin. The assay was performed to examine the capacity of the peptides in inhibiting the binding of the human glycosylated PD-L1-Fc protein to the PD-1 protein located on J-NF- κ B::eGFP PD-1, reporter PD-1. In the assay, as a control, I used Jurkat cells without the expression of PD-1, J-NF- κ B::eGFP Ctrl, reporter Ctrl. Experimental conditions corresponded to the ones described in chapter 2.4. The expression of PD-1 on the reporter PD-1 cell surface was confirmed and described in chapter 3.5. (Figure 66).

Before performing the competition assay, I optimised the conditions of the test by investigating two different anti-human IgG antibodies, PE-labelled donkey anti-human IgG antibody and APC-labelled mouse anti-human IgG antibody. The obtained results are similar to the ones obtained for the detection of PD-1-Fc. The anti-human IgG PE-labelled Ab yielded a stronger response than anti-human IgG APC-labelled Ab, which was preferable for the test outcome as the difference between control and the sample of interest was bigger. Moreover, I tested six different concentrations of the human PD-L1 protein (Figure 62). The results obtained from the titration experiment show that use of a higher concentration of the PD-L1 protein than 1 μ g/ml was not required and this concentration was enough to saturate the PD-1 molecules on the cell surface. The difference between 1 μ g/ml and 2 μ g/ml of PD-L1 was only 4 units of gMFI. The use of lower concentrations of this protein can yield a not sufficiently strong signal to precisely define if the tested peptides displaced the PD-L1 from the complex with PD-1. Taking together, the obtained results for the assay, I chose PE-labelled mouse anti-human IgG antibody and the PD-L1 protein at the concentration of 1 μ g/ml.

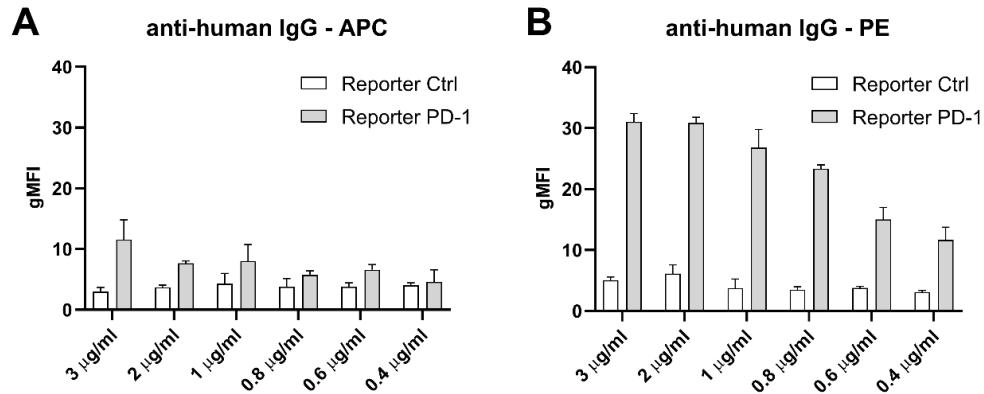


Figure 62. Optimization of the competition test conditions. Comparison of two anti-human IgG antibodies A) APC- and B) PE-labelled detecting human IgG.

Target cells were probed with peptides at three different concentrations from 50 μM to 5.5 μM . In the case of the PD-L1-derived peptides, the titration assay showed that the best inhibitory properties were observed for peptides (L1) and (L11) (Figure 63). These peptides blocked the binding of PD-L1 to PD-1 at a concentration of 50 μM , in 16% and 32%, respectively. Moreover, they had a dose-dependent effect. A slightly weaker blocking effect was also observed for peptides (L9) and (L10) while no concentration-dependent effect was detected for the rest of the tested peptides.

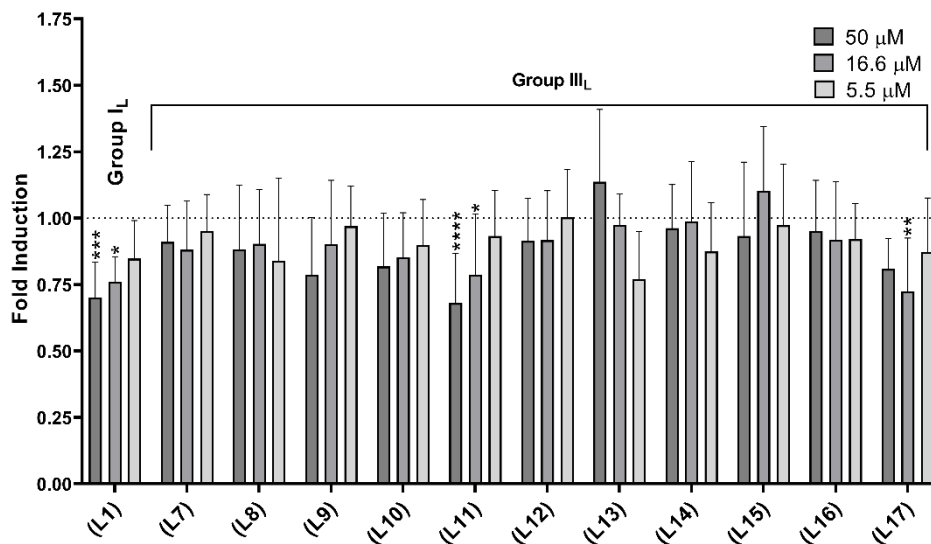


Figure 63. Competitive inhibition of peptides against the PD-1/PD-L1 complex formation. The Jurkat PD-1 cells were incubated with the PD-L1-derived peptides, the final concentration used in the experiment ranged from 50 μM to 5.5 μM . The bar diagram shows the fold induction of gMFI for at least three experiments performed independently in triplicate. Data were normalised to the gMFI received for reporter PD-1 cell line treated by PD-L1. Data are depicted as mean with SD (Mean \pm SD). Statistical analysis was performed using one-way ANOVA followed by the Dunnet's post-hoc test. ****: $p < 0.0001$, ***: $p < 0.001$, **: $p < 0.01$, *: $p < 0.05$.

3.5. Stimulation assay

Evaluation of the inhibitory properties of the PD-L1 derived peptides was performed in the functional cellular assay based on reporter gene expression system, NF- κ B::eGFP, constructed on Jurkat E6.1 cell line, not the commercially available NFAT reporter mediated luminescence cell-based assay used for the PD-1 derived peptides. I performed this part of my research in prof. Peter Steinberger laboratory in the Division of Immune Receptors and T cell Activation at the Medical University of Vienna under the supervision of Ph.D. Claire Battin. I used the T cell reporter platform for the evaluation of ICIs previously established by the group of prof. Peter Steinberger²⁴⁸⁻²⁵⁰.

The inhibitory properties of the peptides were assessed in a coculture assay composed of a reporter gene expression system, NF- κ B::eGFP, constructed on the Jurkat E6.1 cell line expressing PD-1 also known as the reporter cell line (J-NF- κ B::eGFP PD-1) and T cell stimulator expressing PD-L1 (TCS PD-L1). As already mentioned, T cell requires two signals for full activation (Introduction 2.3.). To activate the PD-1 reporter cell line (signal I), I used TCS PD-L1. TCS PD-L1, express membrane-bound anti-human CD3 single-chain variable fragment (scFv) (mb aCD3) that engages the CD3-TCR complex with TCR present on the reporter cells yielding the first signal required to stimulate T cells. Upon stimulation by TCS PD-L1, NF- κ B is upregulated in the PD-1 reporter cells line (J-NF- κ B::eGFP PD-1) and inhibition can be assessed by the measurement of the transcriptional level of eGFP. When PD-1 creates a complex with PD-L1, the eGFP expression is reduced, when the PD-1/PD-L1 complex is disrupted, the eGFP expression increases.

To validate and choose the optimal platform for testing the properties of the peptides for the inhibition of the PD-1/PD-L1 complex formation, I examined different coculture conditions. In this experiment, I used cell lines described in Table 13.

Table 13. Description of the cell lines used in the stimulation assay.

Cell line name	Description of the cell line
J-NF-κB::eGFP Ctrl	the NF- κ B::eGFP reporter cells constructed on the human Jurkat E6.1 cell line expressing CD28 (without expression of PD-1), also known as the reporter Ctrl
J-NF-κB::eGFP PD-1	the NF- κ B::eGFP reporter cells constructed on the human Jurkat E6.1 cell line expressing CD28 and PD-1, also known as the reporter PD-1
TCS Ctrl	the cell line expressing mb aCD3 constructed on the BW5147 cell line
TCS PD-L1	the cell line which express mb aCD3 and PD-L1 constructed on the BW5147 cell line
TCS CD86 Ctrl	the cell line which express mb aCD3 and CD86 (CD86 interacts with CD28 on the J-NF- κ B::eGFP cell line) constructed on the BW5147 cell line
TCS CD86/PD-L1	the cell line which express mb aCD3, CD86 and PD-L1 constructed on the BW5147 cell line
wtBW	wild type of BW5147 cell line – mb aCD3, CD86 and PD-L1 negative.

The schema of cell cocultures performed for experiment optimisation, presenting steps of activation and inhibition of the eGFP expression, is shown in Figure 64. In the experiment, I tested five different combinations of the TCS **1) TCS Ctrl**, **2) TCS PD-L1**, **3) TCS CD86 Ctrl**, **4) TCS CD86/PD-L1** and **5) wild type BW5147 (wtBW)** with two reporter cell lines **1) J-NF- κ B::eGFP Ctrl** and **2) J-NF- κ B::eGFP PD-1**. The wtBW cell line is not included in the schema as it has no influence on the eGFP expression by the reporter cell lines. Two tested reporter cell lines J-NF- κ B::eGFP Ctrl and J-NF- κ B::eGFP PD-1 expressed costimulatory receptor CD28. The introduction of the costimulatory ligand CD86 to the cell line (TCS CD86/PD-L1) enhanced the eGFP expression by additional stimulation of the reporter cells by creating the CD28/CD86 complex. The CD28 is not shown on the cell surface of J-NF- κ B::eGFP Ctrl and J-NF- κ B::eGFP PD-1 in two first experimental systems - TCS Ctrl and TCS PD-L1 as it did not influence the outcome of the experiment due to the lack of CD86. In the final step, I added to the cell coculture the pembrolizumab to measure the variation in the eGFP expression in the presence and absence of the PD-1/PD-L1 complex inhibitor.

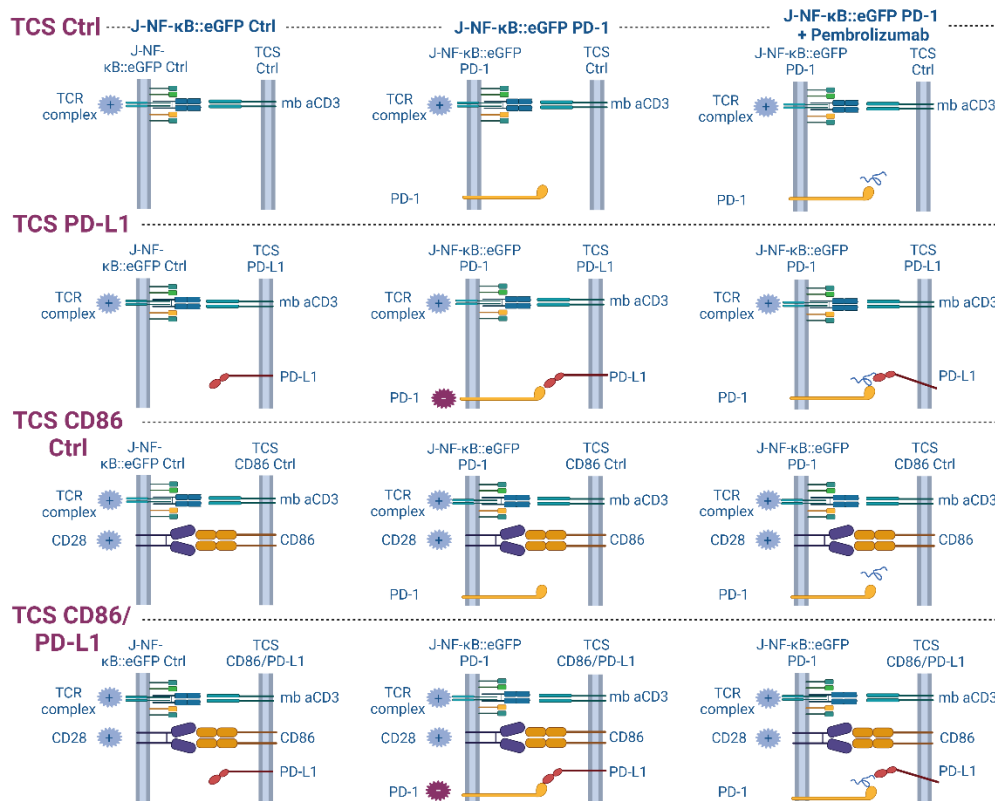


Figure 64. Schematic representation of cell cocultures performed for the experiment optimisation, presenting the steps of activation and inhibition of the eGFP expression. “+” - the eGFP gene expression activated, “-” - the eGFP gene expression inhibited.

The conditions of cell coculture presented in Figure 64 were examined by the eGFP expression. The results are shown in Figure 65. For the J-NF- κ B::eGFP Ctrl, the cell line activation was on a comparable level when TCS Ctrl and TCS PD-L1 were used. Coculturing of J-NF- κ B::eGFP Ctrl with TCS CD86 and TCS CD86/PD-L1, resulted in a higher expression of eGFP compared to the one received for TCS Ctrl and TCS PD-L1. It is an effect of the additional stimulation signal from CD28/CD86. On the contrary to the reporter Ctrl, the expression of eGFP by the J-NF- κ B::eGFP PD-1 reporter cells was diminished upon stimulation by TCS PD-L1 and TCS CD86/PD-L1 due to the formation of the PD-1/PD-L1 complex. This effect was abolished in the presence of a therapeutic anti-PD-1 antibody. The received results indicate that creating the complex between PD-1 and PD-L1 suppressed the reporter gene expression even though the CD28/CD86 complex had been created. The stimulation signal from CD80/CD86 led to a higher reporter gene expression, and in this system, the effect of the reporter gene suppression induced by the PD-1/PD-L1 complex formation was more visible. Taking this into consideration, I chose TCS CD86/PD-L1 as stimulators of the PD-1 reporter cells for the evaluation of the peptides.

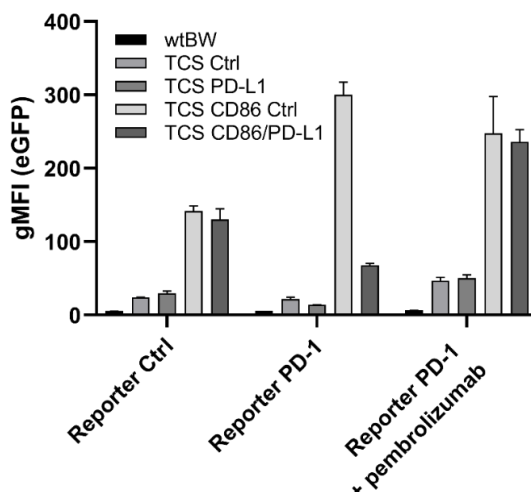


Figure 65. The analyses of the eGFP expression upon the J-NF- κ B::eGFP Ctrl or PD-1 stimulation by wtBW or the TCS (Ctrl, PD-L1, CD86 Ctrl, and CD86/PD-L1). The cells were also stimulated in the presence of pembrolizumab, therapeutic Ab used in the clinical practice.

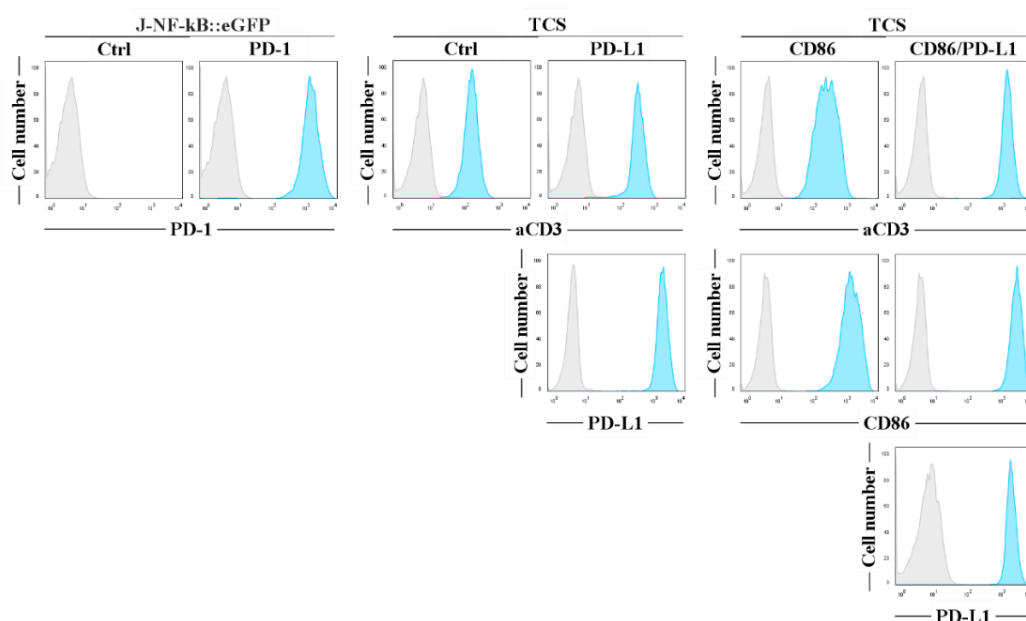


Figure 66. Flow cytometry analysis of the molecular profile of cell lines used in the stimulation assay. The PD-1 expression on reporter J-NF- κ B::eGFP PD-1 and no expression on J-NF- κ B::eGFP Ctrl (left). The flow cytometry analysis of TCS Ctrl and PD-L1 confirming presence or absence of aCD3 and PD-L1 (middle). The flow cytometry analysis of TCS CD86 and TCS CD86/PD-L1 confirming the presence or absence of surface aCD3, CD86 and PD-L1 (right). Light grey histograms: staining of control cells. As a negative control for mb aCD3, wtBW were used. Blue histograms: staining of the indicated molecules.

The molecular profiling of cell lines used in the stimulation assay was performed using the flow cytometry technique. I confirmed the high levels of PD-1 on J-NF- κ B::eGFP PD-1 and the absence of PD-1 on J-NF- κ B::eGFP Ctrl cells (Figure 66 left). Moreover, I also confirmed the presence of mb aCD3 on TCS Ctrl, TCS PD-L1, TCS CD86 Ctrl,

and TCS CD86/PD-L1. As a mb aCD3 negative cell line, I used wtBW. The presence and absence of PD-L1 and CD86 on the selected cell lines were also confirmed (Figure 66, histograms in the middle and right side).

Subsequently, the PD-1 reporter cells were stimulated by TCS CD86 expressing PD-L1 (TCS CD86/PD-L1) in the presence and absence of the PD-L1 derived peptides, at a final concentration in the range 150-5.5 μ M, except the peptides which exhibited the cytotoxic effect on the cell lines used in the assay, namely **(L12)**, **(L13)**, and **(L17)**. Those peptides were examined in the concentration between 50-5.5 μ M. The inhibitory properties of the peptides were measured by reporter gene expression (NF- κ B::eGFP) using flow cytometry and normalised to gMFI of eGFP received for the PD-1 reporter/TCS CD86 cells treated by the selected peptides (Figure 67). Additionally, pembrolizumab, anti-PD-1 mAb, at a concentration 1 μ g/ml was used as a positive control. When a peptide inhibits the PD-1/PD-L1 complex formation, the reporter gene expression should be restored leading to the increase of the signal from eGFP compared with the control - eGFP expression level from the coculture of the PD-1 reporter cells with TCS CD86/PD-L1 without the peptides (Figure 67, dotted line). After normalisation, the signal was restored for all tested peptides at the highest used concentration (Figure 67). For most of the tested peptides, the concentration-dependent effect was observed - **(L1)**, **(L7)**, **(L9)-(L13)**, **(L15)-(L17)**. Although, only the result for peptides **(L11)**, **(L12)** and **(L13)** were statistically significant. However, peptides **(L12)** and **(L13)** had an influence on the eGFP expression by the reporter PD-1 cell stimulated with TCS CD86 Ctrl - without PD-L1 (Figure 68 - light grey bars). This effect, after result normalisation, gives a false positive result. Peptide **(L11)** had no influence on the eGFP expression by the reporter PD-1 cell stimulated with TCS CD86 Ctrl and may be considered as a PD-1/PD-L1 inhibitor.

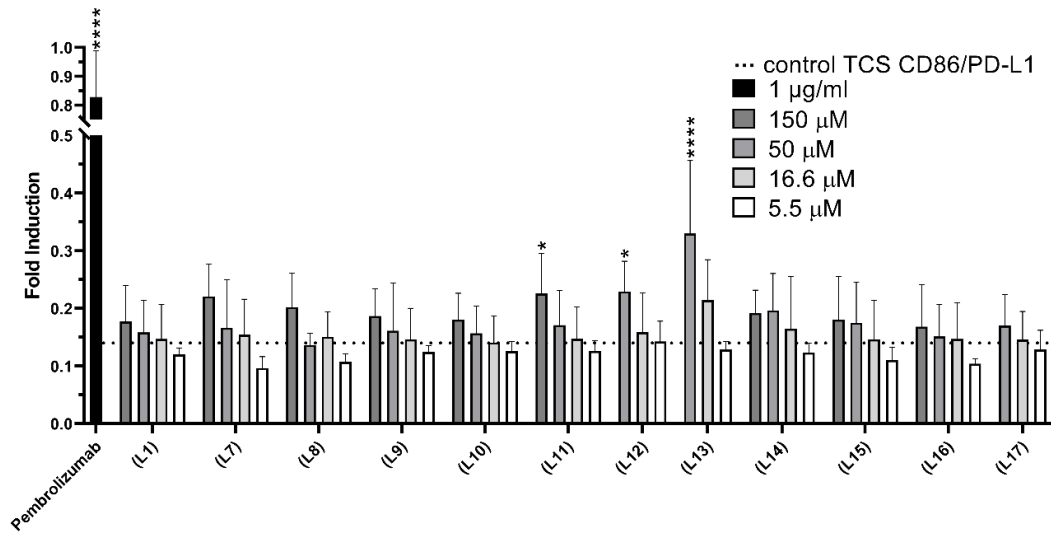


Figure 67. The inhibitory properties of the peptides in the functional cellular assay. The PD-1 reporter cells were stimulated with TCS CD86 expressing PD-L1 in the absence or presence of the peptides. The inhibitory properties of the peptides were measured by the eGFP expression using flow cytometry and normalised to gMFI eGFP received for the PD-1 reporter/TCS CD86 treated by the peptides. The dotted line shows the normalised eGFP expression level from the coculture of the PD-1 reporter cells with TCS CD86/PD-L1. Results are shown for three experiments performed independently in duplicate. Data are depicted as mean with SD. Statistical analysis was performed using one-way ANOVA followed by the Dunnet's post-hoc test. ****: $p < 0.0001$, ***: $p < 0.001$, **: $p < 0.01$, *: $p < 0.05$.

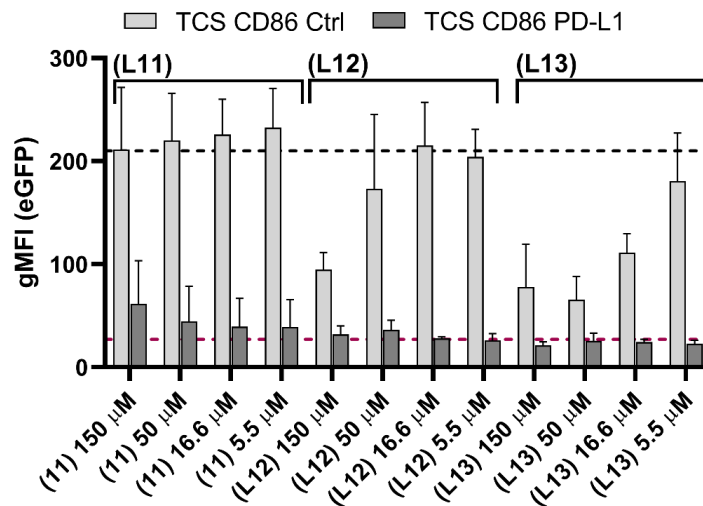


Figure 68. The inhibitory properties in the functional cellular assay for the selected peptides. PD-1 reporter cells were stimulated with TCS CD86 Ctrl and TCS CD86 expressing PD-L1 in the absence or presence of the PD-L1 derived peptides. The grey dotted back lines correspond to the PD-1 reporter cell stimulated with TCS CD86 in the absence of the peptides. The purple dotted back line corresponds to the PD-1 reporter cell stimulated with TCS CD86/PD-L1 in the absence of the peptides. Results are shown for three experiments performed independently in duplicate. Data are depicted as mean with SD (Mean +/- SD).

4. Analogues of PD-1(122-138)^{C123-S137C} targeting PD-L1 protein

4.1. Designing and synthesis of the analogues of PD-1(122-138)^{C123-S137C} targeting the PD-L1 protein

In the NMR conformational studies described in chapter 2.6., it was established that peptide (10) forms a β -hairpin like structure in a solution. This structure is enforced by the introduction of a disulphide bridge. In order to increase the contribution of the β -hairpin structure in peptide (10), I decided to introduce changes in the amino acid sequence in the region of the β -turn in position A129, P130, K131. These changes consisted in replacing the APK sequence with amino acid residues stabilizing the β -turn known from the literature^{251,252}. For further development of peptide (10), I decided to examine the stabilization of the β -turn by introducing to the sequence, in the loop, D-proline, D-alanine, and glycine. Additionally, I decided to change the position of the L-proline and L-alanine in the amino acid sequence. This concept together with the disulphide bridge introduced earlier to the peptide should enable the orientation of the torsion angles in the β -turn in such a way that they force the formation of the β -hairpin structure. Moreover, introducing to the sequence of D-amino acid should improve the peptide stability and decrease hydrolysis by the serum enzymes²⁵³. In the next step, the designed peptides were synthesized. Peptides **A1** and **A2** were rejected from further research due to complications during the oxidation process. Those peptides did not form intermolecular disulphide bonds.

Table 14. The amino acid sequences, position in the protein, and sequence modification of the designed peptides. D-amino acids are marked with a lowercase letter.

Peptide name	Peptide (10) modification in loop (A129, P130, K131)	Amino acid sequence
(10)	PD-1(122-138) ^{C123-S137C} L-alanine-L-proline-L-lysine	Ac-LCGAISLAPKAQIKECL-NH ₂
A1	L-alanine-D-proline-glycine	Ac-LCGAISLApGAQIKECL-NH ₂
A2	L-alanine-D-alanine-glycine	Ac-LCGAISLAaGAQIKECL-NH ₂
A3	glycine-D-proline-L-proline	Ac-LCGAISLGPpAQIKECL-NH ₂
A4	L-proline-D-alanine-L-alanine	Ac-LCGAISLPaAAQIKECL-NH ₂
A5	L-proline-D-alanine-glycine	Ac-LCGAISLPaGAQIKECL-NH ₂
A6	L-proline-D-proline-L-alanine	Ac-LCGAISLPpAAQIKECL-NH ₂

4.2. Study of binding of PD-1(122-138)^{C123-S137C} analogues to PD-L1 using the SPR technique

In the next step, **A3-A6** analogues were subjected to a binding analysis using the SPR technique in the conditions mentioned in chapter 2.2. The obtained sensorgrams are shown in Figure 69 and the binding kinetics parameters have been collected in Table 15. The differences in the strength of interaction with PD-L1 could be observed among three of the four tested peptides; however, the dissociation constants were similar. Peptide **A6** shows no interactions with the PD-L1 protein (Figure 69). The highest affinity was observed for peptide **A4**, the obtained K_D for the PD-L1/**A4** complex was 1.77 μM . What is worth mentioning at this point this peptide aggregated at the highest used concentration (60 nM). These aggregates decreased the effective concentration of peptide **A4** and led to the reduction of the binding²⁵⁴, which can be seen in Figure 69 (purple arrow). Peptides **A3** and **A5** bind to ligand-1 with the same order of magnitude as peptides **A4** and (10). The K_D of their interaction with protein was 6.76 μM for **A3** and 4.28 μM for **A5**.

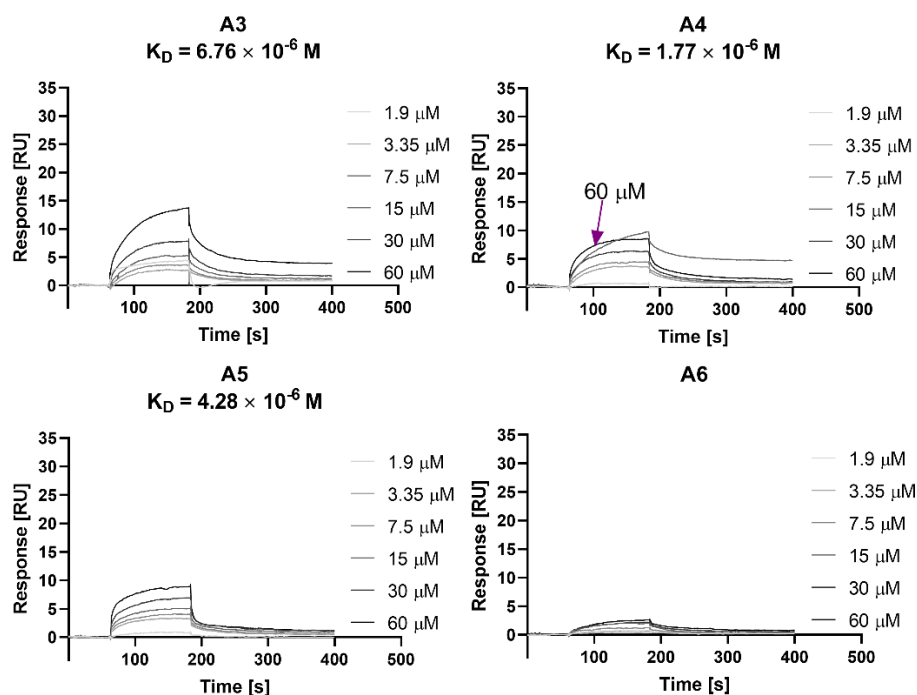


Figure 69. Sensorgrams of the peptide (10) analogues interacting with PD-L1 analysed using the SPR technique.

Table 15. Association and dissociation rates and dissociation constants calculated for the peptide (10) analogues binding to PD-L1 from the SPR data. Results were calculated using the Biacore T200 Evaluation Software from at least three independent titration analyses. The applied binding model 1:1. ND - not determined (no binding detected or binding too weak to establish reliable constants); SD – standard deviation.

Peptides	k_a ($M^{-1}s^{-1}$)	k_d (s^{-1})	K_D (M)	SD
(10)	1.21×10^3	1.80×10^{-3}	1.52×10^{-6}	8.76×10^{-7}
A3	2.35×10^3	2.87×10^{-3}	6.76×10^{-6}	8.48×10^{-6}
A4	1.79×10^3	3.07×10^{-3}	1.77×10^{-6}	4.19×10^{-7}
A5	1.22×10^3	5.17×10^{-3}	4.28×10^{-6}	4.19×10^{-7}
A6	ND	ND	ND	ND

4.3. Stability of the designed analogues and their effects on the viability of chosen cell lines

The next step in my research was the evaluation of the selected peptide (10) analogues regarding their influence on the viability of cell lines used in the planned *in vitro* assays. As in the case of the PD-1 derived peptides, the assessment of their stability in the RPMI 1640 medium with 10% of heat-inactivated FBS used in the cell-based tests was performed. As a control, I used peptides dissolved in water in time 0 h. The procedure for the stability experiment and cell viability assay was described previously in chapter 2.3. The obtained results are presented in Figure 70.

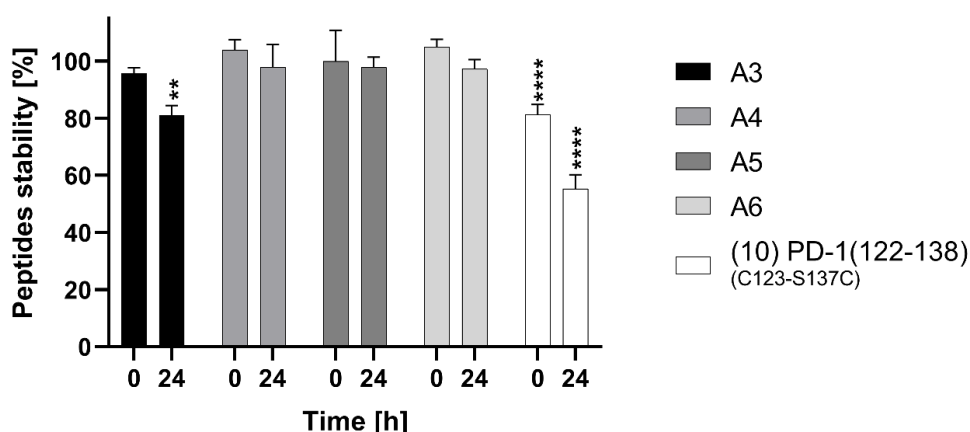


Figure 70. Peptides stability in the RPMI 1640 medium at times 0 and 24 h. The percentage of stability was established by comparing the peak area of control in time 0 h with the peak area for the collected samples. Results were obtained through the RP-HPLC analysis method. Results are shown for three experiments performed independently. Data are depicted as mean with SD (Mean +/- SD). Statistical analysis was performed using one-way ANOVA followed by the Dunnet's post-hoc test. ****: $p < 0.0001$, ***: $p < 0.001$, **: $p < 0.01$, *: $p < 0.05$.

The results for peptide **A3** after 24 h of incubation diverge from the ones obtained for the rest of the peptides from this group. The content of peptide in sample compared to the control was calculated to 81% whereas, for time 0 h, I observed a decrease of about only 4% of the initial signal. Peptides **A4**, **A5**, and **A6** were stable in the tested conditions (Figure 71).

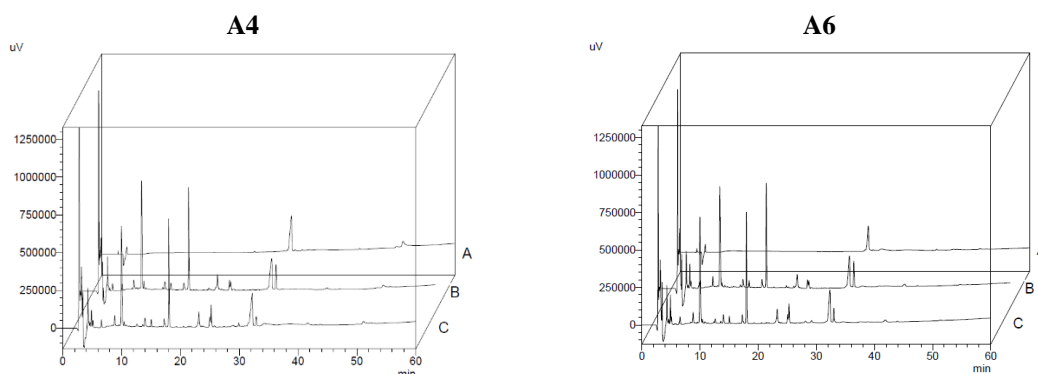


Figure 71. Chromatograms registered for peptides **A4** and **A6**. A) Peptide in water $t=0$ h, B) peptide in medium $t=0$ h, C) peptide in medium $t=24$ h.

Subsequently, I evaluated the viability of the Jurkat E6.1 and TCS Ctrl cell lines after treatment with the peptide (**10**) analogues for 24 h. The test was performed in the same conditions as in the case of peptides derived from the PD-1 protein and was described in chapter 2.3. The examined peptides do not have a negative effect on the viability of both tested cell lines. In the full spectrum of the examined peptide concentrations, the Jurkat E6.1 cells demonstrated a viability of about 100%. A small drop of living cells was observed for the highest concentration of **A5** and **A6** equal to 9% and 6%, respectively (Figure 72). For lower concentrations, the changes were not significant.

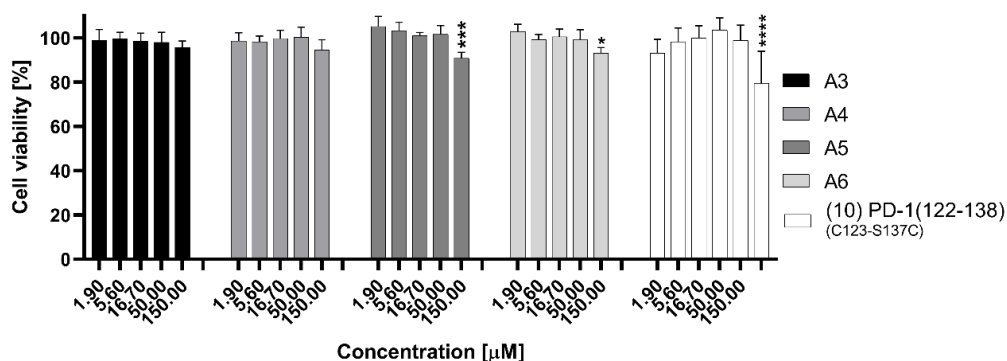


Figure 72. Cell viability assay, used to define the influence of the peptide (**10**) analogues on the Jurkat E6.1 cell line after incubation for 24 hours. Results are shown for three experiments performed independently in triplicate. Data are depicted as mean with SD (Mean \pm SD). Statistical analysis was performed using one-way ANOVA followed by the Dunnet's post-hoc test. ****: $p < 0.0001$, ***: $p < 0.001$, **: $p < 0.01$, *: $p < 0.05$.

In the case of TCS Ctrl, the tested peptides indicated a more intense effect on their viability than on the Jurkat E6.1 cells. The highest concentration of peptides **A5** and **A6** had a negative effect on cell viability. It led to a decrease in the number of living cells to 75% for peptide **A6** and 87% for peptide **A5** compared to the control (Figure 73). The rest of the tested concentrations of peptides led to the TCS Ctrl proliferation. This effect is the most strongly observed for peptide **A6** where I observed an increase of living cells up to 148% for 1.9 μM concentration and 145% for 16.7 μM compared to the control. The percent of living cells was stable for all tested concentrations of **A4** and it increased by about 20% compared to the control.

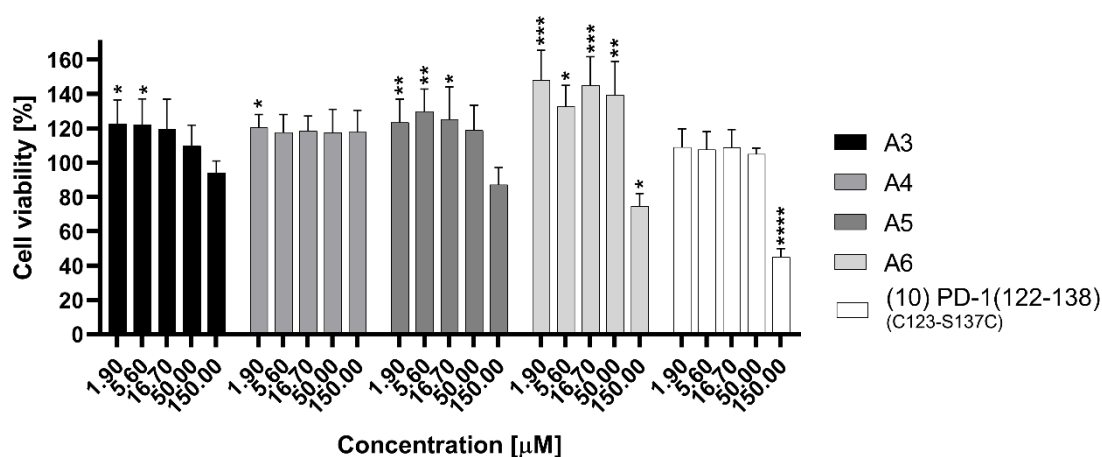


Figure 73. Cell viability assay used to define the influence of the peptide (10) analogues on the TCS Ctrl after incubation for 24 hours. Results are shown for three experiments performed independently in triplicate. Data are depicted as mean with SD (Mean \pm SD). Statistical analysis was performed using one-way ANOVA followed by the Dunnet's post-hoc test. ****: $p < 0.0001$, ***: $p < 0.001$, **: $p < 0.01$, *: $p < 0.05$.

4.4. Cell-Binding Assay and Competitive Inhibition

The properties of the peptide (10) analogues for competing with human glycosylated PD-1-Fc for binding with PD-L1 were studied on TCS cells expressing PD-L1. The assay was performed to examine the capacity of the peptides for inhibiting the binding of the PD-1 to PD-L1 located on the TCS-PD-L1 cells. The target cells were probed with the peptide (10) analogues at three different concentrations from 150 μM to 16.7 μM . Peptide (10) was tested in the concentration range between 50-5.6 μM as it has a negative effect on cell viability at the 150 μM concentration. The experiment conditions corresponded to the ones described in chapter 2.4.

In the titration assay, the best inhibitory properties were observed for peptide **A3** (Figure 74). This peptide significantly blocked the binding of PD-1 to PD-L1 at a concentration of 150 μ M. Moreover, the concentration-dependent effect can be observed for the concentrations in the range from 150 μ M to 16.7 μ M. In inhibit complex formation in 63% in the highest concentration and in 38% in 50 μ M. A weak, concentration-dependent, blocking effect was observed for **A5**. Additionally, peptides **A4** and **A6** competed for binding to PD-L1 with PD-1 but the dose-dependent effect was not observed for them.

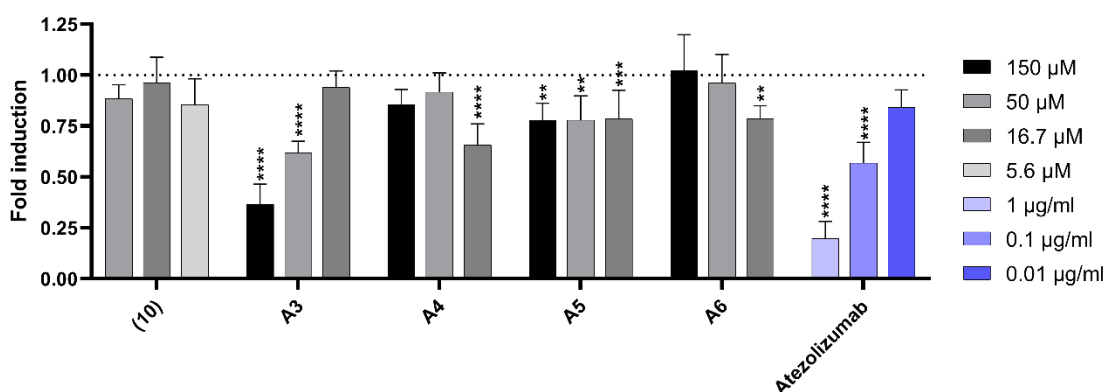


Figure 74. Competitive inhibition of peptides against the PD-1/PD-L1 complex formation. TCS PD-L1 was incubated with the indicated peptides used at final concentrations ranging from 150 μ M to 16.7 μ M. The bar diagram shows the fold induction of gMFI for at least three experiments performed independently in triplicate. Data were normalised to the gMFI received for TCS PD-L1 treated by PD-1. Data are depicted as mean with SD (Mean \pm SD). Statistical analysis was performed using one-way ANOVA followed by the Dunnet's post-hoc test. ****. $p < 0.0001$, ***. $p < 0.001$, **. $p < 0.01$, *. $p < 0.05$.

4.5. Stimulation assay

In the last stage of evaluation of the peptides (**10**) analogues, I examined the inhibitory properties in the functional cellular assay based on reporter gene expression system, NF- κ B::eGFP, constructed on Jurkat E6.1 cell line, described in chapter 3.5. I have also performed these studies in prof. Peter Steinberger laboratory.

Subsequently, the PD-1 reporter cells (J-NF- κ B::eGFP PD-1) were stimulated by TCS CD86/PD-L1 in the presence and absence of peptide (**10**) and its analogues, at a final concentration in the range 150-5.6 μ M for the analogues and 50-5.6 μ M for (**10**). The inhibitory properties of the peptides were measured by the reporter gene expression (NF- κ B::eGFP) using flow cytometry and normalised to gMFI eGFP received for J-NF- κ B::eGFP PD-1/TCS CD86 cells treated by the indicated peptides (Figure 75).

Atezolizumab, anti-PD-L1 mAb, at a concentration 1 $\mu\text{g/ml}$ was used as a positive control. When a peptide inhibits the PD-1/PD-L1 complex formation, the reporter gene expression should be restored leading to the increase of the signal from eGFP compared with the control - eGFP expression level from the coculture of the PD-1 reporter cells with TCS CD86/PD-L1 without the peptides (Figure 75, dotted line). For the tested peptides, the restoration of the signal was observed only for the 150 μM concentration, which was the highest tested concentration. The effect was observed for three from the four analogues, namely **A3**, **A4**, and **A5**. Those peptides at concentrations below 150 μM did not abolish the inhibitory signal from the PD-1/PD-L1 complex. For peptide **A6**, restoration of the signal was not observed for any of the tested concentrations.

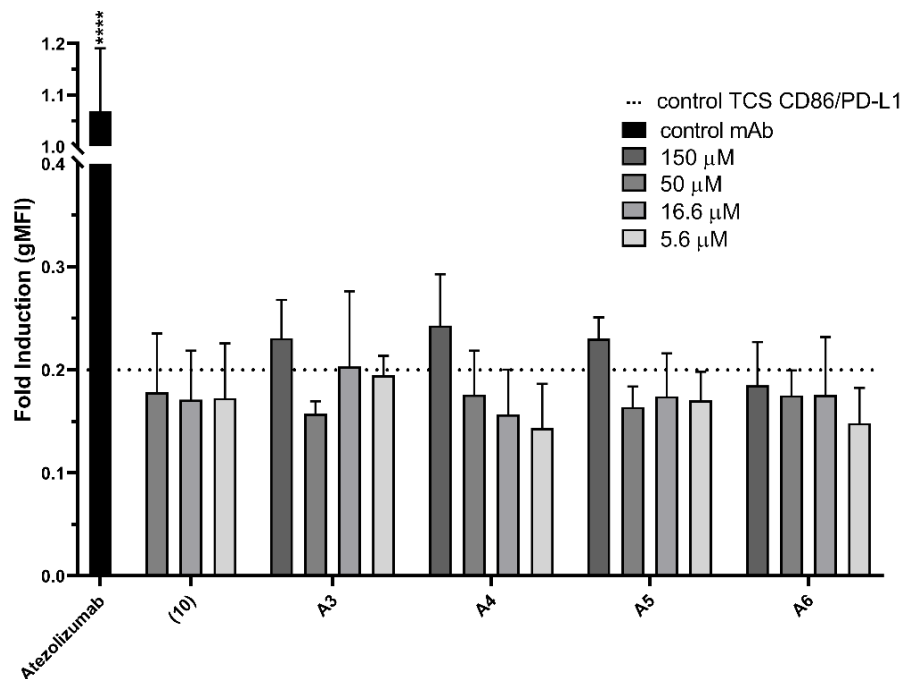


Figure 75. The inhibitory function of the peptides in a reporter cell-based assay. The PD-1 reporter cells were stimulated with TCS CD86/PD-L1 in the absence or presence of the peptides. The inhibitory properties in the form of the eGFP expression were measured using flow cytometry and normalised to gMFI eGFP received for PD-1 reporter/TCS CD86 treated by the peptides. The dotted line show the normalised eGFP expression level from the coculture of PD-1 reporter cells with TCS CD86/PD-L1. Results are shown for three experiments performed independently in duplicate. Data are depicted as mean with SD (Mean \pm SD). Statistical analysis was performed using one-way ANOVA followed by the Dunnet's post-hoc test. ****: $p < 0.0001$, ***: $p < 0.001$, **: $p < 0.01$, *: $p < 0.05$.

IV. Discussion

The PD-1/PD-L1 complex, as a molecular target in immunotherapy, has been the focus of the attention of the scientist since 1990. Throughout the years, the functions of PD-1 and PD-L1 were investigated. The PD-1/PD-L1 complex formation inhibits the activation of the immune system and numerous blocking agents, mostly monoclonal antibodies, were accepted by FDA in cancer therapies. Since 2015, when the first 3D complex of human PD-1 and PD-L1 was obtained by Zak et al.⁶², the rational designing of the compounds blocking the PD-1/PD-L1 complex flourished. The research carried out during my doctoral thesis also fits into this trend. Therefore, the main aim of my research was finding peptide inhibitors of the PD-1/PD-L1 complex formation. I designed, synthesised and examined peptides targeting PD-L1 derived from the amino acid sequences of PD-1 and peptides targeting PD-1 derived from PD-L1.

1. Analysis of the PD-1/PD-L1 interface

In the first stage of my research, I expanded knowledge regarding the interaction between PD-1 and PD-L1. MSc Małgorzata Kogut performed MM/GBSA simulation of the PD-1/PD-L1 complex (PDB ID: 4ZQK) to determine the energy input of individual amino acid residues in the complex formation²³⁸. The obtained results expanded the information on the complex interface obtained by Zak et al in 2015⁶². Both results confirmed that the interface is created by the front faces of the β sheets of the IgV domains from both proteins. Three structures focusing hot spots may be distinguished on the surface of the PD-L1 protein – one groove and two pockets. The residues present in those structures interact with the appropriate amino acid in PD-1. Firstly, I will discuss the influence of PD-1 amino acids on the formation of the PD-1/PD-L1 complex; subsequently, I will move to PD-L1 amino acids taking part in the complex formation. In the discussion, I will focus on two MM/GBSA calculation models: per-residue decomposition, which take into consideration energy input of summed interactions of single residues and pairwise per residue decomposition which calculate the interaction energy among the pair of residues in PD-1 and PD-L1.

1.1. Analysis of the PD-1 interface

Three amino acid residues Y68, Q75 and T76 in PD-1 are accommodated in a shallow groove of PD-L1. Per-residue decomposition confirmed a strong input of Y68 and Q75 (-3.118 kcal/mol and -2.945 kcal/mol, respectively, Figure 30) into binding with PD-L1; however, it is not as significant for T76 (-0.937 kcal/mol). The residues accommodated in the groove are donors and acceptors of hydrogen bonds⁶². Y68 interacts with D122_L (-5.200 kcal/mol) and Y123_L (-2.107 kcal/mol), Q75 interacts with R125_L (-5.768 kcal/mol) and T76 with K124_L (-2.652 kcal/mol) and with R125_L (-2.396 kcal/mol) (Table 6). Although, the architecture of the well is shallow (no cavities) and may generate complications for efficient designing of potential inhibitors, I designed peptides targeting this structure and they are part of Group I derived from PD-1.

The pockets formed in the structure of PD-L1 accommodate I126 and I134 from PD-1. The ΔG value was designated by the MM/GBSA analysis at -3.232 kcal/mol for I126 and -5.129 kcal/mol for I134 (Figure 30). Both these amino acid residues are part of the PD-1 derived peptides from Group II.

The groove and two pockets cover only five from nine hot amino acid residues in PD-1. Based on the crystal structure Zak et al.⁶² (Table 2) additionally points out the importance of N66, K78, A132 and E136⁶². The MM/GBSA calculation run for purposes of my research is in agreement with those results. These amino acids were also included in the sequence of the peptides from Group I and II.

The residues N66, Y68, Q75, K78, E84, I126, L128 and I134 are eight hot spots selected by Huang et al.²⁵⁵ basing on MM/GBSA alanine scanning. The importance of E84 and L128 is not observed by Zak et al. in the crystal structure⁶² and the per-residue energy decomposition for those amino acids designated by MSc Kogut was only -1.130 and -2.085 kcal/mol. The data presented here additionally point out the importance of E136 which is designated as a hot spot by Zak et al.⁶² but not by Huang et al.²⁵⁵. E136 forms a hydrogen bond with Y123_L (-3.642 kcal/mol) and a strong salt bridge with R113_L (-11.303 kcal/mol) and R125_L (-7.319 kcal/mol). However, according to Huang et al.²⁵⁵, its binding free energy is estimated at below 1 kcal/mol while according to the per-residue calculation, run for the purposes of my research, it is -4.228 kcal/mol. Furthermore, these data confirm the formation of hydrogen bonds between K78 and

F19_L (-5.572 kcal/mol), D122_L (-5.245 kcal/mol) and A121_L (-3.996 kcal/mol). The work presented by Ding and Liu²⁵⁶ concentrating on mapping the interface of PD-1/PD-L1 using molecular mechanics Poisson–Boltzmann surface area (MM/PBSA) methods confirms the hot spots designated in the previously described results. Moreover, the results obtained by Ding and Liu²⁵⁶ indicate that the energetically dominant amino acid residues create the hydrophobic core of the interface which is surrounded and protected from the solvent by the polar, less energetically influential, amino acids²⁵⁶. Besides the aforementioned research, Du et al.²⁵⁷ studied the PPI between PD-1 and PD-L1 by MM/PBSA methods. Part of the hot spots, reported by them, overlap the aforementioned hot regions, namely Q75, T76, K78, D85 and E136. However, they also reported that K131, K135 and R104 are important for ligand binding by PD-1. These data stand in contradiction to calculation outcomes collected by MSc Kogut and those of others. The interface designated from the crystal structure does not confirm the relevance of the hot spots selected by Du et al.²⁵⁷ and the data from MM/GBSA summarized in the Table 6 do not indicate an energetical influence of K131, K135 and R104. The authors suggested that the structure obtained from the crystal of PD-1/PD-L1 should not be taken into consideration in inhibitors designing as the PD-1 interface is flexible and the rigid structure of the crystal does not reflect the physiological condition in the solution²⁵⁷. Although, according to the crystal structure and MM/GBSA calculations run in this work, K131 and K135 are not part of the interface, they are included in the sequence of long peptides from Group II, as they are placed in the protein sequence between energetically important amino acid residues.

Moreover, amino acid substitution in protein provides additional information regarding the hot spot amino acids and interface of the complex. Over the years, several PD-1 mutants were described. Lázár-Monlár et al.²⁵⁸ performed the PD-1 protein mutations in positions K78A and I126A. Both of them lead to loss or reduced binding to PD-L1 and PD-L2. The K78 is part of all of the peptides from Group I of the PD-1 derived peptides and I126 is part of almost all of the peptides from Group II except (**13**). Mutations in positions L128A, L128R, I134A and E136A lead to reduced binding to PD-L1 but not to PD-L2²⁵⁸, also those amino acids are part of the peptides from Group II.

1.2. Analysis of the PD-L1 interface

As mentioned before in the PD-L1 interface, three structures focusing hot spots may be distinguished, namely a shallow groove and two pockets. The shallow groove is composed by PD-L1 residues: D122_L, Y123_L, K124_L, R125_L and D26_L⁶². The energy decomposition for these amino acids was already described above. The interaction between D26_L and Q75 was not mentioned before, however, it has an important input for the PPI, and is created through rearrangement in the PD-1 structure occurring during binding with PD-L1⁶². The strong interaction between D26_L and Q75 is supported by MM/GBSA calculation run in this work, and the pairwise per-residue energy decomposition for these two amino acids is -3.090 kcal/mol. The region of this shallow groove is covered by the PD-L1 derived peptides from Group I_L and III_L.

One of the two pockets in PD-L1 consists of M115_L, A121_L and Y123_L, and accommodates I126. According to the pairwise per-residue energy decomposition calculations, the ΔG between the components of the PD-L1 pocket and I126 is not so important for the creation of the complex as the interaction energy is above -1 kcal/mol. However, the energy decomposition on a per-residue basis for a pocket constituent is strong and for M115_L it is -2.349 kcal/mol, for A121_L -4.575 kcal/mol and for Y123_L -3.297 kcal/mol. The aforementioned amino acids residue are part of the peptides from Group III_L.

The second pocket in the PD-L1 interface consists of Y56_L, E58_L, R113_L, M115_L, Y123_L, and accommodates I134⁶². From pairwise per-residues calculation, Y123_L and R113_L interact with I134 and the energy is -2.600 kcal/mol and -1.844 kcal/mol, respectively. For the rest of the amino acid residues of the pocket, the interaction energy with I134 is above -1 kcal/mol. However, considering the input of energy contribution in creating the PPI, basing on per-residue decomposition, it is strong for the aforementioned M115_L (-2.349 kcal/mol) and Y123_L (-3.297 kcal/mol) and for Y56_L (-2.740 kcal/mol), and R113_L (-4.681 kcal/mol). The peptides from Group II_L and III_L comprise the region of the second pocket in PD-L1.

According, to the crystal structure of PD-1/PD-L1 obtained by Zak et al⁶² and MM/GBSA calculation presented in my PhD thesis, there are two more crucial amino acid residues in the PD-L1 structure, important for the complex formation with PD-1, namely, A18_L and F19_L. Corresponding to the energy decomposition on a per-residue

basis, the energy input of A18_L is unfavourable for the PD-1/PD-L1 complex, the ΔG value for A18_L is 3.457 kcal/mol; nonetheless, it strongly interacts with E84 (-9.797 kcal/mol), D85 (-2.057 kcal/mol) and R86 (-3.904 kcal/mol). Inversely, F19_L has a positive impact on the complex creation, because the ΔG for this amino acid residue is -5.584 kcal/mol and the interaction energy with K78 is -5.572 kcal/mol. F19_L is part of the peptide from Group I_L.

The results of MM/GBSA analysis conducted by Huang et al.²⁵⁵ are only partially consistent with the data obtained in this work, pointing out six hot spots for PD-L1: Y56_L, Q66_L, R113_L, M115_L, Y123_L and R125_L. From MM/GBSA analysis run for this dissertation, Q66_L forms the hydrogen bond with A132 and the energy of the interaction is -1.954 kcal/mol, while the energy decomposition per-residue is only -0.296 kcal/mol and it is not marked here as a hot spot. Moreover, Huang et al.²⁵⁵ point out the importance of F19_L, A121_L and D122_L for the complex creation nonetheless, they did not consider those amino acid residues as hot spots. MM/GBSA calculations run in this work point out the importance of F19_L and A121_L for the PD-1/PD-L1 formation. Whereas the work presented by the Ding and Liu²⁵⁶ focusing on mapping the interface of PD-1/PD-L1 did not mention F19_L at all; however, they confirm the rest of the hot spots designated in the previously described results. Additionally, Huang et al.²⁵⁵ mentioned I54_L as a warm spot and data in my PhD dissertation confirm these results, evaluating the ΔG at about -1.389 kcal/mol. Huang et al.²⁵⁵ indicate that I54_L interacts directly with L128.

2. The PD-1 and PD-L1 derived peptides

Basing on the MM/GBSA calculations and the crystal structure of PD-1/PD-L1⁶² complex, I designed 13 peptides derived from PD-1 and 17 peptides derived from the PD-L1 protein. The PD-1 derived peptides have been divided into two groups. Group I contains peptides from N-terminal of PD-1 while Group II consists of peptides from C-terminal of PD-1. In both groups, the linear peptides and their analogues with disulphide bond are present. Peptides derived from PD-L1 have been divided into three groups. Group I_L contains only one peptide from N-terminal of PD-L1, Group II_L consists of five peptides derived from the middle part of the protein while eleven peptides from C-terminal of PD-L1 create Group III_L. In Group I_L and II_L, there are only linear peptides. Peptides from Group II_L were excluded from further research due to

their hindered solubility in aqueous solvents. Group III_L of the PD-L1 derived peptides is the most diverse group of all the designed peptides. The most basic are linear peptides trimmed from the PD-L1 structure with C114_L and M115_L exchanged to their isostere Abu and Nle, respectively. I also designed peptides with a disulphide bond and among them three analogues of (**L8**) with exchanged G120_L, for which the calculated ΔG value is 0.685 kcal/mol, to serine (**L12**), phenylalanine (**L13**) and glutamic acid (**L14**) which can be a donor and an acceptor of additional hydrogen bonds or van der Waals interactions. The last tested modification was examination of the input of exchanging the M115_L with the calculated ΔG value on -2.349 kcal/mol to Nle, this modification was introduced to peptides to prevent methionine oxidation. I introduced the disulphide bond to the peptide structure to examine the influence of the structure organization on their binding properties. To create disulphide bonds, I exchanged the native amino acids to cysteine. The amino acids were selected in such a way as to preserve the key (hot spot) amino acids for the stability of the PD-1/PD-L1 complex. This modification should enable the formation of the β -harpin structure, as it was reported previously, it might be essential for the interaction with the β -sheet-rich proteins such as PD-1 and PD-L1^{204,206,239}. The short linear peptides, probably will not adopt the β -harpin conformation which in protein is stabilized by many interactions, like hydrogen bonds, salt bridges and Van der Waals interactions.

The research conducted by Zhou et al.²⁰⁴, and Abbas et al.²⁰³ confirmed that cyclization and organization of the peptide structure can increase affinity to the targeting molecule. These two groups designed peptides based on the C-terminal part of the PD-L1 protein, interacting with PD-1 (Table 5, no. 33-37 and 25-32). The peptides consist of the amino acids from G110_L to A132_L (DS-II) reported by Zhou et al.²⁰⁴, and from Y112_L to T127_L (YT-16) reported by Abbas et al.²⁰³. Exchanging the amino acids residues V111_L and T127_L to cysteines in peptide DSII and the creation of a disulphide bond increase affinity to PD-1 by almost ~10-fold in comparison to linear peptide (K_D 28 μ M and 109 μ M, respectively)²⁰⁴. In peptide YT-16, to create a disulphide bond, Abbas used C114_L (from PD-L1 sequence) and replaced R125_L with cysteine. Additionally, the peptide's chain was reduced by seven amino acid residues compared with DS-II. Those changes led to a decrease of the dissociation constant to 17.8 nM which is lower than the affinity of PD-1 to PD-L1 for two orders of magnitude²⁰³. This research shows that not only introduction of a disulphide bridge to the peptides structure may have influence

on the affinity to the target but also slight changes in the amino acid sequence may influence the binding strength.

3. SPR analysis of the PD-1/PD-L1 complex – obstacles during analysis condition optimisation

Based on the SPR results, I obtained the K_D value for the PD-1/PD-L1 complex. In literature, there are available experimentally determined values of K_D ^{32,42,128}; however, this constant can slightly differ depending on the applied sensor chip (way of protein immobilization), protein (with or without glycans, tag), number of molecules immobilized on the sensor chip surface (mass transfer effect). When human glycosylated PD-L1 was immobilized to the CM5 sensor chip and titrated with human glycosylated PD-1, the K_D value was 1.56 μ M. In a reversed system, human glycosylated PD-1 immobilized on the CM5 sensor chip and titrated by the glycosylated PD-L1, the K_D value was established at 1.04 μ M, what is in the same order of magnitude (Figure 33 and 50, respectively). When human glycosylated PD-L1 with biotin tag was immobilized on the SA sensor chip and titrated with human PD-1 without glycans, the K_D was lower and its value was 22.6 nM (Figure 52). The association of proteins happens faster in the case of deglycosylated PD-1 what may be an effect of the easier steric access to the binding sites of PD-L1. Moreover the dissociation of PD-1 appears 12 times slower. Literature reports also confirm that the K_D value for the deglycosylated proteins from the PD-1/PD-L1 complex is lower (higher binding) than the one of the glycosylated proteins (Table 16).

Table 16. Equilibrium dissociation constant (K_D) obtained for the PD-1/PD-L1 complex in a different system measured by the SPR. ND – no data; bolt – results received by me.

Immobilized protein	Type of sensor	Glycans	Express system	Analyte	Glycans	Express system	K_D [μ M]
PD-1-Fc ⁴²	CM5	+	ND	His-PD-L1	+	CHO	7.5 \pm 2.2
PD-L1 ⁴²	SA	+	HEK 293	PD-1-Fc		ND	8.2 \pm 0.1
PD-1 ¹²⁸	CM5	-	<i>E.coli</i>	His-PD-L1	+	HEK293	1.15 \pm 0.11
PD-L1 ¹⁸¹	CM5	-	<i>E.coli</i>	PD-1	-	<i>E.coli</i>	0.18
PD-1 ¹⁸¹	CM5	-	<i>E.coli</i>	PD-L1	-	<i>E.coli</i>	0.16
PD-L1-Fc	CM5	+	CHO	HisPD-1	+	HEK 293	1.56 \pm 0.96
PD-1-Fc	CM5	+	CHO	HisPD-L1	+	HEK 293	1.04 \pm 0.87
PD-L1	SA	+	HEK 293	PD-1	-	<i>E.coli</i>	0.023 \pm 0.006

3.1. Differences in binding of the PD-1 derived peptides to PD-L1 - analysis of the SPR data

In the next step, I evaluated the binding of the designed PD-1 derived peptides to the target molecule. From thirteen PD-1 derived peptides, seven bind to PD-L1. Peptides from Group II bind stronger with PD-L1 than the ones from Group I. The strongest binding to PD-L1 is observed for peptide **(10)** and K_D determined for the protein/peptide complex is comparable to K_D obtained for PD-1/PD-L1. The linear analogue of this compound, peptide **(9)**, does not bind to PD-L1. The difference between those two peptides results from introducing the disulphide bridge to peptide **(10)**, which is associated with exchanging S137 to cysteine residues. Additionally, **(9)** contains Abu in position 114. According to MM/GBSA calculation, S137 is not important for creating the PD-1/PD-L1 complex and the energy decomposition on a per-residue basis for it is 0.020 kcal/mol. The same pattern is noticeable for linear peptide **(5)** and its analogue with a disulphide bridge, peptide **(7)**. Peptide **(7)** is longer than peptide **(10)** by seven amino acid residues and has a disulphide bond in the same position. The K_D value for the PD-L1/peptide **(7)** complex is similar to the one obtained for PD-L1/peptide **(10)** and around 12-fold higher than for its linear analogue, peptide **(5)**. The K_D received for the interaction of peptides **(6)** with PD-L1 is around 11-fold higher than for its linear analogue, peptide **(5)**, and only slightly weaker than for peptide **(7)**, the K_D value for **(7)** is 4.66 μ M and for **(6)**, it is 5.36 μ M. Peptides **(6)** and **(7)** differ by the position of the disulphide bridge. To create the disulphide bridge in peptide **(6)**, I exchanged T120 and E141 to cysteine residues and Cys114 to Abu. T120 and E141 are not important for the PD-1/PD-L1 complex formation and their energy input for the complex formation basing on the per-residue energy decomposition is 0.067 kcal/mol and 0.017 kcal/mol, respectively. In peptides **(11)** and in its shorter analogue with the disulphide bridge in the same position, peptide **(12)**, I exchanged A125 and K135 to cysteine. According to MM/GBSA, both those amino acid residues do not have an impact on the formation of the PD-1/PD-L1 complex (per-residue energy decomposition is 0.065 kcal/mol and 0.151 kcal/mol, respectively); however, those peptides do not bind to PD-L1. Du et al.²⁵⁷ pointed out the importance of K135 which was not seen in the MM/GBSA calculations. Whereas, the importance of A125 on the PD-1/PD-L1 complex formation is not mentioned in the available literature. Peptide **(13)** is the last one from Group II, its K_D value for the interaction with PD-L1 is in the

same range of magnitude as for the proteins complex, however, it is 5-fold weaker. This peptide is composed only of five amino acid residues, yet it consists of A132, I134 and E136 for which the energy input for the complex formation is -2.134 kcal/mol, -5.130 kcal/mol and -4.228 kcal/mol, respectively. It is worth to mention the change of binding between peptides (3) and (4) which are analogues that differ by the position of the disulphide bridge in the amino acid sequence. Peptide (4) does not bind to PD-L1 whereas K_D for peptide (3) is 17.8 μM . The loss of binding ability by peptide (4) may result from exchanging D77 to cysteine. D77 interacts with K124_L with energy of about -6.381 kcal/mol (Table 6).

In the drug discovery pipeline, the designation of K_D by SPR is often one of the first steps of a potential drug evaluation. Many reports present the data regarding affinity of the PD-1/PD-L1 peptide inhibitors; however, the majority of published peptides target PD-1, there are few publications deliberately regarding peptides targeting PD-L1. Nonetheless, available reports provide a possibility to compare peptides designed by me with the ones reported in the literature. In chapter 5.2.1 of Introduction, I described and tabulate (Table 4 and 5) reported peptides targeting the PD-1/PD-L1 axis. The PPA-1 and PPA-2 peptides obtained by Chang et al¹⁸¹ bind to PD-L1 with a similar strength as peptide (10), the obtained K_D for them is about 0.51 μM and 1.13 μM , respectively (Table 4, no. 8 and 9), while for peptide (10), it is 1.52 μM . However, the K_D for PD-1/PD-L1 received in the same experimental condition is 0.18 μM ¹⁸¹. Although, the affinity of those peptides to PD-L1 is weaker than the one of PD-1 to PD-L1, peptide PPA-1 disturbs the PD-1/PD-L1 axis in *in vitro* competitive assay and inhibits the growth of CT26-tumour in experiment with tumour bearing mice model¹⁸¹.

3.2. Differences in binding of the PD-L1 derived peptides to PD-1 - analysis of SPR and ELISA data

From twelve PD-L1 derived peptides, the binding with PD-1 is observed for ten of them, when peptides are immobilized to the sensor chip. In this condition, the evaluation of K_D for peptide (L1) was unsuccessful. However, during optimization of the experiment condition, I registered the sensorgrams for this peptide with PD-1 immobilized on a sensor chip and (L1) binds to PD-1 with $K_D = 25.7 \mu\text{M}$ (Figure 50). As already mentioned, the system with peptides immobilized to the sensor chips does

not reflect the biological condition and the length of the **(L1)** peptide may be an obstacles here during measurements. Taking that into consideration, the lack of binding of **(L15)** with PD-1 may be caused by its size. The analogues of peptide **(L9)**, namely **(L12)**, **(L13)**, **(L14)**, with exchanged G120_L to serine, phenylalanine and glutamic acid, respectively bind PD-1 with similar K_D ranging from 33.3-52.4 μM , while K_D for **(L9)** is about 36.0 μM . The longest synthesised peptide with a disulphide bond, namely **(L11)** exhibits a strong interaction with PD-1. The K_D value for the **(L11)**/PD-1 complex is about 100 times stronger than the one for complex of its linear analogue - **(L7)**, with PD-1. Also the strong binding of PD-1 to the peptides **(L16)** and **(L17)** is observed which contain native M115_L not exchanged to Nle. That confirms the importance of this amino acid residue as the analogues of these peptides with Nle instead of methionine, peptides **(L7)** and **(L13)**, bind PD-1 with the K_D value higher by two and one order of magnitude (weaker binding), respectively. The rationally designed peptides based on the PD-L1 structure reported by Zhou et al.²⁰⁴ also contain M115_L in the amino acid sequence and their affinity to PD-L1 differs depending on the length of the amino acid sequence and position of the disulphide bridge. The calculated K_D for these peptides with PD-L1 varies from 109 μM to 11.6 μM (Table 5, no. 34-37)²⁰⁴.

During SPR analyses of the PD-L1 derived peptides, I used PD-1 produced in the *E. coli* system, which is characterized by the lack of protein glycosylation. N58 has been reported as an important glycosylation site which has a significant impact on the stabilization of PD-1 on cell membrane. Furthermore, the mutation at the N-glycosylation sites, especially in position N58Q in PD-1, leads to a decrease in the binding affinity to PD-L1²⁵⁹. PD-L1 glycosylation, like in case of PD-1, influence its stability on the cell surface and T cell activity²⁶⁰. Moreover, deglycosylation of PD-L1 influences its interaction with the anti-PD-L1 mAb used in clinical practise, leading to a decrease of binding by 43-fold in the case of Avelumab (from 0.4 nM to 17 nM) and 3-fold in the case of Atezolizumab (from 4.7 nM to 17.8 nM)²⁶¹. However, the crystal structure of the PD-1/PD-L1 complex was obtained for the human proteins produced in the *E. coli* expression system what confirms that PD-1 and PD-L1 glycosylation is not required for proteins binding, yet it may influence the affinity and kinetics parameters⁶². Taking into consideration all these data, I decided to perform indirect ELISA to confirm if the PD-L1 derived peptides interact with glycolyzed PD-1.

According to the results obtained from indirect ELISA, the glycosylated PD-1 interacts with all the tested peptides. It is important to mention that the peptide concentrations used in the ELISA and SPR analysis differ from each other and I will not compare the received binding strengths of the peptides between those two techniques. The results obtained from ELISA indicate also that PD-1 binds to **(L1)** and **(L15)**. As already mentioned, this interaction was not seen in the SPR analysis performed in the similar system where peptides were immobilized to the sensor chip. This difference may be a result of the number of the molecule binds to the surface (the plate in the case of ELISA and the sensor chip in SPR) and accessibility of the PD-1 binding sites to the peptides. Before ELISA, I optimised the concentration of the peptides immobilized on the plate. In the case of SPR, the optimal theoretical peptide immobilization level was calculated before the immobilization; however, it was not optimised in the experimental approach due to the cost of the sensor chip, what could have influenced the final results.

4. Peptides evaluation in *in vitro* cellular assays

Determining the strength of the interaction between the designed peptides and the target proteins does not provide a full spectrum of information regarding their potential as inhibitors of proteins binding in a biological system. In SPR or ELISA, we have clear system, where only one protein is available for the testing compound. This configuration does not reflect the complexity of cell biology. To better examine the potency of the designed peptides, I decided to run an *in vitro* competitive assay on the cell line with a stable expression of the PD-L1 (TCS PD-L1) and PD-1 (J-PD-1) proteins. Moreover, I performed a stimulation assay to check if the designed peptides are able to restore the biological functions of PD-1 by activating the PD-1 signalling pathway after inhibition of the PD-1/PD-L1 complex. Stimulation assays were run in two different systems basing on the stimulation of the transcription factors responsible for the T cell activation pathway, namely NFAT and NF- κ B. The PD-1 derived peptides were examined on a commercially available platform created on the luciferase reporter gene under the NFAT response element. Whereas the PD-L1 derived peptides were tested using the platform constructed on the eGFP reporter gene under the NF- κ B response element created by prof. Peter Steinberger's group. Different approaches were due to accessibility and cost of the tests. Both platforms differ between each other not only by the transcription factor used but also by the cell lines used in the experiment

(CHO-K1 and BW5147), time of peptides incubation with the cell lines (6h and 24h) or by the measurable effect of inhibition (expression of luciferase or eGFP). The conditions of the experiment could have had an impact on the received results by influencing the peptides behaviour - their stability and degradation. Moreover, the peptides could have also had an influence on the cell line viability. All these distinctions may have a reflection in the received results.

The *in vitro* assays are run on the living cells which may differently react to the tested compounds, sometimes leading to unwanted cell death. Thus, it is important to examine the influence of the tested compounds on cell viability. Moreover, the cells live in a complex medium with the addition of FBS which may have an influence on the peptides stability. Taking this into consideration, before performing the competitive and stimulation assay, I decided to investigate the peptides stability in the RPMI 1640 medium with 10% FBS and the influence of the chosen compounds on cell viability. Basing on the results of SPR analysis, I chose seven peptides binding to PD-L1 and twelve binding to PD-1 for further examination. Peptides showing no affinity to the target protein or not soluble in the aquas solvent were excluded from further research.

The stability results obtained from the HPLC chromatograms show no additional signals. However, the reduction of the signal was observed in the PD-1 and PD-L1 derived peptides. It can be caused by the interaction of the peptides with some components of the medium such as the serum albumin proteins during the sample preparation which includes precipitation of the medium components by ethanol and spinning. Process of non-specific binding of peptides with albumins was observed previously and may occur due to hydrophobic interactions with proteins²⁴¹⁻²⁴³. Besides the non-specific binding of the peptides with albumins, they could have underwent a degradation, and the degradation products exhibit nonspecific binding with some components of the medium, which can result in the lack of additional signals in the registered chromatograms. The albumins are responsible for the transport of endogenous metabolites and exogenous compounds, and affect the pharmacokinetics of many drugs. The non-specific binding of peptides to the human albumins may be an advantage facilitating the transport of the peptides in the serum and prolonging their half-life time^{243,262}.

Subsequently, I performed a viability cell assay on three cell lines – CHO-K1, Jurkat E6.1 and TCS Ctrl – for the peptides derived from the PD-1 and on two cell lines – Jurkat E6.1 and TCS Ctrl – for peptides derived from PD-L1. From the obtained results, it can be seen that the tested peptides influence each cell line differently. The viability of the Jurkat E6.1 cells is demonstrating the slightest changes after the treatment with the peptides and they have a negative influence on cell viability only at the highest tested concentration. It is worth to mention that this cell line originated from a human donor. The CHO-K1 and TCS Ctrl (BW5417) come from hamster and mouse, respectively, and they are more sensitive to peptide treatment, and for some compounds, a cytotoxic effect at the highest tested concentration in the case of the CHO-K1 cells has been observed. For TCS Ctrl (BW5417), the peptides influence on their viability is even stronger.

In the reports published by Ganesan et al.²⁶³, Magiera-Mularz et al.¹⁹⁵ and Zyla et al.¹⁹⁶, regarding macrocyclic peptides p101, p104 and BMS-57 (patented by Bristol-Myers Squibb), the tested peptides do not exhibit a cytotoxic effect on the Jurkat E6.1 and CHO-K1 cell lines; however, the maximal tested concentration did not exceed 10 μM . At this concentration, the obtained peptides synthesised by me also did not exhibit the cytotoxic effect.

After the evaluation of the peptides stability and their cytotoxic effect, I also examined the ability of the PD-1 derived peptides to compete with the PD-1 protein for binding to PD-L1 on the cell surface and to restore NFAT-RE mediated luciferase expression by blocking the PD-1/PD-L1 complex in the cell based assay. Peptides **(7)** and **(10)** inhibit the proteins complex formation in an *in vitro* assay and also exhibit the strongest affinity for the PD-L1 protein among the tested compounds (K_D 1.52 μM and K_D 4.66 μM , respectively). Both those peptides restore the luminescence in an inhibitory bioassay but the effect is not intense and the fold induction for the 50 μM concentration is about 1.2. Moreover, peptide **(7)** prevented the complex formation in the competition assay with the PD-1 protein whereas this effect is not observed for peptide **(10)**. In the competition assay, peptide **(6)** at the highest tested concentration also prevents PD-1 from binding with PD-L1 and possesses a similar affinity to PD-L1 (K_D 5.36 μM) as peptide **(7)** but it does not restore the NFAT-RE mediated luminescence (Figure 46).

For comparison, the aforementioned peptides PPA-1 and PPA-2 reported by Chang et al.¹⁸¹ do not compete with PD-L1 for binding to PD-1 at a similar concentration as tested by me. The inhibitory effect for PPA-1 and PPA-2 (Table 4, no. 9-10) is observed at the 0.2 mg/ml concentration ($\sim 130 \mu\text{M}$), which is almost three times higher than the one used in this work. The data published by Ganesan et al.²⁶³, Magiera-Mularz et al.¹⁹⁵ and Zyla et al.¹⁹⁶ regarding inhibiting PD-1/PD-L1 by restoring the stimulation pathway of NFAT-RE by p101, p104 and BMS-57 show that these compounds restore the stimulation effect two to three times more effective than peptides **(10)** and **(7)**. All these data suggest that the best PD-1 derived peptides, namely peptide **(10)** and **(7)** have a potential to be PD-1/PD-L1 inhibitors used as anticancer drugs, however, their structure has to be further optimised.

The PD-L1 derived peptides were tested in similar approaches, namely, I examined their ability to compete with the PD-L1 protein for binding to PD-1 on the cell surface and to restore the NF- κ B mediated eGFP expression by blocking the PD-1/PD-L1 complex in the cell based assay. Peptides **(L1)** and **(L11)** prevent PD-L1 binding in a competition assay in a concentration-dependent manner; moreover, **(L11)** among all the PD-L1 derived peptides stimulates the eGFP expression by the inhibition of the PD-1/PD-L1 complex formation in a concentration-dependent manner. This peptide also exhibits one of the strongest affinity for the PD-1 protein among the tested peptides (K_D 2.04 μM) and binds the glycosylated PD-1 protein in ELISA assay.

Since the PD-1/PD-L1 complex structure was reported⁶², many peptides basing on the rational designing were tested. Scientist put a lot of interest into the PD-L1 fragment covering Group III_L of the designed peptides. Some of them, investigated by Zhou et al.²⁰⁴ and Abbas et al.²⁰³, were already described in this chapter in the fragment discussing the effect of cyclization and organization of the peptide structure. Moreover, Wang et al.²⁰⁶ reported seven peptides and peptidomimetics (linear, with a disulphide bridge, tryptophan zipper and D-proline in the peptide loop) consisting of the amino acid residues from R113_L to I126_L. Peptide P1.3 (Table 5, no. 44), with D-proline in the loop and tryptophan in the position S117W_L and D121W_L creating a tryptophan zipper, shows the lowest K_D for binding with PD-1 (1.80 μM) and has the ability to restore IL-2 secretion in a co-culture model with the activated Jurkat E6.1 and HCT-116 cell lines. Peptides reported by Zhou et al.²⁰⁴, Abbas et al.²⁰³ and Wang et al.²⁰⁶, depending on the length of the amino acid sequence, the disulphide bridge position and approach to

structure organization, bind to PD-1 with K_D from 0.018 to 474 μM (Table 5, no. 25-37; 42-48). Even the linear peptide PL120131, which is not structured, consisting of the amino acid residues from G120_L to D131_L (Table 5, no. 18), reverses the apoptotic signal in murine primary lymphocytes and the Jurkat cells induced by sPD-L1¹⁷⁷. All those data indicate the importance of this PD-L1 region and show that many approaches can be tested to improve the biological function of those peptides to bring new anticancer drug.

5. Conformation of peptide PD-1(122-138)^{C123-S137C}

To gather more information regarding the conformation and binding site of the leading peptides with PD-L1, the NMR analysis was performed and the received structure was docked to PD-L1. As already mentioned, peptides **(7)** and **(10)** are the best choice for further development from the peptides designed based on the PD-1 structure. Those peptides are analogues with a disulphide bridge in the same position which differ only by the number of amino acids. Peptide **(10)** is shorter by about 3 amino acids on the N-terminal side and 4 amino acids on the C-terminal side than peptide **(7)**. Additionally, they differ in the solubility in aqueous solutions in favour of peptide **(10)**. Due to this aspect, peptide **(10)** was chosen for further research and structure optimization. NMR data show that this peptide possesses the β -hairpin like structure stabilized by intermolecular hydrogen bonds and a disulphide bridge and interacts with PD-L1 in this same place as PD-1. Moreover, the structure of this peptide received from the NMR analysis displays structural similarities with BMS-57 and BMS-71, patented by BMS²¹³ company and investigated by Magiera-Mularz et al.¹⁸⁰. Structures of peptide **(10)** (Figure 76 B) and BMS's (Figure C, D) are more "relaxed" than the fragment trimmed from PD-1 (Figure 76A). BMS-57 and BMS-71 binding sites with PD-L1 partially overlap the PD-1/PD-L1 interface similarly to peptide **(10)**.

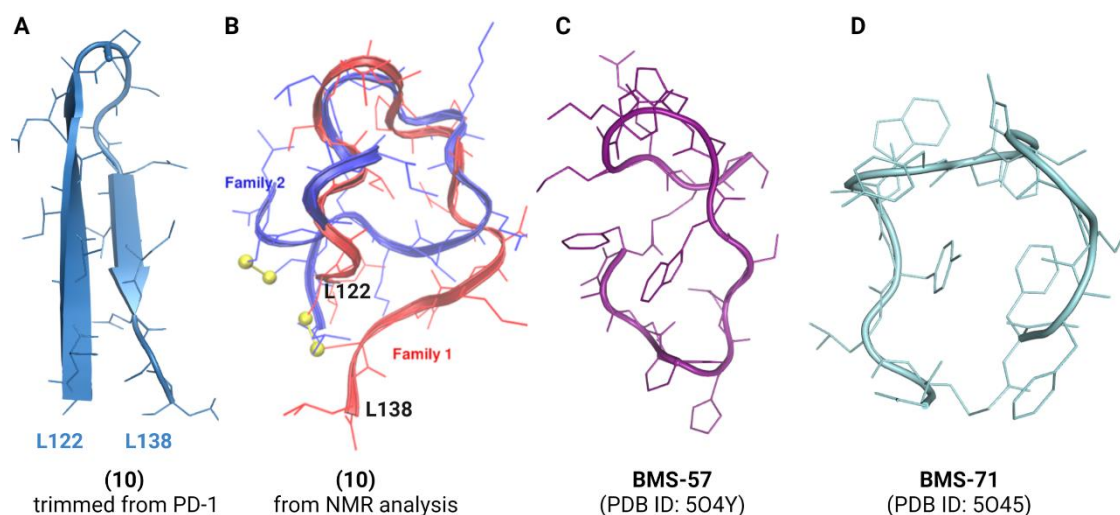


Figure 76. Structure of peptide (10) and patented PD-1/PD-L1 complex inhibitors²¹³. A) Peptide (10) structure trimmed from the PD-1 protein. B) Peptide (10) structure of dominant families from the NMR analysis²³⁸. C) Structure of BMS-51 (PDB ID: 5O4Y)¹⁸⁰. D) Structure of BMS-71 (PDB ID: 5O45)¹⁸⁰.

6. PD-1(122-138)^{C123-S137C} peptide's loop modification and its influence on the interaction with PD-L1

Taking into consideration the inhibitory properties received for peptide (10) and that it forms a β -hairpin-like structure in the loop, however, with the flexibility on the N- and C-terminals, I decided to introduce potential improvements in the structure stabilizing the β -turn which could additionally stabilize the β -hairpin peptide structure (Figure 76B). There are many approaches available in the literature which have a documented influence on the stabilization of β -hairpin, namely:

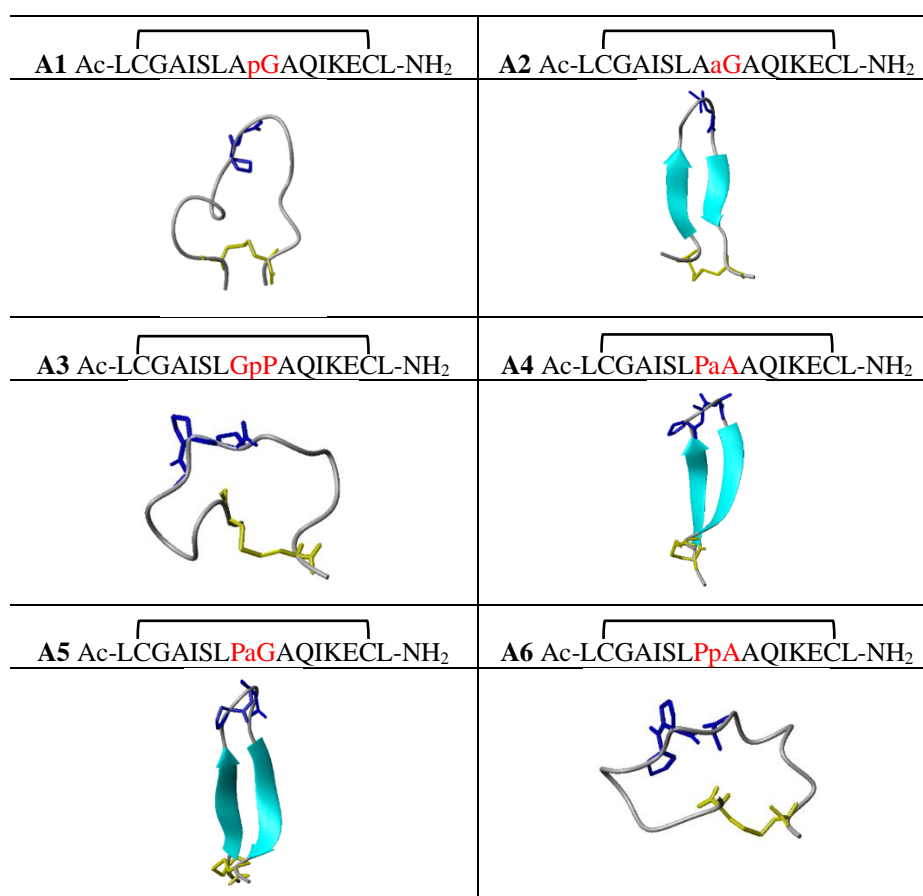
- introducing salt bridges by adding to the peptide sequence amino acids with electrically charged side chains placed opposed to each other²⁶⁴;
- introducing the aryl-aryl interaction^{265,266};
- introducing disulphide bridges^{267,268}, or
- introducing into the loop amino acids with D-configuration, mainly D-proline and D-alanine or D-proline/L-proline, D-proline/glycine^{251,252}.

In my studies, I decided to test the last two mentioned approaches by introducing the changes in the amino acid sequence in the region from A129 to K131, which additionally should enhance the stabilization enforced by the disulphide bridge. The PD-1/PD-L1 complex structure⁶² and MM/GBSA analysis indicate that those amino acid residues are not involved in the proteins complex formation. Their per-residues

energy decomposition is 0.048 kcal/mol for A129, 0.250 kcal/mol for P130 and -0.378 kcal/mol for K131. They were exchanged in varied combinations to D-alanine, glycine and D-proline. D-proline and glycine introduced to **A1** are classical examples of β -turn stabilizing the β -hairpin^{251,252,269,270}. Based on numerous literature publications, it is known that the sequence of connections: L-Pro-D-Ala²⁷¹ or L-Pro-Gly²⁶⁹ and D-Ala-L-Pro-Gly-D-Ala²⁷² or Pro-X (where X= Gly, L-Ala, D-Ala, Aib, Leu)²⁷³ also enforce the formation of the β -turn structure. Based on the above information, I designed five additional analogues in which, together with disulphide bridge introduced earlier to the peptide, aforementioned modifications should enable the orientation of torsion angles in the β -turn in such a way that they force the formation of the β -hairpin structure. Of course, a number of other factors are involved in the stabilization of the β -hairpin, such as hydrophobic and electrostatic interactions as well as hydrogen bonds. Only a thorough analysis using the NMR technique would provide precise information whether the proposed analogues form a structure with a greater contribution of the β -sheet than in the peptide (**10**). Such a conformational analysis could of course be very interesting, but it is not the subject of my PhD thesis; however to investigate the influence of the introduced modification on the formation of β -hairpin, the theoretical structure of peptide (**10**) analogues was designated. The analysis was performed by Ph.D. Adam Sieradzan using All-atom Molecular Dynamics simulation by the AMBER16 software package²⁷⁴. The obtained structures are presented in Table 17. The structures of analogues **A1**, **A3** and **A6** display structural similarities with peptide (**10**) and BMS compounds (Table 17)¹⁸⁰.

Like in case of the PD-1 and PD-L1 derived peptides, I evaluated the new compounds by designating their affinity to PD-L1 by SPR. The received results indicate that the introduced changes in the loop do not improve affinity to PD-L1 compared to peptide (**10**). Exchanging APK to PpA in **A6** even lead to the loss of affinity to the PD-L1 protein. The K_D for the **A4** analogue with PaA in the loop is almost the same as the one received for peptide (**10**). The K_D obtained for **A3** and **A5** is in the same range of magnitude as for their parent peptide, however, their binding to PD-L1 is weaker.

Table 17. Theoretical structures of peptide (**10**) analogues. D-amino acids are marked with a lowercase letter. Red – the exchanged amino acids from the peptide (**10**) loop.



7. Peptide PD-1(122-138)^{C123-S137C} analogues evaluation in the *in vitro* cellular assays

Modification introduced to peptide (**10**) analogues led to changes in their stability and reduced the interaction with the component of the medium. The substitution of L by D amino acids is a common procedure reported in the literature to reduce the interaction with the components of FBS²⁵³ and which is a standard method to enhance the peptide stability to the proteolytic degradation^{181,275}. The strongest drop in concentration was observed for **A3** after 24 h of incubation and it was 19% compared with the control. The results obtained for **A4**, **A5** and **A6** show that the highest decrease in concentration was 3% for **A6** after 24 h of incubation; however, this result is in the range of error. The peptides **A3-A6** display lower affinity to the component of the tested medium than peptide (**10**) for which the concentration in time 0 compared with control was 81% and after 24 h of incubation it decreased to 55%.

Subsequently, I examined the influence of peptide **(10)** analogues on the viability of the Jurkat E6.1 and TCS Ctrl cell lines. Only two tested peptides, **A5** and **A6** exhibited a slight cytotoxicity to the Jurkat E6.1 cells at the highest tested concentration, but it did not exceed 10%. For peptide **(10)**, changes in the cell viability were also observed only for the highest tested concentration. It is worth to mention that the slight proliferation effect on TCS Ctrl cells observed in the case of treating them with peptide **(10)** is strongly amplified in the case of peptides **A5** and **A6**. It is also observed for **A3** and **A4**, however, the effect is not as intense.

In the cell functional assay performed to examine the competitive properties of peptide **(10)** analogues, it can be observed that changes introduced in the sequence of **A3** led to the displacement of PD-1 in a dose-depending manner. For peptide **(10)** and the other analogues, this effect was not observed in the tested conditions. In the stimulation assay, based on a reporter gene expression (NF- κ B::eGFP) system, peptide **(10)** and analogues **A3**, **A4** and **A5** restore the eGFP expression only at the highest concentration used in the test; however, this effect is not statistically significant. Taking into consideration the received results, the modification introduced in the peptide **(10)** loop led to an increase of competitive properties of **A3**, however, it did not improve the ability to restore the eGFP expression by inhibition of the PD-1/PD-L1 complex formation.

The reports published by Wang K. et al.²⁰⁶ regarding stabilization of β -hairpin in peptides targeting PD-1/PD-L1 indicate that the introduction of D-proline to the loop of the peptides and two tryptophan residues increases the affinity of the peptide to PD-1 in SPR analysis and increases the secretion of IL-2 by activated Jurkat cells in a co-culture assay compared to the native peptide trimmed from the PD-L1 structure²⁰⁶. It indicates that improvements of peptide **(10)** or **A3** may lead to the increase of its inhibitory potential. Further improvements of the peptide **(10)** structure are currently being implemented; however, they will not be discussed in this work. It is worth to mention that the research present in this work is a basic research and peptides structures required optimalization and development.

V. Conclusions

In my doctoral thesis, I focused on finding the peptide inhibitors of the PD-1/PD-L1 complex formation which will be able to restore the function of the immune system. Results received by me allowed the following conclusions to be drawn:

- From the PD-1 derived peptides, seven interact with PD-L1, with the strongest binding determined for PD-1(122-138)^{C123-S137C} - peptide **(10)** and PD-1(119-142)^{C123-S137C} - peptide **(7)**. Peptide **(7)** has the ability to displace PD-1 from the complex with PD-L1 in a competitive bioassay while peptide **(10)** exhibits the best inhibitory capacities in the cell-based assay. According to NMR data, peptide **(10)** possesses the β -hairpin like structure and interacts with PD-L1 in the same place as PD-1.
- From the PD-L1 derived peptides, twelve bind to PD-1, with the strongest affinity for peptides PD-L1(111-127)^{(Y112C-I126C)M115Nle} - **(L11)**, and PD-L1(113-126)^{(C114-K124C)G120F} - **(L17)**. Peptide **(L11)** displaces PD-L1 from the complex with PD-1 in a competitive bioassay while **(L17)** does not have such abilities. Moreover, only peptide **(L11)** disrupts the proteins binding in a cellular assays, restoring the PD-1 signaling pathway.
- The designed analogues of peptide **(10)** interact with the PD-L1 protein weaker than the parent peptide but three of them have a binding constant of the same order of magnitude. Introducing the D-amino acids to the loop of peptide **(10)** positively influences the stability of the peptides and their effect on viability of cell lines. Proposed modification in the peptide **(10)** loop led to an increase of the competitive properties of **A3**, however, it did not improve the ability to restore the eGFP expression by inhibition of the PD-1/PD-L1 complex formation.

The results obtained in this doctoral thesis contribute to the development of the knowledge in the field of the PD-1/PD-L1 complex antagonists. The results collected during my research regarding inhibitors of the PD-1/PD-L1 complex formation may be used in the future as a starting point for designing high performance immune-modulators.

VI. Materials and methods

1. Materials and general information

- All proteins used in this work are extracellular domains of recombinant human proteins.
 - Recombinant human PD-L1 protein with C-terminal His Tag, expression system HEK 293 –purchased from GenScript Biotech, USA (#Z03424);
 - Recombinant human PD-1 Chimera protein with C-terminal human Fc tag from IgG1 antibody, expression system CHO - purchased from GenScript Biotech company, USA (#Z03370);
 - Recombinant biotinylated human PD-1 protein with C-terminal His Tag, expression system HEK 293 - purchased from Sino Biological company, China (#10377-H08H-B);
 - Recombinant human PD-1, expression system *E. coli* - purchased from Recepton company, Poland (#R1-001-03);
 - Recombinant human PD-L1 protein with C-terminal His Tag, expression system HEK 293 - purchased from GenScript Biotech, USA (#Z03425);
 - Recombinant human PD-L1 Chimera protein with C-terminal human Fc tag from IgG1 antibody, expression system CHO - purchased from GenScript Biotech company, USA (#Z03371);
 - Recombinant biotinylated human PD-L1 protein with C-terminal His Tag, expression system HEK 293 - purchased from Sino Biological company, China (#10084-H08H-B).
- Materials used in cell culture: PBS (Lonza Group Ltd, Switzerland, #BE17-517Q), FBS (Gibco, #10270-106), RPMI 1640 medium (Sigma-Aldrich, #R8758), F-12 HAM medium (Sigma-Aldrich, #N6658), accutase (Sigma-Aldrich, #SCR005), penicillin-streptomycin (p/s) (Sigma-Aldrich, #N0781).
- The Jurkat E6.1 and CHO-K1 cells were purchased from Cell Line Service GmbH company. The reporter cells and TCS are the property of the laboratory of prof. Peter Steinberger, Institute of Immunology, Medical University of Vienna, Vienna, Austria. Jurkat E6.1, reporter cells, BW5147 and TCS cell lines were maintained

in RPMI 1640, while CHO K-1 cell line were maintained in the HAM-12 medium. All culture media were supplemented with 1% of penicillin and streptomycin with addition of 10% of heat inactivated FBS. The cell lines were incubated at 5% CO₂ atmosphere in a humidified incubator at 37°C. The cell lines culture were maintained according to the manufacturer procedure.

- The following antibodies from Biolegend (USA) were used in the flow cytometry analyses: APC-conjugated anti-human PD-1 Ab (#EH12.2H7), PE-conjugated anti-human PD-L1 Ab (#29E.2A3), APC-conjugated anti-human CD86 Ab (#IT2.2), PE-Cy7-conjugated anti-human CD3 Ab (#UCHT-1), APC-conjugated anti-mouse CD45 Ab (#104) (was used to exclude TCS cells in reporter assays), APC-conjugated mouse anti-human IgG Ab (Fc-specific) (#366906). Additionally, an antibody from Jackson Immuno Research Europe Ltd was used: PE-conjugated donkey anti-human IgG Ab (Fc-specific) (#709-116-098).
- The antibodies used as a positive control: anti-PD-1 antibody was purchased from Promega company, USA (#J1201); atezolizumab (Tecentriq®, Roche) and pembrolizumab (Keytruda®, MSD Sharp & Dohme GmbH) mAbs were a generous gift for prof. Steinberger for the tests.
- In all experiments and the peptide purification, the MiliQ water was used.
- Some figures were self-created on the Biorender.com platform or customized from ready schemes available on this platform.

2. Peptides synthesis

Peptides were synthesised applying the solid-phase peptides synthesis (SPPS) protocol using an automated microwave peptide synthesizer (Liberty Blue, CEM Corporation, Matthews, NC, USA). The peptides synthesis was performed on a polyethylene glycol TentaGel R RAM resin with 0.21 mmol/g loading or a ProTide (CEM) resin with 0.18 mmol/g, using the Fmoc/tBu chemistry. Standard amino acid derivatives were used during the peptides synthesis at concentration 0.2 M. The single cycle of the peptide synthesis using the Liberty Blue microwave synthesiser is presented below.

- Removing Fmoc protecting group from resin or α -amine group of amino acid by the 20% piperidine in the N,N-dimethylformamide (DMF);
- Washing of the resin (peptidyl-resin) by the DMF;
- Coupling of the double excess of amino acid residue to resin loading in the presence of 0.5 M N,N-diisopropylcarbodiimide (DIC) in the DMF (as an activating factor) and 1.0 M ethyle cyano(hydroxyamino)acetate (Oxyma Pure) in the DMF (as an auxiliary nucleophile and racemization suppressor);
- Washing of the peptidyl-resin and removal of the excess of the reagents by the DMF.

After the coupling of the last amino acid from the peptide sequence, the Fmoc protecting group from the α -amine group of amino acid was removed by the 20% piperidine in the DMF and peptidyl-resin was washed by the DMF to remove the excess of the reagents. Subsequently, the N-terminal part of the peptide was modified depending on the required product:

- Peptides with acetyl groups on N-terminal - amine group of the peptides was acetylated by the reaction with 1-acetylimidazole. Peptidyl-resin was mixed with 1-acetylimidazole (1.10 g/1 g of resin) in the DMF (10 mL) and stirred at ambient temperature for 24 h. At the end, the peptidyl-resin was washed: 3 times in the DMF, 3 times in the DMF/dichloromethane (DCM) (1:1, v:v), and 3 times in the DCM.
- Peptides with biotin on N-terminal – the reaction of biotin coupling was run manually using: 2.5 eq. of biotin (relative to resin loading), 2.36 eq. of TBTU (relative to resin loading), and 2 eq. of DIPEA (N,N-diisopropylethylamine) (relative to biotin). Primarily, the biotin with 2-(1H-benzotriazole-1-yl)-1, 1, 3, 3-tetramethylaminium tetrafluoroborate (TBTU) was mixed in a small amount of the DMF (3 ml) and then DIPEA was added. After 3 minutes, the mixture was added to the peptidyl-resin. The coupling reaction was run for 1 h with constant shaking and repeated once with a new portion of the reagents. At the end, the peptidyl-resin was washed: 3 times in the DMF, 3 times in the DMF/ DCM (1:1, v:v), and 3 times in the DCM.

3. Peptides cleavage

Following the synthesis, the peptides were cleaved from the resin with the simultaneous removal of the side-chain protection groups by the mixture of 88% trifluoroacetic acid (TFA), 5% phenol, 5% H₂O, and 2% triisopropylsilane (TIPS) (v:v:v:v). The mixture was added to the peptidyl-resin in the ratio of 10 ml to 1g of the resin and the reaction was conducted for 2 h at ambient temperature. Subsequently, the solution was filtered from the resin, vacuum-concentrated, and suspended in ice-cold Et₂O. The peptides in Et₂O were centrifuged – 15 min, 4,000 rpm at 4°C and decanted. The step of peptide centrifugation and decantation was repeated thrice, each time with the addition of a new portion of Et₂O. Crude peptide was dried in vacuum desiccator, then dissolved in H₂O, and lyophilized.

4. Formation of disulphide bridges

To form intramolecular disulphide bonds between sulfhydryl groups of cysteine residues, the peptides were dissolved in H₂O:MeOH:AcOH (1:9:1, v:v:v) to a final concentration of 40 mg/l. Next, the solution of iodine in MeOH was added to receive the straw-yellow colour of the solution. The reaction was conducted at ambient temperature for 1 h with continuous stirring. After the reaction, iodine was removed from the solution by the filtration through the ion exchange resin - Dowex. Subsequently, the solution was evaporated under reduced pressure, the peptide was dissolved in H₂O, and lyophilised. The product of the reaction was analysed using RP-HPLC and LC ESI-IT-TOF MS according to the conditions described in the peptide purification section.

5. Peptide Purification

Peptides were purified using the RP-HPLC technique. Before the purification, the peptides were dissolved in H₂O or in the AcOH and then adjusted with the H₂O to the final concentration of AcOH not exceeding 15%. To the peptides with free sulfhydryl groups, 10-fold molar excess of dithiothreitol (DTT) was added. The solution of peptide with DTT in H₂O was heated for 30 min in an ultrasonic bath at 50°C. Peptides were purified on the semi-preparative Luna C8 (2) (250 mm × 20 mm, 5 μm) column from Phenomenex (Torrance, CA, USA) using the mobile phase:

(I)

Buffer A - 0.01 M ammonium acetate (6 ml acetic acid and 7.7 g of ammonium acetate for 1 l) in H₂O, the buffer was adjusted to pH 4.75

Buffer B - 0.01 M ammonium acetate (6 ml acetic acid and 7.7 g of ammonium acetate for 1 l) in 60% (v:v) acetonitrile (ACN) in H₂O, the buffer was adjusted to pH 4.75

(II)

Solution A - 0.1% TFA in H₂O

Solution B - 0.08% TFA in 80% ACN in H₂O.

All peptides were purified in a linear gradient characterised in the tables below (Table 18-21). The analysis was monitored by UV absorbance at 223 and 254 nm. After purification, the peptides purity was confirmed by the RP-HPLC technique using:

(III)

UFLC LC-20A with ELSD-LT detector (Shimadzu, Shimpol, Warsaw, Poland) using a linear gradient from 5% to 100% B in A over 60 min using the mobile phase described in (II) on a Kromasil C8 (250 mm x 4.6 mm, 5 µm) analytical column from Phenomenex (Torrance, CA, USA) with the flow rate volume of 1 ml/min, or

(IV)

NEXERA X2 with two detectors ELSD-LTII and SPD-M20A (Shimadzu, Shimpol, Warsaw, Poland), using a linear gradient from 5% to 100% B in A over 15 min using the mobile phase described in (II) on a Kinetex C8 column (2.1 x 100 mm, 2.6 µm) analytical column from Phenomenex (Torrance, CA, USA) with the flow rate volume of 0.5 ml/min.

Additionally, the molecular mass of the received peptides was confirmed by:

(V)

liquid chromatography coupled with electrospray ionization, ion trap, and time-of-flight mass spectroscopy (LC ESI-IT-TOF MS) (Shimadzu, Shimpol, Warsaw, Poland), or

(VI)

matrix assisted laser desorption ionization with time-of-flight mass spectroscopy
MALDI-TOF MS Biflex III or autoflex maX (Bruker, Daltonics).

6. Peptides characterization

Table 18. Characterization of the PD-1 derived peptides. The methods of defining the peptides' molecular mass, mobile phase used during purification and technic used for defining the peptides purity are mark by the Roman numerals from I-VI which are decoded in the previous chapter.

No.	PD-1 derived peptides	M _{theoretical}	M _{observed}	Peptides purification condition (linear gradient and mobile phase)	Retention time on analytical column [min]	Peptide purity [%]
(1)	PD-1(68-78) Ac-YRNleSPSNQTDK-NH ₂	1348.58	1348.613 (V)	10-30% B in A over 90 min; mobile phase (I)	14.94 (III)	99.2
(2)	PD-1(62-80) Ac-SFVLNWYRNleSPSNQTDKLA-NH ₂	2279.06	2279.996 (V)	20-50% B in A over 90 min; mobile phase (I)	28.62 (III)	99.9
(3)	PD-1(62-80)^{W67C-L79C} Ac-SFVLN YC YRNleSPSNQTDK CA -NH ₂	2183.93	2184.887 (V)	20-50% B in A over 90 min; mobile phase (I)	24.09 (III)	99.0
(4)	PD-1(62-80)^{R69C-D77C} Ac-SFVLNWY CN leSPSNQ TCK LA-NH ₂	2211.97	2211.954 (V)	20-50% B in A over 90 min; mobile phase (I)	31.59 (III)	90.3
(5)	PD-1(119-142) Ac-GTYLAbuGAISLAPKAQIKESLRAEL-NH ₂	2554.36	2555.25 [M+H] ⁺ (VI)	20-50% B in A over 90 min; mobile phase (I)	28.0 (III)	94
(6)	PD-1(119-142)^{T120C-E141C} Ac-GCYLAbuGAISLAPKAQIKESLRA EL -NH ₂	2528.31	2529.59 [M+H] ⁺ (VI)	20-50% B in A over 90 min; mobile phase (I)	28.8 (III)	96.6
(7)	PD-1(119-142)^{C123-S137C} Ac-GTYL CG AISLAPKAQIK ECL RAEL-NH ₂	2586.37	2587.66 [M+H] ⁺ (VI)	20-50% B in A over 90 min; mobile phase (I)	29.6 (III)	94.9
(8)	PD-1(119-142)^{A125C-K135C} Ac-GTYLAbu GC ISLAPKAQ ICES LRAEL-NH ₂	2559.27	2560.99 [M+H] ⁺ (VI)	-	-	-
(9)	PD-1(122-138) Ac-LAbuGAISLAPKAQIKESL-NH ₂	1763.99	1763.66 (V)	20-50% B in A over 90 min; mobile phase (I)	25.99 (III)	99.9

(10)	PD-1(122-138)^{C123-SI37C} Ac-LCGAISLAPKAQIKECL-NH ₂	1795.97	1796.90 [M+H] ⁺ (VI)	20-50% B in A over 90 min; mobile phase (I)	27.94 (III)	94.0
(11)	PD-1(122-138)^{A125C-KI35C} Ac-LAbuGCISLAPKAQICESL-NH ₂	1768.87	1769.93 (V)	20-50% B in A over 90 min; mobile phase (I)	30.59 (III)	96.6
(12)	PD-1(124-136)^{A125C-KI35C} Ac-GCISLAPKAQICE-NH ₂	1370.67	1371.66 (V)	20-50% B in A over 90 min; mobile phase (I)	25.15 (III)	99.4
(13)	PD-1(132-136) Ac-AQIKE-NH ₂	628.34	628.32 (V)	5-30% B in A over 75 min; mobile phase (I)	10.24 (III)	100

Table 19. Characterization of peptide (10) analogues. The methods of defining the peptides' molecular mass, mobile phase used during purification and technic used for defining the peptides purity are mark by the Roman numerals from I-VI which are decoded in the previous chapter.

No.	Peptide (10) analogues	M _{theoretical}	M _{observed}	Peptides purification condition (linear gradient and mobile phase)	Retention time on analytical column [min]	Peptide purity [%]
A1	Ac-LCGAISLApGAQIKECL-NH ₂	1724.90	1725.82 [M+H] ⁺ (VI)	25-55% B in A over 90 min; mobile phase (I)	-	-
A2	Ac-LCGAISLAaGAQIKECL-NH ₂	1698.86	1698.89	25-55% B in A over 90 min; mobile phase (I)	-	-
A3	Ac-LCGAISLpPAQIKECL-NH ₂	1750.92	1750.93 (V)	25-55% B in A over 90 min; mobile phase (I)	8.107 (IV)	91.3
A4	Ac-LCGAISLPaAAQIKECL-NH ₂	1738.92	1738.94 (V)	25-55% B in A over 90 min; mobile phase (I)	7.688 (IV)	95.8
A5	Ac-LCGAISLPaGAQIKECL-NH ₂	1724.90	1725.84 [M+H] ⁺ (VI)	25-55% B in A over 90 min; mobile phase (I)	8.002 (IV)	87.7
A6	Ac-LCGAISLPpAAQIKECL-NH ₂	1764.93	1787.94 [M+Na] ⁺ (VI)	25-55% B in A over 90 min; mobile phase (I)	7.508 (IV)	94.6

Table 20. Characterization of the PD-L1 derived peptides. The methods of defining the peptides' molecular mass, mobile phase used during purification and technic used for defining the peptides purity are mark by the Roman numerals from I-VI which are decoded in the previous chapter.

No.	PD-L1 derived peptides	M _{theoretical}	M _{observed}	Peptides purification condition (linear gradient and mobile phase)	Retention time on analytical column [min]	Peptide purity [%]
(L1)	PD-L1(19-26) Ac-FTVTVPKD-NH ₂	946.50	946.48 (V)	15-35% B in A over 90 min; mobile phase (I)	20.97 (III)	99.0
(L2)	PD-L1(52-68) Ac-ALIVYWENleEDKNIIQFV-NH ₂	2133.07	2133.68 (V)	35-65% B in A over 90 min; mobile phase (I)	40.24 (III)	-
(L3)	PD-L1(52-73) Ac-ALIVYWENleEDKNIIQFVHGEEED-NH ₂	2700.25	2700.39 (V)	35-65% B in A over 90 min; mobile phase (I)	40.30 (III)	-
(L4)	PD-L1(52-79) Ac-ALIVYWENleEDKNIIQFVHGEEEDLKVQHS-NH ₂	3392.65	3392.50 (V)	35-65% B in A over 90 min; mobile phase (I)	45.07 (III)	-
(L5)	PD-L1(45-68) Ac-EKQLDLAALIVYWENleEDKNIIQFV-NH ₂	2930.48	2930.37 (V)	-	-	-
(L6)	PD-L1(56-66) Ac-YWENleEDKNIIQ-NH ₂	1490.65	1490.58 (V)	25-55% B in A over 90 min; mobile phase (I)	29.74 (III)	99.0
(L7)	PD-L1(111-127) ^{M115Nle} Ac-VYRAbuNleISYGGADYKRIT-NH ₂	1999.94	1999.94 (V)	30-60% B in A over 90 min; mobile phase (I)	35.14 (III)	96.2
(L8)	PD-L1(113-126) ^{M115Nle} Ac-RAbuNleISYGGADYKRI-NH ₂	1636.76	1636.88 (V)	20-50% B in A over 90 min; mobile phase (I)	5.719 (IV)	99.1
(L9)	PD-L1(113-126) ^{(C114-K124C) M115Nle} Ac-RCNleISYGGADYCRINH ₂	1629.68	1627.51 (V)	20-50% B in A over 90 min; mobile phase (I)	25.58 (III)	99.8
(L10)	PD-L1(110-128) ^{(V111C-T127C) M115Nle} Ac-GCYRAbuNleISYGGADYKRICV-NH ₂	2159.93	2161.46 [M+H] ⁺ (VI)	20-50% B in A over 90 min; mobile phase (I)	25.11 (III)	95.7
(L11)	PD-L1(111-127) ^{(Y112C-I126C) M115Nle} Ac-VCRAbuNleISYGGADYKRCT-NH ₂	1927.81	1927.95 (V)	20-50% B in A over 90 min; mobile phase (I)	22.43 (III)	95.7
(L12)	PD-L1(113-126) ^{(C114-K124C) G120S; M115Nle} Ac-RCNleISYGSADYCRINH ₂	1657.69	1658.86 [M+H] ⁺ (VI)	20-50% B in A over 90 min; mobile phase (I)	5.719 (IV)	99.5

(L13)	PD-L1(113-126) ^{(C114-K124C) G120F; M115Nle} Ac-RCNleISYGFADYCRl-NH ₂	1717.73	1718.94 (V)	20-50% B in A over 90 min; mobile phase (I)	6.402 (IV)	99.0
(L14)	PD-L1(113-126) ^{(C114-K124C) G120E; M115Nle} Ac-RCNleISYGEADYCRl-NH ₂	1699.70	1700.85 [M+H] ⁺ (VI)	20-50% B in A over 90 min; mobile phase (I)	5.615 (IV)	99.0
(L15)	PD-L1(121-125) Ac-ADYKR-NH ₂	692.35	693.345 (V)	05-25% B in A over 60 min; mobile phase (I)	10.21 (III)	99.5
(L16)	PD-L1(111-127) Ac-VYRABuMISYGGADYKRIT-NH ₂	2017.98	2017.59 (V)	20-50% B in A over 90 min; mobile phase (I)	6.008 (IV)	99.9
(L17)	PD-L1(113-126) ^{(C114-K124C) G120F} Ac-RCMISYGFADYCRl-NH ₂	1735.77	1735.79 (V)	20-50% B in A over 90 min; mobile phase (I)	6.602 (IV)	99.0

Table 21. Characterization of the PD-L1 derived peptides with 5-glycine and biotin on N-terminal. The methods of defining the peptides' molecular mass, mobile phase used during purification and technic used for defining the peptides purity are mark by the Roman numerals from I-VI which are decoded in the previous chapter.

No.	PD-L1 derived peptides	M _{theoretical}	M _{observed}	Peptides purification condition (linear gradient and mobile phase)	Retention time on analytical column [min]	Peptide purity [%]
(L1)	PD-L1(19-26) B-GGGGG-FTVTVPKD-NH ₂	1415.92	1415.42 (V)	20-50% B in A over 90 min; mobile phase (II)	21.16 (III)	99.2
(L3)	PD-L1(52-73) B-GGGGG-ALIVYWENleEDKNIIQFVHGEEED-NH ₂	3169.67	3169.58 (V)	25-55% B in A over 90 min; mobile phase (II)	25.69 (III)	-
(L4)	PD-L1(52-79) B-GGGGG- ALIVYWENleEDKNIIQFVHGEEEDLKVQHS-NH ₂	3862.06	3861.78 (V)	30-60% B in A over 90 min; mobile phase (II)	35.10 (III)	-
(L5)	PD-L1(45-68) B-GGGGG- EKQLDLAALIVYWENleEDKNIIQFV-NH ₂	3399.90	3399.98 (V)	-	39.47 (III)	-
(L6)	PD-L1(56-66) B-GGGGG-YWENleEDKNIIQ-NH ₂	1960.06	1959.88 (V)	-	24.94 (III)	96.6
(L7)	PD-L1(111-127) ^{M115Nle} B-GGGGG-VYRABuNleISYGGADYKRIT-NH ₂	2469.35	2469.16 (V)	25-55% B in A over 90 min; mobile phase (II)	27.77 (III)	99.6

(L8)	PD-L1(113-126) ^{M115Nle} B-GGGGG-RAbuNleISYGGADYKRI-NH ₂	2106.17	2106.05 (V)	25-55% B in A over 90 min; mobile phase (II)	5.061 (IV)	99.5
(L9)	PD-L1(113-126) ^{(C114-K124C) M115Nle} B-GGGGG-RCNleISYGGADYCRINle-NH ₂	2097.00	2096.55 (V)	25-55% B in A over 90 min; mobile phase (II)	23.79 (III)	90.3
(L10)	PD-L1(110-128) ^{(V111C-T127C) M115Nle} B-GGGGG-GCYRABuNleISYGGADYKRICV-NH ₂	2629.35	2629.05 (V)	25-55% B in A over 90 min; mobile phase (II)	24.81 (III)	98.6
(L11)	PD-L1(111-127) ^{(Y112C-I126C) M115Nle} B-GGGGG-VCRAbuNleISYGGADYKRCT-NH ₂	2397.22	2396.94 (V)	25-55% B in A over 90 min; mobile phase (II)	23.30 (III)	99.5
(L12)	PD-L1(113-126) ^{(C114-K124C) G120S; M115Nle} B-GGGGG-RCNleISYGSADYCRINle-NH ₂	2127.11	2128.05 [M+H] ⁺ (VI)	25-55% B in A over 90 min; mobile phase (II)	5.539 (IV)	99.5
(L13)	PD-L1(113-126) ^{(C114-K124C) G120F; M115Nle} B-GGGGG-RCNleISYGFADYCRINle-NH ₂	2187.14	2187.25 (V)	25-55% B in A over 90 min; mobile phase (II)	6.387 (IV)	98.8
(L14)	PD-L1(113-126) ^{(C114-K124C) G120E; M115Nle} B-GGGGG-RCNleISYGEADYCRINle-NH ₂	2169.12	2169.93 (V)	25-55% B in A over 90 min; mobile phase (II)	5.615 (IV)	99.8
(L15)	PD-L1(121-125) B-GGGGG-ADYKR-NH ₂	1161.77	1162.52 (V)	5-25% B in A over 60 min; mobile phase (I)	10.50 (III)	97.5
(L16)	PD-L1(111-127) B-GGGGG-VYRABuMISYGGADYKRIT-NH ₂	2487.39	2486.67 (V)	25-55% B in A over 90 min; mobile phase (II)	25.31 (III)	99.1
(L17)	PD-L1(113-126) ^{(C114-K124C) G120F} B-GGGGG-RCMISYGFADYCRINle-NH ₂	2205.19	2205.29 (V)	25-55% B in A over 90 min; mobile phase (II)	6.36 (IV)	90.2

7. Testing of the peptides binding properties

The binding properties of the designed peptides to the target molecules were examined in two different systems of the SPR analysis and indirect ELISA depending on the peptides. The PD-1 derived peptides and the peptide (**10**) analogues were examined using the SPR analysis on a CM5 sensor chips. The PD-L1 derived peptides were evaluated using the SPR analysis on an SA sensor chips and by indirect ELISA.

7.1. The SPR Analysis on a CM5 sensor chips

The SPR analyses were performed using the Biacore T200 equipment (Cytiva, Malborough, USA) according to the manufacturer's manual. The interaction of the PD-1 derived peptides with PD-L1 was analysed in the system where the His-PD-L1 protein was immobilized on the surface of a CM5 sensor chip (Cytiva, Malborough, USA). PD-L1 was suspended in a 10 mM sodium acetate buffer, pH 4.5, as described previously¹⁸¹. The immobilization level was 6500 RU \pm 880 RU. The peptides concentrations were prepared by the serial dilution method in the PBS-P buffer (Cytiva, Malborough, USA #28995084) and injected over the CM5 sensor chip with immobilized PD-L1. As a control, PD-1-Fc was injected. All analyses were run with PBS-P as a running buffer at 25°C and the flow rate was set to 30 μ l/min. The regeneration step was done with 1.5 M NaCl and 10 mM glycine, pH 3 with further wash with a 50% DMSO solution. The obtained data were analysed using the Biacore T200 Evaluation Software (Cytiva, Malborough, USA). The titration of the peptides or the PD-1 protein was performed at least three times on the sensor surface with at least two independent PD-L1 immobilizations. The sensorgrams are presented for the results from which the background signal from the reference cell was subtracted.

7.2. The SPR Analysis on an SA sensor chips

The SPR analyses were performed using the Biacore T200 equipment (Cytiva, Malborough, USA) according to the manufacturer's manual. The interaction of the PD-L1 derived peptides with PD-1 was analysed in the system where the peptides were immobilized on the surface of an SA sensor chip (Cytiva, Malborough, USA). Peptides were suspended in the PBS-P buffer. The immobilization level was \sim 800 RU, with an

exception for (L1) which was immobilized to a final value of ~500 RU. The PD-1 concentrations were prepared by the serial dilution method in the PBS-P buffer and injected over the SA sensor chip with the immobilized peptides. As a control, biotinylated PD-L1 was immobilized on an SA sensor chip. All analyses were run with PBS-P as a running buffer at 25°C and the flow rate was set to 30 µl/min. The regeneration step was done with 1.5 M NaCl and 10 mM glycine, pH 3. The obtained data were analysed using the Biacore T200 Evaluation Software (Cytiva, Malborough, USA). The titration of the PD-1 protein was performed at least three times on the sensor surface. The sensorgrams are presented for the results from which the background signal from the reference cell was subtracted.

7.3. Indirect ELISA

Indirect ELISA was performed according to the following steps.

1. 96-well streptavidin plates (Nunc, Thermo Fisher Scientific) were washed 3 times with 200 µl of PBS-T (0.05% Tween-20 in PBS with 0.3 M NaCl, pH 7.4).
2. Wells were covered with 100 µl of biotinylated peptides dissolved in water or biotinylated PD-L1 protein dissolved in PBS (positive control) and incubated for 1 h at 37 °C with continuous shaking.
3. Wells were washed 5×200 µl by PBS-T.
4. 100 µl of 2-fold serial dilutions of PD-1-Fc in PBS-T was added to the wells with peptides or PD-L1 and incubated for 2 h at 37 °C with continuous shaking.
5. Wells were washed 5×200 µl by PBS-T.
6. 100 µl of HRP conjugated goat anti-human IgG (Bio-Rad, #1721050) Ab in PBS-T at the concentration of 1:3000 (v:v) was added to each well and incubated for 1 h at 37 °C with continuous shaking.
7. Wells were washed 5×200 µl by PBS-T.
8. 100 µl of TMB (Thermo Scientific, #N301) was added to each well and incubated for 15 min. After the incubation time, the absorbance was measured on the Infinite M200 Pro (Tecan, USA) plates reader, at a measurement wavelength of 650 nm and a reference length of 492 nm.

The assay was performed at least three times, in duplicate and the results were analysed using the GraphPad Prism 8 software.

8. Peptides stability in RPMI 1640

Chosen peptides from all groups were subjected to the stability studies. The tests were performed using the RPMI 1640 medium with the addition of 10% FBS at pH 8.0. Peptides were dissolved in H₂O and added to the medium in the ratio 1:3 (v:v). The final peptides concentration in the sample was 100 μM. The samples were collected at two times, 0 h and after 24 h of incubation. The incubation was performed at 37°C with continuous stirring. Then, the samples were immersed in liquid N₂ and stored at -80°C until the end of the experiment. To prepare the samples for analysis, they were thawed on ice and suspended in a 4-fold excess of absolute ethanol (v:v). Subsequently, the samples were centrifuge at 15,000 rpm at 4°C for 20 min, after this step, the supernatant was transferred to the test tubes and evaporated using the vacuum concentrator. Concentrated samples were dissolved in 100 μL of 0.1% TFA in H₂O. The analysis was run on the analytical RP-HPLC using Luna C18(2) (250 mm x 4.6 mm, 5 μm) column and a linear gradient from 5% B to 100% B in A over 60 min. As the mobile phase, the following solutions were used: a - 0.1% TFA in H₂O, B - 0.08% TFA in 80% ACN in H₂O. Two controls, peptides dissolved in water and the medium with the 10% FBS (without the peptides), were simultaneously tested - to check the effect of the procedure on the peptides and the medium, respectively.

9. Jurkat E6.1, CHO-K1, and BW5417 (TCS Ctrl) cell lines viability assay

Cell line viability was examined on the three cell lines – Jurkat E.6.1, CHO-K1, and TCS Ctrl. The experiments were performed on the 96-well solid white plates for cell culture. Jurkat E6.1 and TCS Ctrl were seeded into wells on the day of the experiment at the density of 2×10^4 cells per well in 50 μl of the RPMI 1640 medium with 10% FBS and 50 μl of peptides were added to the wells. CHO-K1 cells were seeded the day before the experiment at the density of 1×10^4 cells per well in 100 μl of the HAM-12 medium with 10% FBS. On the day of the experiment, the medium was removed and immediately converted to a fresh one with peptides. The peptides were prepared on the day of the assay at six concentrations by the 3-fold serial dilutions in the cell culture medium. The final peptides concentration range was from 150 μM to 0.62 μM. The peptides were added to the cells and incubated for 24 h in the standard cell culture conditions. After the incubation period, the plates were equilibrated to

ambient temperature for 15 min and 100 μ l of Cell Titter-Glo (Promega Corporation, #G7570) was added to each well. The plates were shook on the plate shaker for 2 minutes at 250 rpm to induce cell lysis and then equilibrated for 10 minutes to stabilize the luminescence signal. The luminescence was measured on the Spark M10 (Tecan, Switzerland) plate reader with the integration time of 0.5 s. The experiment was performed at least three times, in triplicate, and the results were analysed by the GraphPad Prism 8 software.

10. Competitive assay at the cellular level

The competitive potency of the PD-1 derived peptides and the peptide (**10**) analogues were tested using the BW5417 cell line expressing PD-L1 (TCS PD-L1). The peptides were dissolved in H₂O and diluted to the final concentration of 12% of H₂O by PBS with 0.5% FBS. The three-fold serial dilutions of peptides were prepared starting from 150 μ M or 50 μ M to 0.62 μ M. The experiment was run in 5 ml conical bottom tubes for flow cytometry. Peptides were incubated at the indicated concentrations with 10⁵ TSC PD-L1 cells for 120 min at 4°C. Then, human PD-1-Fc was added at the concentration of 1 μ g/ml and incubated for 15 min at 4°C. Binding of PD-1-Fc was detected by PE-labelled donkey anti-human IgG antibody which was incubated with each sample at the concentration of 1:300 (v:v) in PBS with 0.5% FBS for 20 min at 4°C. As a positive control, atezolizumab (Tecentriq®, Roche) mAb anti-PD-L1 was used. Each step of the experiment was followed by the spinning (5 min, 500 rpm at 4°C) and washing of the samples. This step was performed using PBS with 0.5% FBS. The samples were analysed via flow cytometry, and mean and standard deviation of gMFI of the viable cell population were determined²⁴⁹. The experiment was performed at least three times, in triplicate.

The PD-L1 derived peptides were tested using the J-NF- κ B::eGFP expressing PD-1 cells (J-PD-1). As a peptides competitor, the PD-L1-Fc protein was used at a concentration of 1 μ g/ml. Binding of PD-L1-Fc was detected with PE-labeled donkey anti-human IgG antibody at the concentration described above. The rest of the experimental conditions corresponded to the ones described for the PD-1 derived peptides.

The Flow cytometry analysis was performed on a FACSCalibur flow cytometer (Becton Dickinson Immunocytometry System, USA) using the CellQuest software. Data were analyzed with FlowJo (version 10.0.6, Tree Star, Ashland, OR) and GraphPad Prism (version 8, GraphPad Software, Inc., La Jolla, CA).

11. Testing of the peptides inhibition properties for the PD-1/PD-L1 complex formation

The inhibitory properties of the designed peptides were examined in two different systems depending on the examined peptides; the PD-1 derived peptides were examined in the PD-1/PD-L1 blocking bioassay – based on NFAT-RE induced luciferase. Peptide (**10**) analogues and the PD-L1 derived peptides were evaluated in the PD-1/PD-L1 blocking bioassay – based on NF- κ B-RE induced eGFP.

11.1. The PD-1/PD-L1 blocking bioassay – based on NFAT-RE induced luciferase

The assay was performed using a PD-1/PD-L1 Blockade Bioassay kit (Promega Corporation, Madison, WI, USA, #J1250) according to the manufacturer's procedure. The experiments were performed on the 96-well solid white plates for cell culture (Corning, #3917). APC/CHO-K1 with expression of the PD-L1 cells were seeded the day before the experiment at the density of 1×10^4 cells per well in the 100 μ l of the HAM-12 medium with 10% FBS and incubated at 37°C in an atmosphere of 5% CO₂. On the day of the experiment, the medium was removed and immediately converted to a fresh one with peptides. The PD-1 derived peptides were prepared on the day of the assay at five concentration by the 3-fold serial dilutions in the assay medium (RPMI 1640 with 1% FBS). The final peptide concentration ranged from 50 μ M to 0.62 μ M. The 40 μ l peptides were added to the APC/CHO-K1 cells and incubated for 90 min in the standard cell culture conditions. As a positive control, I used an anti-PD-1 antibody (Promega). Subsequently, the effector Jurkat E6.1 cells with the expression of PD-1 were seeded into wells at the density of 2×10^4 cells per well in 40 μ l of the assay medium and incubated for 6 h in the standard cell culture conditions. After the incubation period, the plates were equilibrated to the ambient temperature for 10 min and 80 μ l of the Bio-Glo reagent was added and incubated for 15 more minutes.

After this time, the luminescence was measured on the Spark M10 (Tecan, Switzerland) plate reader with the integration time of 0.5 s. The experiment was performed at least three times, in triplicate, and the results were analysed using the GraphPad Prism 8 software.

11.2. The PD-1/PD-L1 blocking bioassay – based on NF- κ B-RE induced eGFP

The assay was performed using the reporter system established by prof Steinberger's group^{248–250}. The PD-L1 derived peptides and the peptide (**10**) analogues were tested using the reporter assay constructed on the J-NF- κ B::eGFP and TCS cell lines.

The experiments were performed on the 96-well tissue culture treated transparent plates. The seeding density was 5×10^4 cells per well in 50 μ l of the RPMI 1640 medium with 10% FBS for the reporter cells and 2×10^4 cells per well in 50 μ l of the RPMI 1640 medium with 10% FBS for TCS. In the case of the peptide (**10**) analogues, first TCS cells were seeded on the plates to which the peptides or the medium (control) were added and incubated for 90 min. In the case of the PD-L1 derived peptides, the peptides were preincubated with the reporter cells for 90 min. Subsequently, the second cell line was added. The cells with the peptides were cocultured for 24 h at 37°C in an atmosphere of 5% CO₂. The peptides were dissolved in H₂O and diluted to the final concentration in RPMI 1640 with 10% of FBS, the H₂O concentration did not exceed 12%. As a positive control, atezolizumab mAb anti-PD-L1 was used when the peptide (**10**) analogues were tested and pembrolizumab mAb anti-PD-1 was used when the PD-L1 derived peptides were evaluated. After 24 h, the cells were harvested and the eGFP expression was measured by flow cytometry. TCS were excluded from the analysis by APC-conjugated mCD45 mAb. The mean and standard deviation of the geometric mean of the fluorescence intensity (gMFI) of the viable cell population were determined. The experiment was performed at least three times, in duplicate. The flow cytometry analysis was performed on a FACSCalibur flow cytometer (Becton Dickinson Immunocytometry System, USA) using the CellQuest software. Data were analysed with FlowJo (version 10.0.6, Tree Star, Ashland, OR) and GraphPad Prism (version 8, GraphPad Software, Inc., La Jolla, CA).

Publications:

1. **Bojko, M.**, Węgrzyn, K., Sikorska, E., Kocikowski, M., Parys, M., Battin, C., Steinberger, P., Kogut, M., Winnicki, M., Sieradzan, A., Spodzieja, M., & Rodziewicz-Motowidło, S. (2022). *Design, synthesis and biological evaluation of PD-1 derived peptides as inhibitors of PD-1/PD-L1 complex formation for cancer therapy*. *Bioorganic Chemistry*, 128, 1–15.
<https://doi.org/10.1016/j.bioorg.2022.106047>
2. Niedziałkowski, P., **Bojko, M.**, Ryl, J., Wcisło, A., Spodzieja, M., Magiera-Mularz, K., Guzik, K., Dubin, G., Holak, T., Ossowski, T., & Rodziewicz-Motowidło, S. (2021). *Ultrasensitive electrochemical determination of the cancer biomarker protein sPD-L1 based on a BMS-8-modified gold electrode*. *Bioelectrochemistry*, 139, 1–10.
<https://doi.org/10.1016/j.bioelechem.2021.107742>
3. **Bojko, M.**, Falandysz, J., & Maćkiewicz, Z. (2015). Oznaczanie witamin rozpuszczalnych w tłuszczach zawartych w grzybach z zastosowaniem HPLC. W H. Koroniak & J. Barciszewski (red.), *Na pograniczu chemii i biologii, t. 35* (s. 151–158). Wydawnictwo Naukowe Uniwersytetu im. Adama Mickiewicza.

Scientific Communications

Oral presentations:

1. Bojko, M., Spodzieja, M., & Rodziewicz-Motowidło, S. (2017). *Punkty kontrolne układu immunologicznego jako strategię wykorzystywane w immunoterapii*.
2. Bojko, M., Kostrzewa, T., & Maćkiewicz, Z. (2016). *Badania stabilności wybranych peptydów o właściwościach hydrofobowych w pH charakterystycznym dla jelita grubego*.
3. Jurkiewicz, A., Bojko, M., Łubkowska, B., & Maćkiewicz, Z. (2016). *Badanie właściwości peptydów rozkurczających na przykładzie oligopeptydów o sekwencjach Ac-GGHK i Ac-GGQPR*. Bojko, M., Falandysz, J., & Maćkiewicz, Z. (2015). *Oznaczanie witamin rozpuszczalnych w tłuszczach w *Suillus luteus*: HPLC*.
4. Bojko, M., Falandysz, J., & Maćkiewicz, Z. (2015). *Oznaczanie witamin rozpuszczalnych w tłuszczach w *Suillus luteus*: HPLC*.
5. *Bojko, M. (2015). Witaminy w grzybach*.
6. Pallach, M., Czerwicka, M., Bojko, M., Orłowski, K., Stepnowski, P., & Kaczyński, Z. (2015). *Qualitative and quantitative analysis of volatile organic compounds in dried spruce (*Picea abies*) wood*.
7. Bojko, M., & Pallach, M. (2014). *Termiczna modyfikacja drewna*.

- Pallach, M., Czerwicka, M., Bojko, M., Orłowski, K., & Stepnowski, P. (2014). *Wpływ temperatury na zawartość i emisję lotnych związków organicznych podczas obróbki termicznej drewna.*

Poster presentations:

- Niedziałkowski, P., Ryl, J., Koterwa, A., Bojko, M., Wcisło, A., Spodzieja, M., Magiera-Mularz, K., Guzik, K., Dubin, G., Holak, T. A., Ossowski, T., & Rodziewicz-Motowidło, S. (2022). *Electrochemical detection of the cancer biomarkers on modified electrodes.*
- Bojko, M., Niedziałkowski, P., Spodzieja, M., Ossowski, T., Magiera, K., Holak, T., Dubin, G., & Rodziewicz-Motowidło, S. (2019). *Use of sPD-L1 as a biomarker in cancer.*
- Kuncewicz, K., Sieradzan, A., Karczyńska, A., Battin, C., Orlikowska, M., Bojko, M., Steinberger, P., Rodziewicz-Motowidło, S., & Spodzieja, M. (2019). *Fragments of gD protein as potential inhibitors of BTLA-HVEM and CD160-HVEM complexes formation.*
- Bojko, M., Spodzieja, M., Parys, M., Hupp, T., Magiera, K., Holak, T., Dubin, G., & Rodziewicz-Motowidło, S. (2018). *Exploitation of PD-1/PD-L1 complex structure to design potential peptides immunotherapeutic agents.*
- Bojko, M., Spodzieja, M., Magiera, K., Holak, T., Dubin, G., & Rodziewicz-Motowidło, S. (2018). *Peptides as potential inhibitors of the PD-1/PD-L1.*
- Bojko, M., Spodzieja, M., Niedziałkowski, P., Ossowski, T., Magiera, K., Holak, T., Dubin, G., & Rodziewicz-Motowidło, S. (2018). *Small peptides as potential inhibitors targeting immune checkpoints.*
- Bojko, M., Spodzieja, M., Magiera, K., Holak, T., Dubin, G., & Rodziewicz-Motowidło, S. (2018). *Wykorzystanie struktury kompleksu PD-1/PD-L1 do projektowania peptydów o potencjale immunoterapeutycznym.*
- Bojko, M., Spodzieja, M., Magiera, K., Holak, T., Dubin, G., & Rodziewicz-Motowidło, S. (2017). *Design and synthesis of small peptides inhibiting PD-1/PD-L1 binding.*
- Bojko, M., Spodzieja, M., Fularczyk, M., Jędrzejewska, K., Magiera, K., Holak, T., Dubin, G., & Rodziewicz-Motowidło, S. (2017). *Searching for potential peptide inhibitors targeting the PD-1/PD-L1 complex.*
- Fularczyk, M., Dzierżyńska, M., Jędrzejewska, K., Sawicka, J., Bojko, M., Rodziewicz-Motowidło, S., & Kasprzykowski, F. (2017). *Design and synthesis of new peptide hydrogels for medical and related application.*
- Jędrzejewska, K., Kropidłowska, M., Fularczyk, M., Bojko, M., Jankowska, E., & Wiczerzak, E. (2017). *Modulation of 20S proteasome activity by peptides derived from VCP (Valosin-Containing Protein).*
- Bojko, M., Jurkiewicz, A., Łubkowska, B., & Maćkiewicz, Z. (2016). *Porównanie stopnia uwodnienia modelowego naskórka po aplikacji maseczek hydrożelowych z palmitoilowanymi i acetylowanymi pochodnymi peptydów o sekwencji GGHK i GGQPR.*

13. Kostrzewa, T., Bojko, M., Kawczyński, M., & Maćkiewicz, Z. (2016). *Defensyny jako integralny element w patogenezie nieswoistych zapaleń jelita grubego.*
14. Kostrzewa, T., Kawczyński, M., Bojko, M., & Maćkiewicz, Z. (2015). *Chemiczna synteza koniugatu peptydu penetrującego ze znacznikiem fluorescencyjnym.*
15. Bojko, M., Pallach, M., Czerwicka, M., Orłowski, K., & Stepnowski, P. (2014). *Analiza jakościowa i ilościowa LZO w drewnie jesionowym i bukowym.*
16. Pallach, M., Czerwicka, M., Bojko, M., Orłowski, K., & Stepnowski, P. (2014). *Analiza jakościowa lotnych związków organicznych w suszonym drewnie świerkowym.*

Scientific Internships

1. Division of Immune Receptor and T cell Activation, Institute of Immunology, Medical University of Vienna, Austria; Erasmus+ program, 20.09.2021-20.09.2021.
2. The Roslin Institute, The University of Edinburgh, Scotland; NAWA PROM, 21-27.08.2021.

1. Paul WE. Fundamental Immunology-Seventh Edition. *Fundam Immunol* 2013;7:1312, DOI: 10.1017/CBO9781107415324.004.
2. Bray F, Ferlay J, Soerjomataram I, Siegel RL, Torre LA, Jemal A. Global Cancer Statistics 2018: GLOBOCAN Estimates of Incidence and Mortality Worldwide for 36 Cancers in 185 Countries. *CA Cancer J Clin* 2018;68(6):394–424, DOI: 10.3322/caac.21492.
3. Ladik J, Förner W, Ladik J, Förner W. *The Beginnings of Cancer in the Cell*. Springer Berlin Heidelberg, 1994, DOI: 10.1007/978-3-642-78984-7_1.
4. Sung H, Ferlay J, Siegel RL, Laversanne M, Soerjomataram I, Jemal A, Bray F. Global Cancer Statistics 2020: GLOBOCAN Estimates of Incidence and Mortality Worldwide for 36 Cancers in 185 Countries. *CA Cancer J Clin* 2021;71(3):209–249, DOI: 10.3322/CAAC.21660.
5. Shin HR. Global Activity of Cancer Registries and Cancer Control and Cancer Incidence Statistics in Korea. *J Prev Med Public Heal* 2008;41(2):84–91, DOI: 10.3961/jpmph.2008.41.2.84.
6. Pilleron S, Soto-Perez-de-Celis E, Vignat J, Ferlay J, Soerjomataram I, Bray F, Sarfati D. Estimated Global Cancer Incidence in the Oldest Adults in 2018 and Projections to 2050. *Int J Cancer* 2021;148(3):601–608, DOI: 10.1002/ijc.33232.
7. Papaioannou NE, Beniata O V., Vitsos P, Tsitsilonis O, Samara P. Harnessing the Immune System to Improve Cancer Therapy. *Ann Transl Med* 2016;4(14):261–261, DOI: 10.21037/atm.2016.04.01.
8. Types of Cancer Treatment | American Cancer Society <https://www.cancer.org/treatment/treatments-and-side-effects/treatment-types.html> (accessed May 25, 2020).
9. Types of Cancer Treatment - National Cancer Institute <https://www.cancer.gov/about-cancer/treatment/types> (accessed Dec 11, 2021).
10. Kamta J, Chaar M, Ande A, Altomare DA, Ait-Oudhia S. Advancing Cancer Therapy with Present and Emerging Immuno-Oncology Approaches. *Front Oncol* 2017;7(APR):64, DOI: 10.3389/fonc.2017.00064.
11. Hoos A. Development of Immuno-Oncology Drugs-from CTLA4 to PD1 to the next Generations. *Nat Rev Drug Discov* 2016;15(4):235–247, DOI: 10.1038/nrd.2015.35.
12. Schultz M. Rudolf Virchow. *Emerg Infect Dis* 2008;14(9):1480–1481, DOI: 10.3201/eid1409.086672.
13. Delves PJ, Roitt IM. The Immune System. *N Engl J Med* 2000;343(1):37–49, DOI: 10.1056/NEJM200007063430107.
14. Cells of the Immune System • iBiology <https://www.ibiology.org/immunology/cells-immune-system/> (accessed Jan 11, 2022).
15. Actor JK. T Lymphocytes: Ringleaders of Adaptive Immune Function. In *Introductory Immunology*. Elsevier, 2019; 45–62, DOI: 10.1016/B978-0-12-816572-0.00004-8.
16. Hamrah P, Dana R. Antigen-Presenting Cells in the Eye and Ocular Surface. *Encycl Eye* 2010;120–127, DOI: 10.1016/B978-0-12-374203-2.00007-5.
17. *Immunology Guidebook*. Elsevier, 2004, DOI: 10.1016/B978-0-12-198382-6.X5022-5.
18. Wilson IA, Christopher Garcia K. T-Cell Receptor Structure and TCR Complexes. *Curr Opin Struct Biol* 1997;7(6):839–848, DOI: 10.1016/S0959-440X(97)80156-X.

19. Neefjes J, Jongsma MLM, Paul P, Bakke O. Towards a Systems Understanding of MHC Class I and MHC Class II Antigen Presentation. *Nat Rev Immunol* 2011;11(12):823–836, DOI: 10.1038/nri3084.
20. Van Coillie S, Wiernicki B, Xu J. Molecular and Cellular Functions of CTLA-4. In *Advances in Experimental Medicine and Biology*, Vol. 1248. Springer, 2020; 7–32, DOI: 10.1007/978-981-15-3266-5_2.
21. Kaiser J, Couzin-Frankel J. Cancer Immunotherapy Sweeps Nobel for Medicine. *Science* 2018;362(6410):13, DOI: 10.1126/science.362.6410.13.
22. Yasinska IM, Sakhnevych SS, Pavlova L, Teo Hansen Selnø A, Teuscher Abeleira AM, Benlaouer O, Gonçalves Silva I, Mosimann M, Varani L, Bardelli M, Hussain R, Siligardi G, Cholewa D, Berger SM, Gibbs BF, Ushkaryov YA, Fasler-Kan E, Klenova E, Sumbayev V V. The Tim-3-Galectin-9 Pathway and Its Regulatory Mechanisms in Human Breast Cancer. *Front Immunol* 2019;10(JULY):1594, DOI: 10.3389/fimmu.2019.01594.
23. Immune checkpoint analysis | Flow cytometry assays | Norge
<https://www.miltenyibiotec.com/NO-en/applications/flow-cytometry-applications/immune-checkpoint-analysis.html?countryRedirected=1#gref> (accessed Feb 16, 2021).
24. Vanamee ÉS, Faustman DL. On the TRAIL of Better Therapies: Understanding TNFRSF Structure-Function. *Cells* 2020;9(3):764, DOI: 10.3390/cells9030764.
25. Ward-Kavanagh LK, Lin WW, Šedý JR, Ware CF. The TNF Receptor Superfamily in Co-Stimulating and Co-Inhibitory Responses. *Immunity* 2016;44(5):1005–1019, DOI: 10.1016/j.immuni.2016.04.019.
26. Liu W, Zang X. Structures of Immune Checkpoints: An Overview on the CD28-B7 Family. In *Advances in Experimental Medicine and Biology*, Vol. 1172. Springer New York LLC, 2019; 63–78, DOI: 10.1007/978-981-13-9367-9_3.
27. Gelfand IM, Chothia C, Kister AE. Immunoglobulin Fold: Structures of Proteins in the Immunoglobulin Superfamily. *eLS* 2001;1–8, DOI: 10.1038/npg.els.0003051.
28. Smith DK, Xue H. Sequence Profiles of Immunoglobulin and Immunoglobulin-like Domains. *J Mol Biol* 1997;274(4):530–545, DOI: 10.1006/jmbi.1997.1432.
29. Bork P, Holm L, Sander C. The Immunoglobulin Fold. *J Mol Biol* 1994;242(4):309–320, DOI: 10.1006/jmbi.1994.1582.
30. Bodelón G, Palomino C, Fernández LÁ. Immunoglobulin Domains in Escherichia Coli and Other Enterobacteria: From Pathogenesis to Applications in Antibody Technologies. *FEMS Microbiol Rev* 2013;37(2):204–250, DOI: 10.1111/j.1574-6976.2012.00347.x.
31. Shinohara T, Taniwaki M, Ishida Y, Kawaichi M, Honjo T. Structure and Chromosomal Localization of the Human PD-1 Gene (PDCD1). *Genomics* 1994;23(3):704–706, DOI: 10.1006/geno.1994.1562.
32. Lazar-Molnar E, Yan Q, Cao E, Ramagopal U, Nathenson SG, Almo SC. Crystal Structure of the Complex between Programmed Death-1 (PD-1) and Its Ligand PD-L2. *Proc Natl Acad Sci* 2008;105(30):10483–10488, DOI: 10.1073/pnas.0804453105.
33. Greenwald RJ, Freeman GJ, Sharpe AH. The B7 Family Revisited. *Annu Rev Immunol* 2005;23(1):515–548, DOI: 10.1146/annurev.immunol.23.021704.115611.
34. Ishida Y, Agata Y, Shibahara K, Honjo T. Induced Expression of PD-1, a Novel Member of the Immunoglobulin Gene Superfamily, upon Programmed Cell Death.

- EMBO J* 1992;11(11):3887–3895.
35. Folkl A, Bienzle D. Structure and Function of Programmed Death (PD) Molecules. *Vet Immunol Immunopathol* 2010;134(1–2):33–38, DOI: 10.1016/J.VETIMM.2009.10.006.
 36. Okazaki T, Honjo T. PD-1 and PD-1 Ligands: From Discovery to Clinical Application. *Int Immunol* 2007;19(7):813–824, DOI: 10.1093/intimm/dxm057.
 37. PDCD1 - Programmed cell death protein 1 precursor - Homo sapiens (Human) - PDCD1 gene & protein <https://www.uniprot.org/uniprot/Q15116> (accessed Jan 4, 2022).
 38. Tan S, Zhang H, Chai Y, Song H, Tong Z, Wang Q, Qi J, Wong G, Zhu X, Liu WJ, Gao S, Wang Z, Shi Y, Yang F, Gao GF, Yan J. An Unexpected N-Terminal Loop in PD-1 Dominates Binding by Nivolumab. *Nat Commun* 2017;8, DOI: 10.1038/ncomms14369.
 39. Okazaki T, Maeda A, Nishimura H, Kurosaki T, Honjo T. PD-1 Immunoreceptor Inhibits B Cell Receptor-Mediated Signaling by Recruiting Src Homology 2-Domain-Containing Tyrosine Phosphatase 2 to Phosphotyrosine. *Proc Natl Acad Sci U S A* 2001;98(24):13866–13871, DOI: 10.1073/pnas.231486598.
 40. Long EO. Regulation of Immune Responses by Inhibitory Receptors. *Adv Exp Med Biol* 1998;452:19–28, DOI: 10.1146/annurev.immunol.17.1.875.
 41. Zhang X, Schwartz JCD, Guo X, Bhatia S, Cao E, Lorenz M, Cammer M, Chen L, Zhang ZY, Edidin MA, Nathenson SG, Almo SC. Structural and Functional Analysis of the Costimulatory Receptor Programmed Death-1 (Immunity (March 2004) 20 (337–347)). *Immunity* 2004;20(5):651, DOI: 10.1016/S1074-7613(04)00114-1.
 42. Cheng X, Veverka V, Radhakrishnan A, Waters LC, Muskett FW, Morgan SH, Huo J, Yu C, Evans EJ, Leslie AJ, Griffiths M, Stubberfield C, Griffin R, Henry AJ, Jansson A, Ladbury JE, Ikemizu S, Carr MD, Davis SJ. Structure and Interactions of the Human Programmed Cell Death 1 Receptor. *J Biol Chem* 2013;288(17):11771–11785, DOI: 10.1074/jbc.M112.448126.
 43. Greenwald RJ, Freeman GJ, Sharpe AH. The B7 Family Revisited. *Annu Rev Immunol* 2005;23(1):515–548, DOI: 10.1146/annurev.immunol.23.021704.115611.
 44. Nielsen C, Ohm-Laursen L, Barington T, Husby S, Lillevang ST. Alternative Splice Variants of the Human PD-1 Gene. *Cell Immunol* 2005;235(2):109–116, DOI: 10.1016/j.cellimm.2005.07.007.
 45. Marasco M, Berteotti A, Weyershaeuser J, Thorausch N, Sikorska J, Krausze J, Brandt HJ, Kirkpatrick J, Rios P, Schamel WW, Köhn M, Carlomagno T. Molecular Mechanism of SHP2 Activation by PD-1 Stimulation. *Sci Adv* 2020;6(5), DOI: 10.1126/sciadv.aay4458.
 46. Rota G, Niogret C, Dang AT, Barros CR, Fonta NP, Alfei F, Morgado L, Zehn D, Birchmeier W, Vivier E, Guarda G. Shp-2 Is Dispensable for Establishing T Cell Exhaustion and for PD-1 Signaling In Vivo. *Cell Rep* 2018;23(1):39–49, DOI: 10.1016/j.celrep.2018.03.026.
 47. Patsoukis N, Duke-Cohan JS, Chaudhri A, Aksoylar H-I, Wang Q, Council A, Berg A, Freeman GJ, Boussiotis VA. Interaction of SHP-2 SH2 Domains with PD-1 ITSM Induces PD-1 Dimerization and SHP-2 Activation. *Commun Biol* 2020;3(1):128, DOI: 10.1038/s42003-020-0845-0.
 48. Quigley M, Pereyra F, Nilsson B, Porichis F, Fonseca C, Eichbaum Q, Julg B, Jesneck JL, Brosnahan K, Imam S, Russell K, Toth I, Piechocka-Trocha A, Dolfi D, Angelosanto J, Crawford A, Shin H, Kwon DS, Zupkosky J, Francisco L, Freeman GJ, Wherry EJ, Kaufmann DE, Walker BD, Ebert B, Haining WN. Transcriptional Analysis of HIV-

- Specific CD8⁺ T Cells Shows That PD-1 Inhibits T Cell Function by Upregulating BATF. *Nat Med* 2010;16(10):1147–1151, DOI: 10.1038/nm.2232.
49. Sharpe AH, Pauken KE. The Diverse Functions of the PD1 Inhibitory Pathway. *Nat Rev Immunol* 2018;18(3):153–167, DOI: 10.1038/nri.2017.108.
 50. Curran CS, Gupta S, Sanz I, Sharon E. PD-1 Immunobiology in Systemic Lupus Erythematosus. *J Autoimmun* 2019;97:1–9, DOI: 10.1016/j.jaut.2018.10.025.
 51. Prokunina L, Castillejo-López C, Öberg F, Gunnarsson I, Berg L, Magnusson V, Brookes AJ, Tentler D, Kristjansdóttir H, Gróndal G, Isine Bolstad A, Svenungsson E, Lundberg I, Sturfelt G, Jönssen A, Truedsson L, Lima G, Alcocer-Varela J, Jonsson R, Gyllenstein UB, Harley JB, Alarcón-Segovia D, Steinsson K, Alarcón-Riquelme ME. A Regulatory Polymorphism in PDCD1 Is Associated with Susceptibility to Systemic Lupus Erythematosus in Humans. *Nat Genet* 2002;32(4):666–669, DOI: 10.1038/ng1020.
 52. Okazaki T, Tanaka Y, Nishio R, Mitsuiye T, Mizoguchi A, Wang J, Ishida M, Hiai H, Matsumori A, Minato N, Honjo T. Autoantibodies against Cardiac Troponin I Are Responsible for Dilated Cardiomyopathy in PD-1-Deficient Mice. *Nat Med* 2003;9(12):1477–1483, DOI: 10.1038/nm955.
 53. Ansari MJI, Salama AD, Chitnis T, Smith RN, Yagita H, Akiba H, Yamazaki T, Azuma M, Iwai H, Khoury SJ, Auchincloss H, Sayegh MH. The Programmed Death-1 (PD-1) Pathway Regulates Autoimmune Diabetes in Nonobese Diabetic (NOD) Mice. *J Exp Med* 2003;198(1):63–69, DOI: 10.1084/jem.20022125.
 54. Wang J, Yoshida T, Nakaki F, Hiai H, Okazaki T, Honjo T. Establishment of NOD-Pdcd1^{-/-} Mice as an Efficient Animal Model of Type I Diabetes. *Proc Natl Acad Sci U S A* 2005;102(33):11823–11828, DOI: 10.1073/pnas.0505497102.
 55. Wan B, Nie H, Liu A, Feng G, He D, Xu R, Zhang Q, Dong C, Zhang JZ. Aberrant Regulation of Synovial T Cell Activation by Soluble Costimulatory Molecules in Rheumatoid Arthritis. *J Immunol* 2006;177(12):8844–8850, DOI: 10.4049/jimmunol.177.12.8844.
 56. James ES, Harney S, Wordsworth BP, Cookson WOCM, Davis SJ, Moffatt MF. PDCD1: A Tissue-Specific Susceptibility Locus for Inherited Inflammatory Disorders. *Genes Immun* 2005;6(5):430–437, DOI: 10.1038/sj.gene.6364223.
 57. Du S, McCall N, Park K, Guan Q, Fontina P, Ertel A, Zhan T, Dicker AP, Lu B. Blockade of Tumor-Expressed PD-1 Promotes Lung Cancer Growth. *Oncoimmunology* 2018;7(4):e1408747, DOI: 10.1080/2162402X.2017.1408747.
 58. Kleffel S, Posch C, Barthel SR, Mueller H, Schlapbach C, Guenova E, Elco CP, Lee N, Juneja VR, Zhan Q, Lian CG, Thomi R, Hoetzenecker W, Cozzio A, Dummer R, Mihm MC, Flaherty KT, Frank MH, Murphy GF, Sharpe AH, Kupper TS, Schatton T. Melanoma Cell-Intrinsic PD-1 Receptor Functions Promote Tumor Growth. *Cell* 2015;162(6):1242–1256, DOI: 10.1016/j.cell.2015.08.052.
 59. D'Angelo SP, Shoushtari AN, Agaram NP, Kuk D, Qin L-X, Carvajal RD, Dickson MA, Gounder M, Keohan ML, Schwartz GK, Tap WD. Prevalence of Tumor-Infiltrating Lymphocytes and PD-L1 Expression in the Soft Tissue Sarcoma Microenvironment. *Hum Pathol* 2015;46(3):357–365, DOI: 10.1016/j.humpath.2014.11.001.
 60. Tseng SY, Otsuji M, Gorski K, Huang X, Slansky JE, Pai SI, Shalabi A, Shin T, Pardoll DM, Tsuchiya H. B7-DC, a New Dendritic Cell Molecule with Potent Costimulatory Properties for T Cells. *J Exp Med* 2001;193(7):839–845, DOI: 10.1084/jem.193.7.839.
 61. Lin DYW, Tanaka Y, Iwasaki M, Gittis AG, Su HP, Mikami B, Okazaki T, Honjo T,

- Minato N, Garboczi DN. The PD-1/PD-L1 Complex Resembles the Antigen-Binding Fv Domains of Antibodies and T Cell Receptors. *Proc Natl Acad Sci U S A* 2008;105(8):3011–3016, DOI: 10.1073/pnas.0712278105.
62. Zak KM, Kitel R, Przetocka S, Golik P, Guzik K, Musielak B, Dömling A, Dubin G, Holak TA. Structure of the Complex of Human Programmed Death 1, PD-1, and Its Ligand PD-L1. *Structure* 2015;23(12):2341–2348, DOI: 10.1016/j.str.2015.09.010.
 63. Chen Y, Liu P, Gao F, Cheng H, Qi J, Gao GF. A Dimeric Structure of PD-L1: Functional Units or Evolutionary Relics? *Protein Cell* 2010;1(2):153–160, DOI: 10.1007/s13238-010-0022-1.
 64. PDCD1LG2 - Programmed cell death 1 ligand 2 precursor - Homo sapiens (Human) - PDCD1LG2 gene & protein <https://www.uniprot.org/uniprot/Q9BQ51> (accessed Oct 26, 2021).
 65. Dong H, Zhu G, Tamada K, Chen L. B7-H1, a Third Member of the B7 Family, Co-Stimulates T-Cell Proliferation and Interleukin-10 Secretion. *Nat Med* 1999;5(12):1365–1369, DOI: 10.1038/70932.
 66. Mueller SN, Vanguri VK, Ha SJ, West EE, Keir ME, Glickman JN, Sharpe AH, Ahmed R. PD-L1 Has Distinct Functions in Hematopoietic and Nonhematopoietic Cells in Regulating T Cell Responses during Chronic Infection in Mice. *J Clin Invest* 2010;120(7):2508–2515, DOI: 10.1172/JCI40040.
 67. Iwai Y, Ishida M, Tanaka Y, Okazaki T, Honjo T, Minato N. Involvement of PD-L1 on Tumor Cells in the Escape from Host Immune System and Tumor Immunotherapy by PD-L1 Blockade. *Proc Natl Acad Sci U S A* 2002;99(19):12293–12297, DOI: 10.1073/pnas.192461099.
 68. Qiao X, Jiang J, Pang X, Huang M, Tang Y, Liang X, Tang Y. The Evolving Landscape of PD-1/PD-L1 Pathway in Head and Neck Cancer. *Front Immunol* 2020;11:1721, DOI: 10.3389/fimmu.2020.01721.
 69. Moratin J, Metzger K, Safaltin A, Herpel E, Hoffmann J, Freier K, Hess J, Horn D. Upregulation of PD-L1 and PD-L2 in Neck Node Metastases of Head and Neck Squamous Cell Carcinoma. *Head Neck* 2019;41(8):2484–2491, DOI: 10.1002/hed.25713.
 70. Chen K, Wang X, Yang L, Chen Z. The Anti-PD-1/PD-L1 Immunotherapy for Gastric Esophageal Cancer: A Systematic Review and Meta-Analysis and Literature Review. *Cancer Control* 2021;28:107327482199743, DOI: 10.1177/1073274821997430.
 71. Hsieh C-C, Hsu H-S, Li AF-Y, Chen Y-J. Clinical Relevance of PD-L1 and PD-L2 Overexpression in Patients with Esophageal Squamous Cell Carcinoma. *J Thorac Dis* 2018;10(7):4433–4444, DOI: 10.21037/jtd.2018.06.167.
 72. Baptista MZ, Sarian LO, Derchain SFM, Pinto GA, Vassallo J. Prognostic Significance of PD-L1 and PD-L2 in Breast Cancer. *Hum Pathol* 2016;47(1):78–84, DOI: 10.1016/j.humpath.2015.09.006.
 73. Miyazawa T, Marushima H, Saji H, Kojima K, Hoshikawa M, Takagi M, Nakamura H. PD-L1 Expression in Non-Small-Cell Lung Cancer Including Various Adenocarcinoma Subtypes. *Ann Thorac Cardiovasc Surg* 2019;25(1):1–9, DOI: 10.5761/atcs.0a.18-00163.
 74. Yearley JH, Gibson C, Yu N, Moon C, Murphy E, Juco J, Lunceford J, Cheng J, Chow LQM, Seiwert TY, Handa M, Tomassini JE, McClanahan T. PD-L2 Expression in Human Tumors: Relevance to Anti-PD-1 Therapy in Cancer. *Clin Cancer Res* 2017;23(12):3158–3167, DOI: 10.1158/1078-0432.CCR-16-1761.

75. Tokunaga R, Xiu J, Johnston C, Goldberg RM, Philip PA, Seeber A, Naseem M, Lo JH, Arai H, Battaglin F, Puccini A, Berger MD, Soni S, Zhang W, Hwang JJ, Shields AF, Marshall JL, Baba H, Korn WM, Lenz H-J. Molecular Profiling of Appendiceal Adenocarcinoma and Comparison with Right-Sided and Left-Sided Colorectal Cancer. *Clin Cancer Res* 2019;25(10):3096–3103, DOI: 10.1158/1078-0432.CCR-18-3388.
76. Topalian SL, Hodi FS, Brahmer JR, Gettinger SN, Smith DC, McDermott DF, Powderly JD, Carvajal RD, Sosman JA, Atkins MB, Leming PD, Spigel DR, Antonia SJ, Horn L, Drake CG, Pardoll DM, Chen L, Sharfman WH, Anders RA, Taube JM, McMiller TL, Xu H, Korman AJ, Jure-Kunkel M, Agrawal S, McDonald D, Kollia GD, Gupta A, Wigginton JM, Sznol M. Safety, Activity, and Immune Correlates of Anti-PD-1 Antibody in Cancer. *N Engl J Med* 2012;366(26):2443–2454, DOI: 10.1056/NEJMoa1200690.
77. Wang H, Yao H, Li C, Liang L, Zhang Y, Shi H, Zhou C, Chen Y, Fang J-Y, Xu J. PD-L2 Expression in Colorectal Cancer: Independent Prognostic Effect and Targetability by Deglycosylation. *Oncoimmunology* 2017;6(7):e1327494, DOI: 10.1080/2162402X.2017.1327494.
78. Zheng L. PD-L1 Expression in Pancreatic Cancer. *J Natl Cancer Inst* 2017;109(6):djw304, DOI: 10.1093/jnci/djw304.
79. Fay AP, Signoretti S, Callea M, Teló GH, McKay RR, Song J, Carvo I, Lampron ME, Kaymakcalan MD, Poli-de-Figueiredo CE, Bellmunt J, Hodi FS, Freeman GJ, Elfiky A, Choueiri TK. Programmed Death Ligand-1 Expression in Adrenocortical Carcinoma: An Exploratory Biomarker Study. *J Immunother Cancer* 2015;3(1):3, DOI: 10.1186/s40425-015-0047-3.
80. Hamanishi J, Mandai M, Iwasaki M, Okazaki T, Tanaka Y, Yamaguchi K, Higuchi T, Yagi H, Takakura K, Minato N, Honjo T, Fujii S. Programmed Cell Death 1 Ligand 1 and Tumor-Infiltrating CD8+ T Lymphocytes Are Prognostic Factors of Human Ovarian Cancer. *Proc Natl Acad Sci* 2007;104(9):3360–3365, DOI: 10.1073/pnas.0611533104.
81. Koirala P, Roth ME, Gill J, Piperdi S, Chinai JM, Geller DS, Hoang BH, Park A, Fremed MA, Zang X, Gorlick R. Immune Infiltration and PD-L1 Expression in the Tumor Microenvironment Are Prognostic in Osteosarcoma. *Sci Rep* 2016;6(1):30093, DOI: 10.1038/srep30093.
82. Ren T, Zheng B, Huang Y, Wang S, Bao X, Liu K, Guo W. Osteosarcoma Cell Intrinsic PD-L2 Signals Promote Invasion and Metastasis via the RhoA-ROCK-LIMK2 and Autophagy Pathways. *Cell Death Dis* 2019;10(4):261, DOI: 10.1038/s41419-019-1497-1.
83. Lee B-H, Park Y, Kim JH, Kang K-W, Lee SJ, Kim SJ, Kim BS. PD-L1 Expression in Bone Marrow Plasma Cells as a Biomarker to Predict Multiple Myeloma Prognosis: Developing a Nomogram-Based Prognostic Model. *Sci Rep* 2020;10(1):12641, DOI: 10.1038/s41598-020-69616-5.
84. Dail M, Yang L, Green C, Ma C, Robert A, Kadel EE, Koeppen H, Adamkewicz J, Byon J, Woodard J, Rodig SJ, Venstrom JM. Distinct Patterns of PD-L1 and PD-L2 Expression By Tumor and Non-Tumor Cells in Patients with MM, MDS and AML. *Blood* 2016;128(22):1340–1340, DOI: 10.1182/blood.V128.22.1340.1340.
85. Ricklefs FL, Alayo Q, Krenzlin H, Mahmoud AB, Speranza MC, Nakashima H, Hayes JL, Lee K, Balaj L, Passaro C, Rooj AK, Krasemann S, Carter BS, Chen CC, Steed T, Treiber J, Rodig S, Yang K, Nakano I, Lee H, Weissleder R, Breakefield XO, Godlewski J, Westphal M, Lamszus K, Freeman GJ, Bronisz A, Lawler SE, Chiocca EA. Immune Evasion Mediated by PD-L1 on Glioblastoma-Derived Extracellular Vesicles. *Sci Adv* 2018;4(3), DOI: 10.1126/sciadv.aar2766.

86. Fu Y, Liu CJ, Kobayashi DK, Johanns TM, Bowman-Kirigin JA, Schaeffler MO, Mao DD, Bender D, Kelley DG, Uppaluri R, Bi WL, Dunn IF, Tao Y, Luo J, Kim AH, Dunn GP. GATA2 Regulates Constitutive PD-L1 and PD-L2 Expression in Brain Tumors. *Sci Rep* 2020;10(1):9027, DOI: 10.1038/s41598-020-65915-z.
87. Ansell SM, Lesokhin AM, Borrello I, Halwani A, Scott EC, Gutierrez M, Schuster SJ, Millenson MM, Cattray D, Freeman GJ, Rodig SJ, Chapuy B, Ligon AH, Zhu L, Grosso JF, Kim SY, Timmerman JM, Shipp MA, Armand P. PD-1 Blockade with Nivolumab in Relapsed or Refractory Hodgkin's Lymphoma. *N Engl J Med* 2015;372(4):311–319, DOI: 10.1056/NEJMoa1411087.
88. Panjwani PK, Charu V, DeLisser M, Molina-Kirsch H, Natkunam Y, Zhao S. Programmed Death-1 Ligands PD-L1 and PD-L2 Show Distinctive and Restricted Patterns of Expression in Lymphoma Subtypes. *Hum Pathol* 2018;71:91–99, DOI: 10.1016/j.humpath.2017.10.029.
89. Brusa D, Serra S, Coscia M, Rossi D, D'Arena G, Laurenti L, Jaksic O, Fedele G, Inghirami G, Gaidano G, Malavasi F, Deaglio S. The PD-1/PD-L1 Axis Contributes to T-Cell Dysfunction in Chronic Lymphocytic Leukemia. *Haematologica* 2013;98(6):953–963, DOI: 10.3324/haematol.2012.077537.
90. Chen C, Liang C, Wang S, Chio CL, Zhang Y, Zeng C, Chen S, Wang C, Li Y. Expression Patterns of Immune Checkpoints in Acute Myeloid Leukemia. *J Hematol Oncol* 2020;13(1):28, DOI: 10.1186/s13045-020-00853-x.
91. Calderaro J, Rousseau B, Amaddeo G, Mercey M, Charpy C, Costentin C, Luciani A, Zafrani E-S, Laurent A, Azoulay D, Lafdil F, Pawlotsky J-M. Programmed Death Ligand 1 Expression in Hepatocellular Carcinoma: Relationship With Clinical and Pathological Features. *Hepatology* 2016;64(6):2038–2046, DOI: 10.1002/hep.28710.
92. Jung H Il, Jeong D, Ji S, Ahn TS, Bae SH, Chin S, Chung JC, Kim HC, Lee MS, Baek M-J. Overexpression of PD-L1 and PD-L2 Is Associated with Poor Prognosis in Patients with Hepatocellular Carcinoma. *Cancer Res Treat* 2017;49(1):246–254, DOI: 10.4143/crt.2016.066.
93. Neyaz A, Husain N, Kumari S, Gupta S, Shukla S, Arshad S, Anand N, Chaturvedi A. Clinical Relevance of PD-L1 Expression in Gallbladder Cancer: A Potential Target for Therapy. *Histopathology* 2018;73(4):622–633, DOI: 10.1111/his.13669.
94. Böger C, Behrens H-M, Mathiak M, Krüger S, Kalthoff H, Röcken C. PD-L1 Is an Independent Prognostic Predictor in Gastric Cancer of Western Patients. *Oncotarget* 2016;7(17):24269–24283, DOI: 10.18632/oncotarget.8169.
95. Shanes ED, Friedman LA, Mills AM. PD-L1 Expression and Tumor-Infiltrating Lymphocytes in Uterine Smooth Muscle Tumors. *Am J Surg Pathol* 2019;43(6):792–801, DOI: 10.1097/PAS.0000000000001254.
96. Mo Z, Liu J, Zhang Q, Chen Z, Mei J, Liu L, Yang S, Li H, Zhou L, You Z. Expression of PD-1, PD-L1 and PD-L2 Is Associated with Differentiation Status and Histological Type of Endometrial Cancer. *Oncol Lett* 2016;12(2):944–950, DOI: 10.3892/ol.2016.4744.
97. Liu Y, Wu L, Tong R, Yang F, Yin L, Li M, You L, Xue J, Lu Y. PD-1/PD-L1 Inhibitors in Cervical Cancer. *Front Pharmacol* 2019;10(FEB):65, DOI: 10.3389/fphar.2019.00065.
98. Zhao SG, Lehrer J, Chang SL, Das R, Erho N, Liu Y, Sjöström M, Den RB, Freedland SJ, Klein EA, Karnes RJ, Schaeffer EM, Xu M, Speers C, Nguyen PL, Ross AE, Chan JM, Cooperberg MR, Carroll PR, Davicioni E, Fong L, Spratt DE, Feng FY. The

Immune Landscape of Prostate Cancer and Nomination of PD-L2 as a Potential Therapeutic Target. *JNCI J Natl Cancer Inst* 2019;111(3):301–310, DOI: 10.1093/jnci/djy141.

99. Fankhauser CD, Curioni-Fontecedro A, Allmann V, Beyer J, Tischler V, Sulser T, Moch H, Bode PK. Frequent PD-L1 Expression in Testicular Germ Cell Tumors. *Br J Cancer* 2015;113(3):411–413, DOI: 10.1038/bjc.2015.244.
100. Kostine M, Briaire-de Bruijn IH, Cleven AHG, Vervat C, Corver WE, Schilham MW, Van Beelen E, van Boven H, Haas RL, Italiano A, Cleton-Jansen A-M, Bovée JVMG. Increased Infiltration of M2-Macrophages, T-Cells and PD-L1 Expression in High Grade Leiomyosarcomas Supports Immunotherapeutic Strategies. *Oncoimmunology* 2018;7(2):e1386828, DOI: 10.1080/2162402X.2017.1386828.
101. Robert C, Long G V., Brady B, Dutriaux C, Maio M, Mortier L, Hassel JC, Rutkowski P, McNeil C, Kalinka-Warzocho E, Savage KJ, Hernberg MM, Lebbé C, Charles J, Mihalciou C, Chiarion-Sileni V, Mauch C, Cognetti F, Arance A, Schmidt H, Schadendorf D, Gogas H, Lundgren-Eriksson L, Horak C, Sharkey B, Waxman IM, Atkinson V, Ascierto PA. Nivolumab in Previously Untreated Melanoma without BRAF Mutation. *N Engl J Med* 2015;372(4):320–330, DOI: 10.1056/NEJMoa1412082.
102. Frigola X, Inman BA, Krco CJ, Liu X, Harrington SM, Bulur PA, Dietz AB, Dong H, Kwon ED. Soluble B7-H1: Differences in Production between Dendritic Cells and T Cells. *Immunol Lett* 2012;142(1–2):78–82, DOI: 10.1016/J.IMLET.2011.11.001.
103. Manos MP, Zhao F, Butterfield LH, Liao X, Wu X, Mahoney KM, Zhou J, Giobbie-Hurder A, Lee S, Hodi FS, Freeman GJ, Piesche M, Rodig S, Li J, Dranoff G, Eastman LM. Soluble PD-L1 as a Biomarker in Malignant Melanoma Treated with Checkpoint Blockade. *Cancer Immunol Res* 2017;5(6):480–492, DOI: 10.1158/2326-6066.cir-16-0329.
104. Bi X, Wang H, Zhang W, Wang J, Liu W, Xia Z, Huang H, Jiang W, Zhang Y, Wang L. PD-L1 Is Upregulated by EBV-Driven LMP1 through NF-KB Pathway and Correlates with Poor Prognosis in Natural Killer/T-Cell Lymphoma. *J Hematol Oncol* 2016;9(1):109, DOI: 10.1186/s13045-016-0341-7.
105. Nagato T, Ohkuri T, Ohara K, Hirata Y, Kishibe K, Komabayashi Y, Ueda S, Takahara M, Kumai T, Ishibashi K, Kosaka A, Aoki N, Oikawa K, Uno Y, Akiyama N, Sado M, Takei H, Celis E, Harabuchi Y, Kobayashi H. Programmed Death-Ligand 1 and Its Soluble Form Are Highly Expressed in Nasal Natural Killer/T-Cell Lymphoma: A Potential Rationale for Immunotherapy. *Cancer Immunol Immunother* 2017;66(7):877–890, DOI: 10.1007/s00262-017-1987-x.
106. Rossille D, Gressier M, Damotte D, Maucourt-Boulch D, Pangault C, Semana G, Le Gouill S, Haioun C, Tarte K, Lamy T, Milpied N, Fest T, Sang for the GO-E des L et AM du, Damaj G, Clavert A, Jijakli A Al, Banos A, Dutel J-L, Deconinck E, Rodon P, Bouabdallah K, Soubeyran P, Choufi B, Maakaroun A, Tournilhac O, Fleury J, Gressin R, Maisonneuve H, Laribi K, Solal-Celigny P, Moreau P, Rossi J-F, Cartron G, Morineau N, Harousseau JL, Jourdan E, Alexis M, Dreyfus F, Delwail V, Cornillon J, Garidi R, Gyan E, Colombat P, Godemer P. High Level of Soluble Programmed Cell Death Ligand 1 in Blood Impacts Overall Survival in Aggressive Diffuse Large B-Cell Lymphoma: Results from a French Multicenter Clinical Trial. *Leukemia* 2014;28(12):2367–2375, DOI: 10.1038/leu.2014.137.
107. Wang L, Wang H, Chen H, Wang W, Chen X, Geng Q, Xia Z, Lu Y, Wang L, Wang H, Chen H, Wang W, Chen X, Geng Q, Xia Z, Lu Y, Wang L, Wang H, Chen H, Wang W, Chen X, Geng Q, Xia Z, Lu Y. Serum Levels of Soluble Programmed Death Ligand 1 Predict Treatment Response and Progression Free Survival in Multiple Myeloma.

Oncotarget 2015;6(38):41228–41236, DOI: 10.18632/oncotarget.5682.

108. Schmidt M, Greten FR, Finkelmeier F, Pleli T, Piiper A, Waidmann O, Kronenberger B, Tal A, Trojan J, Canli Ö, Zeuzem S. High Levels of the Soluble Programmed Death-Ligand (SPD-L1) Identify Hepatocellular Carcinoma Patients with a Poor Prognosis. *Eur J Cancer* 2016;59:152–159, DOI: 10.1016/j.ejca.2016.03.002.
109. Frigola X, Inman BA, Lohse CM, Krco CJ, Cheville JC, Thompson RH, Leibovich B, Blute ML, Dong H, Kwon ED. Identification of a Soluble Form of B7-H1 That Retains Immunosuppressive Activity and Is Associated with Aggressive Renal Cell Carcinoma. *Clin Cancer Res* 2011;17(7):1915–1923, DOI: 10.1158/1078-0432.CCR-10-0250.
110. Guleria I, Khosroshahi A, Ansari MJ, Habicht A, Azuma M, Yagita H, Noelle RJ, Coyle A, Mellor AL, Khoury SJ, Sayegh MH. A Critical Role for the Programmed Death Ligand 1 in Fetomaternal Tolerance. *J Exp Med* 2005;202(2):231–237, DOI: 10.1084/jem.20050019.
111. Latchman Y, Wood CR, Chernova T, Chaudhary D, Borde M, Chernova I, Iwai Y, Long AJ, Brown JA, Nunes R, Greenfield EA, Bourque K, Bousiotis VA, Carter LL, Carreno BM, Malenkovich N, Nishimura H, Okazaki T, Honjo T, Sharpe AH, Freeman GJ. PD-L2 Is a Second Ligand for PD-1 and Inhibits T Cell Activation. *Nat Immunol* 2001;2(3):261–268, DOI: 10.1038/85330.
112. Xiao Y, Yu S, Zhu B, Bedoret D, Bu X, Duke-Cohan LMF, Umetsu DT, Sharpe AH, DeKruyff RH, Freeman GJ. RGMb Is a Novel Binding Partner for PD-L2 and Its Engagement with PD-L2 Promotes Respiratory Tolerance. *J Exp Med* 2014;211(5):943–959, DOI: 10.1084/jem.20130790.
113. Nie X, Chen W, Zhu Y, Huang B, Yu W, Wu Z, Guo S, Zhu Y, Luo L, Wang S, Chen L. B7-DC (PD-L2) Costimulation of CD4+ T-Helper 1 Response via RGMb. *Cell Mol Immunol* 2018;15(10):888–897, DOI: 10.1038/cmi.2017.17.
114. Mortensen JB, Monrad I, Enemark MB, Ludvigsen M, Kamper P, Bjerre M, D’Amore F. Soluble Programmed Cell Death Protein 1 (SPD-1) and the Soluble Programmed Cell Death Ligands 1 and 2 (SPD-L1 and SPD-L2) in Lymphoid Malignancies. *Eur J Haematol* 2021;107(1):81–91, DOI: 10.1111/ejh.13621.
115. Buderath P, Schwich E, Jensen C, Horn PA, Kimmig R, Kasimir-Bauer S, Rebmann V. Soluble Programmed Death Receptor Ligands SPD-L1 and SPD-L2 as Liquid Biopsy Markers for Prognosis and Platinum Response in Epithelial Ovarian Cancer. *Front Oncol* 2019;9:1015, DOI: 10.3389/fonc.2019.01015.
116. Dowell AC, Munford H, Goel A, Gordon NS, James ND, Cheng KK, Zeegers MP, Ward DG, Bryan RT. PD-L2 Is Constitutively Expressed in Normal and Malignant Urothelium. *Front Oncol* 2021;11, DOI: 10.3389/fonc.2021.626748.
117. Wang Q, Zhang J, Tu H, Liang D, Chang DW, Ye Y, Wu X. Soluble Immune Checkpoint-Related Proteins as Predictors of Tumor Recurrence, Survival, and T Cell Phenotypes in Clear Cell Renal Cell Carcinoma Patients. *J Immunother Cancer* 2019;7(1):334, DOI: 10.1186/s40425-019-0810-y.
118. Mortensen JB, Yoanna V, Hansen IM, Bjerre M, D’Amore F. Characterization of Soluble Immune Checkpoint Protein PD-1, PD-L1 and PD-L2 Levels in Different Types of Lymphoid Malignancies. *Blood* 2018;132(Supplement 1):5306–5306, DOI: 10.1182/blood-2018-99-114509.
119. Takeuchi M, Doi T, Obayashi K, Hirai A, Yoneda K, Tanaka F, Iwai Y. Soluble PD-L1 with PD-1-Binding Capacity Exists in the Plasma of Patients with Non-Small Cell Lung Cancer. *Immunol Lett* 2018;196:155–160, DOI: 10.1016/j.imlet.2018.01.007.

120. Tong M, Fang X, Yang J, Wu P, Guo Y, Sun J. Abnormal Membrane-Bound and Soluble Programmed Death Ligand 2 (PD-L2) Expression in Systemic Lupus Erythematosus Is Associated with Disease Activity. *Immunol Lett* 2020;227:96–101, DOI: 10.1016/j.imlet.2020.09.001.
121. Fukasawa T, Yoshizaki A, Ebata S, Nakamura K, Saigusa R, Miura S, Yamashita T, Hirabayashi M, Ichimura Y, Taniguchi T, Asano Y, Shimizu H, Kazoe Y, Mawatari K, Kitamori T, Sato S. Contribution of Soluble Forms of Programmed Death 1 and Programmed Death Ligand 2 to Disease Severity and Progression in Systemic Sclerosis. *Arthritis Rheumatol* 2017;69(9):1879–1890, DOI: 10.1002/art.40164.
122. Raftery MJ, Abdelaziz MO, Hofmann J, Schönrich G. Hantavirus-Driven PD-L1/PD-L2 Upregulation: An Imperfect Viral Immune Evasion Mechanism. *Front Immunol* 2018;9:2560, DOI: 10.3389/fimmu.2018.02560.
123. Kong Y, Wang Y, Wu X, Han J, Li G, Hua M, Han K, Zhang H, Li A, Zeng H. Storm of Soluble Immune Checkpoints Associated with Disease Severity of COVID-19. *Signal Transduct Target Ther* 2020;5(1):192, DOI: 10.1038/s41392-020-00308-2.
124. Greisen SR, Kragstrup TW, Thomsen JS, Hansen AS, Krishnamurthy A, Hørslev-Petersen K, Hetland ML, Stengaard-Pedersen K, Østergaard M, Ørnbjerg LM, Junker P, Sharpe AH, Freeman GJ, Annamalai L, Hvid M, Moestrup SK, Hauge E-M, Catrina AI, Deleuran B. Programmed Death Ligand 2 – A Link between Inflammation and Bone Loss in Rheumatoid Arthritis. *J Transl Autoimmun* 2020;3:100028, DOI: 10.1016/j.jtauto.2019.100028.
125. Liu W, Huang B, Kuang Y, Liu G. Molecular Dynamics Simulations Elucidate Conformational Selection and Induced Fit Mechanisms in the Binding of PD-1 and PD-L1. *Mol Biosyst* 2017;13(5):892–900, DOI: 10.1039/c7mb00036g.
126. Tang S, Kim PS. A High-Affinity Human PD-1/PD-L2 Complex Informs Avenues for Small-Molecule Immune Checkpoint Drug Discovery. *Proc Natl Acad Sci* 2019;116(49):24500–24506, DOI: 10.1073/pnas.1916916116.
127. Viricel C, Ahmed M, Barakat K. Human PD-1 Binds Differently to Its Human Ligands: A Comprehensive Modeling Study. *J Mol Graph Model* 2015;57:131–142, DOI: 10.1016/j.jmgm.2015.01.015.
128. Li Q, Quan L, Lyu J, He Z, Wang X, Meng J, Zhao Z, Zhu L, Liu X, Li H. Discovery of Peptide Inhibitors Targeting Human Programmed Death 1 (PD-1) Receptor. *Oncotarget* 2016;7(40), DOI: 10.18632/oncotarget.11274.
129. Whiteside TL. The Local Tumor Microenvironment. In *General Principles of Tumor Immunotherapy: Basic and Clinical Applications of Tumor Immunology*. Springer Netherlands, 2008; 145–167, DOI: 10.1007/978-1-4020-6087-8_7.
130. Whiteside TL. Immune Suppression in Cancer: Effects on Immune Cells, Mechanisms and Future Therapeutic Intervention. *Semin Cancer Biol* 2006;16(1):3–15, DOI: 10.1016/j.semcancer.2005.07.008.
131. Cui Y, Guo G. Immunomodulatory Function of the Tumor Suppressor P53 in Host Immune Response and the Tumor Microenvironment. *Int J Mol Sci* 2016;17(11):1942, DOI: 10.3390/ijms17111942.
132. Ribas A, Wolchok JD. Cancer Immunotherapy Using Checkpoint Blockade. *Science (80-)* 2018;359(6382):1350–1355, DOI: 10.1126/science.aar4060.
133. Cameron F, Whiteside G, Perry C. Ipilimumab: First Global Approval. *Drugs* 2011;71(8):1093–1104, DOI: 10.2165/11594010-000000000-00000.

134. Wolchok JD, Hoos A, O'Day S, Weber JS, Hamid O, Lebbé C, Maio M, Binder M, Bohnsack O, Nichol G, Humphrey R, Hodi FS. Guidelines for the Evaluation of Immune Therapy Activity in Solid Tumors: Immune-Related Response Criteria. *Clin Cancer Res* 2009;15(23):7412–7420, DOI: 10.1158/1078-0432.CCR-09-1624.
135. Spain L, Diem S, Larkin J. Management of Toxicities of Immune Checkpoint Inhibitors. *Cancer Treat Rev* 2016;44:51–60, DOI: 10.1016/j.ctrv.2016.02.001.
136. Poole RM. Pembrolizumab: First Global Approval. *Drugs* 2014;74(16):1973–1981, DOI: 10.1007/s40265-014-0314-5.
137. Markham A. Atezolizumab: First Global Approval. *Drugs* 2016;76(12):1227–1232, DOI: 10.1007/s40265-016-0618-8.
138. Syed YY. Durvalumab: First Global Approval. *Drugs* 2017;77(12):1369–1376, DOI: 10.1007/s40265-017-0782-5.
139. Mcdermott DF, Atkins MB. PD-1 as a Potential Target in Cancer Therapy. *Cancer Medicine*, 2013, 2, 662–673, DOI: 10.1002/cam4.106.
140. Zhao Y, Harrison DL, Song Y, Ji J, Huang J, Hui E. Antigen-Presenting Cell-Intrinsic PD-1 Neutralizes PD-L1 in Cis to Attenuate PD-1 Signaling in T Cells. *Cell Rep* 2018;24(2):379-390.e6, DOI: 10.1016/j.celrep.2018.06.054.
141. Patsoukis N, Wang Q, Strauss L, Boussiotis VA. Revisiting the PD-1 Pathway. *Sci Adv* 2020;6(38), DOI: 10.1126/sciadv.abd2712.
142. Chaudhri A, Xiao Y, Klee AN, Wang X, Zhu B, Freeman GJ. PD-L1 Binds to B7-1 Only In Cis on the Same Cell Surface. *Cancer Immunol Res* 2018;6(8):921–929, DOI: 10.1158/2326-6066.CIR-17-0316.
143. Sugiura D, Maruhashi T, Okazaki I, Shimizu K, Maeda TK, Takemoto T, Okazaki T. Restriction of PD-1 Function by Cis -PD-L1/CD80 Interactions Is Required for Optimal T Cell Responses. *Science (80-)* 2019;364(6440):558–566, DOI: 10.1126/science.aav7062.
144. Zhao Y, Lee CK, Lin C-H, Gassen RB, Xu X, Huang Z, Xiao C, Bonorino C, Lu L-F, Bui JD, Hui E. PD-L1:CD80 Cis-Heterodimer Triggers the Co-Stimulatory Receptor CD28 While Repressing the Inhibitory PD-1 and CTLA-4 Pathways. *Immunity* 2019;51(6):1059-1073.e9, DOI: 10.1016/j.immuni.2019.11.003.
145. Search of: PD-L1 | Recruiting, Not yet recruiting, Active, not recruiting, Enrolling by invitation Studies - List Results - ClinicalTrials.gov
https://clinicaltrials.gov/ct2/results?term=PD-L1&Search=Apply&recrs=b&recrs=a&recrs=f&recrs=d&age_v=&gndr=&type=&rslt=
(accessed Aug 23, 2022).
146. Search of: PD-1 | Recruiting, Not yet recruiting, Active, not recruiting, Enrolling by invitation Studies - List Results - ClinicalTrials.gov
https://clinicaltrials.gov/ct2/results?term=PD-1&Search=Apply&recrs=b&recrs=a&recrs=f&recrs=d&age_v=&gndr=&type=&rslt=
(accessed Aug 23, 2022).
147. Na Z, Yeo SP, Bharath SR, Bowler MW, Balıkcı E, Wang CI, Song H. Structural Basis for Blocking PD-1-Mediated Immune Suppression by Therapeutic Antibody Pembrolizumab. *Cell Research*, 2017, 27, 147–150, DOI: 10.1038/cr.2016.77.
148. Lee HT, Lee JY, Lim H, Lee SH, Moon YJ, Pyo HJ, Ryu SE, Shin W, Heo YS. Molecular Mechanism of PD-1/PD-L1 Blockade via Anti-PD-L1 Antibodies Atezolizumab and Durvalumab. *Sci Rep* 2017;7(1):1–12, DOI: 10.1038/s41598-017-

06002-8.

149. Horita S, Nomura Y, Sato Y, Shimamura T, Iwata S, Nomura N. High-Resolution Crystal Structure of the Therapeutic Antibody Pembrolizumab Bound to the Human PD-1. *Sci Rep* 2016;6(1):1–8, DOI: 10.1038/srep35297.
150. Scapin G, Yang X, Prorise WW, McCoy M, Reichert P, Johnston JM, Kashi RS, Strickland C. Structure of Full-Length Human Anti-PD1 Therapeutic IgG4 Antibody Pembrolizumab. *Nat Struct Mol Biol* 2015;22(12):953–958, DOI: 10.1038/nsmb.3129.
151. Lee JY, Lee HT, Shin W, Chae J, Choi J, Kim SH, Lim H, Won Heo T, Park KY, Lee YJ, Ryu SE, Son JY, Lee JU, Heo YS. Structural Basis of Checkpoint Blockade by Monoclonal Antibodies in Cancer Immunotherapy. *Nat Commun* 2016;7:1–10, DOI: 10.1038/ncomms13354.
152. Lee SH, Lee HT, Lim H, Kim Y, Park UB, Heo Y-S. Crystal Structure of PD-1 in Complex with an Antibody-Drug Tislelizumab Used in Tumor Immune Checkpoint Therapy. *Biochem Biophys Res Commun* 2020;527(1):226–231, DOI: 10.1016/j.bbrc.2020.04.121.
153. Hong Y, Feng Y, Sun H, Zhang B, Wu H, Zhu Q, Li Y, Zhang T, Zhang Y, Cui X, Li Z, Song X, Li K, Liu M, Liu Y. Tislelizumab Uniquely Binds to the CC' Loop of PD-1 with Slow-dissociated Rate and Complete PD-L1 Blockage. *FEBS Open Bio* 2021;11(3):782–792, DOI: 10.1002/2211-5463.13102.
154. Markham A, Duggan S. Cemiplimab: First Global Approval. *Drugs* 2018;(January), DOI: 10.1007/s40265-018-1012-5.
155. Herbst RS, Soria J-C, Kowanzetz M, Fine GD, Hamid O, Gordon MS, Sosman JA, McDermott DF, Powderly JD, Gettinger SN, Kohrt HEK, Horn L, Lawrence DP, Rost S, Leabman M, Xiao Y, Mokatrín A, Koeppen H, Hegde PS, Mellman I, Chen DS, Hodi FS. Predictive Correlates of Response to the Anti-PD-L1 Antibody MPDL3280A in Cancer Patients. *Nature* 2014;515(7528):563–567, DOI: 10.1038/nature14011.
156. Liu K, Tan S, Chai Y, Chen D, Song H, Zhang CWH, Shi Y, Liu J, Tan W, Lyu J, Gao S, Yan J, Qi J, Gao GF. Structural Basis of Anti-PD-L1 Monoclonal Antibody Avelumab for Tumor Therapy. *Cell Research*, 2017, 27, 151–153, DOI: 10.1038/cr.2016.102.
157. Tan S, Liu K, Chai Y, Zhang CWH, Gao S, Gao GF, Qi J. Distinct PD-L1 Binding Characteristics of Therapeutic Monoclonal Antibody Durvalumab. *Protein Cell* 2018;9(1):135–139, DOI: 10.1007/s13238-017-0412-8.
158. Smyth MJ, Ngíow SF, Ribas A, Teng MWL. Combination Cancer Immunotherapies Tailored to the Tumour Microenvironment. *Nat Rev Clin Oncol* 2016;13(3):143–158, DOI: 10.1038/nrclinonc.2015.209.
159. Borghaei H, Paz-Ares L, Horn L, Spigel DR, Steins M, Ready NE, Chow LQ, Vokes EE, Felip E, Holgado E, Barlesi F, Kohlhäufel M, Arrieta O, Burgio MA, Fayette J, Lena H, Poddubskaya E, Gerber DE, Gettinger SN, Rudin CM, Rizvi N, Crinò L, Blumenschein GR, Antonia SJ, Dorange C, Harbison CT, Graf Finckenstein F, Brahmer JR. Nivolumab versus Docetaxel in Advanced Nonsquamous Non-Small-Cell Lung Cancer. *N Engl J Med* 2015;373(17):1627–1639, DOI: 10.1056/nejmoa1507643.
160. Larkin J, Chiarion-Sileni V, Gonzalez R, Grob JJ, Cowey CL, Lao CD, Schadendorf D, Dummer R, Smylie M, Rutkowski P, Ferrucci PF, Hill A, Wagstaff J, Carlino MS, Haanen JB, Maio M, Marquez-Rodas I, McArthur GA, Ascierto PA, Long G V., Callahan MK, Postow MA, Grossmann K, Sznol M, Dreno B, Bastholt L, Yang A, Rollin LM, Horak C, Hodi FS, Wolchok JD. Combined Nivolumab and Ipilimumab or

- Monotherapy in Untreated Melanoma. *N Engl J Med* 2015;373(13):1270–1271, DOI: 10.1056/NEJMc1509660.
161. Andrews A. Treating with Checkpoint Inhibitors-Figure \$1 Million per Patient. *Am Heal drug benefits* 2015;8(Spec Issue):9.
 162. Vergnenegre A, Chouaid C. Economic Analyses of Immune-Checkpoint Inhibitors to Treat Lung Cancer. *Expert Rev Pharmacoeconomics Outcomes Res* 2020;0(0), DOI: 10.1080/14737167.2021.1863790.
 163. Kourie HR, Klastersky J. Immune Checkpoint Inhibitors Side Effects and Management. *Immunotherapy* 2016;8(7):799–807, DOI: 10.2217/imt-2016-0029.
 164. Combined Nivolumab and Ipilimumab or Monotherapy in Untreated Melanoma. *N Engl J Med* 2015;373(13):1270–1271, DOI: 10.1056/NEJMc1509660.
 165. Zhang Y, La B, Liang B, Gu Y. Treatment-Related Adverse Events with PD-1 or PD-L1 Inhibitors: A Systematic Review and Meta-Analysis. *Life* 2021;11(11):1277, DOI: 10.3390/life11111277.
 166. Yun K, Daniels G, Gold K, McCowen K, Patel SP. Rapid Onset Type 1 Diabetes with Anti-PD-1 Directed Therapy. *Oncotarget* 2020;11(28):2740–2746, DOI: 10.18632/oncotarget.27665.
 167. Zak KM, Grudnik P, Magiera K, Dömling A, Dubin G, Holak TA. Structural Biology of the Immune Checkpoint Receptor PD-1 and Its Ligands PD-L1/PD-L2. *Structure* 2017;25(8):1163–1174, DOI: 10.1016/j.str.2017.06.011.
 168. Martins F, Sofiya L, Sykiotis GP, Lamine F, Maillard M, Fraga M, Shabafrouz K, Ribi C, Cairoli A, Guex-Crosier Y, Kuntzer T, Michielin O, Peters S, Coukos G, Spertini F, Thompson JA, Obeid M. Adverse Effects of Immune-Checkpoint Inhibitors: Epidemiology, Management and Surveillance. *Nat Rev Clin Oncol* 2019;16(9):563–580, DOI: 10.1038/s41571-019-0218-0.
 169. Peptide Therapeutics Market Size & Growth, 2019-2026
<https://www.reportsanddata.com/report-detail/peptide-therapeutics-market> (accessed Apr 6, 2020).
 170. Craik DJ, Fairlie DP, Liras S, Price D. The Future of Peptide-Based Drugs. *Chem Biol Drug Des* 2013;81(1):136–147, DOI: 10.1111/cbdd.12055.
 171. Pelay-Gimeno M, Glas A, Koch O, Grossmann TN. Structure-Based Design of Inhibitors of Protein-Protein Interactions: Mimicking Peptide Binding Epitopes. *Angew Chemie - Int Ed* 2015;54(31):8896–8927, DOI: 10.1002/anie.201412070.
 172. Nevola L, Giralt E. Modulating Protein-Protein Interactions: The Potential of Peptides. *Chem Commun* 2015;51(16):3302–3315, DOI: 10.1039/c4cc08565e.
 173. Vlieghe P, Lisowski V, Martinez J, Khrestchatisky M. Synthetic Therapeutic Peptides: Science and Market. *Drug Discov Today* 2010;15(1–2):40–56, DOI: 10.1016/J.DRUDIS.2009.10.009.
 174. Sasikumar PG, Ramachandra M. Small-Molecule Immune Checkpoint Inhibitors Targeting PD-1/PD-L1 and Other Emerging Checkpoint Pathways. *BioDrugs* 2018;32(5):481–497, DOI: 10.1007/s40259-018-0303-4.
 175. Bumbaca B, Li Z, Shah DK. Pharmacokinetics of Protein and Peptide Conjugates. *Drug Metab Pharmacokinet* 2019;34(1):42–54, DOI: 10.1016/j.dmpk.2018.11.001.
 176. Darwin P, Toor SM, Sasidharan Nair V, Elkord E. Immune Checkpoint Inhibitors: Recent Progress and Potential Biomarkers. *Experimental and Molecular Medicine*, 2018,

50, 165, DOI: 10.1038/s12276-018-0191-1.

177. Boohaker RJ, Sambandam V, Segura I, Miller J, Suto M, Xu B. Rational Design and Development of a Peptide Inhibitor for the PD-1/PD-L1 Interaction. *Cancer Lett* 2018;434:11–21, DOI: 10.1016/j.canlet.2018.04.031.
178. Differding E, Aurigene Discovery Technologies, Fabre P. A Novel Peptide Therapeutic Targeting Pd-1 Immune Checkpoint Pathway for Cancer Immunotherapy ± Structure Activity Relationships & Peptide / Peptidomimetic. 2014;1–12.
179. WO 2013/144704 A1 - Immunomodulating Cyclic Compounds From The Bc Loop Of Human Pd1 - The Lens - Free & Open Patent and Scholarly Search <https://www.lens.org/lens/patent/012-160-659-090-701> (accessed Apr 21, 2020).
180. Magiera-Mularz K, Skalniak L, Zak KM, Musielak B, Rudzinska-Szostak E, Berlicki Ł, Kocik J, Grudnik P, Sala D, Zarganes-Tzitzikas T, Shaabani S, Dömling A, Dubin G, Holak TA. Bioactive Macrocyclic Inhibitors of the PD-1/PD-L1 Immune Checkpoint. *Angew Chemie - Int Ed* 2017;56(44):13732–13735, DOI: 10.1002/anie.201707707.
181. Chang H-N, Liu B, Qi Y, Zhou Y, Chen Y-P, Pan K-M, Li W-W, Zhou X-M, Ma W-W, Fu C-Y, Qi Y-M, Liu L, Gao Y-F. Blocking of the PD-1/PD-L1 Interaction by a <sc>D</sc>-Peptide Antagonist for Cancer Immunotherapy. *Angew Chemie Int Ed* 2015;54(40):11760–11764, DOI: 10.1002/anie.201506225.
182. Konieczny M, Musielak B, Kocik J, Skalniak L, Sala D, Czub M, Magiera-Mularz K, Rodriguez I, Myrcha M, Stec M, Siedlar M, Holak TA, Plewka J. Di-Bromo-Based Small-Molecule Inhibitors of the PD-1/PD-L1 Immune Checkpoint. *J Med Chem* 2020;63(19):11271–11285, DOI: 10.1021/acs.jmedchem.0c01260.
183. Orafaie A, Sadeghian H, Bahrami AR, Rafatpanah H, Matin MM. Design, Synthesis and Evaluation of PD-L1 Peptide Antagonists as New Anticancer Agents for Immunotherapy. *Bioorg Med Chem* 2021;30(October 2020):115951, DOI: 10.1016/j.bmc.2020.115951.
184. Sasikumar PGN, Ramachandra M, Vadlamani SK, Vemula KR, Satyam LK, Subbarao K, Shrimali RK, Kandepu S. IMMUNOSUPPRESSION MODULATING COMPOUNDS, 2011.
185. Sasikumar P, Shrimali R, Adurthi S, Ramachandra R, Satyam L, Dhudashiya A, Samiulla D, Sunilkumar KB, Ramachandra M. A Novel Peptide Therapeutic Targeting PD1 Immune Checkpoint with Equipotent Antagonism of Both Ligands and a Potential for Better Management of Immune-Related Adverse Events. *J Immunother Cancer* 2013;1(Suppl 1):O24, DOI: 10.1186/2051-1426-1-s1-o24.
186. Musielak B, Kocik J, Skalniak L, Magiera-Mularz K, Sala D, Czub M, Stec M, Siedlar M, Holak TA, Plewka J. CA-170 – A Potent Small-Molecule PD-L1 Inhibitor or Not? *Molecules* 2019;24(15):2804, DOI: 10.3390/molecules24152804.
187. Wang F, Ma J, Liu J, Jin H, Huang D. Synthetic Small Peptides Acting on B7H1 Enhance Apoptosis in Pancreatic Cancer Cells. *Mol Med Rep* 2012;6(3):553–557, DOI: 10.3892/mmr.2012.970.
188. Li C, Zhang N, Zhou J, Ding C, Jin Y, Cui X, Pu K, Zhu Y. Peptide Blocking of PD-1/PD-L1 Interaction for Cancer Immunotherapy. *Cancer Immunol Res* 2018;6(2):178–188, DOI: 10.1158/2326-6066.CIR-17-0035.
189. Sasikumar PG, Satyam LK, Shrimali RK, Subbarao K, Ramachandra R, Vadlamani S, Reddy A, Kumar A, Srinivas A, Reddy S, Gopinath S, Samiulla DS, Ramachandra M. Abstract 2850: Demonstration of Anti-Tumor Efficacy in Multiple Preclinical Cancer Models Using a Novel Peptide Inhibitor (Aurigene-012) of the PD1 Signaling Pathway.

- In *Cancer Research*, Vol. 72. American Association for Cancer Research (AACR), 2012; 2850–2850, DOI: 10.1158/1538-7445.am2012-2850.
190. Sasikumar PG, Ramachandra RK, Adurthi S, Dhudashiya AA, Vadlamani S, Vemula K, Vunnum S, Satyam LK, Samiulla DS, Subbarao K, Nair R, Shrimali R, Gowda N, Ramachandra M. A Rationally Designed Peptide Antagonist of the PD-1 Signaling Pathway as an Immunomodulatory Agent for Cancer Therapy. *Mol Cancer Ther* 2019;18(6):1081–1091, DOI: 10.1158/1535-7163.MCT-18-0737.
 191. A Kind of PD-1 Albumen Extracellular Fragment Affinity Peptide L8 and Application Thereof, March 24, 2014.
 192. PD-L1 IgV Affinity Peptide with Antineoplastic Activity, and Preparation Method and Application of Thereof, June 30, 2014.
 193. PD-L1 IgV Affinity Peptide S10 with Antitumor Activity, May 29, 2014.
 194. M. Miller, C. Mapelli, M. P. Allen, M. S. Bowsher, K. M. Boy, E. P. Gillis, D. R. Langley, E. Mull, M. A. Poirier, N. Sanghvi, L.-Q. Sun, D. J. Tenney, K.-S. Yeung, J. Zhu, P. C. Reid PMS. WO2014151634A1 - Macrocyclic Inhibitors of the Pd-1/Pd-L1 and Cd80(B7-1)/Pd-L1 Protein/Protein Interactions - Google Patents, 2014.
 195. Magiera-Mularz K, Kuska K, Skalniak L, Grudnik P, Musielak B, Plewka J, Kocik J, Stec M, Weglarczyk K, Sala D, Wladyka B, Siedlar M, Holak TA, Dubin G. Macrocyclic Peptide Inhibitor of PD-1/PD-L1 Immune Checkpoint. *Adv Ther* 2021;4(2):2000195, DOI: 10.1002/adtp.202000195.
 196. Zyla E, Musielak B, Holak TA, Dubin G. Structural Characterization of a Macrocyclic Peptide Modulator of the PD-1/PD-L1 Immune Checkpoint Axis. *Molecules* 2021;26(16):4848, DOI: 10.3390/molecules26164848.
 197. Zou S, Liu J, Sun Z, Feng X, Wang Z, Jin Y, Yang Z. Discovery of HPRDX5-Based Peptide Inhibitors Blocking PD-1/PD-L1 Interaction through in Silico Proteolysis and Rational Design. *Cancer Chemother Pharmacol* 2020;85(1):185–193, DOI: 10.1007/s00280-019-03995-z.
 198. Munir S, Lundsager MT, Jørgensen MA, Hansen M, Petersen TH, Bonefeld CM, Friese C, Met Ö, Straten P thor, Andersen MH. Inflammation Induced PD-L1-Specific T Cells. *Cell Stress* 2019;3(10):319–327, DOI: 10.15698/cst2019.10.201.
 199. Gurung S, Khan F, Gunassekaran GR, Yoo J Do, Poongkavithai Vadevo SM, Permpoon U, Kim S-H, Kim H-J, Kim I-S, Han H, Park J, Kim S, Lee B. Phage Display-Identified PD-L1-Binding Peptides Reinvigorate T-Cell Activity and Inhibit Tumor Progression. *Biomaterials* 2020;247:119984, DOI: 10.1016/j.biomaterials.2020.119984.
 200. Li W, Zhu X, Zhou X, Wang X, Zhai W, Li B, Du J, Li G, Sui X, Wu Y, Zhai M, Qi Y, Chen G, Gao Y. An Orally Available PD-1/PD-L1 Blocking Peptide OPBP-1-Loaded Trimethyl Chitosan Hydrogel for Cancer Immunotherapy. *J Control Release* 2021;334(April):376–388, DOI: 10.1016/j.jconrel.2021.04.036.
 201. Munir Ahmad S, Martinenaite E, Hansen M, Junker N, Borch TH, Met Ö, Donia M, Svane IM, Andersen MH. PD-L1 Peptide Co-Stimulation Increases Immunogenicity of a Dendritic Cell-Based Cancer Vaccine. *Oncoimmunology* 2016;5(8), DOI: 10.1080/2162402X.2016.1202391.
 202. Wang Y, Guo H, Feng Z, Wang S, Wang Y, He Q, Li G, Lin W, Xie XQ, Lin Z. PD-1-Targeted Discovery of Peptide Inhibitors by Virtual Screening, Molecular Dynamics Simulation, and Surface Plasmon Resonance. *Molecules* 2019;24(20):1–15, DOI: 10.3390/molecules24203784.

203. Abbas A, Lin B, Liu C, Morshed A, Hu J, Xu H. Design and Synthesis of A PD-1 Binding Peptide and Evaluation of Its Anti-Tumor Activity. *Int J Mol Sci* 2019;20(3):572, DOI: 10.3390/ijms20030572.
204. Zhou K, Lu J, Yin X, Xu H, Li L, Ma B. Structure-Based Derivation and Intramolecular Cyclization of Peptide Inhibitors from PD-1/PD-L1 Complex Interface as Immune Checkpoint Blockade for Breast Cancer Immunotherapy. *Biophys Chem* 2019;253(June), DOI: 10.1016/j.bpc.2019.106213.
205. Liu H, Zhao Z, Zhang L, Li Y, Jain A, Barve A, Jin W, Liu Y, Fetse J, Cheng K. Discovery of Low-Molecular Weight Anti-PD-L1 Peptides for Cancer Immunotherapy. *J Immunother Cancer* 2019;7(1):270, DOI: 10.1186/s40425-019-0705-y.
206. Wang K, Song Y, Su Y, Liang Y, Wang L. Effect of the Hairpin Structure of Peptide Inhibitors on the Blockade of PD-1/PD-L1 Axis. *Biochem Biophys Res Commun* 2020;527(2):453–457, DOI: 10.1016/j.bbrc.2020.04.018.
207. Zhang P, Li C, Ji X, Gao M, Lyu S, Dai X, Du J. In Silico Screening and Surface Plasma Resonance-Based Verification of Programmed Death 1-Targeted Peptides. *Chem Biol Drug Des* 2020;95(3):332–342, DOI: 10.1111/cbdd.13647.
208. Guardiola S, Varese M, Roig X, Garcia J, Giralt E. A Target-Based Method for Designing Heterochiral Cyclic Peptide Binders: De Novo Inhibitors of the PD-1/PD-L1 Interaction., DOI: 10.26434/chemrxiv.11663337.v1.
209. Kotraiah V, Phares TW, Browne CD, Pannucci J, Mansour M, Noe AR, Tucker KD, Christen JM, Reed C, MacKay A, Weir GM, Rajagopalan R, Stanford MM, Chung C-S, Ayala A, Huang J, Tsuji M, Gutierrez GM. Novel Peptide-Based PD1 Immunomodulators Demonstrate Efficacy in Infectious Disease Vaccines and Therapeutics. *Front Immunol* 2020;11:264, DOI: 10.3389/fimmu.2020.00264.
210. Zhai W, Zhou X, Zhai M, Li W, Ran Y, Sun Y, Du J, Zhao W, Xing L, Qi Y, Gao Y. Blocking of the PD-1/PD-L1 Interaction by a Novel Cyclic Peptide Inhibitor for Cancer Immunotherapy. *Sci China Life Sci* 2020;1–15, DOI: 10.1007/s11427-020-1740-8.
211. Chen Y, Huang H, Liu Y, Wang Z, Wang Q, Zhang Y, Wang H. Engineering a High-Affinity PD-1 Peptide for Optimized Immune Cell-Mediated Tumor Therapy. *Cancer Res Treat* 2021;1–31, DOI: 10.4143/crt.2021.424.
212. Li G, Guo H, Zhao L, Feng H, He H, Chen Y, Wang Y, Lin Z. Discovery of Modulators for the PD-1/PD-L1 Interaction by Molecular Simulation and Bioassay. *New J Chem* 2021;45(39):18497–18508, DOI: 10.1039/D1NJ02030G.
213. US10538555B2 - Macrocyclic inhibitors of the PD-1/PD-L1 and CD80(B7-1)/PD-L1 protein/protein interactions - Google Patents <https://patents.google.com/patent/US10538555B2/en> (accessed Apr 22, 2020).
214. Miao Q, Zhang W, Zhang K, Li H, Zhu J, Jiang S. Rational Design of a Potent Macrocyclic Peptide Inhibitor Targeting the PD-1/PD-L1 Protein–Protein Interaction. *RSC Adv* 2021;11(38):23270–23279, DOI: 10.1039/D1RA03118J.
215. Guzik K, Tomala M, Muszak D, Konieczny M, Hec A, Błaszkiwicz U, Pustuła M, Butera R, Dömling A, Holak TA, Guzik K, Tomala M, Muszak D, Konieczny M, Hec A, Błaszkiwicz U, Pustuła M, Butera R, Dömling A, Holak TA. Development of the Inhibitors That Target the PD-1/PD-L1 Interaction—A Brief Look at Progress on Small Molecules, Peptides and Macrocycles. *Molecules* 2019;24(11):2071, DOI: 10.3390/molecules24112071.
216. Li K, Tian H. Development of Small-Molecule Immune Checkpoint Inhibitors of PD-1/PD-L1 as a New Therapeutic Strategy for Tumour Immunotherapy. *J Drug Target*

- 2019;27(3):244–256, DOI: 10.1080/1061186X.2018.1440400.
217. Chen T, Li Q, Liu Z, Chen Y, Feng F, Sun H. Peptide-Based and Small Synthetic Molecule Inhibitors on PD-1/PD-L1 Pathway: A New Choice for Immunotherapy? *Eur J Med Chem* 2019;161:378–398, DOI: 10.1016/J.EJMECH.2018.10.044.
 218. Wu Q, Jiang L, Li S cheng, He Q jun, Yang B, Cao J. Small Molecule Inhibitors Targeting the PD-1/PD-L1 Signaling Pathway. *Acta Pharmacol Sin* 2020;(October 2019), DOI: 10.1038/s41401-020-0366-x.
 219. Shaabani S, Huizinga HPS, Butera R, Kouchi A, Guzik K, Magiera-Mularz K, Holak TA, Dömling A. A Patent Review on PD-1/PD-L1 Antagonists: Small Molecules, Peptides and Macrocycles (2015-2018) HHS Public Access. *Expert Opin Ther Pat* 2018;28(9):665–678, DOI: 10.1080/13543776.2018.1512706.
 220. Zarganes-Tzitzikas T, Konstantinidou M, Gao Y, Krzemien D, Zak K, Dubin G, Holak TA, Dömling A. Inhibitors of Programmed Cell Death 1 (PD-1): A Patent Review (2010-2015). *Expert Opin Ther Pat* 2016;26(9):973–977, DOI: 10.1080/13543776.2016.1206527.
 221. Zhu W, Bai Y, Zhang N, Yan J, Chen J, He Z, Sun Q, Pu Y, He B, Ye X. A Tumor Extracellular PH-Sensitive PD-L1 Binding Peptide Nanoparticle for Chemo-Immunotherapy of Cancer. *J Mater Chem B* 2021;9(20):4201–4210, DOI: 10.1039/D1TB00537E.
 222. Gautam A, Beiss V, Wang C, Wang L, Steinmetz NF. Plant Viral Nanoparticle Conjugated with Anti-PD-1 Peptide for Ovarian Cancer Immunotherapy. *Int J Mol Sci* 2021;22(18):9733, DOI: 10.3390/ijms22189733.
 223. Hughes J, Rees S, Kalindjian S, Philpott K. Principles of Early Drug Discovery. *Br J Pharmacol* 2011;162(6):1239–1249, DOI: 10.1111/j.1476-5381.2010.01127.x.
 224. Liu C, Seeram NP, Ma H. Small Molecule Inhibitors against PD-1/PD-L1 Immune Checkpoints and Current Methodologies for Their Development: A Review. *Cancer Cell Int* 2021;21(1):239, DOI: 10.1186/s12935-021-01946-4.
 225. Zeidan E, Kepley CL, Sayes C, Sandros MG. Surface Plasmon Resonance: A Label-Free Tool for Cellular Analysis. *Nanomedicine* 2015;10(11):1833–1846, DOI: 10.2217/nmm.15.31.
 226. De Crescenzo G, Boucher C, Durocher Y, Jolicoeur M. Kinetic Characterization by Surface Plasmon Resonance-Based Biosensors: Principle and Emerging Trends. *Cell Mol Bioeng* 2008;1(4):204–215, DOI: 10.1007/s12195-008-0035-5.
 227. GE Healthcare. *Biacore Sensor Surface Handbook*. 2016.
 228. Swinney DC. Molecular Mechanism of Action (MMoA) in Drug Discovery. In *Annual Reports in Medicinal Chemistry*, Vol. 46. Elsevier Inc., 2011; 301–317, DOI: 10.1016/B978-0-12-386009-5.00009-6.
 229. Principle and Protocol of Surface Plasmon Resonance (SPR) - Creative BioMart <https://www.creativebiomart.net/resource/principle-protocol-principle-and-protocol-of-surface-plasmon-resonance-spr-361.htm> (accessed May 22, 2022).
 230. Fossceco SL, Company KP, Curtis NA. Exploring Enzyme-Linked Immunosorbent Assay (ELISA) Data with the SAS ® Analyst Application Introduction. 1996.
 231. Lequin RM. Enzyme Immunoassay (EIA)/Enzyme-Linked Immunosorbent Assay (ELISA). *Clin Chem* 2005;51(12):2415–2418, DOI: 10.1373/clinchem.2005.051532.
 232. Voller A, Bartlett A, Bidwell DE. Enzyme Immunoassays with Special Reference to

- ELISA Techniques. *J Clin Pathol* 1978;31(6):507–520, DOI: 10.1136/jcp.31.6.507.
233. McKinnon KM. Flow Cytometry: An Overview. *Curr Protoc Immunol* 2018;120(1):5.1.1, DOI: 10.1002/cpim.40.
234. Adan A, Alizada G, Kiraz Y, Baran Y, Nalbant A. Flow Cytometry: Basic Principles and Applications. *Crit Rev Biotechnol* 2017;37(2):163–176, DOI: 10.3109/07388551.2015.1128876.
235. DeLay M, Rieger A. *Flow Cytometry Handbook Available Fluorochrome Options by Laser Conjugate*. 2019.
236. Garofalo M, Grazioso G, Cavalli A, Sgrignani J. How Computational Chemistry and Drug Delivery Techniques Can Support the Development of New Anticancer Drugs. *Molecules*, 2020, 25, DOI: 10.3390/molecules25071756.
237. Miller BR, McGee TD, Swails JM, Homeyer N, Gohlke H, Roitberg AE. MMPBSA.Py : An Efficient Program for End-State Free Energy Calculations. *J Chem Theory Comput* 2012;8(9):3314–3321, DOI: 10.1021/ct300418h.
238. Bojko M, Węgrzyn K, Sikorska E, Kocikowski M, Parys M, Battin C, Steinberger P, Kogut MM, Winnicki M, Sieradzan AK, Spodzieja M, Rodziewicz-Motowidło S. Design, Synthesis and Biological Evaluation of PD-1 Derived Peptides as Inhibitors of PD-1/PD-L1 Complex Formation for Cancer Therapy. *Bioorg Chem* 2022;128:106047, DOI: 10.1016/j.bioorg.2022.106047.
239. Jeong W jin, Bu J, Han Y, Drelich AJ, Nair A, Král P, Hong S. Nanoparticle Conjugation Stabilizes and Multimerizes β -Hairpin Peptides to Effectively Target PD-1/PD-L1 β -Sheet-Rich Interfaces. *J Am Chem Soc* 2020;142(4):1832–1837, DOI: 10.1021/jacs.9b10160.
240. Moore GE, Gerner RE, Franklin HA. Culture of Normal Human Leukocytes. *JAMA J Am Med Assoc* 1967;199(8):519–524, DOI: 10.1001/jama.1967.03120080053007.
241. Kuncewicz K, Battin C, Sieradzan A, Karczyńska A, Orlikowska M, Wardowska A, Piękła M, Steinberger P, Rodziewicz-Motowidło S, Spodzieja M. Fragments of Gd Protein as Inhibitors of Btla/Hvem Complex Formation—Design, Synthesis, and Cellular Studies. *Int J Mol Sci* 2020;21(22):1–19, DOI: 10.3390/ijms21228876.
242. Yang F, Zhang Y, Liang H. Interactive Association of Drugs Binding to Human Serum Albumin. *Int J Mol Sci* 2014;15:3580–3595, DOI: 10.3390/ijms15033580.
243. Zorzi A, Linciano S, Angelini A. Non-Covalent Albumin-Binding Ligands for Extending the Circulating Half-Life of Small Biotherapeutics. *Medchemcomm* 2019;10(7):1068–1081, DOI: 10.1039/C9MD00018F.
244. Riss T, Ph D. CELL TITER -G LO™ LUMINESCENT CELL VIABILITY ASSAY : A SENSITIVE AND RAPID METHOD FOR DETERMINING CELL. 11–13.
245. CellTiter-Glo® Luminescent Cell Viability Assay https://pl.promega.com/products/cell-health-assays/cell-viability-and-cytotoxicity-assays/celltiter_glo-luminescent-cell-viability-assay/?catNum=G7570 (accessed May 16, 2022).
246. Gould SJ, Subramani S. Firefly Luciferase as a Tool in Molecular and Cell Biology. *Anal Biochem* 1988;175(1):5–13, DOI: 10.1016/0003-2697(88)90353-3.
247. PD-1 PD-L1 Blockade Bioassay | PD1 PDL1 | PD1 PDL1 Interactions https://pl.promega.com/products/reporter-bioassays/immune-checkpoint-bioassays/pd1_pdl1-blockade-bioassays/?catNum=J1250 (accessed Aug 26, 2022).

248. Jutz S, Hennig A, Paster W, Asrak Ö, Dijanovic D, Kellner F, Pickl WF, Huppa JB, Leitner J, Steinberger P, Jutz S, Hennig A, Paster W, Asrak Ö, Dijanovic D, Kellner F, Pickl WF, Huppa JB, Leitner J, Steinberger P. A Cellular Platform for the Evaluation of Immune Checkpoint Molecules. *Oncotarget* 2017;8(39):64892–64906, DOI: 10.18632/ONCOTARGET.17615.
249. De Sousa Linhares A, Battin C, Jutz S, Leitner J, Hafner C, Tobias J, Wiedermann U, Kundi M, Zlabinger GJ, Grabmeier-Pfistershammer K, Steinberger P. Therapeutic PD-L1 Antibodies Are More Effective than PD-1 Antibodies in Blocking PD-1/PD-L1 Signaling. *Sci Rep* 2019;9(1):1–9, DOI: 10.1038/s41598-019-47910-1.
250. Jutz S, Leitner J, Schmetterer K, Doel-Perez I, Majdic O, Grabmeier-Pfistershammer K, Paster W, Huppa JB, Steinberger P. Assessment of Costimulation and Coinhibition in a Triple Parameter T Cell Reporter Line: Simultaneous Measurement of NF- κ B, NFAT and AP-1. *J Immunol Methods* 2016;430:10–20, DOI: 10.1016/j.jim.2016.01.007.
251. Liang GB, Rito CJ, Gellman SH. Thermodynamic Analysis of β -Turn Formation in Pro-Ala, Pro-Gly, and Pro-Val Model Peptides in Methylene Chloride. *J Am Chem Soc* 1992;114(11):4440–4442, DOI: 10.1021/ja00037a083.
252. Nowick JS, Brower JO. A New Turn Structure for the Formation of β -Hairpins in Peptides. *J Am Chem Soc* 2003;125(4):876–877, DOI: 10.1021/ja028938a.
253. Hong SY, Oh JE, Lee K-H. Effect of D-Amino Acid Substitution on the Stability, the Secondary Structure, and the Activity of Membrane-Active Peptide. *Biochem Pharmacol* 1999;58(11):1775–1780, DOI: 10.1016/S0006-2952(99)00259-2.
254. Studies S. White Paper Wyatt Technology Corporation Protein Quality Control in SPR and BLI High-Throughput <https://www.wyatt.com/files/literature/white-papers/protein-quality-control-high-throughput-screening-studies.pdf> (accessed May 22, 2022).
255. Huang D, Wen W, Liu X, Li Y, Zhang JZH. Computational Analysis of Hot Spots and Binding Mechanism in the PD-1/PD-L1 Interaction. *RSC Adv* 2019;9(26):14944–14956, DOI: 10.1039/C9RA01369E.
256. Ding H, Liu H. Mapping the Binding Hot Spots on Human Programmed Cell Death 1 and Its Ligand with Free-Energy Simulations. *J Chem Inf Model* 2019;59(10):4339–4349, DOI: 10.1021/acs.jcim.9b00337.
257. Du J, Qin Y, Wu Y, Zhao W, Zhai W, Qi Y, Wang C, Gao Y. The Design of High Affinity Human PD-1 Mutants by Using Molecular Dynamics Simulations (MD). *Cell Commun Signal* 2018;16(1):25, DOI: 10.1186/s12964-018-0239-9.
258. Lázár-Molnár E, Scanduzzi L, Basu I, Quinn T, Sylvestre E, Palmieri E, Ramagopal UA, Nathenson SG, Guha C, Almo SC. Structure-Guided Development of a High-Affinity Human Programmed Cell Death-1: Implications for Tumor Immunotherapy. *EBioMedicine* 2017;17:30–44, DOI: 10.1016/j.ebiom.2017.02.004.
259. Sun L, Li C-W, Chung EM, Yang R, Kim Y-S, Park AH, Lai Y-J, Yang Y, Wang Y-H, Liu J, Qiu Y, Khoo K-H, Yao J, Hsu JL, Cha J-H, Chan L-C, Hsu J-M, Lee H-H, Yoo SS, Hung M-C. Targeting Glycosylated PD-1 Induces Potent Antitumor Immunity. *Cancer Res* 2020;80(11):2298–2310, DOI: 10.1158/0008-5472.CAN-19-3133.
260. Li C-W, Lim S-O, Xia W, Lee H-H, Chan L-C, Kuo C-W, Khoo K-H, Chang S-S, Cha J-H, Kim T, Hsu JL, Wu Y, Hsu J-M, Yamaguchi H, Ding Q, Wang Y, Yao J, Lee C-C, Wu H-J, Sahin AA, Allison JP, Yu D, Hortobagyi GN, Hung M-C. Glycosylation and Stabilization of Programmed Death Ligand-1 Suppresses T-Cell Activity. *Nat Commun* 2016;7(1):12632, DOI: 10.1038/ncomms12632.
261. Benicky J, Sanda M, Brnakova Kennedy Z, Grant OC, Woods RJ, Zwart A, Goldman R.

- PD-L1 Glycosylation and Its Impact on Binding to Clinical Antibodies. *J Proteome Res* 2021;20(1):485–497, DOI: 10.1021/acs.jproteome.0c00521.
262. Fanali G, di Masi A, Trezza V, Marino M, Fasano M, Ascenzi P. Human Serum Albumin: From Bench to Bedside. *Mol Aspects Med* 2012;33(3):209–290, DOI: 10.1016/j.mam.2011.12.002.
263. Ganesan A, Ahmed M, Okoye I, Arutyunova E, Babu D, Turnbull WL, Kundu JK, Shields J, Agopsowicz KC, Xu L, Tabana Y, Srivastava N, Zhang G, Moon TC, Belovodskiy A, Hena M, Kandadai AS, Hosseini SN, Hitt M, Walker J, Smylie M, West FG, Siraki AG, Lemieux MJ, Elahi S, Nieman JA, Tyrrell DL, Houghton M, Barakat K. Comprehensive in Vitro Characterization of PD-L1 Small Molecule Inhibitors. *Sci Rep* 2019;9(1):12392, DOI: 10.1038/s41598-019-48826-6.
264. Ciani B, Jourdan M, Searle MS. Stabilization of β -Hairpin Peptides by Salt Bridges: Role of Preorganization in the Energetic Contribution of Weak Interactions. *J Am Chem Soc* 2003;125(30):9038–9047, DOI: 10.1021/ja030074l.
265. Makwana KM, Mahalakshmi R. Implications of Aromatic-Aromatic Interactions: From Protein Structures to Peptide Models. *Protein Sci* 2015;24(12):1920–1933, DOI: 10.1002/pro.2814.
266. Cochran AG, Skelton NJ, Starovasnik MA. Tryptophan Zippers: Stable, Monomeric β -Hairpins. *Proc Natl Acad Sci* 2001;98(10):5578–5583, DOI: 10.1073/pnas.091100898.
267. Cochran AG, Tong RT, Starovasnik MA, Park EJ, McDowell RS, Theaker JE, Skelton NJ. A Minimal Peptide Scaffold for β -Turn Display: Optimizing a Strand Position in Disulfide-Cyclized β -Hairpins. *J Am Chem Soc* 2001;123(4):625–632, DOI: 10.1021/ja003369x.
268. Spodzieja M, Kuncewicz K, Sieradzan A, Karczyńska A, Iwaszkiewicz J, Cesson V, Węgrzyn K, Zhukov I, Maszota-Zieleniak M, Michielin O, Speiser DE, Zoete V, Derré L, Rodziewicz-Motowidło S. Disulfide-Linked Peptides for Blocking BTLA/HVEM Binding. *Int J Mol Sci* 2020;21(2):636, DOI: 10.3390/ijms21020636.
269. Rao MHVR, Kumar SK, Kunwar AC. Formation of β -Hairpins in l-Pro-Gly Containing Peptides Facilitated by 3-Amino Benzoic Acid. *Tetrahedron Lett* 2003;44(39):7369–7372, DOI: 10.1016/j.tetlet.2003.07.003.
270. Haque TS, Little JC, Gellman SH. Stereochemical Requirements for β -Hairpin Formation: Model Studies with Four-Residue Peptides and Depsipeptides. *J Am Chem Soc* 1996;118(29):6975–6985, DOI: 10.1021/ja960429j.
271. Ananthanarayanan VS, Shyamasundar N. Circular Dichroism of Type 13 β -Turn in Linear Tripeptides Containing L-Proline and D-Alanine. *Biochem Biophys Res Commun* 1981;102(1):295–301, DOI: 10.1016/0006-291X(81)91520-5.
272. Buděšínský M, Šebestík J, Bednářová L, Baumruk V, Šafařík M, Bouř P. Conformational Properties of the Pro-Gly Motif in the $\langle d \rangle$ -Ala- $\langle l \rangle$ -Pro-Gly- $\langle d \rangle$ -Ala Model Peptide Explored by a Statistical Analysis of the NMR, Raman, and Raman Optical Activity Spectra. *J Org Chem* 2008;73(4):1481–1489, DOI: 10.1021/jo702297y.
273. Ravi A, Balaram P. Stabilization of β -Turn Conformations in Pro-X Sequences by Disulphide Bridging. Synthesis and Solution Conformations of Five Cyclic Cystine Peptides. *Tetrahedron* 1984;40(13):2577–2583, DOI: 10.1016/S0040-4020(01)83512-2.
274. Case DA, Betz RM, Cerutti DS, T.E. CI, Darden TA, Duke RE, Giese TJ, Gohlke H, Goetz AW, Homeyer N, Izadi S, Janowski P, Kaus J, Kovalenko A, Lee TS, LeGrand S, Li P, C.Lin, Luchko T, Luo R, Madej B, Mermelstein D, Merz KM, Monard G, Nguyen

H, Nguyen HT, Omelyan I, Onufriev A, Roe DR, Roitberg A, Sagui C, Simmerling CL, Botello-Smith WM, Swails J, Walker RC, Wang J, Wolf RM, Wu X, Xiao L, Kollman PA. Amber 2016. *Univ California, San Fr* 2016.

275. Miller SM, Simon RJ, Ng S, Zuckermann RN, Kerr JM, Moos WH. Comparison of the Proteolytic Susceptibilities of Homologous L-Amino Acid, D-Amino Acid, and N-Substituted Glycine Peptide and Peptoid Oligomers. *Drug Dev Res* 1995;35(1):20–32, DOI: 10.1002/ddr.430350105.